THE MINERALOGY AND CHEMISTRY OF PULVERISED FUEL ASH PRODUCED BY THREE SOUTH AFRICAN COAL-BURNING POWER STATIONS.

by

GORDON L. BOSCH

Thesis submitted in fulfilment of the requirement for the degree of Master of Science.

Department of Geochemistry
University of Cape Town

March 1990

DECLARATION

I hereby declare that all the work presented in this thesis is my own, except where otherwise stated in the text.

Signed by candidate

G. L. BOSCH

March 1990

We shall not cease from exploration

And the end of all our exploring

Will be to arrive where we started

And know the place for the first time

T. S. Elliot (extract from Little Gidding)

TABLE OF CONTENTS

LIST OF TABLES

LIST OF FIGURES

LIST OF APPENDICES

ABSTRACT

The chemical and mineral compositions are presented for 63 pulverized fuel ash (PFA) and 16 input coal samples collected from Lethabo, Duvha and Matla power stations over the period 1987-1988. Bulk chemical composition was determined by X-ray fluorescence spectrometry. The mineral concentrations were determined by semi-quantitative X-ray diffraction based on integrated counts over peak areas, with silicon used as an internal standard. The particle size distributions were determined for two sample sets from each power station with a Malvern Instruments Particle Sizer. The major phases present in the ash are glass (45-75%), mullite (16-39%) and quartz (1.5-16%). The quartz concentration decreases in PFA from fields 1 to 4 in all the stations, and is positively correlated with the SiO_2 concentration. The concentrations of glass, mullite and quartz in PFA generally vary within well defined limits which remain constant with time. An exception is the glass concentration in Duvha PFA. Spinel concentration generally decreases in concentration in PFA from fields 1 to 4, and is positively correlated with the Fe_2O_3 concentration. Of the trace elements determined, Zr, Rb and Mn generally have no or very low enrichment in concentration in PFA from fields 1 to 4. The highest enrichment factors (> 5) were found for As, Ge and Se in Duvha PFA. The composition of the glass and ferrite spinel phases were determined by electron microprobe analysis. The glass consists of SiO_2 (21-100%) and Al_2O_3 (0.1-49%), with significant proportions of CaO, TiO_2, Fe_2O_3 and MgO. Al_2O_3, MgO and TiO_2 substitute for FeO in the spinel structure, with MgO substitution dominant in Duvha spinels. Chemical mass balance calculations suggest that of the elements determined for Lethabo PFA, the only one released in a significant proportion to the atmosphere is S (92%).

CHAPTER 1

INTRODUCTION

Pulverised fuel ash (PFA) is the mineral and glass residue produced in the combustion chamber of pulverised coal burning power stations. PFA is composed of fly ash (FA) which is removed along with the flue gas, and of bottom ash (BA) which is collected on the bottom of the combustion chamber. FA and BA ashes are made up predominantly of the inorganic fraction of the input coal which has undergone heating, with possible melting, vaporisation and new mineral growth as a result of the high temperatures in the combustion chamber of the power station. FA and BA also contain small amounts of carbon from unburnt coal particles which escaped the combustion process.

Coal burnt in South African power stations is mostly bituminous. In 1988 64.5 million tons of coal with an average ash content of 28% were burnt to generate electricity, which produced 18 million tons of FA and 0.5 million tons of BA (Eskom Annual Report 1988; Willis et al 1989). Table 1.1 gives details of the main coal-burning power stations in South Africa.

Power Station	Total Installed Rating (MW)	Coal (Mtons)	Ash (Mtons)
Arnot	2100	5.4	1.5
Camden	1600	1.0	0.28
Duvha	3600	10.0	2.8
Grootvlei	1200	1.0	0.28
Hendrina	2000	4.3	1.2
Kendal	686	1.5	0.42
Komati	1000	1.8	0.5
Kriel	3000	8.4	2.3
Lethabo	2472	8.4	2.3
Matimba	1995	6.0	1.68
Matla	3600	10.4	2.9
Tutuka	3045	6.7	1.87

Table 1.1 : Details of the main coal-burning power stations in South Africa. The data are correct for 31 December 1988 (Eskom Annual Report 1988).

Most of the FA is removed from the flue gas by a series of sequential precipitators (mechanical in the older stations and electrostatic in the modern stations) before the ash is released to the atmosphere. The majority of the ash is removed by the first precipitator field, with subsequently less ash removed by each of the following sequential precipitators, and with an associated decrease in particle size. Most modern stations use four sequential electrostatic precipitator fields. However, Lethabo uses seven fields due to the unusually high ash content of the input coal (±40% ash) which is ground to finer particle sizes than elsewhere.

PFA consists of a heterogeneous combination of solid glass spheres, hollow glass spheres (cenospheres), hollow glass spheres filled with other glass spheres (plerospheres), unfused quartz grains derived from the original coal, solid iron metal (rare) and iron oxide spheres, and unburnt coal particles (Fischer et al 1976, Lauf 1982). FA particles vary in size from approximately 500μm to < 0.1μm. The glass spheres are mainly aluminosilicates which also contain other oxides such as Fe_2O_3 and CaO. The mineralogy of ash derived from high rank coals is relatively simple and consists of glass, mullite, quartz, magnetite (ferrite spinel) and hematite. The mineralogy of ash derived from coals of lower rank is more complex (McCarthy 1988). Glass is a component of all ashes. Mullite crystallites ($3Al_2O_3.2SiO_2$) are found in the glass and have an acicular habit (Hulett et al 1980) and together with the glass are thought to be decomposition products of kaolinite. Iron is found as hematite and as a ferrite spinel (McCarthy 1988), and as dissolved Fe_2O_3 in the glass. Free lime and its alteration products portlandite ($Ca(OH)_2$) and calcite ($CaCO_3$) have been observed in PFA.

The chemical composition of FA has been extensively researched and is well known both for South African ashes (Willis 1987) and for other coal-burning countries (Valkovic et al 1984; Block and Dams 1976; Furuya et al 1987; Klein et al 1975; Grossman 1983). Oxides of the refractory elements such as CaO, Al_2O_3, SiO_2 and Fe_2O_3 form the major minerals present in the ash (Fischer et al 1976, Hulett et al 1980). Volatile elements such as As, S, Pb and Mo are found as gases at combustion chamber temperatures, but are believed to condense onto the fly ash particles as the flue gas temperature drops (Davidson et al 1974, Linton et al 1976). Enrichment of trace elements such as Se, Ge, As and Pb in the smaller particle size fraction has been well established both for South African FA (Willis 1987) and for FA from other countries.

Recent work in the USA has sought to provide further understanding of the mineralogy of fly ash (McCarthy 1988). Semi-quantitative analysis of the phases present in fly ash have been

carried out both on South African fly ash (Lesch and Cornell 1987) and for American fly ash (McCarthy and Thedchanamoorthy 1989). The latter authors have developed an easily applied method of semi-quantitative X-ray diffraction which is currently being employed to generate a data base of fly ash mineralogy.

Attention both in South Africa and internationally has recently been focused on the development of PFA as a utilisable resource, rather than dumping it as a waste product. This was the central issue of a recent international conference on coal ash held in South Africa (*Ash:* A Valuable Resource, CSIR, 1987).

During 1988 only 278 505 tons of S. African coal ash was utilised in other than backfill or landfill operations. Of this amount 26.7% was used for cement blends, 22.1% for mine support, 15.1% in dams, 12.8% in structural concrete, 9.8% in concrete products, 8.8% in ready-mix concrete and 5% in "bags" used mainly for canal linings. Concrete products consist of bricks and blocks, fibre cement (asbestos), refractories, roof tiles, pipes and other minor products (Willis et al 1989).

Other areas of utilisation which are presently undergoing research are in mass concrete and agricultural applications (Willis et al 1989). Fly ash is currently being tested for use as a soil ameliorant in the acidic soils of the maize-producing areas of the Transvaal. Cenospheres have been commercially recovered from ashes in the UK and the USA, and on an experimental basis in South Africa, primarily for use as a filler in the polymer industry (Kruger et al 1989). The recovery from the ash of Al, Ge, Ga, U and Mo, as well as other elements, has been investigated (Verbaan 1987; Kruger et al 1989), and has been reviewed by Burnet et al (1984). Recovery is presently uneconomical and thus is not practised on South African fly ashes to date.

This work has aimed to provide the basic chemical and mineralogical data necessary to assist in the development and promotion of PFA utilisation in South Africa. Ash from three of South Africa's largest power stations, Duvha, Lethabo and Matla, has been collected over the period 1987-1988 to determine the long-term variations in the chemical and mineralogical composition and particle size distribution of the ash. The mineralogy of the PFA was determined using a semi-quantitative X-ray diffraction method developed by the author. Bulk chemical composition was determined using X-ray fluorescence spectrometry. Compositions of the glass and ferrite spinel phases were determined by electron microprobe analysis.

Particle size distributions were determined with a Malvern Instruments Particle Sizer on FA in both dry and slurry form, with comparative results obtained for some samples with a Micromeritics Sedigraph.

CHAPTER 2

SAMPLES

2.1 CHOICE OF POWER STATION

The samples studied in this project were taken from three South African power stations, namely Lethabo, Matla and Duvha. PFA produced by these three stations was selected for study for the following reasons: The glass and calcium content is lower in Duvha PFA and higher in Matla PFA than in most other South African fly ashes (Lesch and Cornell 1987; Willis 1987); and Lethabo coal is ground to a finer size than normal, has the highest ash content of all South African power stations, and seven sequential electrostatic precipitator fields are used where Duvha and Matla use four. Matla and Lethabo were visited during February 1987 to gain a working knowledge of power station operating conditions.

Each power station has been built adjacent to the colliery which supplies all the coal used in that station. Only in exceptional instances is coal brought in from other collieries. Fig. 2.1 shows the location of the three power stations.

2.2 SAMPLE COLLECTION

A diagrammatic representation of a typical power station studied in this project, and on which the sampling sites have been indicated, is shown in Fig. 2.2. Sample collection was kindly undertaken by the power station staff under the supervision of Dr. Richard Kruger, then of the CSIR, over a period of 2 years. Samples were taken at regular intervals from the precipitator fields, and occasionally from mixed ash and bottom ash. Details of the samples and date of sampling are listed in Table 2.1.

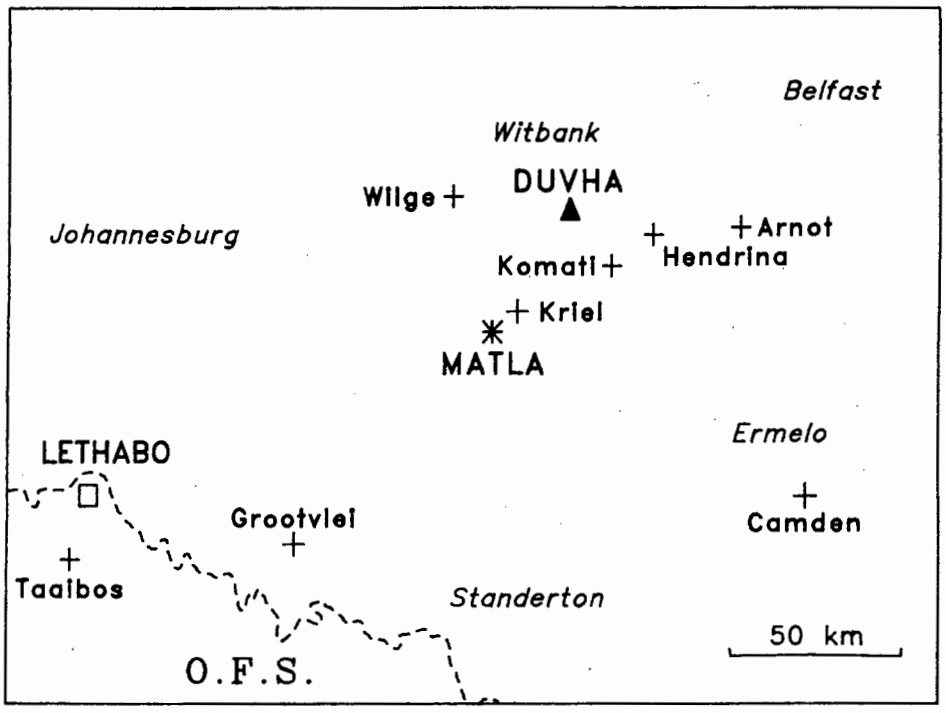

Fig. 2.1 : Location of power stations and collieries.

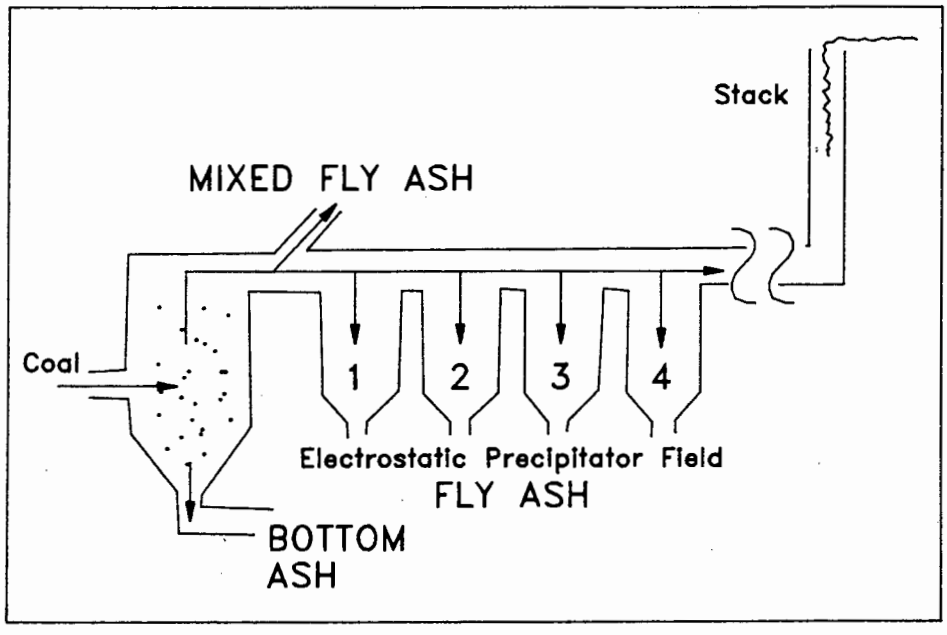

Fig. 2.2 : Diagram representing the sampling sites in the power stations studied. In the case of Lethabo there are 7 precipitator fields.

Table 2.1 : List of sample labels, type of sample, field and date of collection for Lethabo, Matla and Duvha samples, and for unclassified samples.

Lethabo				Matla				Duvha				Unknown			
Label	Type	Field	Date	Label	Type	Field	Date	Label	Type	Field	Date	Label	Type	Field	Date
L1_PF	pf		Feb 87	M4_PF	pf		Jan 88	D1_PFA1	fa	1	Jun 87	D2_COAL	coal		Aug 87
TH8_16	coal		Feb 87					D1_PFA2	comp		Jun 87	D2_PFA1	fa	1	Aug 87
TH8_17	coal		Feb 87	M2_PF	pf		Mar 88	D1_PFA3	fa	2	Jun 87	D2_PFA2	fa	2	Aug 87
L1_BA	bot		Feb 87	M2_PFA1	fa	1	Mar 88	D1_PFA4	fa	3	Jun 87	D2_PFA3	fa	3	Aug 87
L1_MA	mix		Feb 87	M2_PFA2	fa	2	Mar 88	D1_PFA5	fa	4	Jun 87	D2_PFA4	fa	4	Aug 87
L1_PFA1	fa	1	Feb 87	M2_PFA3	fa	3	Mar 88								
L1_PFA2	fa	2	Feb 87	M2_PFA4	fa	4	Mar 88	D4_PF	pf		Mar 88	D3_COAL	coal		Oct 87
L1_PFA3	fa	3	Feb 87					D4_PFA1	fa	1	Mar 88	D3_COMP	comp		Oct 87
L1_PFA4	fa	4	Feb 87	M5_COAL	coal		Jun 88	D4_PFA2	fa	2	Mar 88	D3_PFA1	fa	1	Oct 87
L1_PFA5	fa	5	Feb 87	M5_PFA1	fa	1	Jun 88	D4_PFA3	fa	3	Mar 88	D3_PFA2	fa	2	Oct 87
L2_PFA5	fa	5	Feb 87	M5_PFA2	fa	2	Jun 88	D4_PFA4	fa	4	Mar 88	D3_PFA3	fa	3	Oct 87
L2_PFA6	fa	6	Feb 87	M5_PFA3	fa	3	Jun 88					D3_PFA4	fa	4	Oct 87
L1_PFA7	fa	7	Feb 87	M5_PFA4	fa	4	Jun 88	D5_COAL	coal		Jun 88				
								D5_PFA1	fa	1	Jun 88				
L3_PF	pf		Mar 88	M6_PF	pf		Sep 88	D5_PFA2	fa	2	Jun 88				
L3_PFA1	fa	1	Mar 88	M6_LH1	fa	1	Sep 88	D5_PFA3	fa	3	Jun 88				
L3_PFA2	fa	2	Mar 88	M6_LH2	fa	2	Sep 88	D5_PFA4	fa	4	Jun 88				
L3_PFA3	fa	3	Mar 88	M6_LH3	fa	3	Sep 88								
L3_PFA4	fa	4	Mar 88	M6_LH4	fa	4	Sep 88	D6_PF	pf		Sep 88				
				M6_RH1	fa	1	Sep 88	D6_PFA1	fa	1	Sep 88				
L4_PF	pf		Jun 88	M6_RH2	fa	2	Sep 88	D6_PFA2	fa	1	Sep 88				
L4_PFA1	fa	1	Jun 88	M6_RH3	fa	3	Sep 88	D6_PFA3	fa	1	Sep 88				
L4_PFA2	fa	2	Jun 88	M6_RH4	fa	4	Sep 88	D6_PFA4	fa	1	Sep 88				
L4_PFA3	fa	3	Jun 88												
L4_PFA4	fa	4	Jun 88												
L5_PF	pf		Sep 88												
L5_PFA1	fa	1	Sep 88												
L5_PFA2	fa	2	Sep 88												
L5_PFA3	fa	3	Sep 88												
L5_PFA4	fa	4	Sep 88												

pf = pulverised fuel
coal = coal received as chips
bot = bottom ash
mix = mixed ash
fa = fly ash
comp = composite ash

CHAPTER 3

ANALYTICAL METHODS (I)

QUANTITATIVE MINERALOGY

3.1 INTRODUCTION

Mineral concentrations in the PFA samples were determined by Quantitative X-Ray Diffraction (QXRD). The theoretical and practical aspects of X-Ray diffraction are well known and are covered by Klug and Alexander (1974). The technique is ideally suited to the quantification of mineral phases in complex samples having small grain size.

The theoretical basis for all QXRD methods is that the intensity of a particular Bragg reflection is proportional to the concentration of the phase which produced it. The basis for QXRD was first proposed by Hull (1919), but no further work was done until Clark and Reynolds (1936) determined the concentration of quartz in mine dust, making use of an internal standard to correct for absorption effects. Since then, many attempts at QXRD have been made, and various methods have been developed to reduce the causes of error in quantitative analysis.

3.2 CAUSES OF ERROR

There are various causes of error in QXRD which are related to the sample and which can be minimised by using appropriate procedures. These are:

3.2.1 Particle and Crystallite Size

Particle size and crystallite size are important factors effecting the accuracy of QXRD measurements. Particle size refers to the grain size of the powdered state, and crystallite size refers to the size of the individual domains which diffract the X-rays coherently (Tatlock 1966). Parrish and Huang (1983) have shown that the reproducibility of the diffracted beam

intensity is equal to that expected by the counting error only when the crystallite size is less than 5μm. Jenkins et al (1988) state that the most reproducible XRD traces are obtained when the crystallite size is less than 10μm and preferably about 1μm. When the crystallite size is less than 0.2μm the very small crystallites cause peak broadening.

3.2.2 Orientation Effects

Orientation effects are extremely important in all XRD work, but play a minor role in this study, as there are no free oriented particles in the PFA. Mullite, which has an acicular morphology and would thus be oriented in the sample holder, occurs as crystallites within glass spheres (Lesch and Cornell 1987). The association of glass and mullite was noted in optical work undertaken in this study. The powdered glass grains are irregular in shape and thus are not oriented in the holder.

3.2.3 Absorption Effects

Absorption effects in the sample are of two types: macroabsorption and microabsorption. Macroabsorption is the absorption of both the incident and the diffracted X-ray beam by the sample, and is a function of the bulk chemical composition of the sample. The result is a reduction in the intensity of all the diffraction peaks by a constant factor for each sample. The use of an internal standard automatically corrects for macroabsorption effects.

When the X-ray beam is diffracted by a component in the mixture it is then passing preferentially through that component rather than the bulk sample (Clark and Preston 1974). This leads to microabsorption, which is a function of both the particle size and the difference in the mass absorption coefficient of the components from that of the bulk sample (Brindley 1945). The effect is minimised by keeping the particle size of the components as small as possible (Klug and Alexander 1974; Jenkins et al 1988).

3.2.4 Extinction Effects

Primary extinction occurs in a perfect crystal when incoming X-ray photons are reflected off the underside of atomic planes in the crystal and travel back toward the incident beam. This results in a decreased intensity of the incoming beam. Natural crystals are not perfect however and approximate the mosaic type of structure. Different areas in the crystal diffract incoming X-rays at slightly different positions and the intensity of the X-ray beam travelling against the incident beam is thus reduced compared with a perfect crystal. This is known as secondary extinction and its effect is less than that of primary extinction. Secondary extinction

does not occur in fine particles less than 0.1-0.01mm in diameter (Klug and Alexander 1974), and is thus reduced by effective grinding of the sample.

3.3 QUANTITATIVE METHODS

There are various methods employed in QXRD as discussed below.

3.3.1 Internal Standard Method

A fixed quantity of an internal standard is added to both samples and standards. The analyte concentration is found either with the use of calibration curves or by the Reference Intensity Ratio (RIR) method (Klug and Alexander 1974; Chung 1974). Both methods have the advantage of automatically correcting for macroabsorption, but not for microabsorption, of the X-ray beam by the sample. Klug and Alexander (1974) consider the internal standard method to be the most reliable procedure for large numbers of samples, or when the composition of the samples varies greatly.

3.3.2 Direct Method

This method compares the intensity of the analyte peak to the intensity of the same peak in a pure standard (Klug and Alexander 1974; Lennox 1957; Leroux et al 1953). A correction is made for differences in the mass absorption coefficient of the sample and the standard where these are different. This method is not recommended by Klug and Alexander (1974) for multi-component systems.

3.3.3 Spiking Method

The spiking (or doping) method was applied to QXRD by Copeland and Bragg (1958). In this method the unknown containing the analyte phase is spiked by the addition of aliquots containing the phase of interest. The concentration of the analyte in the original sample is calculated from the change in intensity ratio of the analyte peak and a peak of any naturally occurring second phase. This method is most useful for samples which contain relatively small amounts of the analyte (Alexander 1977).

3.3.4 Dilution Method

This method employs the dilution of the unknown by addition of another phase (preferably amorphous) and was developed for QXRD by Clark and Preston (1974). The method has the

advantage of not requiring mass absorption measurements of the sample and of automatically compensating for microabsorption effects. A major limitation of the method is an increase in the minimum detectable concentration of the analyte due to the reduction in intensity of the diffracted beam.

3.3.5 Standardless Method

A method developed by Zevin (1977) is noteworthy in that no standards are used. In order to determine 'n' phases in a sample, a sample set consisting of 'n' samples must be analysed, and 'n' linear equations must be satisfied. A limitation of the method is that the error greatly increases when different samples contain similar concentrations of a particular phase.

3.3.6 This Work

For this work the internal standard method has been used to determine the quantitative mineralogy as it eliminates the effects of macroabsorption, is accurate over a wide range of concentrations and is appropriate where a large number of samples are to be analysed.

3.4 MATHEMATICAL BASIS FOR THE INTERNAL STANDARD METHOD

The mathematical basis for the method was developed by Alexander and Klug (1948). Assuming that extinction, microabsorption and preferred orientation were negligible, they showed that for a flat sample of infinite thickness the integrated intensity 'I' of diffraction peak 'i' of component J is given by:

$$I_{iJ} = \frac{K_{iJ}.x_J}{\rho_J[x_J(\mu_J-\mu_M)+\mu_M]} \qquad (3.1)$$

K_{iJ} = constant

x_J = weight fraction of the analyte

ρ_J = density of the analyte

μ_J = mass absorption coefficient of the analyte

μ_M = mass absorption coefficient of the matrix

Equation (3.1) can be rewritten as:

$$I_{iJ} = \frac{K_{iJ}.x_J}{\rho_J.\mu} \qquad (3.2)$$

μ = mass absorption coefficient of the specimen

If a constant weight fraction of an internal standard is added, then

$$x_J = k' \times \left(\frac{I_{iJ}}{I_{kS}} \right) \qquad (3.3)$$

k' = constant

I_{kS} = intensity of reflection k of the internal standard

3.5 INSTRUMENTAL OPERATING CONDITIONS

All QXRD data were obtained with a Philips PW1130/90 X-ray diffractometer housed in the Department of Geology, University of Cape Town and operated at the following settings, unless otherwise stated:

Cu K_α radiation
45 kV, 40 mA
divergence slit: 1°
pre-slit (fixed): 2mm
receiving slit: 1°
anti-scatter slit: none
curved graphite crystal monochromator
PHS set to pass 95% pulse amplitude peak
Scintillation counter

3.6 SAMPLE PREPARATION

Samples, interference standards and standards were mixed by hand in an agate pestle-and-mortar, and were then ground for 2 hours in an automatic agate pestle-and-mortar to ensure

a fine grain size.

3.7 CHOICE OF THE INTERNAL STANDARD

Some internal standards mentioned in the literature for QXRD are Al_2O_3 (corundum), CaF_2 (calcium fluoride), TiO_2 (rutile) and others. The internal standard chosen for this work needed to satisfy the following criteria:

1. There should be no, or at least very few, peak overlaps caused by the internal standard on the selected analyte peaks.
2. The linear absorption coefficient of the internal standard must as far as possible be close to that of the standards, the analyte and the unknowns (McCarthy et al 1981). This will limit microabsorption effects.
3. The internal standard must be stable under normal operating conditions, including sample preparation, and must be capable of being ground to a fine grain size (-10μm).

The internal standard selected for use in this project was laboratory grade Silicon manufactured by BDH Chemicals Ltd (Poole, England). A concentration of 5% silicon in all standards and samples was used so as to minimise the dilution factor.

3.8 PEAK HEIGHT vs PEAK AREA

Analyte peak intensities were measured using integrated peak areas rather than peak heights. Peak area is considered to be more reproducible than peak height for varying degrees of crystallinity and solid solution of a single phase (Bayliss 1986; McCarthy et al 1981), and compensates for the reduced height and increased width of peaks produced by crystallites with a size below approximately 0.1μm (Alexander and Klug 1974). In PFA many of the crystallite sizes will be very small ($< 1\mu$m).

3.9 INTERFERENCE STANDARDS

Interference standards are preferably pure specimens of the phases of interest, and are used to determine, and to estimate correction factors for, peak overlap problems. They should meet the same requirements as standards, namely that they should be similar in all possible ways to the same phase in the unknown (Bayliss 1986; McCarthy et al 1981). This includes thermal history, degree of crystallinity, solid solution, and particle and crystallite size. It has not always been possible to meet the requirement that interference standards duplicate the same phase in the sample in all possible ways. Analyte peaks of the interference standards were scanned at 1/8°2θ per minute, and backgrounds were counted for 400 seconds each. The following is a list of the interference standards used.

3.9.1 Silicon

The silicon interference standard was prepared from the silicon used for the internal standard.

3.9.2 Quartz

The quartz interference standard was natural quartz available in the Geochemistry Department, UCT.

3.9.3 Mullite

Mullite is an important phase in PFA due to its high aluminium content. It was thus particularly important that the mullite used in the interference standards and in the standards should be representative of the mullite found in PFA. Mullite prepared by different methods can have different RIR ratios (McCarthy and Thedchanamoorthy 1989). The mullite interference standard used here was prepared from Lethabo PFA from which the carbon had been removed by heating overnight to 800°C, and from which the magnetic phases had been extracted with the aid of a powerful electromagnet, with the PFA dispersed in acetone. This separation was repeated until the magnetic phases were no longer detectable on an X-ray diffractogram. The aluminosilicate fraction remaining was then ground in an automatic pestle-and-mortar to a fine grain size, prior to the removal of the glass phase with a 1% HF solution (Hussein and Gad 1966).

HF leaches were initially left for periods of 1, 2, 3, 4, 6, 16 and 65 hours to determine the optimum leaching time to remove all the glass. The only mineral phases remaining after

leaching were quartz and mullite. Comparison of the backgrounds for these leachates indicates that there is no further reduction in the glass bulge after approximately 16 hours leaching (Fig. 3.1). The advantage of this method is that the mullite used for the interference standards is the same as that found in the samples. This was not considered a pure interference standard as it comprised a mixture of quartz and mullite.

3.9.4 Spinel

The spinel interference standard was prepared from Duvha PFA by extracting the iron-rich phases using the electromagnetic method described for mullite. Duvha PFA was selected due to its high iron and low glass content (data from Lesch and Cornell 1987, and Willis 1987) as this would assist in extracting fewer contaminating phases along with the oxide. This also was not a pure interference standard as hematite was extracted with the spinel.

3.9.5 Hematite

The hematite interference standard was laboratory grade Fe_2O_3 manufactured by BDH Chemicals.

3.9.6 Lime

The lime interference standard was prepared from CaO heated at 850°C overnight to convert any portlandite and calcite present to lime. To prevent the lime altering back to portlandite and calcite after heating, the material was allowed to cool in a vacuum desiccator and was stored under vacuum in the presence of silica gel (to absorb moisture) and a large amount of CaO (to absorb CO_2).

3.9.7 Portlandite

The portlandite interference standard was prepared by mixing an aliquot of the lime interference standard with distilled water and allowing it to hydrate. The portlandite formed in this way was then dried at 110°C and immediately removed to a vacuum desiccator in the presence of CaO to prevent alteration to calcite.

3.9.8 Calcite

The calcite interference standard was prepared from natural calcite.

3.9.9 Glass

The glass interference standard was prepared from finely crushed bottle glass. The position of the glass bulge maximum is not constant, and is known to be dependent on the CaO

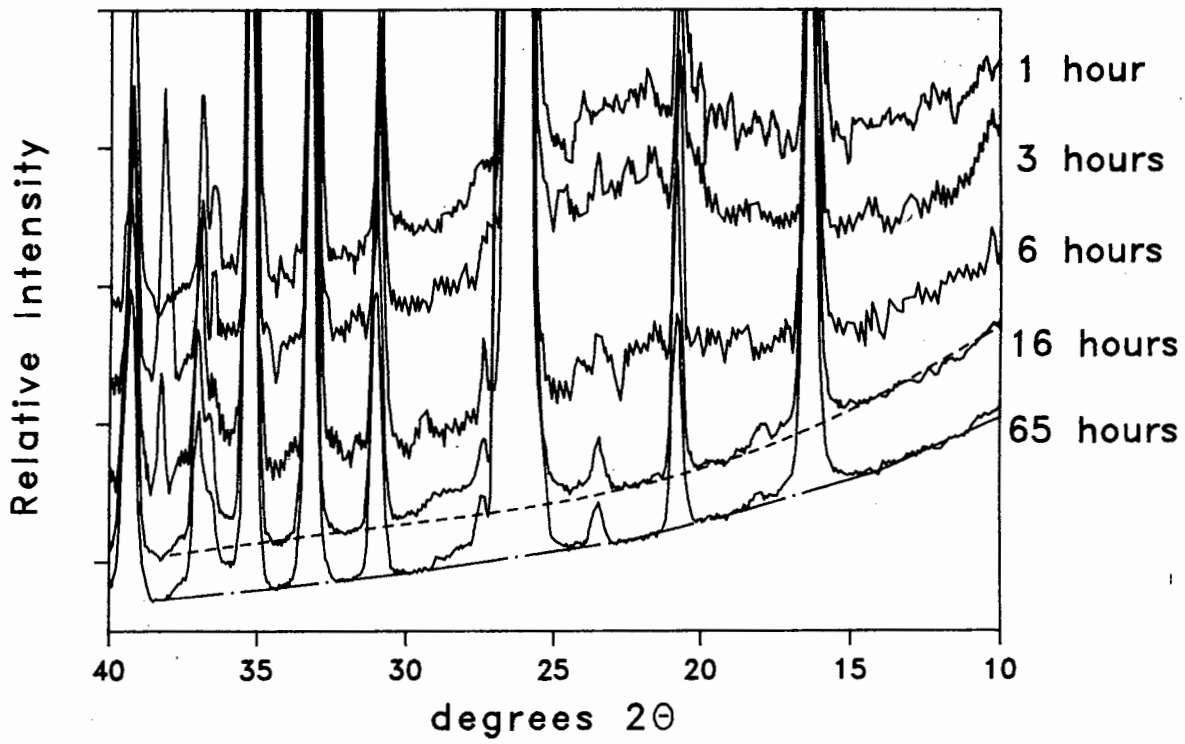

Fig. 3.1 : The effect of various leaching times on removal of the glass bulge with a 1% HF acid leach. The diffractograms have been positioned vertically above each other for clarity.

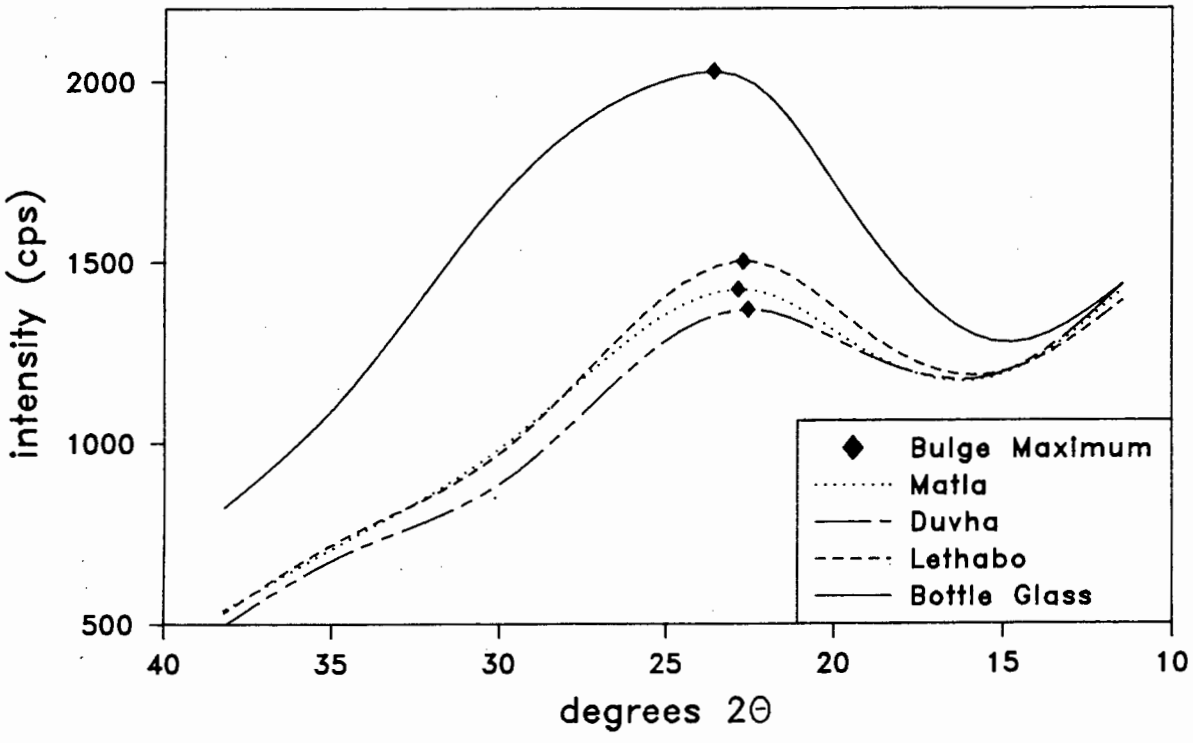

Fig. 3.2 : Relative positions of the glass bulge maxima for glass from Lethabo, Duvha and Matla, and for the bottle glass used for the interference standards.

concentration of the glass (Lesch 1987; Diamond 1983; McCarthy 1988). Fig. 3.2 shows the minor differences in the positions of the glass bulge maxima for samples from Lethabo, Duvha and Matla power stations compared with the bottle glass. The bottle glass bulge maximum and shape are similar to those of the PFA glass.

3.10 CHOICE OF ANALYTE PEAK AND BACKGROUND POSITIONS

One analyte peak from each phase was selected, and had to meet the following criteria:

1. The nett analyte peak should be a large component of the gross counts collected over the angular window, i.e. contributions to the gross counts from background or overlapping peaks should be as small as possible.
2. It should be possible to accurately calculate the background below the peak.

Background positions were chosen so as to minimise peak interference (Fig. 3.3).

The mineral phases found in Matla and Duvha PFA are well known and have been described by Lesch and Cornell (1987). Lethabo has only recently become operative, but X-ray diffractograms of the ash showed no new phases to be present. Figs 3.3 and 3.4 show overlays of the interference standards for all major and minor phases found in South African PFA, as well as the background positions used for the samples and the standards, and the angular range over which the detector was scanned for the selected analyte peaks. These are summarised in Appendix 1.

3.11 BACKGROUND CALCULATION

Corrections for background below the peak can be dealt with in several ways. Klug and Alexander (1974), and McCarthy and Thedchanamoorthy (1989) consider that a straight line approximation between two backgrounds measured on either side of the analyte peak is sufficiently accurate. This method over-estimates the background intensity on a concave background, and under-estimates the intensity on a convex background. Both background shapes are found in the PFA samples (due to the presence of the glass bulge). Only concave

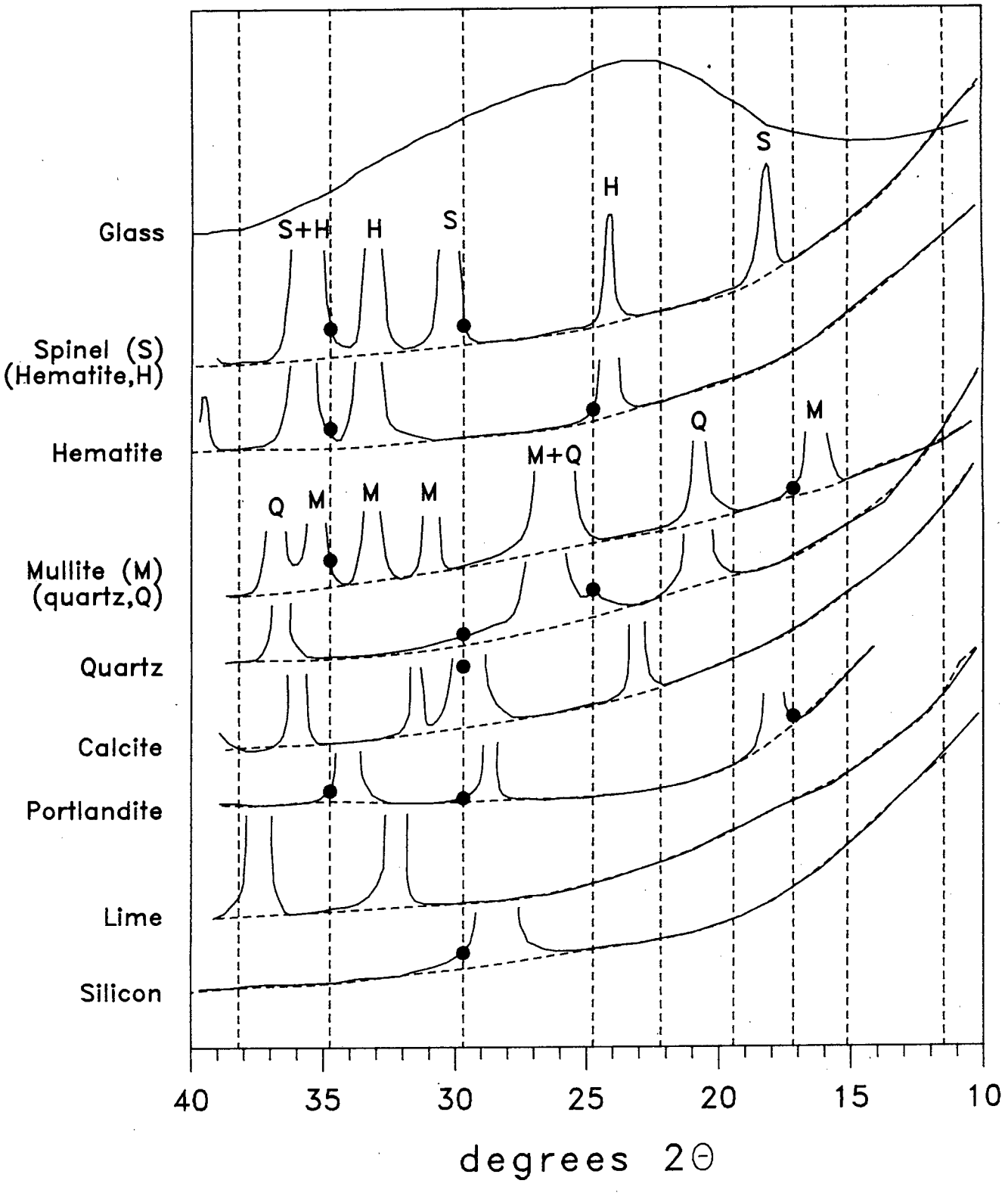

Fig. 3.3 : Vertically staggered overlay of the interference standards used to determine background positions (vertical dashed lines). A solid dot indicates interference at that position.

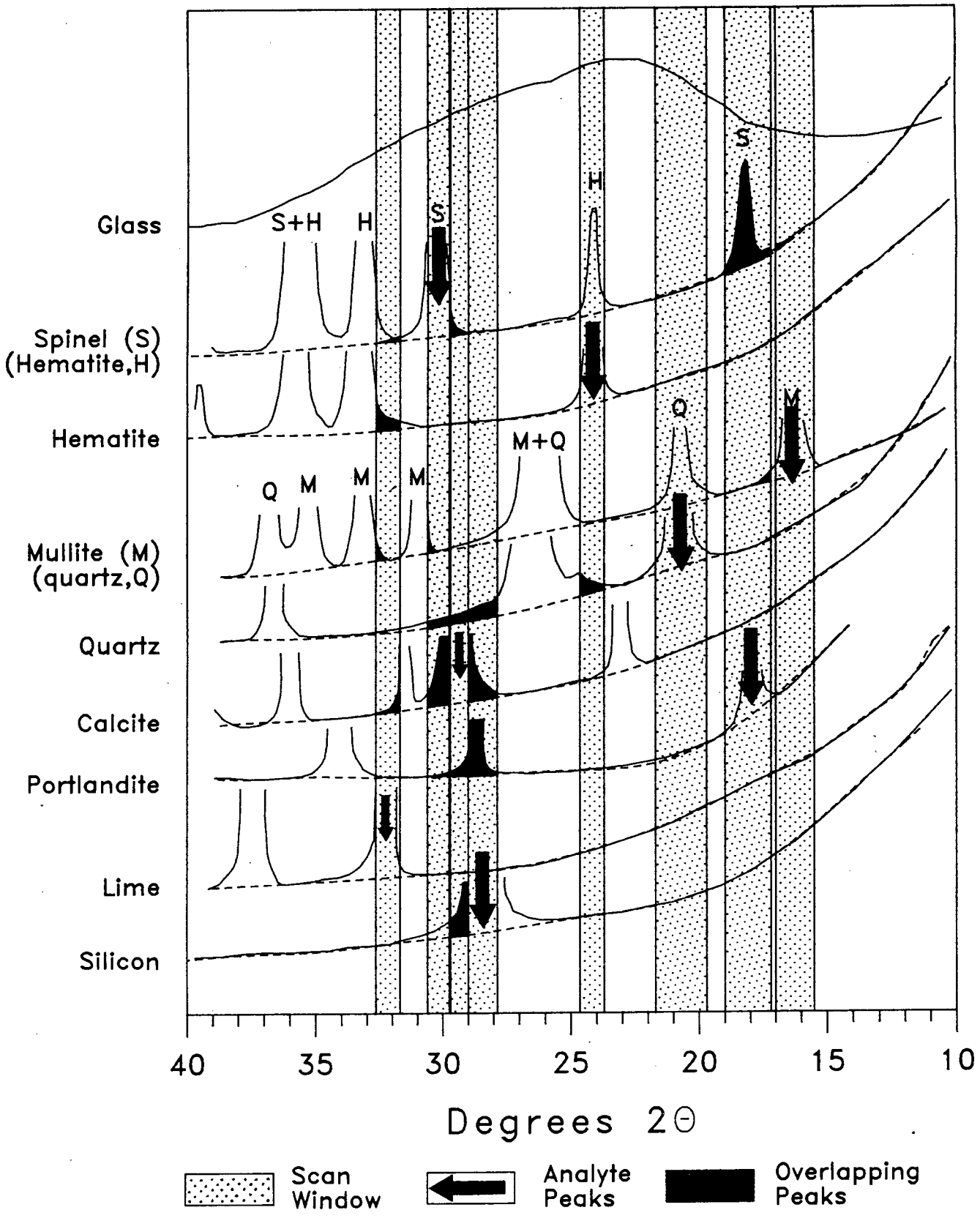

Fig. 3.4 : Vertically staggered overlay of the interference standards used to determine the 2θ ranges over which the analyte peaks were counted.

shapes are present in those standards which contain no glass. In order to be consistent in both the standards and the samples, and to minimise errors, the background below each peak was calculated from the best fit quadratic equation passed through three adjacent backgrounds. Background positions used for the samples and the standards are listed in Appendix 2(a). These backgrounds were chosen close to the analyte peak, and included the peak within their angular range. The area of the background within a peak window was then calculated using the equation:

$$B_p = \frac{\int_{2\theta_{min}}^{2\theta_{max}} Q}{2\theta_{max}-2\theta_{min}} \qquad (3.4)$$

B_p = background area below peak (in counts)
Q = quadratic equation through the background
$2\theta_{min}$ = start of analyte detection window
$2\theta_{max}$ = end of analyte detection window

Division by the denominator $2\theta_{max}-2\theta_{min}$ (the angular range) is necessary to convert the calculated units of area (degrees 2θ x counts) to the measured units of area (counts).

3.12 GLASS AREA CALCULATION

Lesch (1987) attempted to relate the area of the glass bulge to the glass concentration using standards prepared from window glass, but could not match the measured concentrations in the unknowns with concentrations found by difference. This work also attempted to relate the area of the glass bulge to glass concentration, using the method outlined below.

In order to calculate the area of the glass bulge, it was necessary to first estimate the background below the bulge. Fig. 3.5 shows that the degree of curvature of the mullite-quartz background is not as pronounced as that of pure quartz, and that the mullite-quartz background has a higher intensity than the quartz background. The intensity difference between the mullite-quartz and quartz backgrounds was assumed to be proportional to the mullite concentration. Thus for any position 'p':

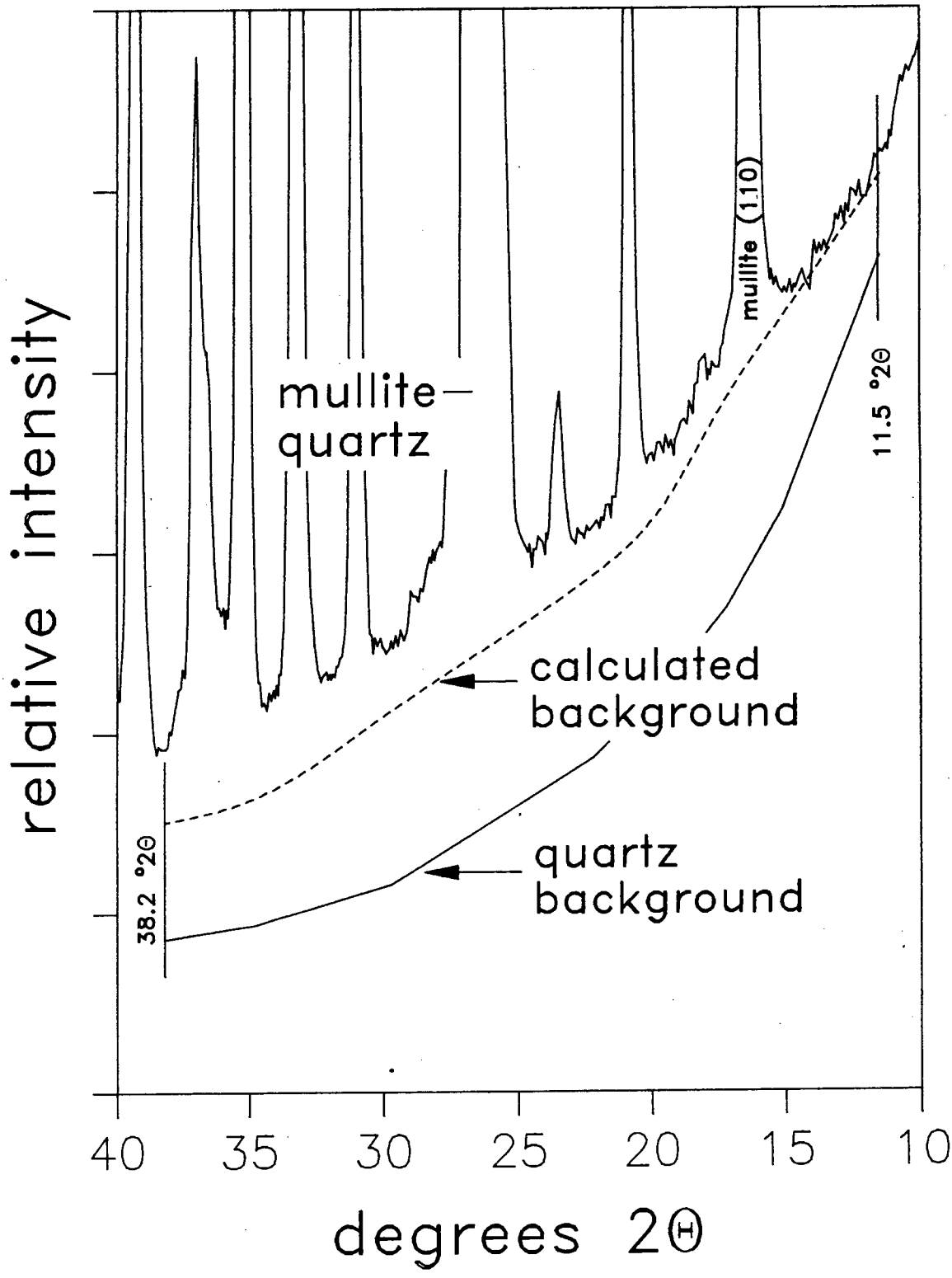

Fig. 3.5 : Diffractograms of the mullite/quartz and quartz interference standards indicating the elevation of the background due to the presence of mullite, and the more pronounced curvature of the quartz background.

$$MFAC_p = \frac{B^p_{mullite} - B^p_{quartz}}{MUL(110)} \qquad (3.5)$$

$MFAC_p$ = correction factor at position 'p' for the raised background due to mullite
$B^p_{mullite}$ = background intensity at position 'p' measured with the mullite interference standard
B^p_{quartz} = background intensity at position 'p' measured with the quartz interference standard
MUL(110) = nett intensity in the MUL(110) analytical window

A list of MFAC values is included in Appendix 1. The effect of other mineral species, e. g. spinel, hematite, lime and portlandite, was ignored due to the relatively low concentrations of these minerals. In the glass standards and the samples, the calculated background below the glass bulge becomes:

$$B^p_{glass} = B^p_{quartz} + \left[MFAC_p \times MUL(110)\right] \qquad (3.6)$$

B^p_{glass} = intensity of background below the glass bulge at position 'p'

In order to calculate the area of the glass bulge, the 2θ range covered by the bulge (approximately 12-38°2θ) was divided into 6 domains:
11.50-17.19, 17.19-19.45, 19.45-22.20, 22.20-24.75, 24.75-34.75 and 34.75-38.20°2θ. Quadratic equations were calculated in each domain for the measured background through the bulge, and for the corrected background below the bulge. The domain limits which gave the best fit quadratic equations were determined by trial and error using the glass interference standard. Each calculated area was divided by the 2θ range to convert the calculated units of area (degrees 2θ x counts) to the measured units of area (counts). The domain limits and backgrounds used to calculate the quadratic equations in each domain are listed in Appendix 2(b). The total area of the bulge is the sum of the areas of the individual domains:

$$A_p = \sum_{i=I}^{VI} \left\{ \frac{\int_{2\theta_{min}}^{2\theta_{max}} Q_{glass} - \int_{2\theta_{min}}^{2\theta_{max}} Q_{bkg}}{2\theta_{max} - 2\theta_{min}} \right\} \qquad (3.7)$$

A_p = area below peak in counts
Q_{glass} = quadratic equation passed through glass bulge

Q_{bkg} = quadratic equation passed through background below glass

3.13 ERRORS

Statistics and figure of merit (FOM) calculations have been used to determine the choice of sample holder, certain of the operating conditions, and the counting times. Percentage standard deviation was calculated from the following equations (Bertin 1975):

$$SD_b(\%) = \frac{100}{\sqrt{cps_b \times t_b}} \tag{3.8}$$

$SD_b(\%)$ = percentage standard deviation of the background counts
cps_b = count rate on background
t_b = time on background

$$SD_p(\%) = \frac{\sqrt{\frac{cps_p}{t_p} + \frac{cps_b}{t_b}}}{cps_p - cps_b} \times 100 \tag{3.9}$$

$SD_p(\%)$ = percentage standard deviation of the nett peak
cps_p = count rate on gross peak
t_p = time on peak

$$FOM = \sqrt{cps_p} - \sqrt{cps_b} \tag{3.10}$$

FOM = figure of merit for nett peak intensity

3.13.1 Choice of Sample Holder

The choice of optimum sample holder was determined after reloading a mixture of mullite and quartz (68.9% mullite, 29.8% quartz and 1.4% glass) into a variety of standard XRD holders. The holders tested were a back-loaded aluminium holder, a top-loaded perspex holder, and a rotating top-loaded holder. The results are listed in Table 3.1. The measured standard deviation is always greater than the value due to the counting error because of errors introduced by reloading the specimen. The standard deviations of the backgrounds from the back-loaded holder are closer to calculated values than those from the rotated top-

		Aluminium Holder Back-loaded n=4			Perspex Holder Top-loaded n=4			Rotated Holder Top-loaded n=4		
Position	time (secs)	SD(%) calc	meas	FOM	SD(%) calc	meas	FOM	SD(%) calc	meas	FOM
Background	400	.15	.65		.08	1.94		.15	1.24	
Background	400	.16	.69		.10	4.13		.16	1.37	
Background	400	.17	.80		.12	6.45		.18	1.34	
Background	400	.18	1.02		.15	6.39		.19	1.42	
Background	400	.19	.86		.18	4.52		.20	1.38	
Background	400	.23	2.53		.22	.91		.23	1.42	
Silicon(111)	552	.22	18.77	15.47	.21	23.32	14.79	.18	2.30	17.19
Mullite(110)	720	.31	1.74	8.49	.49	1.52	5.57	.28	1.62	9.57
Quartz(100)	480	.23	1.74	14.08	.28	2.31	11.50	.22	2.68	14.82
Mullite(110)/Silicon(111)			17.20			23.81			3.17	
Quartz(100)/Silicon(111)			17.30			26.32			5.21	

Table 3.1 : Total error for backgrounds, nett peaks and nett peak ratios, measured with three different sample holders for a sample consisting of 68.9% mullite, 29.8% quartz and 1.4% glass.

	Slit Sizes	
Position	divergence = 1° receiving = 1° FOM	divergence = 1/2° receiving = 1/2° FOM
Silicon(111)	14.0	7.2
Mullite(110)	4.5	2.1
Quartz(100)	16.0	7.0

Table 3.2 : Figures of Merit (FOM) for the same sample as in table 3.1 with 1°,1° and 1/2°,1/2° divergence and receiving slits, using a rotating top-loaded holder.

		Counting Error n=10		Reloading Error (calculated)	Total Error n=8
Position	time (secs)	SD(%) calc	meas	SD(%) calc	SD(%) meas
Background	400	.56	.70	2.47	2.57
Background	400	.64	.76	1.63	1.80
Background	400	.64	3.89	-	3.07
Background	400	.87	.88	1.63	1.85
Background	400	.81	1.08	1.74	2.05
Background	400	.76	1.48	1.46	2.08
Silicon(111)	552	.64	.99	3.22	3.37
Mullite(110)	720	.73	.71	3.01	3.09
Quartz(100)	960	2.06	2.34	2.71	3.58
Mullite(110)/Silicon(111)			2.33	4.93	5.45
Quartz(100)/Silicon(111)			3.08	3.25	4.48

Table 3.3 : Counting, reloading and total error for backgrounds, nett peaks, and nett peak ratios, in a sample containing 12.2% quartz, 86.1% mullite and 1.7% glass, measured with the rotating top-loaded holder.

loaded holder. Results from the top-loaded perspex holder are in very poor agreement compared with calculated values.

Figures of merit were determined for silicon (111), mullite (110) and quartz (100). Silicon showed no appreciable difference in FOM between the different holders. Mullite and quartz both have low FOM values in the top-loaded perspex holder. There was no appreciable difference in the standard deviations of quartz and mullite for the different holders. The standard deviation of the nett silicon intensity however was unacceptably high in both the back-loaded holder and the top-loaded perspex holder (18.8 and 23.3% respectively), but was acceptable in the rotated top-loaded holder (2.3%). This large standard deviation for the stationary holders is probably due either to an inhomogeneous distribution of silicon in the sample, or to preferred orientation effects. The rotating holder seemed to compensate for this heterogeneity. The variation of the nett silicon intensity resulted in large standard deviations of the mullite/silicon and quartz/silicon ratios for all except the rotating holder.

The rotating top-loaded holder gave the most reproducible silicon intensities, as well as acceptable standard deviations on the mullite and quartz nett intensities and on background measurements, and was thus selected as the standard holder for all the QXRD work done for this project.

3.13.2 Choice of Slit Sizes

Table 3.2 lists the FOM values found for a rotating top-loaded holder with divergent and receiving slits of 1/2°,1/2° and 1°,1° respectively. The pre-slit was fixed at 2mm and there was no anti-scatter slit. FOM values for the 1°,1° slits are approximately twice those of the 1/2°,1/2° slits, and thus these slit sizes were selected for the analytical work. The 1°,1° slits have a slightly poorer resolution than the 1/2°,1/2° slits, which results in greater peak overlap. This has been corrected for by overlap correction factors.

3.13.3 Counting and Particle-Induced Errors

Counting errors due only to the variation in intensity of the diffracted X-ray beam were determined from consecutive analyses without reloading the sample, and were not corrected for peak interference. Particle-induced effects such as preferred orientation, particle and crystallite size, and microabsorption thus remain constant in all measurements. Measured standard deviation should then be equal to the calculated standard deviation due to counting errors, if no other errors are present. The measured and calculated values for counting and total errors determined with the rotating top-loaded holder are listed in Table 3.3 and are shown graphically in Fig. 3.6. To determine the total error (counting error + error introduced by reloading the sample), the sample was reloaded before each analysis.

Measured and calculated counting errors are similar for both the background and the mineral phases. The total error is significantly greater than that due to counting errors, but does not exceed approximately 3.5% for nett peak intensities and 5.5% for peak/silicon ratios. The single unusually high value of 3.89 for the measured standard deviation of one of the backgrounds (counting error) was also high in the determination of total error. This may be due to interference from a mullite peak on the background position (34.75°2theta). The greatest contribution to the total error is from reloading the sample.

3.14 PEAK OVERLAP AND BACKGROUND INTERFERENCE

Peak overlap problems occur where a peak from one phase overlaps the analyte peak of another phase. This problem is exacerbated when peak areas are measured rather than peak heights. Background interference occurs when any peak overlaps a background position. These problems can sometimes be solved by choosing either a different background position

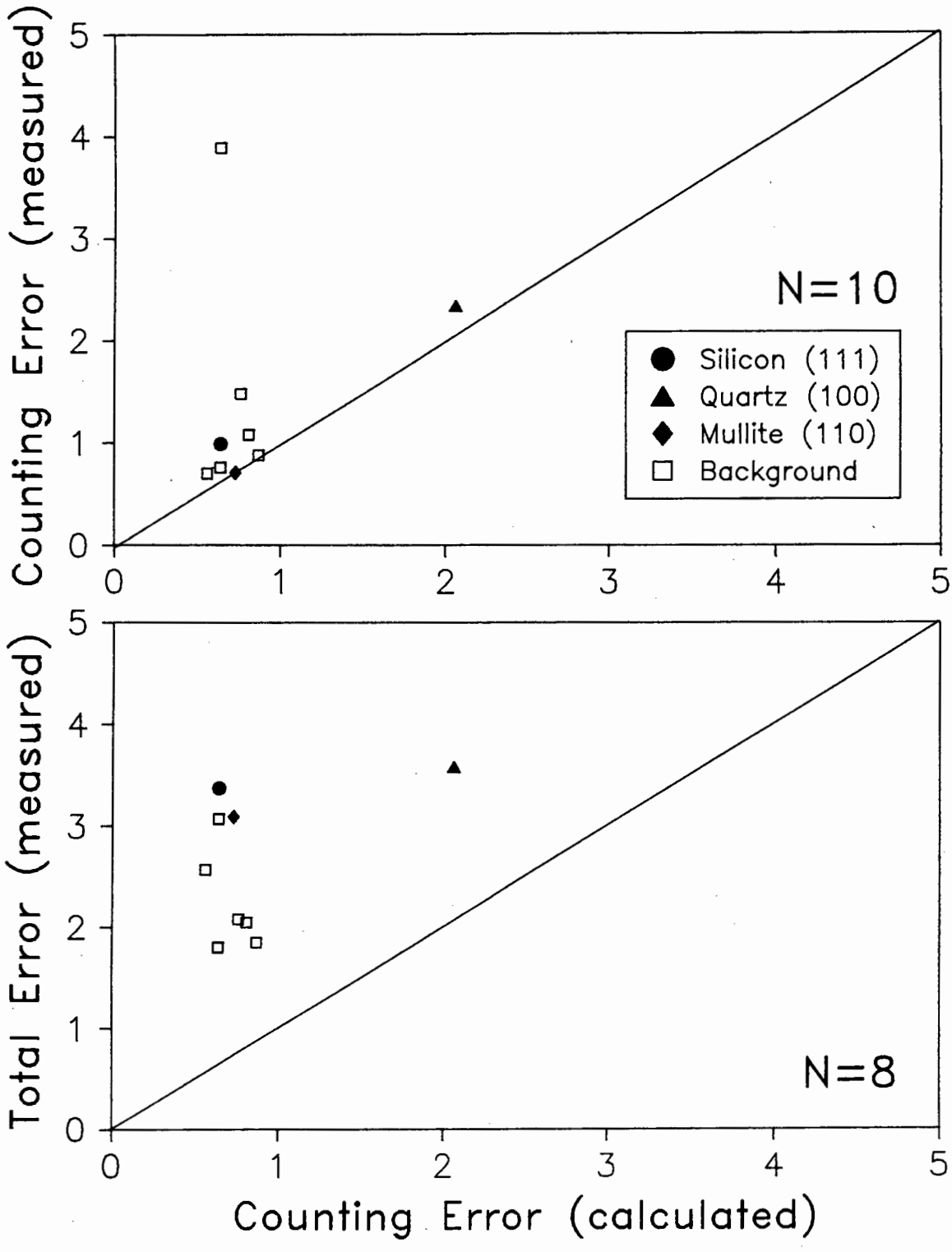

Fig. 3.6 : Comparison of calculated and measured counting statistics, and of the total error determined by reloading the same sample.

or selecting another peak of the analyte mineral. Peak on background interferences were determined by visually inspecting diffractograms of the interference standards for raised backgrounds due to peak tails (Fig. 3.3). Overlapping peaks were also determined from a visual inspection of the diffractograms and are shown graphically in Fig. 3.4.

3.14.1 Peak Overlap

Overlap must be corrected for by using correction factors determined with the interference standards.

Correction factors for overlap on peak positions were obtained in the following way: where the analyte peak for phase A and a peak of phase B both contribute to the nett intensity measured in the analytical window 'q' for phase A (Fig. 3.7), and where 'n' is an interference free peak in phase B, then from the interference standard for phase B,

$$PFAC^{A_q}_{B_m n} = \frac{I_{q_m B}}{I_{nB}} \tag{3.11}$$

$PFAC^{A_q}_{B_m n}$ = correction factor for overlap of nett peak 'm' of phase B on peak 'q' of phase A

$I_{q_m B}$ = nett intensity of peak 'm' of phase B in analyte window 'q'

I_{nB} = nett intensity of a peak 'n' of phase B that can also be measured in the unknown (the analyte peak)

In the sample, for the corrected nett peak intensity,

$$I_{qA} = I_{qA_o} - \left(I_{nB} \times PFAC^{A_q}_{B_m n}\right) \tag{3.12}$$

I_{qA} = corrected nett intensity of phase A in analyte window 'q'

I_{qA_o} = measured (uncorrected) nett intensity of phase A in analyte window 'q'

3.14.2 Background Interference

Correction factors for background interferences have been obtained in the following way: where peak 'm' of phase A overlaps background position 'b' (Fig. 3.8), then from the interference standard for phase A:

$$BFAC^{b}_{A_m n} = \frac{I_{b_m A}}{I_{nA}} \tag{3.13}$$

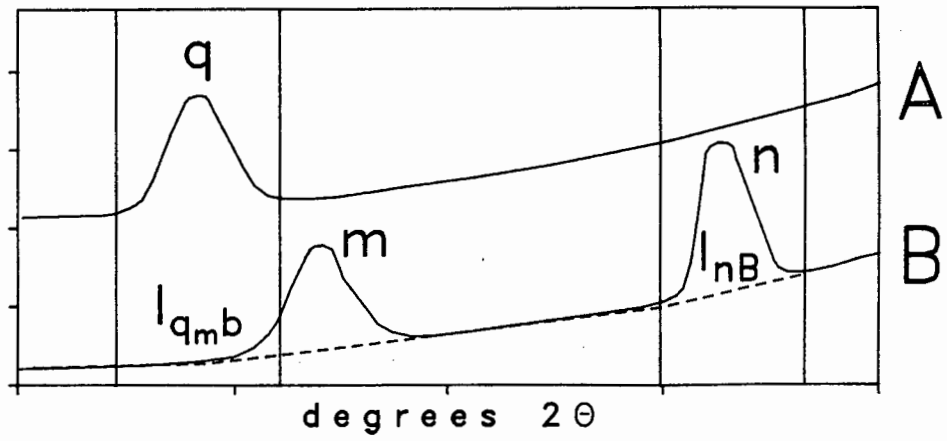

Fig. 3.7 : Peak positions and measurements used to determine the factor $PFAC^{Aq}_{B_m n}$.

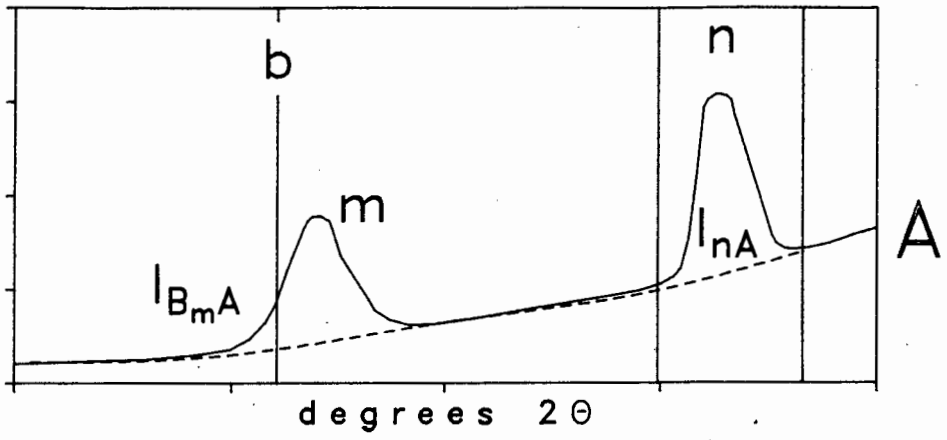

Fig. 3.8 : Peak and background positions and the intensities which must be measured to determine the factor $BFAC^{b}_{A_m n}$.

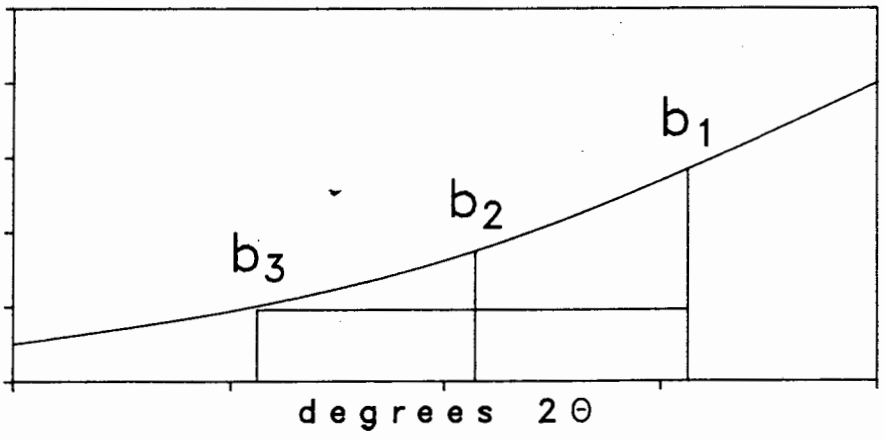

Fig. 3.9 : Background positions used to derive a factor for the direct calculation of intensity at position b_2.

$BFAC^{b}_{A_{m}n}$ = correction factor for interference from peak 'm' of phase A on background position 'b'

$I_{b_{m}A}$ = nett intensity of peak 'm' of phase A at background position 'b'

I_{nA} = nett intensity of a peak 'n' of phase A that can also be measured in the sample

then in the sample:

$$B = B_o - \left(I_{nA} \times BFAC^{b}_{A_{m}n}\right) \tag{3.14}$$

B = corrected intensity of background at position 'b'

B_o = measured (uncorrected intensity of background at position 'b'

3.14.3 Direct Background Calculation

Background intensities can also be calculated directly provided at least two adjacent backgrounds can be measured (Feather and Willis 1976). A background factor is calculated from a sample which has a similar background curvature to the unknown, but in which there is no background interference over the background of interest, i.e. a blank (Fig. 3.9). Quartz was frequently used in this respect. This method has been used to calculate the intensity of the background below the glass bulge from a quartz blank. The equation used to calculate the background factor from the blank (Willis 1989) is:

$$BFAC_{b_2} = \frac{I_{b_2} - I_{b_3}}{I_{b_1} - I_{b_3}} \tag{3.15}$$

$BFAC_{b_2}$ = background factor for direct calculation of background at position b_2

I_{b_1} = background intensity measured at position b_1

I_{b_2} = background intensity measured at position b_2

I_{b_3} = background intensity measured at position b_3

In the sample, the equation used to calculate the background intensity at position b_2 is then

$$I_{b_2} = \left[BFAC_{b_2} \times (I_{b_1} - I_{b_3})\right] + I_{b_3} \tag{3.16}$$

In theory, there is no limit to the number of corrections applied to any particular peak or background, as these can be corrected using the method of iteration. In practice, each correction increases the error of the final intensity, and thus corrections should be kept to a

minimum.

3.14.4 Correction Factor Measurements

Overlap and interference correction factors for silicon, quartz, mullite, hematite, portlandite and calcite were determined from the interference standards using the method described, and are listed in Appendix 1.

3.14.5 Corrections for Glass

The presence of the glass bulge causes the calculated background below some of the peaks to be consistently overestimated or underestimated. This error has been corrected by using factors found from the glass interference standard. The factors are listed in Appendix 1.

$$GFAC^{w} = \frac{I_{wG}}{Ag} \qquad (3.17)$$

$GFAC^{w}$ = correction factor for glass in window 'w'

I_{wG} = nett intensity measured in window 'w' with glass interference standard

Ag = total area of the glass bulge in counts

3.14.6 Correction Factors for Calcite and Portlandite

Lime and portlandite are unstable under normal atmospheric conditions. Lime alters to portlandite by absorbing moisture from the atmosphere, and within a few hours both lime and portlandite alter to calcite with the addition of CO_2 from the atmosphere. The alteration of portlandite to calcite is shown in Fig. 3.10 and the alteration of lime to both portlandite and calcite is shown in Fig. 3.11. Portlandite and calcite both interfere on (a) the background at 29.70°2θ and (b) the analyte peaks for silicon and lime (Figs 3.3 and 3.4). It was therefore necessary to correct for the contribution from calcite in the portlandite standards, and for portlandite and calcite in the lime standards.

Calcite produced from the alteration of portlandite has a broader peak shape than the natural calcite used to prepare the calcite interference standard (Fig. 3.12), and will thus have different correction factors. The peak broadening is probably attributable to the very small crystallite size of the alteration calcite.

The calcite and portlandite correction factors for the portlandite standards were determined using the changing calcite/portlandite ratio in the portlandite interference standard, and calcite and portlandite corrections for the lime standards were similarly determined from the

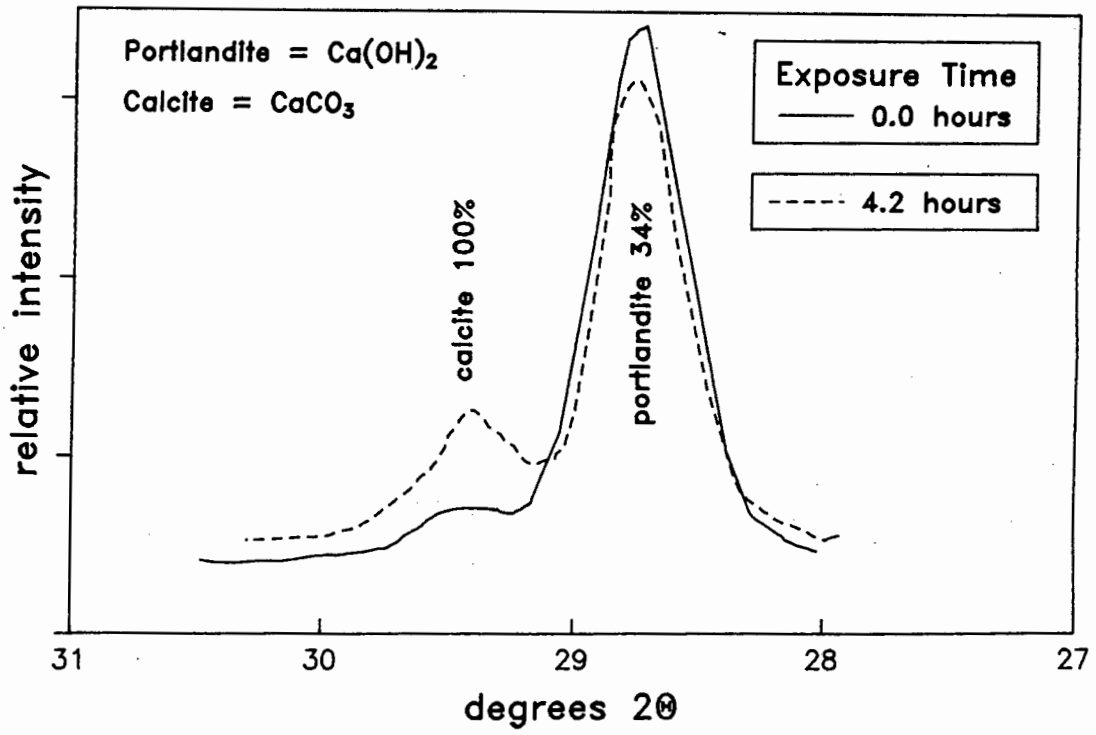

Fig. 3.10 : Diffractogram showing the alteration with time of portlandite to calcite on exposure to air. The percentage is the relative intensity of each peak compared with the strongest peak of that phase.

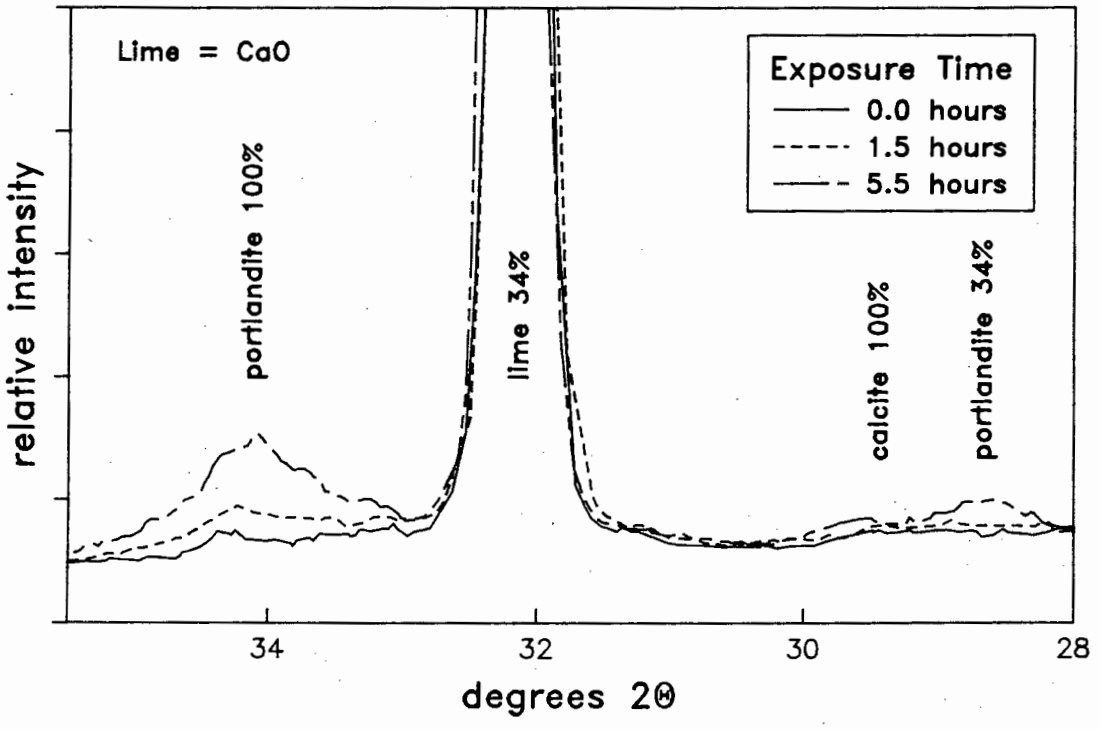

Fig. 3.11 : Diffractogram showing the alteration with time of lime to portlandite and calcite.

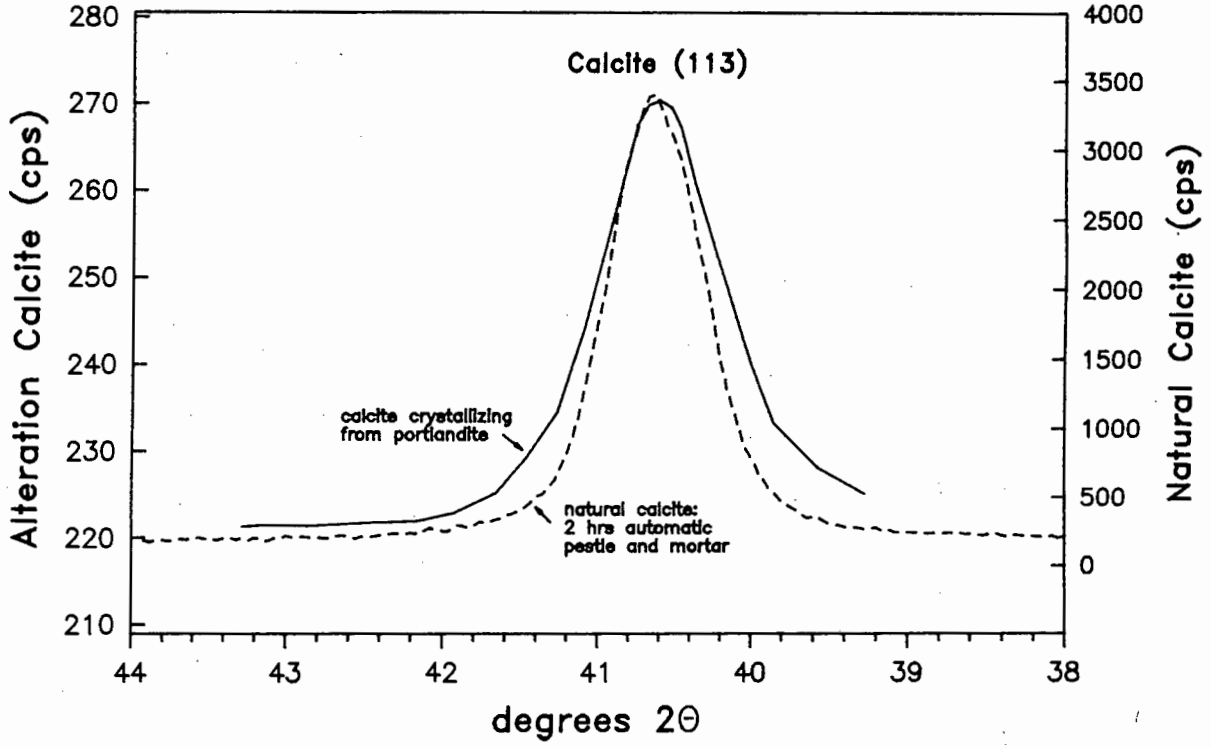

Fig. 3.12 : Comparison of the Calcite (113) peak shape for natural calcite and for calcite produced from the alteration of portlandite.

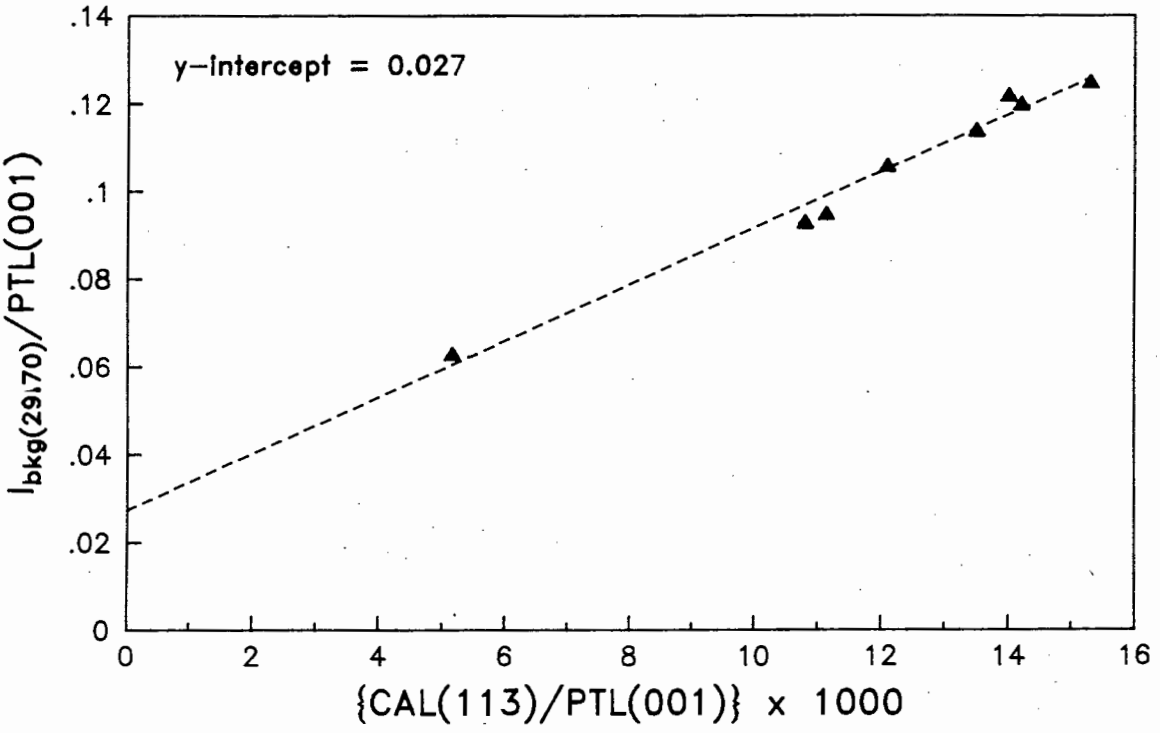

Fig. 3.13 : Determination of the background interference factor, $BFAC_{PTL(001)}^{bkg(29.70)}$, from the portlandite interference standard when calcite and portlandite both overlap on the background position.

lime interference standard. Calcite correction factors used for the calcite standards were determined from the calcite interference standard. These factors are listed in Appendix 1.

The portlandite interference standard was exposed to air over a period of time and allowed to alter to calcite, and the lime interference standard was similarly allowed to alter to calcite and portlandite. Analyte peak intensities were measured in the lime and portlandite interference standards as the reactions progressed. Each analysis is the result of normalising the background and peak intensities from two consecutive analyses to a particular time, assuming a linear drift in intensities. This was done so as to correct for any change in intensity during the course of an analysis.

In the discussion which follows, the following terminology is used:

$I_{p(hkl)}$ = the measured (uncorrected) intensity in the analyte window of phase p with Miller Index (hkl), e.g. cal(104)
P(HKL) = the corrected nett intensity in the analyte window of phase P with Miller Index (HKL), e.g. PTL(001) for portlandite (001)
$I_{bkg(b)}$ = the measured (uncorrected) background intensity at b°2θ, e.g. $I_{bkg(29.70)}$
$PFAC^{p(hkl)}_{A(HKL)}$ = correction factor for phase A overlapping analyte window p(hkl)
$BFAC^{bkg(b)}_{A(HKL)}$ = correction factor for phase A interfering on background at position b°2θ

3.14.6.1 Determination of Factors From the Portlandite Interference Standard:
The problem caused by calcite (CAL) and portlandite (PTL) interfering on the same positions was solved by mathematically removing the contribution from calcite, making use of the increasing calcite/portlandite ratio as calcite grew at the expense of portlandite. The correction factor for portlandite overlap in window 'p' ($PFAC^{p(hkl)}_{PTL(001)}$) , when calcite overlapped in the same window, was determined graphically by plotting the term ($I_{p(hkl)}$/PTL(001) against the term CAL(113)/PTL(001). The correction factor for portlandite interference on background at b°2θ ($BFAC^{bkg(b)}_{PTL(001)}$), when calcite interfered on the same background, was similarly determined by plotting the term $I_{bkg(b)}$/PTL(001) against the term CAL(113)/PTL(001). Calcite (113) was selected as this peak has no contribution from portlandite and thus $I_{calcite(113)}$ = 0 when the calcite concentration is zero. There is no overlap on PTL(001) from any other peak.

When there is no calcite in the sample the term CAL(113)/PTL(001) becomes zero and the intercept on the y-axis of the best fit linear regression through the data points was taken as the correction factors, $PFAC^{(hkl)}_{PTL(001)}$ and $BFAC^{bkg(b)}_{PTL(001)}$. Graphical determinations of these corrections are shown in Figs. 3.13-3.16.

Calcite and portlandite both overlap the silicon window and interfere on the background at 29.70°2θ. The correction factor for calcite on silicon and background (29.70°2θ) was calculated in the normal way after first correcting the nett intensities for the contribution from portlandite.

3.14.6.2 Determination of Factors from the Lime Interference Standard:
Correction factors for calcite and portlandite were also found from the lime interference standard using a modification of the method described above. These factors have been used for the lime standards as well as for the samples, as calcite and portlandite are alteration products of lime in both the unknowns and the interference standard. The steps involved in calculating the overlap and interference factors for portlandite and calcite in the lime interference standard are summarised below:

$PFAC^{cal(104)}_{PTL(001)}$ was calculated for each analysis using the following method. The term $I_{cal(104)}$/PTL(001) was plotted on the y-axis, and the term CAL(113)/PTL(001) was plotted on the x-axis, where $I_{cal(104)}$ has contributions from both calcite and portlandite. This plot is shown in Fig. 3.17. The y-intercept of the tangent to the curve at the position of the data points is taken as the factor, $PFAC^{cal(104)}_{PTL(001)}$, at that time. This factor changes from approximately 0.2 at t = 0 hours, to 0.048 after 24.25 hours. This reduction in $PFAC^{cal(104)}_{PTL(001)}$ with time is to be expected if the initial portlandite microcrystallites were small enough (< 0.2μm) so as to cause peak broadening. Data from the portlandite interference standard are also plotted on Fig. 3.17. These two data sets define very different trends, but have similar values for $PFAC^{cal(104)}_{PTL(001)}$.

CAL(104) was then corrected for interference from portlandite for each analysis by applying the following equation:

$$CAL(104) = I_{cal(104)} - \left[PFAC^{cal(104)}_{PTL(001)} \times PTL(001)\right] \qquad (3.18)$$

CAL(104) = corrected nett intensity of calcite (104) in the CAL(104) analytical window
$I_{cal(104)}$ = measured nett intensity in the Calcite (104) window
$PFAC^{cal(104)}_{PTL(001)}$ = correction factor for overlap from portlandite in the CAL(104) window

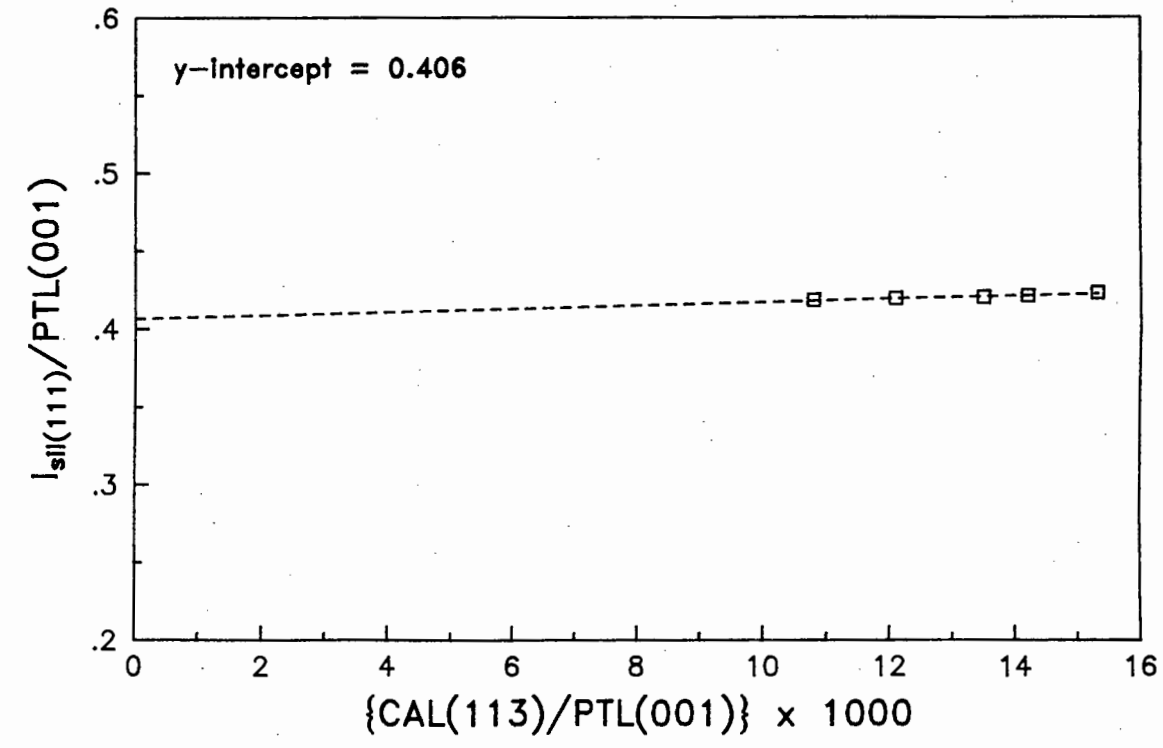

Fig. 3.14 : Determination of the peak overlap factor, $PFAC^{sil(111)}_{PTL(001)}$, from the portlandite interference standard when calcite and portlandite both overlap in the Silicon (111) analytical window.

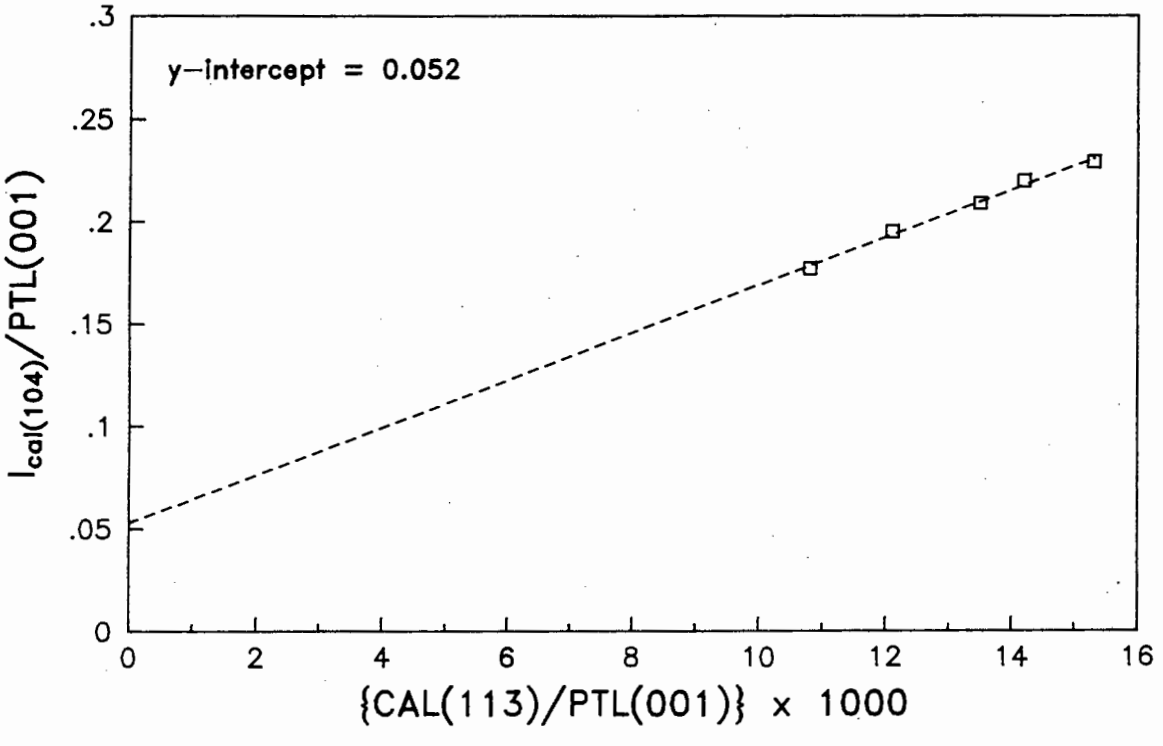

Fig. 3.15 : Determination of the peak overlap factor, $PFAC^{cal(104)}_{PTL(001)}$, from the portlandite interference standard when calcite and portlandite both overlap in the Calcite (104) analytical window.

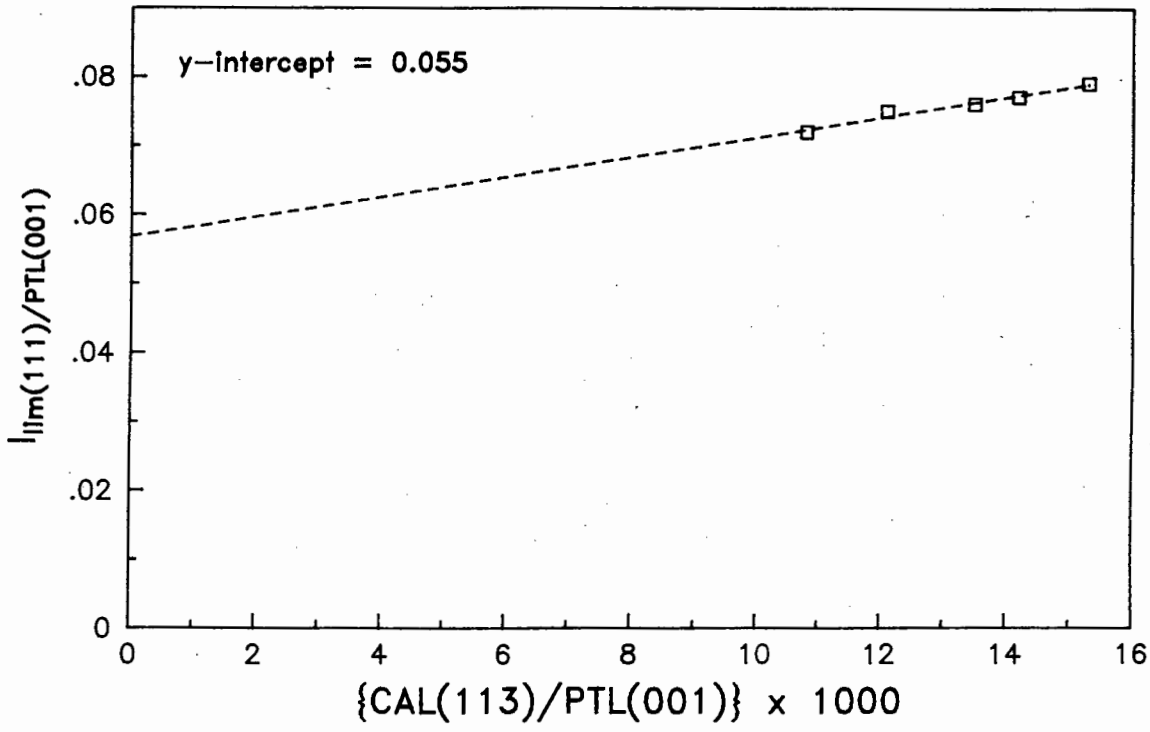

Fig. 3.16 : Determination of the peak overlap factor, $PFAC^{lim(111)}_{PTL(001)}$, from the portlandite interference standard when calcite and portlandite both overlap in the Lime (111) analytical window.

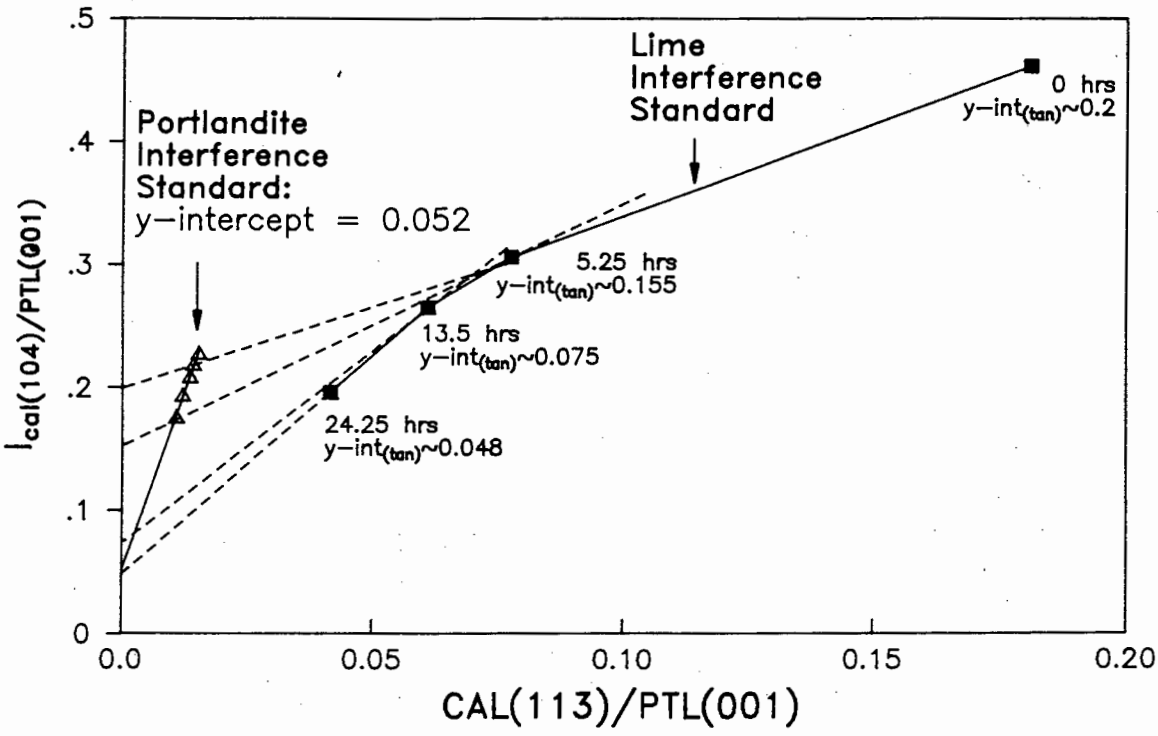

Fig. 3.17 : Determination of the peak overlap factor, $PFAC^{cal(104)}_{PTL(001)}$, from the lime interference standard as lime alters to portlandite and calcite.

PTL(001) = nett intensity of portlandite (001)

The background at 29.7°2θ has interference from both portlandite and calcite. $BFAC^{bkg(29.70)}_{PTL(001)}$ is the intercept on the y-axis of the best fit linear regression through the data points plotted on the graph in Fig. 3.18 using the reasoning described above. Similarly, $BFAC^{bkg(29.70)}_{CAL(104)}$ is the intercept on the y-axis of the linear regression shown in Fig. 3.19.

Portlandite and calcite both interfere on the lime (LIM(111)) scan window. To calculate $PFAC^{lim(111)}_{CAL(104)}$, the term $I_{lim(111)}$/CAL(104) has been plotted against [LIM(200)+PTL(001)]/CAL(104) (Fig. 3.20), where LIM(200) has no contributions from calcite or portlandite. As the calcite concentration approaches 100%, the term [LIM(200)+PTL(001)]/CAL(104) approaches 0. $PFAC^{lim(111)}_{CAL(104)}$ for an equilibrium condition is taken as the y-intercept of the curve when x=0, which was estimated by passing a straight line through points 6 and 7 in Fig. 3.20.

Similarly, $PFAC^{lim(111)}_{PTL(001)}$ was calculated from the graph shown in Fig. 3.21. Data point 7 appears to be a spurious data point as it lies off the trend defined by points 1 to 6, and the straight line was thus projected through points 5 and 6.

$PFAC^{sil(111)}_{CAL(104)}$ was calculated from the data shown in Fig. 3.22, which removes the contribution from portlandite. Points 1-5 represent the situation where portlandite is increasing at a greater rate than calcite. Points 5-7 represent the reverse situation, i.e. where calcite is increasing at the expense of portlandite. The latter trend is defined by a straight line indicating that the shape of the calcite peak has reached equilibrium. A linear regression curve passed through data points 5-7 has a y-intercept equal to $PFAC^{sil(111)}_{CAL(104)}$.

$PFAC^{sil(111)}_{PTL(001)}$ was calculated from the data shown in Fig. 3.23, which removes the contribution from calcite. Points 5, 6 and 7 represent an equilibrium condition. The mean $I_{sil(111)}$/PTL(001) value for these three points was taken as $PFAC^{sil(111)}_{PTL(001)}$.

3.15 COMPUTER PROGRAM

A computer program (XRDGLASS) was written (in FORTRAN 77 on an HP9000/823S) to process the intensity data received from the X-ray diffractometer and to perform the extensive overlap and interference corrections required. Information such as peak and background

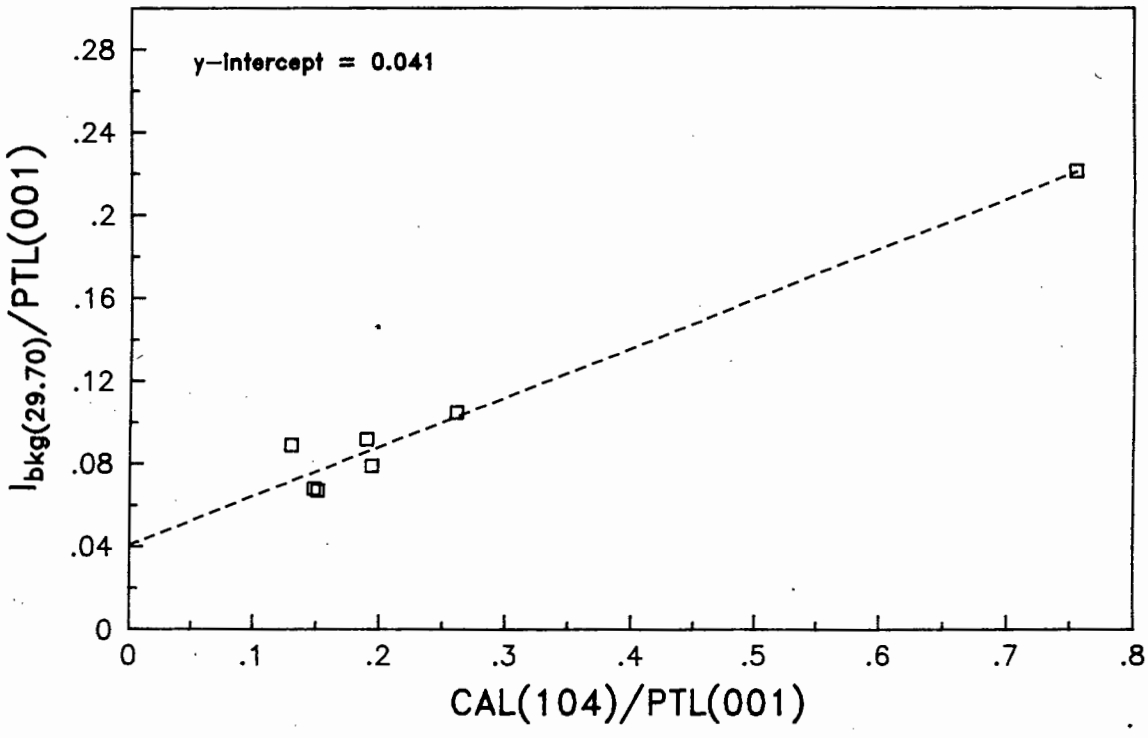

Fig. 3.18 : Determination of the background interference factor, $BFAC^{bkg(29.70)}_{PTL(001)}$, from the lime interference standard when calcite and portlandite both interfere on the background at 29.70°2θ.

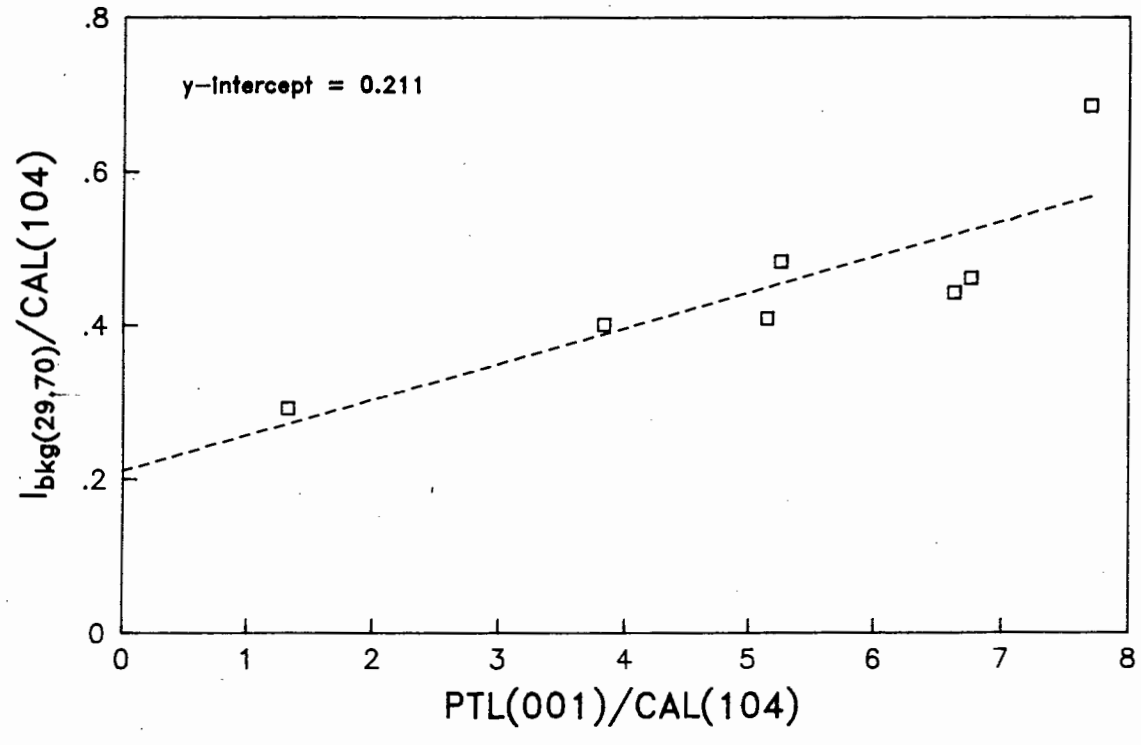

Fig. 3.19 : Determination of the background interference factor, $BFAC^{bkg(29.70)}_{CAL(104)}$, from the lime interference standard when calcite and portlandite both interfere on the background at 29.70°2θ.

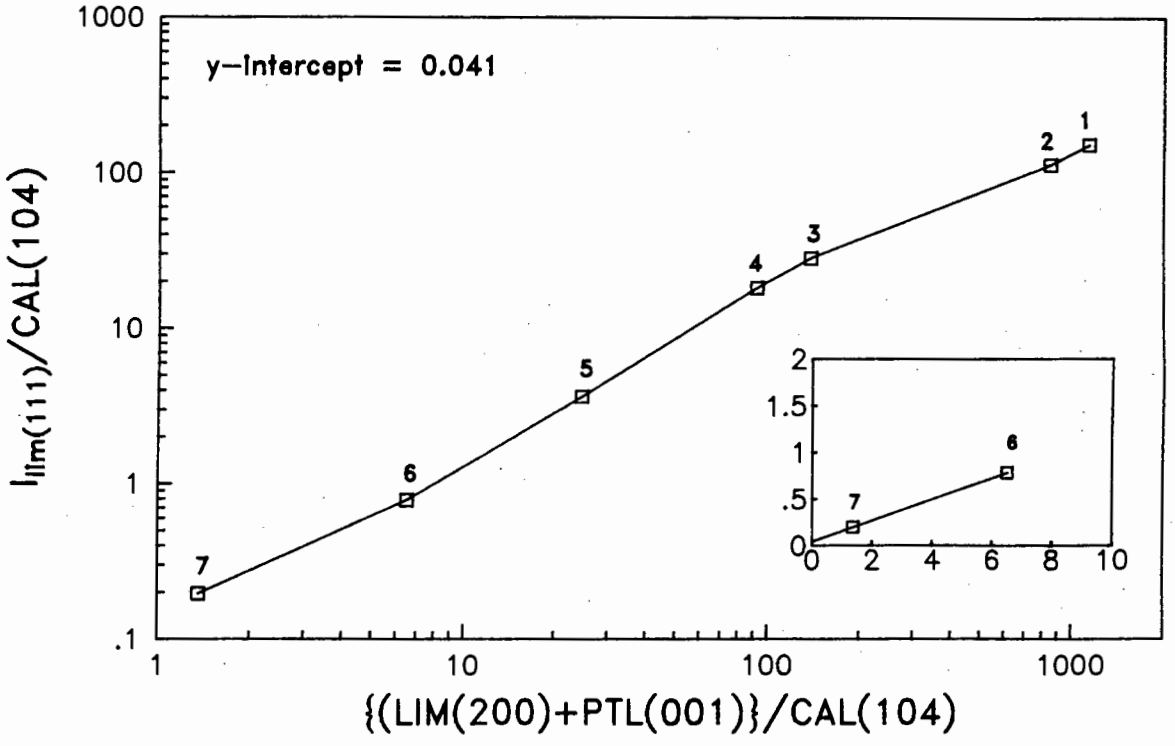

Fig. 3.20 : Determination of the peak overlap factor, $PFAC^{lim(111)}_{CAL(104)}$, from the lime interference standard when calcite and portlandite both overlap on the Lime (111) analytical window. CAL(104) has been corrected for overlap.

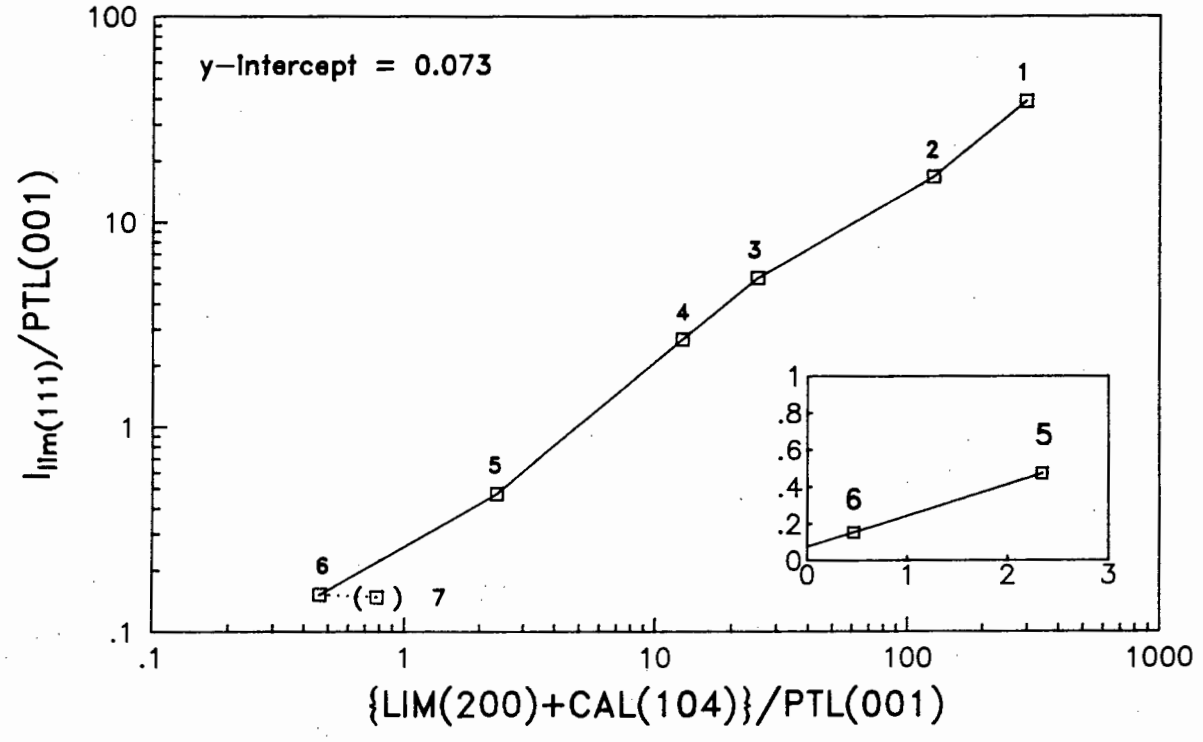

Fig. 3.21 : Determination of the peak overlap factor, $PFAC^{lim(111)}_{PTL(001)}$, from the lime interference standard when calcite and portlandite both overlap in the Lime (111) analytical window. Data point 7 is an outlier and has been excluded from the calculation.

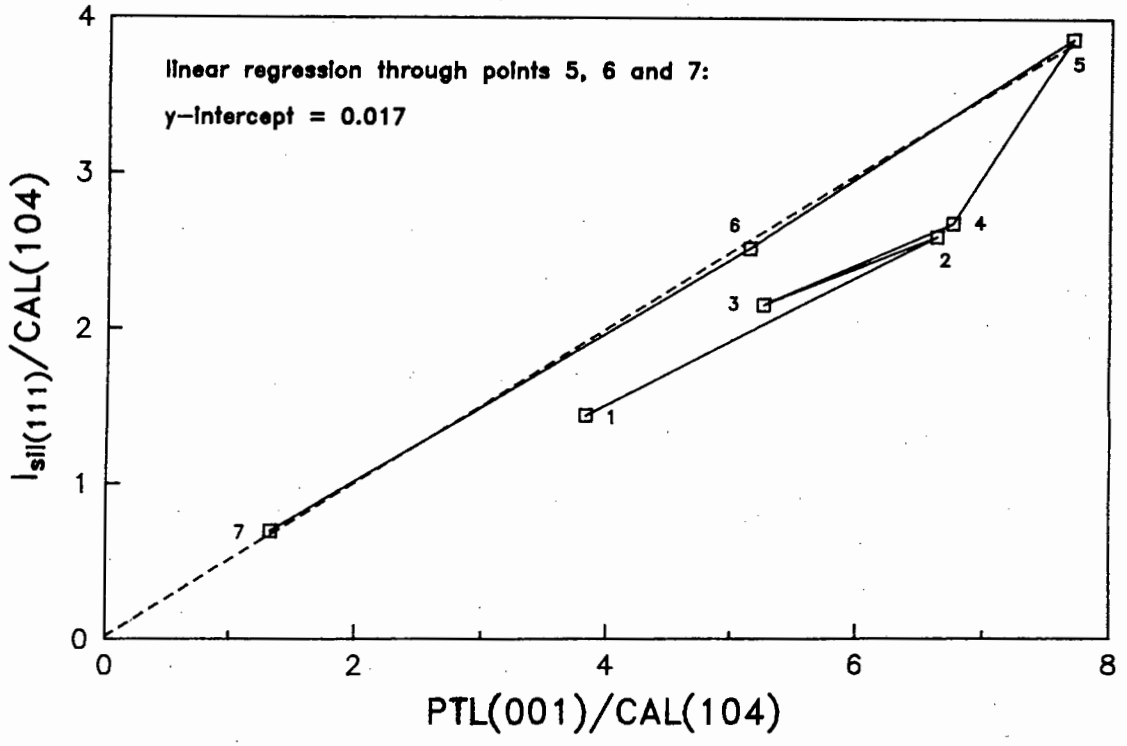

Fig. 3.22 : Determination of the peak overlap factor, $PFAC^{sil(111)}_{CAL(104)}$, from the lime interference standard when calcite and portlandite both overlap on the Silicon (111) analytical window. CAL(104) has been corrected for overlap.

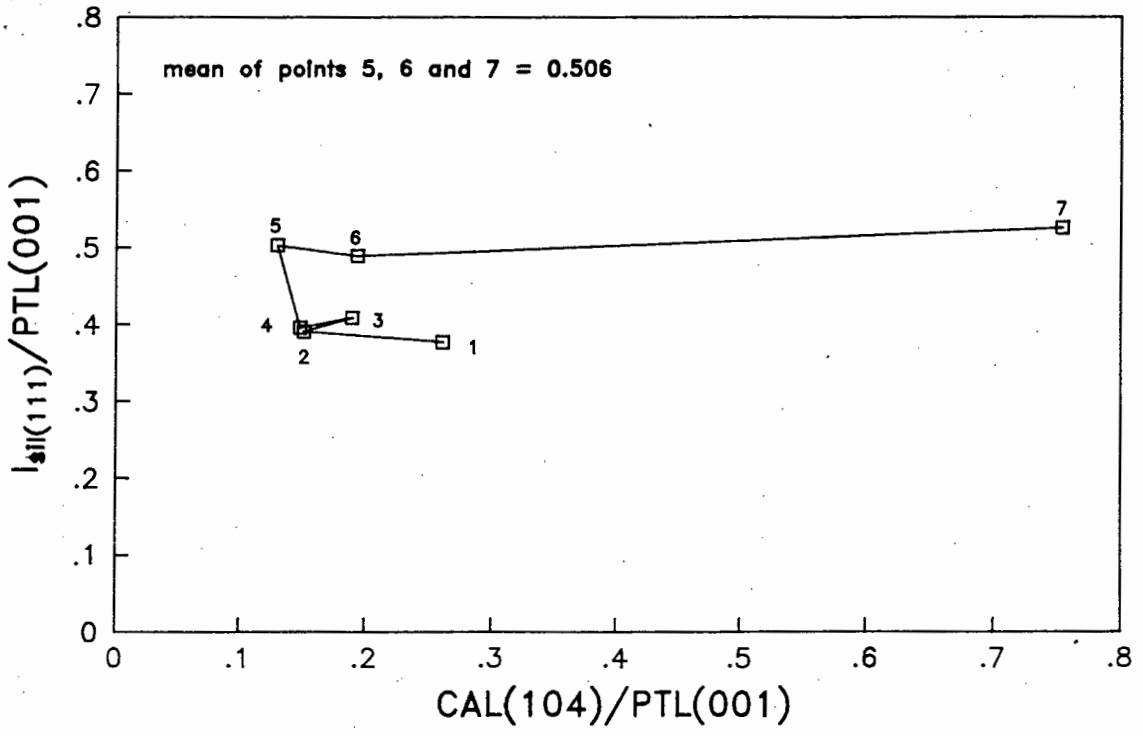

Fig. 3.23 : Determination of the peak overlap factor, $PFAC^{sil(111)}_{PTL(001)}$, from the lime interference standard when calcite and portlandite both overlap on the Silicon (111) analytical window. CAL(104) has been corrected for overlap.

names, interference and overlap factors, and the backgrounds used to calculate each of the quadratic equations, were stored in a parameter file. Intensity data were stored in a separate file. Appendices 3(a) and 3(b) contain examples of these file types. The program steps are listed in Appendix 3(c). Examples of the output data files are included in Appendices 3(d) and 3(e). An example of the printout is included in Appendix 3(f).

The program performs the following steps:

1. Read data.
2. Convert all intensities to counts per second.
3. Calculate background area below each peak using the best-fit quadratic equation passed through three adjacent backgrounds.
4. Uncorrected nett peak = gross peak - background below peak
5. Corrected nett peak = uncorrected nett peak - contributions from overlapping peaks - contribution from glass
6. Corrected background intensity = measured background intensity - contributions from interfering peaks
7. Background below glass bulge = background due to quartz + background due to mullite
8. Calculate the area of the glass in each domain and sum these to calculate the total glass area.
9. Steps 3-8 are repeated until each corrected nett peak calculated in step 5 remains constant.
10. Calculate the counting error for each peak and background and write data to file and print the data. Corrected background intensity and position data are written to a separate file readable by the graph program GRAFIT (Graphicus, Inc.) to provide a visual check of the background corrections.

3.16 STANDARDS

The standards used to construct the calibration curves were prepared from the same material as the interference standards. Standards have a concentration range equal to or greater than that expected in the PFA (data taken from Willis 1987, and Lesch and Cornell 1987). A minimum of three points was used to determine the slope of each calibration curve, which was

calculated from the best fit linear regression through zero and the data points. Analyte peaks were scanned at 1/8°2θ per minute and backgrounds were counted for 400 seconds each. Calibration curve slopes for the standards are included in Appendix 1. Data for the standards are listed in Appendix 4.

Where standards were prepared from mixtures spiked with aliquots of the pure standard material, the following equation was used to calculate the concentration of the standard material in the unspiked mixture (Bertin 1975)

$$C = \frac{\frac{I_o}{I_1} \times C_s}{1 - \left(\frac{I_o}{I_1} \times C_o \right)} \qquad (3.19)$$

C = concentration of the analyte in the unspiked mixture

C_s = concentration of standard in spiked mixture

C_o = concentration of starting material in spiked mixture

I_o = nett intensity of analyte peak in unspiked mixture

I_1 = nett intensity of analyte peak in spiked mixture

3.16.1 Glass

The glass standard was prepared from Duvha FA spiked with the crushed bottle glass used for the interference standard, and diluted with quartz. Duvha FA was chosen as this had the lowest glass concentration of all South African produced FA (Lesch and Cornell 1987). The glass concentration of 43.3% in the undiluted interference standard was determined using equation (3.19). The concentration of glass in each standard was then calculated. The glass calibration curve is shown in Fig. 3.24.

3.16.2 Quartz

The quartz calibration curve was prepared from two sets of quartz standard data.

i. 5, 15 and 25% quartz was added to glass.

ii. The mullite interference standard consisting of mullite and quartz was spiked with the addition of 40, 60 and 80% quartz. The quartz concentration of 22.2% in the undiluted interference standard was calculated using equation (3.19), from which the total quartz in

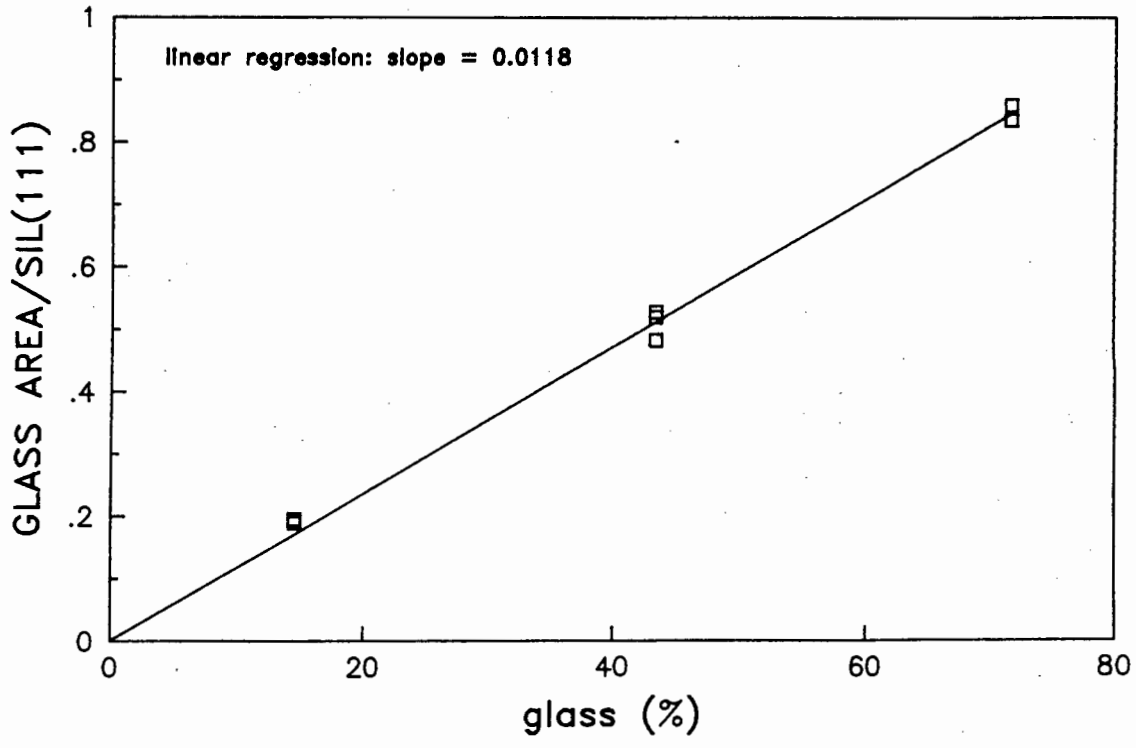

Fig. 3.24 : The glass calibration curve used to determine the glass concentration in the samples.

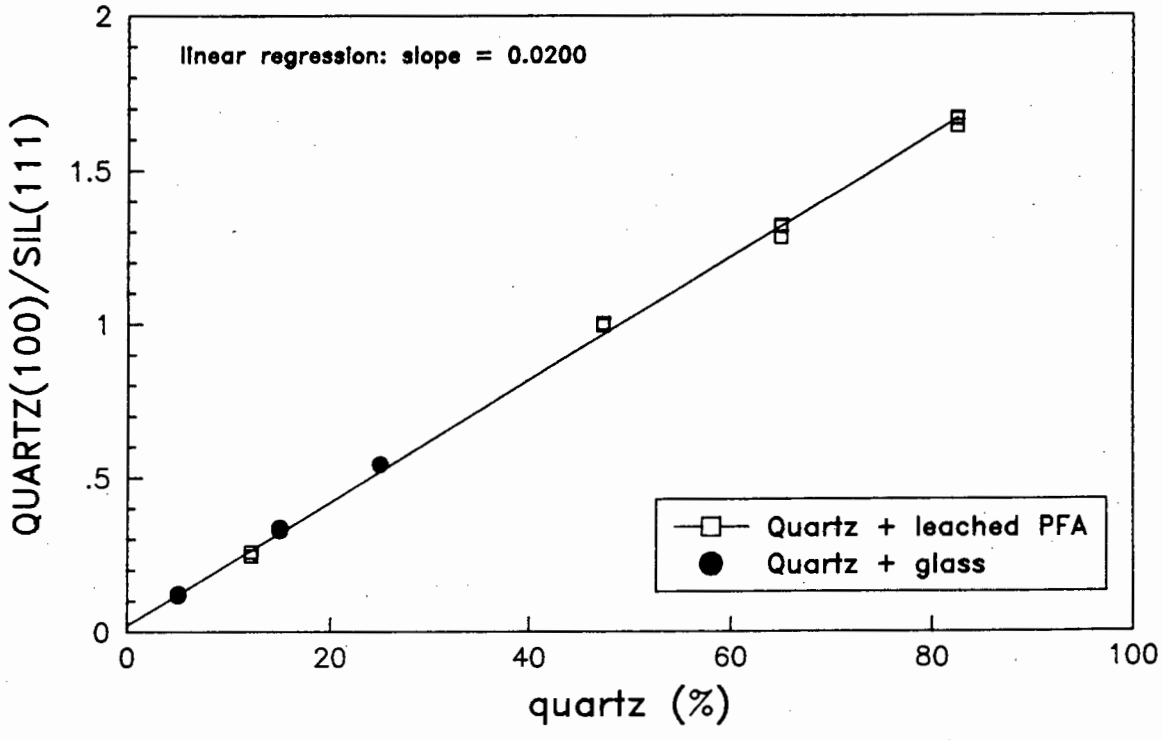

Fig. 3.25 : The quartz calibration curve used to determine the quartz concentration in the samples.

each standard could be calculated.

The quartz calibration curve is shown in Fig. 3.25.

3.16.3 Hematite

The hematite standards were prepared from the spinel interference standard spiked with the addition of hematite and diluted with quartz. The hematite concentration of 4.3% in the starting mixture was calculated using equation (3.19). The hematite calibration curve is shown in Fig. 3.26.

3.16.4 Spinel

The hematite standards were also used for the spinel standards except that the spinel concentration was calculated by difference. The spinel calibration curve is shown in Fig. 3.27.

3.16.5 Calcite

The calcite standard consisted of a mixture of the quartz and the natural calcite used for the interference standards. The calibration curve is shown in Fig. 3.28.

3.16.6 Portlandite

The portlandite standard was prepared from the artificial portlandite manufactured for the portlandite interference standard, using portlandite and calcite correction factors found from that interference standard. The calcite concentration (from the alteration of portlandite) was determined for each standard. The amount of portlandite that remained was then calculated from

$$C_{ptl} = C_{cal} \times \left(\frac{MM_{ptl}}{MM_{cal}} \right) \qquad (3.20)$$

C_{ptl} = portlandite concentration

C_{cal} = calcite concentration

MM_{ptl} = molar mass of portlandite

MM_{cal} = molar mass of calcite

The remaining portlandite concentration was plotted against PTL(001)/SIL(111) to derive the calibration curve shown in Fig. 3.29.

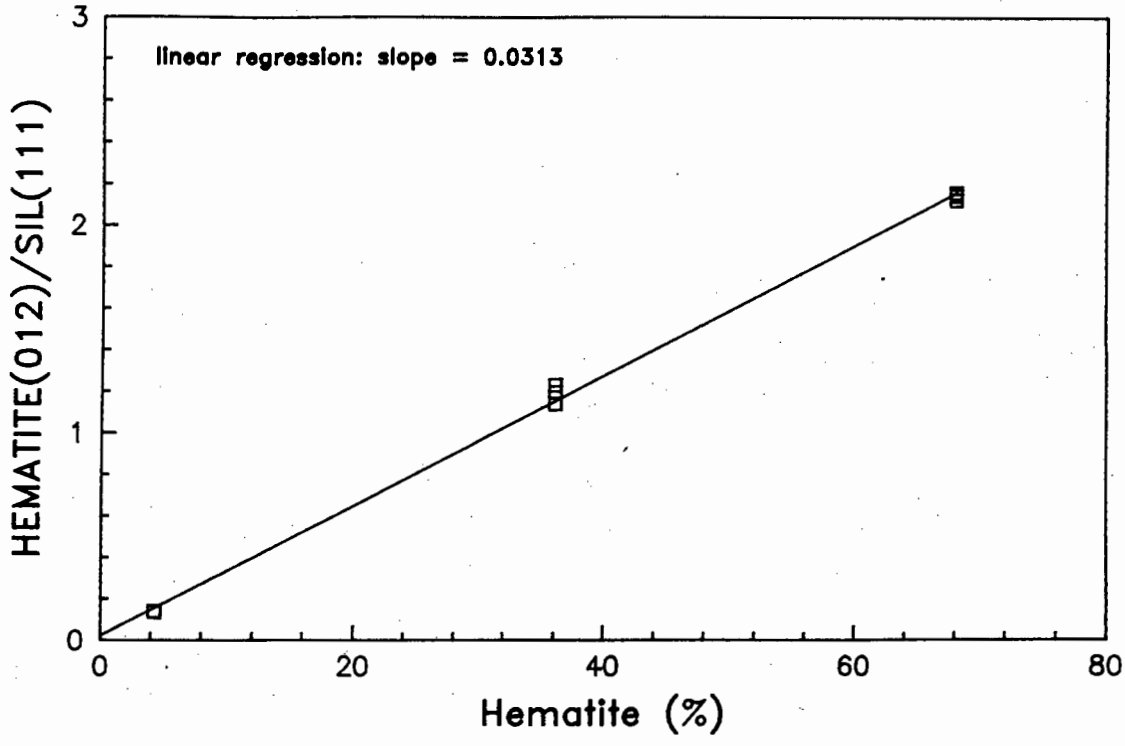

Fig. 3.26 : The hematite calibration curve used to determine the hematite concentration in the samples.

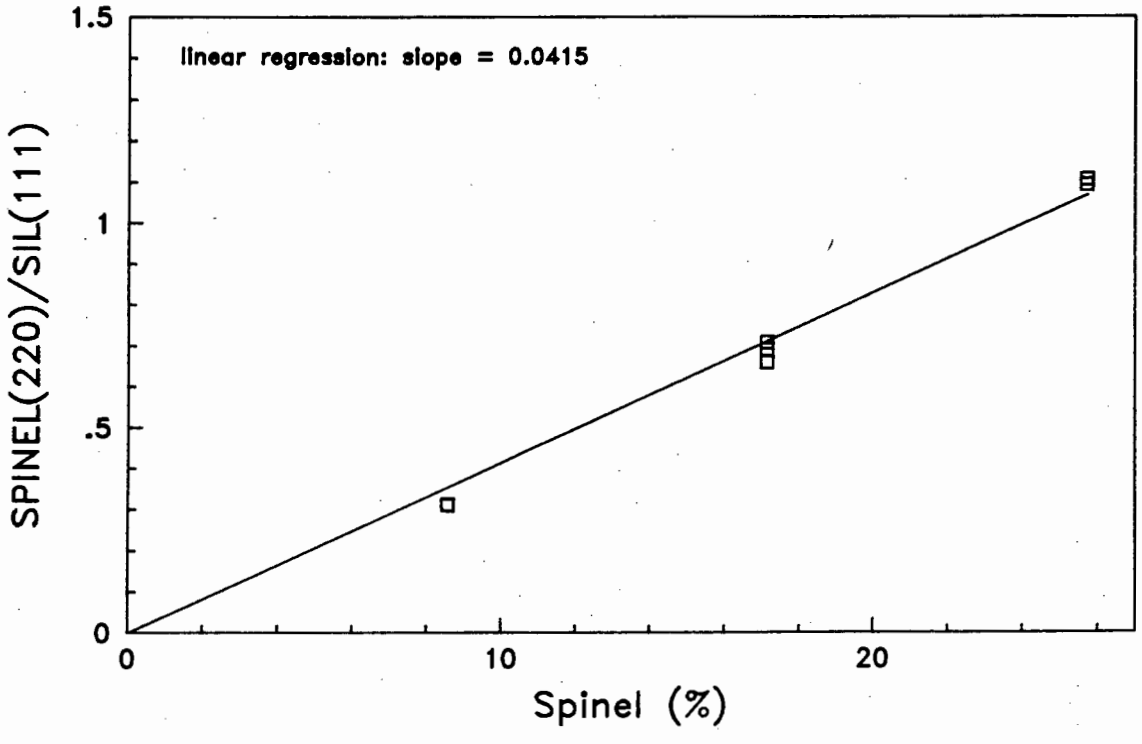

Fig. 3.27 : The spinel calibration curve used to determine the spinel concentration in the samples.

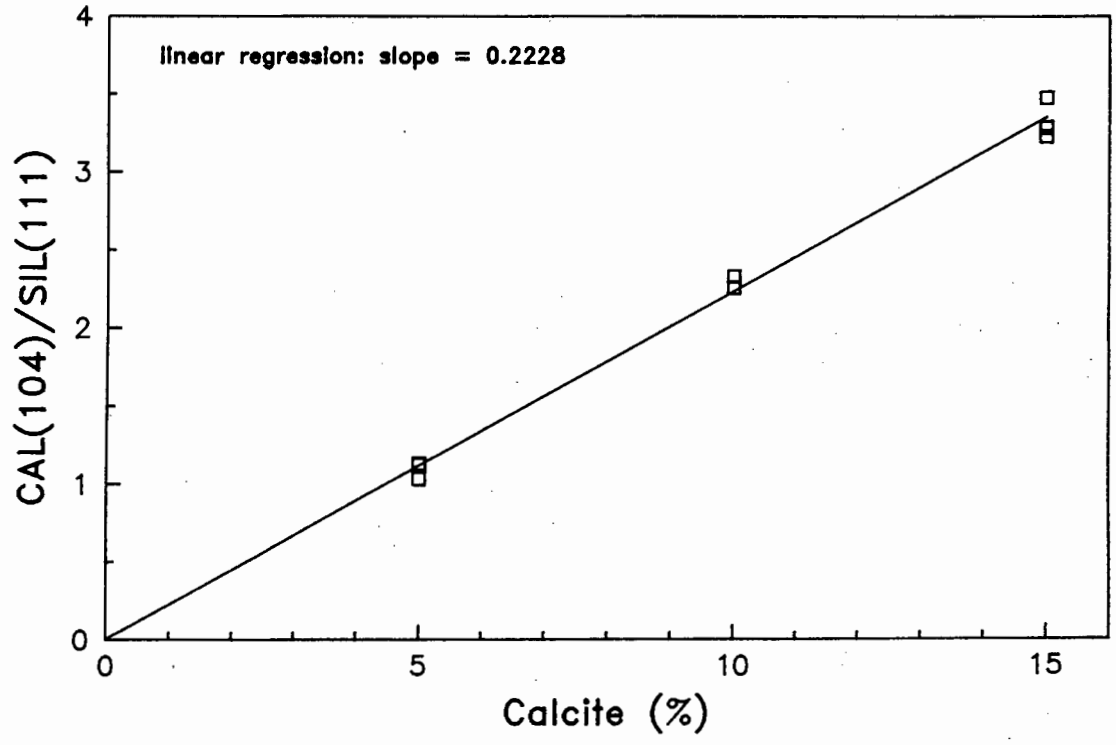

Fig. 3.28 : The calcite calibration curve used to determine the calcite concentration in the samples.

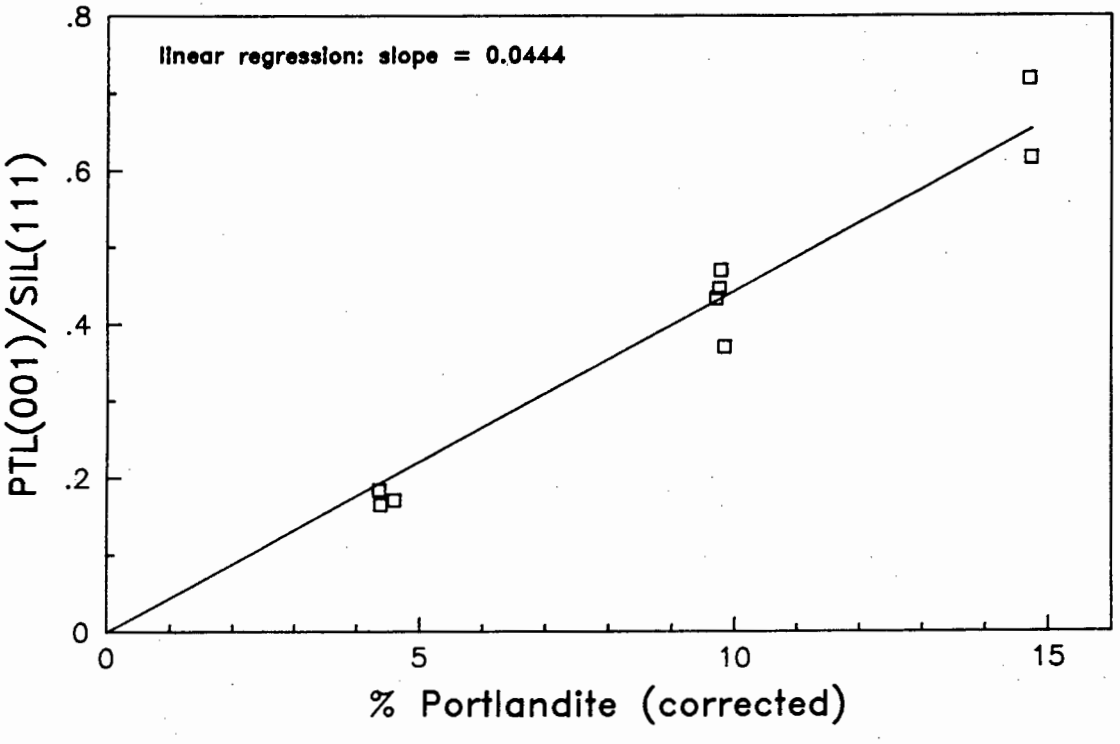

Fig. 3.29 : The portlandite calibration curve used to determine the portlandite concentration in the samples. The portlandite concentration has been corrected for the alteration of portlandite to calcite.

3.16.7 Lime

The lime standard was prepared from the lime used for the interference standard, from which the portlandite and calcite correction factors were derived. The portlandite and calcite concentrations in each standard were determined at the same time as the lime peak was measured. The amount of lime that had undergone alteration was then

$$C_{lime} = C_{cal} \times \left(\frac{MM_{lime}}{MM_{cal}} \right) + C_{ptl} \times \left(\frac{MM_{lime}}{MM_{ptl}} \right) \qquad (3.21)$$

C_{lime} = lime concentration

MM_{lime} = molar mass of lime

The remaining lime concentration was plotted against LIM(111)/SIL(111) to derive the calibration curve shown in Fig. 3.30.

3.16.8 Mullite

The mullite standards were the same as the second set of quartz standards described above. The unspiked mullite-quartz mixture contained small amounts of quartz (12.2%) and glass. The glass concentration was calculated in two ways:

1. The glass concentration in the unspiked mixture was measured directly using the glass calibration curve found above. This method gave a glass concentration of 1.6%.

2. The glass concentration was determined by spiking the mullite-quartz mixture with 10% glass, and then equation (3.19) was used to calculate the amount of glass. This method gave a glass concentration of 1.8% in the unspiked mixture. The glass concentration found by both methods was in good agreement. The glass concentration in the unspiked mixture was taken to be the mean concentration from the two methods, namely 1.7%.

The concentration of mullite in the unspiked mixture was therefore 86.1%, from which the concentration in each of the standards was calculated. Data points for the mullite standards are shown in Fig. 3.31. Also shown is the mullite concentration found by difference in the glass standards, a 32 hour HF leach, and two synthetic ashes, PFASYN1 and PFASYN2, prepared from the components used for the interference standards. The mullite calibration curve shown in Fig. 3.31 was derived using all these data points.

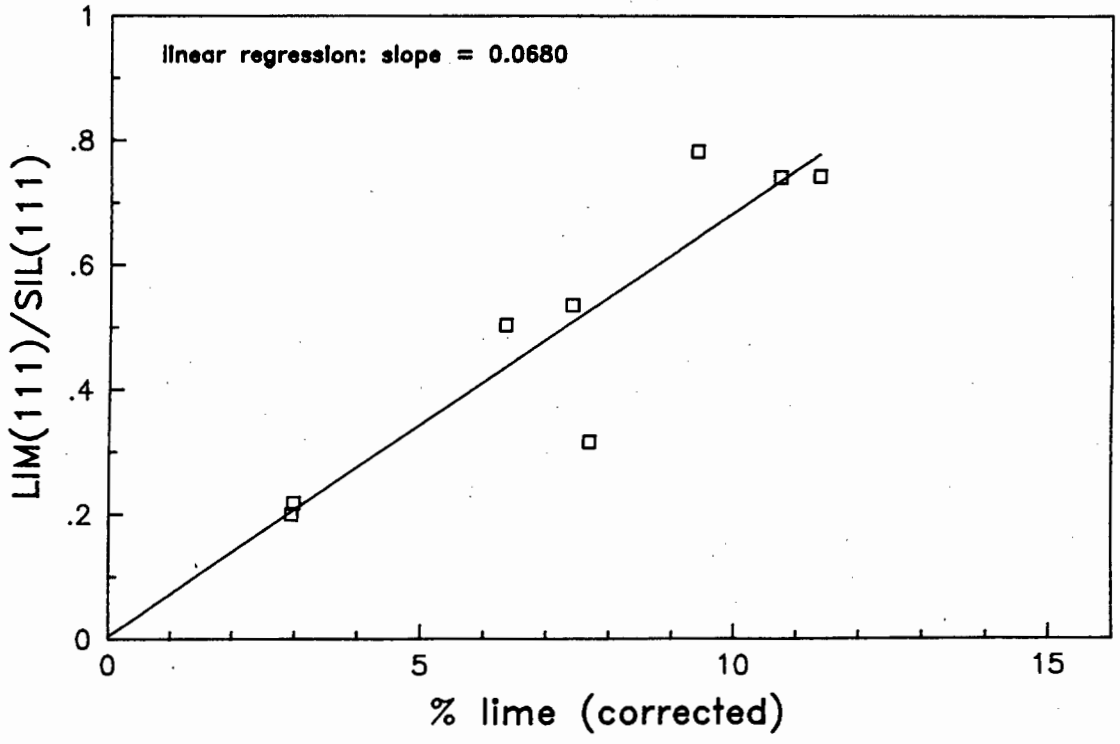

Fig. 3.30 : The lime calibration curve used to determine the lime concentration in the samples. The lime concentration has been corrected for the alteration of lime to portlandite and calcite.

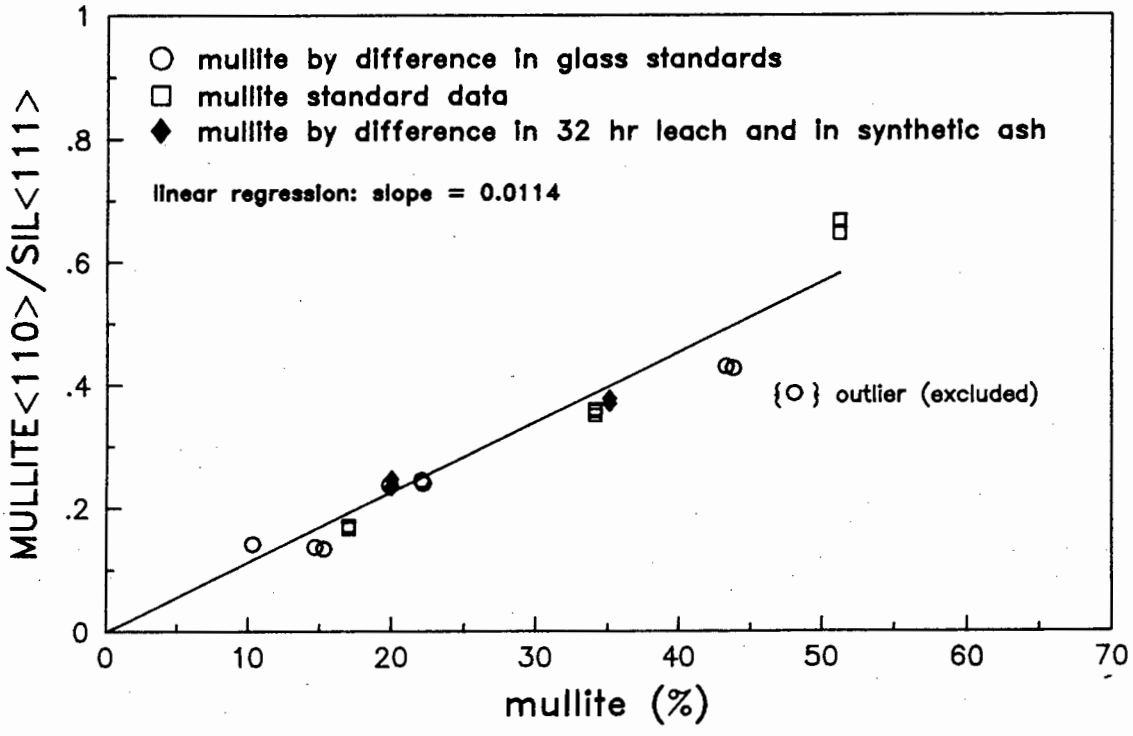

Fig. 3.31 : The mullite calibration curve used to determine the mullite concentration in the samples.

3.16.9 Interlaboratory Comparisons and Accuracy

The accuracy of the method has been tested against the calculated values for two synthetic fly ashes as well as against two National Bureau Standards (NBS) fly ashes (NBS2689 and NBS2690). The concentrations of the NBS fly ashes were compared with data from McCarthy and Thedchanamoorthy (1989), which were calculated using the RIR method based on peak heights and visually estimated backgrounds, with rutile as an internal standard. Fig. 3.32 shows a comparison of the data from the two laboratories, as well as a comparison of calculated and measured data for two synthetic ashes prepared from the material used for the interference standards. The data are tabulated in Table 3.4.

The agreement between data from the two laboratories is very good, and generally within the analytical error of both methods. Quartz is slightly higher in both NBS ashes with the UCT method, and lime is lower. Mullite, glass, hematite and spinel show no consistent differences.

	NBS2689		NBS2690		PFASYN1		PFASYN2	
Phase	UCT[1]	MT[2]	UCT[1]	MT[2]	meas	calc	meas	calc
Glass	71.0	77.8	76.4	76.3	62.1	62.3	53.6	48.5
Mullite	12.1	9.4	8.8	11.2	21.1	20.6	32.9	35.4
Quartz	6.6	4.0	13.4	11.4	11.2	11.0	10.2	11.5
Lime	-0.4		-0.6		2.5	3.0	2.9	3.6
Spinel	6.2	4.9	0.8	1.2	2.4	3.0	0.1	0.7
Hematite	2.6	3.6	0.5		0.8	0.7	0.1	0.1

Table 3.4 : Comparison of concentration data (%) between laboratories for two NBS ashes, and between the measured and calculated values of two synthetic ashes prepared for this work (pfasyn1 and pfasyn2) .

1 = this work

2 = data taken from McCarthy and Thedchanamoorthy (1989)

3.16.10 Effect of Grinding Time on Rutile Intensity

Two NBS fly ashes (NBS2689 and NBS2690) were crushed in the UCT Geochemistry Department for two hours using an automatic pestle-and-mortar, and then mixed by hand with 10% rutile (received from McCarthy, Department of Chemistry, North Dakota State University as NDSU rutile), which had been fired at 1190°C and passed through a 325 mesh sieve: (i) using the rutile as received, and (ii) using rutile that had been first mixed with the sample and then further crushed in the UCT Geochemistry Department for 2 hours. All

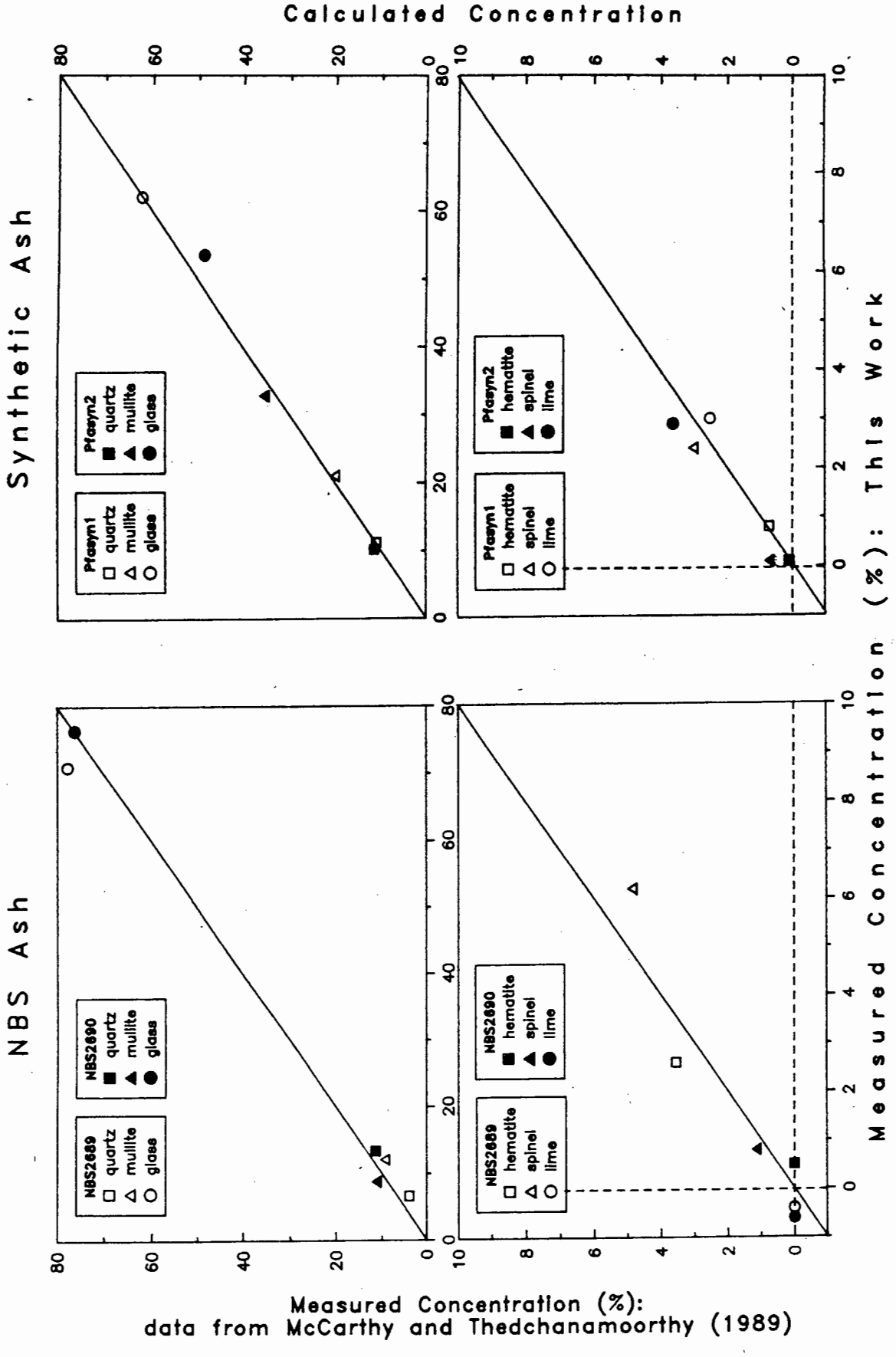

Fig. 3.32 : Comparison of data between laboratories for two NBS ashes; and between the theoretical and measured concentrations of two synthetic ashes prepared from the same material used for the interference standards.

samples were side loaded in the sample holder and were step scanned using 40 kV and 30 mA.

Method (ii) broadened the rutile peak and reduced the height to approximately half that of method (i) (Fig. 3.33). This could be due to overgrinding of the rutile in method (ii). The change in rutile peak height with grinding time is very disturbing and suggests that consistency of sample preparation methods is critical for reliable analytical work, particularly when using the RIR technique. Calibration curve slopes and RIR values taken from the literature and subsequently used for quantitative determinations may result in errors which could be as large as a factor of 2.

3.17 SAMPLES

All the samples received for this study have been analysed in duplicate using the QXRD method outlined above. The analyte peaks were scanned at $1/4°2\theta$ per minute, and background intensities were counted for 200 seconds each. Corrected nett peak areas were calculated with the program XRDGLASS and then converted to concentrations using the slopes of the calibration curves. Lower limits of detection (LLD) for each of the mineral phases are listed in Appendix 1. The analytical errors for a typical PFA sample are listed in Table 3.5.

Phase	Concentration Weight (%)	Absolute Error (%)	Relative Error (%)
Mullite	33.3	2.7	8.3
Quartz	13.6	1.2	8.6
Glass	45.5	4.7	10.4
Hematite	0.4	0.2	62.7
Spinel	3.6	0.3	9.2
Portlandite	0.6	0.1	22.6
Lime	0.3	0.1	23.2

Table 3.5 : Analytical error in the QXRD analysis of PFA for a typical sample (D1_PFA1).

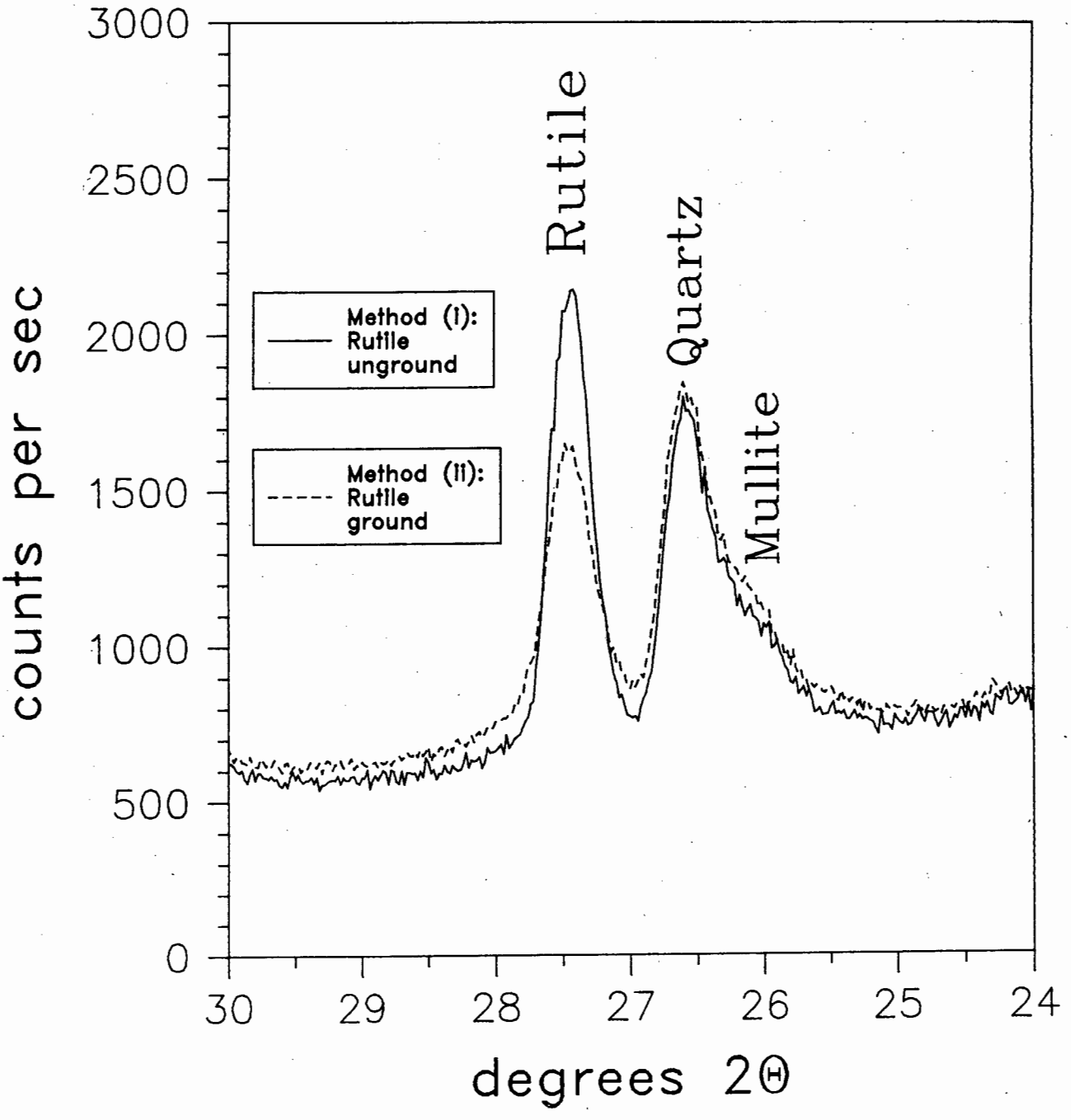

Fig. 3.33 : Diffractogram of NBS2689 showing the effect of excessive grinding on the rutile peak height.

CHAPTER 4

ANALYTICAL METHODS (II)

4.1 X-RAY FLUORESCENCE SPECTROMETRY

X-Ray Fluorescence spectrometry (XRF) was used to determine the bulk element chemistry for 10 major and minor elements and 29 trace elements for both the PFA and the coal samples. Analyses were determined with a Siemens SRS-303AS and a Philips PW1400 XRF Spectrometer. The intensity data were converted to concentrations with the aid of the Hewlett-Packard 9000 computer system and the in-house data-processing programs MJSRT, MAJOR, TRACE, and modified versions of the NBSGSC programs CALCO and CALCOMP21 (Tao et al 1985).

4.1.1 H_2O^- *and LOI*

4.1.1.1 PFA Samples:

The H_2O^- concentrations in the PFA were determined from the mass lost by heating the sample at 110°C for 4 hours, and the loss of ignition (LOI) was determined from the further loss in mass found by heating at 850°C for a further 4 hours.

4.1.1.2 Coal Samples:

The H_2O^- concentrations were determined from the mass lost by heating the coal at 110°C for 4 hours, and the LOI was determined from the mass lost by increasing the temperature stepwise to 1000°C (Table 4.1) to minimise the loss of material through the production of smoke.

4.1.2 Sample Preparation

4.1.2.1 PFA Samples:

PFA samples were ground in a Carbon-Steel swingmill after having been dried at 110°C for 4 hours. Powder pellets were prepared from a mixture of 16g PFA with 4g (20%) Hoechst Wax C Micropowder as binder, and pressed at 10 tons. Undiluted powder pellets were prepared from 2g PFA mixed with a few drops of a Mowiol solution (20% Hoechst N 70-88 in distilled water) as a binder, and pressed into 30mm diameter pellets with boric acid backing at 10 tons pressure.

Temperature (°C)	Time
110	4 hours
150	15 minutes
250	15 minutes
350	15 minutes
450	15 minutes
500	30 minutes
815	30 minutes
950	1 hour
1000	Overnight

Table 4.1 : Coal ashing procedure so as to minimise the production of smoke.

4.1.2.2 Coal Samples:

Coal samples were ground at slow speed in an Agate swingmill after initial drying at 110°C. Powder pellets were prepared by mixing 32g coal with 8g (20%) Hoechst Wax C Micropowder and pressing into 40mm diameter pellets at 10 tons pressure.

4.1.3 Major Elements

4.1.3.1 PFA:

Major and minor elements in the PFA samples (SiO_2, TiO_2, Al_2O_3, Fe_2O_3, MgO, CaO, K_2O and P_2O_5) were determined using the fusion disk method of Norrish and Hutton (1969), in which the ashed samples were mixed with a Lithium Tetraborate flux with La as heavy absorber (Johnson Matthey Spectroflux 105) and cast into a glass disk. Na_2O and SO_3 were determined separately on the undiluted powder briquettes. The intensity data were converted to concentrations with the programs MJSRT and MAJOR.

4.1.3.2 Coal:

Major and minor oxide concentrations (SiO_2, TiO_2, Al_2O_3, FeO, MgO, CaO, Na_2O, K_2O, P_2O_5 and S) were determined in the powder pellets with the aid of the program CALCOMP21, and with a correction for dilution by the wax.

4.1.4 Trace Elements

4.1.4.1 PFA:

For the PFA samples, the Rh K_α Compton peak was measured in order to determine the mass absorption coefficient (MAC) at the Mo K_α wavelength. MAC values for S, K, Sc, V, Cr, Rb, La and Ce were calculated from the major element concentrations using the in-house program XRMAC.

Concentrations of the trace elements Rb, Sr, Y, Zr, Nb, Mo, U, Th, Pb, As, Se, Bi, Ge, W, Ga and Br were measured using powder pellets diluted with 20% wax. All concentration data were corrected for dilution by the wax binder. The trace elements Zn, Cu, Ni, Mn, Co, Cr, V, Ba, Sc, La, Ce and Nd were determined in the undiluted powder briquettes. Intensity data were converted to concentrations using the program TRACE.

4.1.4.2 Coal:

For the coal samples, the W L_{β_1} Compton peak was measured in order to determine the MAC at that wavelength. MAC values for K, Cr, Sc, Mo, V, Mn, Co, La, Ce, Rb and W were calculated from the major element concentrations using the in-house program HIMAC. All trace element concentrations in coal were measured in the powder briquettes.

4.2 MICROPROBE ANALYSES

A Cameca Camebax Electron Microprobe has been used to determine the chemistry of the glass and spinel phases in the PFA. The electron beam was operated at 39.0 nA and 15kV, with a defocused beam diameter of 10μm for the glass analyses so as not to volatilise K_2O, Na_2O and P_2O_5. Spinel analyses were determined with the electron beam focused as fine as possible so as to limit interference from the glass matrix. Intensity data were converted to concentrations using the standard ZAF correction and CAMECA software. The lower limits of detection are listed in Table 4.2.

Samples were prepared for analysis by dispersing an aliquot of the PFA in resin which was mounted on a standard glass slide when dry. The resin was then ground to a thickness of 30μm and polished. The polished surface was coated with carbon prior to analysis.

Fe-Oxides		Glass	
Oxide	LLD(%)	Oxide	LLD(%)
SiO_2	0.047	SiO_2	0.030
TiO_2	0.045	TiO_2	0.040
Al_2O_3	0.043	Al_2O_3	0.034
Cr_2O_3	0.047		
FeO	0.101	Fe_2O_3	0.082
MnO	0.079	MnO	0.059
MgO	0.039	MgO	0.022
CaO	0.032	CaO	0.028
		P_2O_5	0.046
		SrO	0.209
		BaO	0.147
		K_2O	0.021
		Na_2O	0.024

Table 4.2 : Lower limits of detection (LLD) for oxides determined by electron microprobe analysis.

4.3 PARTICLE SIZE ANALYSIS

4.3.1 Sedigraph

The particle size distributions for the L1 data set were determined in the Marine Geoscience Unit at UCT. Each sample was separated by wet- sieving into a greater than and less than 63μm fraction, and the relative proportions were determined from the dried mass of each fraction. The particle size distribution of the coarser fraction was measured using a settling tube calibrated against quartz, and that of the finer fraction was measured using a Micromeritics Sedigraph with Calgon solution as the dispersing medium. Samples were ultrasounded before analysis and densities were taken from Heinichen and Willis (1987). The disadvantage of this method is that the analysis time for each sample can be as long as 3 hours when a large proportion of fine material is present. An advantage of the method is that particle sizes as small as 0.12μm can be measured.

4.3.2 Malvern Particle Sizer

Initially particle size distributions were determined on dry PFA and coal samples with a Malvern 2600 C Particle Sizer at the Pretoria Portland Cement laboratory at De Hoek. Samples were sieved through a 300μm sieve prior to analysis. Aggregation of the particles occurred, presumably due to absorption of moisture from the atmosphere as the samples were left exposed to the air over a period of several days of high humidity. These results unfortunately proved unusable (see Chapter 6).

Subsequently, particle size distributions of two PFA samples from each power station were determined with the Malvern 2600 HSD Particle Sizer in the Department of Physics at UCT. Samples were analysed as slurries, and tests were conducted with both water and 0.005 and 0.05 molar Sodium Pyrophosphate as dispersing solutions. Teepol was added in all cases to assist in wetting the particles. Three lenses were used: a 300mm lens able to measure a particle size range of 564.0-5.8μm, a 100mm lens able to measure a particle size range of 188.0-1.9μm and a 63mm lens able to measure a range of 118-1.2μm. No particles should be present in the sample which are larger than the maximum size which each lens can determine. All samples were ultrasounded prior to analysis with the 300mm lens. If a significant proportion was finer than 5.8μm the sample was then sieved wet through an 80μm sieve, prior to analysis with either the 100mm or the 63mm lens.

CHAPTER 5

DATA

5.1 INTRODUCTION

The following data are presented:

Table 5.1: Bulk chemical and mineralogical data. Fe is reported as Fe_2O_3 in the PFA samples and as FeO in the coal. S is reported as SO_3 in the PFA samples and as S in the coal. The coal major and minor element data are expressed as H_2O^- free. A '< x' in the chemical composition data indicates that the measured concentration was below the lower limit of detection (x). Lime (meas) is the measured lime concentration, and lime(calc) is the total lime concentration corrected for alteration to portlandite. The high Pb value for L4_PF is an outlier and has been excluded from the discussion.

Table 5.2: Major and minor oxide concentrations in the PFA microprobe glass analyses.

Table 5.3: Major and minor oxide concentrations in the PFA microprobe Fe oxide analyses.

Table 5.4: Particle size distributions of selected PFA samples expressed as cumulative weight percent. Data is from the UCT Physics Department Malvern Instruments Particle Sizer unless otherwise stated.

5.2.1 **Table 5.1 : Major and trace element concentrations in coal and bulk fly ash samples from XRF analyses, and mineral concentrations from QXRD analyses.**

	TH8_16	TH8_17	L1_PF	L1_BA	L1_MA	L1_PFA1	L1_PFA2	L1_PFA3	L1_PFA4
SiO_2	21.68	20.26	21.16	50.27	50.77	51.35	48.99	47.83	48.48
TiO_2	.69	.67	.69	1.57	1.67	1.67	1.76	1.77	1.89
Al_2O_3	14.06	12.63	13.63	33.35	35.23	35.75	36.85	36.87	38.05
Fe_2O_3				3.97	3.41	3.06	3.00	2.83	2.79
FeO	1.04	1.03	.99						
MgO	.44	.42	.41	1.06	1.20	1.11	1.23	1.34	1.39
CaO	1.77	1.80	1.85	4.46	4.36	4.32	4.66	4.61	4.71
Na_2O	.09	.14	.11	.31	.28	.27	.31	.43	.33
K_2O	.18	.20	.18	.42	.46	.46	.49	.55	.52
P_2O_5	.16	.14	.14	.22	.36	.30	.45	.58	.65
SO_3				.39	.41	.14	.21	.36	.35
S	.40	.35	.39						
H_2O^-				.29	.39	.10	.22	.10	.11
LOI	61.38	60.50	59.00	4.35	2.25	1.72	2.26	3.21	1.20
TOTAL	101.48	97.67	98.20	100.68	100.80	100.24	100.43	100.46	100.46
Rb	11	13	13	27	31	30	33	37	35
Sr	343	328	312	759	837	767	870	945	993
Y	34	32	34	88	94	94	105	108	110
Zr	209	199	216	567	571	586	600	594	586
Nb	17	16	17	46	47	47	51	52	54
Mo	2	2	2	3	6	5	9	10	10
U	5	5	5	11	12	12	12	14	14
Th	19	18	20	45	49	49	55	56	60
Pb	28	69	28	31	79	70	115	151	166
As	5	4	5	3	14	15	23	29	31
Se	.8	.5	.9	<.9	2	2	2	4	4
Bi	<1.7	<1.6	<1.7	<3.0	3	<3.0	6	11	12
Ge	.8	1	.9	<.9	2	2	5	6	7
W	3	5	4	7	7	7	12	14	14
Ga	21	20	21	33	56	55	79	97	105
Br	<.6	<.6	<.6	<1.1	<1.1	<1.1	<1.1	<1.1	<1.1
Zn	26	26	32	35	81	79	137	183	204
Cu	19	20	28	50	59	61	75	78	83
Ni	30	30	33	88	92	96	112	126	129
Mn	127	132	140	413	371	358	388	413	483
Cs	5	4	5	11	13	13	15	14	14
Co	9	9	9	23	24	24	28	29	32
Cr	102	97	103	231	257	257	285	287	293
V	84	80	88	164	191	192	233	260	273
Ba	345	382	336	743	868	800	937	1123	1148
Sc	17		17	39	43	44	50	52	56
La	45	43	46	102	113	110	119	124	128
Ce	97	88	97	217	234	232	247	260	268
Nd	43	40	43	99	104	106	113	118	120
Quartz				7.9	6.8	6.5	3.3	2.1	1.9
Mullite				30.8	36.2	36.0	35.7	35.1	36.7
Glass				56.3	54.5	54.3	57.3	58.5	60.0
Hematite				.6					
Spinel				.5	.6	1.2	.9	.9	.4
Calcite				.1	.2	-0.1	-0.1	-0.1	-0.1
Portlandite				.1			.1		
Lime (meas)				-0.7	-0.6	.4	.5	.3	0.0
Lime (corr)				-0.6	-0.6	.4	.6	.3	0.0

Table 5.1 : (Continued)

	L1_PFA5	L2_PFA5	L2_PFA6	L1_PFA7	L3_PF	L3_PFA1	L3_PFA2	L3_PFA3	L3_PFA4
SiO_2	48.24	48.41	48.52	48.56	21.89	51.47	45.17	47.55	47.35
TiO_2	1.90	1.90	1.90	1.91	.63	1.59	1.59	1.78	1.82
Al_2O_3	38.21	38.07	38.24	38.13	13.23	34.65	33.01	35.98	36.50
Fe_2O_3	2.83	2.84	2.89	2.98		3.97	4.16	3.96	3.84
FeO					1.42				
MgO	1.44	1.44	1.44	1.47	.57	1.17	1.35	1.49	1.55
CaO	4.79	4.80	4.46	4.56	1.90	4.24	4.86	4.95	4.72
Na_2O	.32	.32	.45	.43	.10	.31	.39	.42	.43
K_2O	.50	.51	.56	.56	.28	.49	.49	.53	.50
P_2O_5	.68	.68	.66	.73	.18	.41	.61	.75	.81
SO_3	.31	.29	.29	.29		.17	.35	.51	.45
S					.66				
H_2O^-	.08	.08	.07	.10		.09	5.74	.19	.43
LOI	1.08	1.01	.87	.67	59.52	1.96	1.82	.87	.36
TOTAL	100.39	100.37	100.36	100.39	100.01	100.51	99.53	98.98	98.75
Rb	35	35	37	38	17	30	32	39	34
Sr	1058	1045	1089	1185	449	1009	1386	1745	1558
Y	113	113	109	112	28	78	90	112	99
Zr	582	581	573	566	175	542	560	655	555
Nb	55	55	55	57	15	48	52	65	57
Mo	10	10	7	7	1	5	7	9	8
U	15	14	13	14	5	11	13	15	14
Th	59	59	61	63	18	49	55	68	62
Pb	178	176	179	185	40	65	107	166	166
As	31	31	25	26	5	13	28	37	33
Se	5	5	6	7	.7	2	3	3	6
Bi	14	14	16	18	<1.6	<3.0	7	11	16
Ge	7	6	5	6	1	2	4	7	7
W	15	17	15	15	6	10	10	12	15
Ga	108	107	107	110	18	49	74	108	105
Br	<1.1	<1.1	<1.1	<1.1	<.6	<1.1	<1.1	<1.2	<1.1
Zn	214	217	226	235	28	47	104	126	148
Cu	84	84	88	96	24	40	53	60	63
Ni	132	131	127	128	23	58	69	79	86
Mn	466	487	495	518	137	278	341	373	410
Cs	14	14	15	14					
Co	34	33	34	34	9	19	20	24	25
Cr	289	290	277	269	100	227	236	255	250
V	270	271	239	241	74	134	159	180	187
Ba	1213	1206	1358	1437	544	973	1243	1480	1623
Sc	55	56	54	54	18	35	39	45	48
La	132	130	133	139	47	97	107	120	121
Ce	271	272	270	275	98	203	216	242	246
Nd	121	122	122	124	44	91	97	109	112
Quartz	2.5		1.9	2.0		7.0	3.5	2.5	1.7
Mullite	38.0		35.0	35.3		35.5	33.0	31.4	29.7
Glass	58.7		62.2	62.7		54.2	59.3	64.2	67.3
Hematite									
Spinel	.4		.4	.2		1.4	1.7	1.0	.9
Calcite	-0.1		-0.1	-0.1		-0.1	-0.1	-0.1	-0.1
Portlandite			.1	<.1		.1			
Lime (meas)	-0.5		-0.3	-0.6		-0.1	.8	.2	.1
Lime (corr)	-0.5		-0.2	-0.7			.8	.2	.1

Table 5.1 : (Continued)

	L4_PF	L4_PFA1	L4_PFA2	L4_PFA3	L4_PFA4	L4_PFA5	L4_PFA6	L5_PF	L5_PFA1
SiO_2	22.59	52.83	49.81	49.17	48.32	47.54	52.89	22.32	55.87
TiO_2	.88	1.76	1.87	1.94	1.99	1.96	1.78	.64	1.54
Al_2O_3	14.38	36.33	37.40	36.72	38.07	37.59	34.31	12.98	30.06
Fe_2O_3		3.99	3.72	3.41	3.52	3.49	3.90		4.49
FeO	1.95							1.45	
MgO	.49	1.26	1.41	1.49	1.44	1.51	1.31	.49	1.31
CaO	2.28	5.07	5.34	5.38	4.82	4.95	4.52	1.92	4.73
Na_2O	.09	.22	.25	.26	.27	.29	.20	.07	.16
K_2O	.21	.40	.47	.56	.48	.49	.58	.21	.62
P_2O_5	.26	.57	.77	.99	.90	.96	.47	.21	.37
SO_3		.29	.50	.55	.58	1.54	.35		.20
S	.87							1.80	
H_2O^-		.16	.08	.15	.15	.42	.16		.04
LOI	58.76	.37	.15	.75	.28	.34	.33	59.86	.60
TOTAL	102.18	103.24	101.77	101.37	100.81	101.08	100.79	103.17	99.99
Rb	11	27	30	38	31	32	39	9	39
Sr	479	1306	1573	1452	1653	1699	1029	259	1005
Y	27	74	81	82	86	89	76	19	69
Zr	190	504	514	502	509	496	454	129	452
Nb	17	46	50	51	54	54	47	10	41
Mo	3	6	9	10	9	10	8	3	5
U	4	12	14	12	11	12	11	3	9
Th	17	50	57	58	60	62	52	11	45
Pb	2755	77	117	154	159	180	134	16	65
As	7	14	24	31	26	28	17	3	9
Se	<.5	1	3	5	5	6	4	.8	1
Bi	<1.8	<3.0	7	11	12	17	9	<1.5	<3.0
Ge	<.6	1	4	6	5	5	4	1	2
W	6	10	13	16	13	14	12	3	10
Ga	22	47	75	88	94	103	66	12	36
Br	<.9	<1.5	<1.6	<1.5	<1.5	<1.6	<1.5	1	<1.5
Zn	26	63	70	106	106	122	75	15	35
Cu	24	51	55	61	67	70	54	14	39
Ni	26	58	68	72	85	90	61	17	45
Mn	126	292	327	361	373	406	318	121	248
Cs									
Co	7	16	19	24	24	26	19	11	18
Cr	101	238	267	245	268	275	231	66	177
V	77	144	177	192	195	213	153	59	119
Ba	532	1124	1393	1301	1579	1643	1119	441	907
Sc	18	36	42	42	45	47	40	9	32
La	49	103	114	112	119	123	103	38	97
Ce	105	215	242	235	253	258	222	80	202
Nd	46	92	104	104	107	114	94	36	83
Quartz		8.6	4.6	3.3	2.2	1.5	6.1		11.0
Mullite		37.9	37.4	35.4	33.1	32.6	28.9		25.0
Glass		50.3	55.7	59.4	63.3	65.3	63.6		61.5
Hematite						.3			
Spinel		2.0	1.5	1.1	.9	.5	.9		1.7
Calcite		-0.1	-0.1	-0.1	-0.1	-0.1	-0.1		-0.1
Portlandite		.2	.2			<.2			
Lime (meas)		.7	.6	.1	.2	-0.2	.4		.2
Lime (corr)		.8	.7	.1	.2	-0.3	.4		.2

Table 5.1 : (Continued)

	L5_PFA2	L5_PFA3	L5_PFA4	D1_PFA2	D1_PFA1	D1_PFA3	D1_PFA4	D1_PFA5	D4_PF
SiO_2	52.11	50.61	48.08	51.98	52.22	49.21	48.44	47.15	12.79
TiO_2	1.65	1.81	1.98	1.65	1.63	1.80	1.85	1.90	.38
Al_2O_3	31.76	34.69	37.52	31.34	31.15	32.86	33.91	34.22	7.36
Fe_2O_3	4.30	3.88	3.53	5.01	5.04	5.06	4.54	4.34	
FeO									.34
MgO	1.47	1.58	1.46	.82	.83	.83	.86	.99	.54
CaO	5.39	5.32	4.82	4.89	4.87	5.30	5.13	5.20	1.88
Na_2O	.19	.22	.26	.07	.07	.09	.10	.12	.10
K_2O	.67	.63	.47	.62	.63	.61	.64	.69	.24
P_2O_5	.55	.78	.88	.75	.73	.90	1.09	1.46	.13
SO_3	.38	.52	.68	.27	.23	.87	.68	.93	3.31
S									1.33
H_2O^-	.32	.17	.27	.12	.12	.57	.11	.10	
LOI	.54	.53	.80	2.74	2.86	2.22	2.84	3.03	73.75
TOTAL	99.34	100.75	100.74	100.25	100.38	100.32	100.19	100.14	100.50
Rb	44	42	32	38	39	40	43	44	11
Sr	1173	1420	1627	1034	1003	1307	1397	1574	312
Y	76	82	84	90	89	105	110	117	20
Zr	458	470	504	546	530	603	594	593	125
Nb	46	49	54	46	45	53	55	57	10
Mo	8	10	10	7	6	11	18	28	2
U	12	14	12	9	9	10	15	17	4
Th	50	54	60	43	41	53	58	64	11
Pb	104	134	158	52	47	83	103	135	27
As	24	30	26	11	10	21	35	53	4
Se	3	5	5	<.9	1	1	3	4	.7
Bi	6	11	12	<3.2	<3.2	7	8	8	<1.5
Ge	5	7	4	3	3	7	12	20	2
W	10	16	13	7	8	10	14	18	4
Ga	58	78	94	38	37	55	76	107	13
Br	<1.6	<1.5	<1.5	<1.1	<1.2	<1.2	<1.2	<1.2	2
Zn	62	90	101	82	73	125	157	209	17
Cu	48	55	61	49	45	60	64	74	18
Ni	53	67	79	93	90	113	121	145	21
Mn	278	315	378	233	233	241	244	258	83
Cs				10	10	13	14	15	
Co	21	24	23	33	33	40	46	56	9
Cr	211	241	262	163	157	194	210	237	52
V	153	188	196	129	130	151	180	226	59
Ba	1090	1344	1564	974	925	1245	1384	1617	371
Sc	37	43	45	30	29	36	40	45	10
La	103	110	120	105	109	122	127	133	35
Ce	215	230	250	196	196	228	244	260	72
Nd	86	95	99	99	98	111	117	124	33
Quartz	6.7	4.2	2.3	13.4	13.6	9.7	8.7	6.5	
Mullite	25.2	28.9	31.2	33.7	33.3	36.1	38.5	38.2	
Glass	65.0	64.6	65.0	45.7	45.5	46.7	46.6	48.2	
Hematite				.4	.4	1.1	.6	.6	
Spinel	1.7	1.2	.8	3.5	3.6	3.3	2.5	2.6	
Calcite	-0.1	-0.1	-0.1	-0.1	-0.1	-0.1	-0.1	-0.1	
Portlandite				.4	.6	.5	.2	.1	
Lime (meas)	.9	.6		.1	.3	.5	.3	.8	
Lime (corr)	.9	.6		.4	.8	.9	.4	.9	

Table 5.1 : (Continued)

	D4_PFA1	D4_PFA2	D4_PFA3	D4_PFA4	D5_COAL	D5_PFA1	D5_PFA2	D5_PFA3	D5_PFA4
SiO_2	47.08	48.45	45.88	45.09	13.50	51.30	46.89	44.86	43.66
TiO_2	1.19	1.42	1.63	1.69	.47	1.59	1.81	1.82	1.82
Al_2O_3	23.83	28.84	30.90	31.09	7.65	28.26	32.92	32.99	32.51
Fe_2O_3	7.97	5.87	5.69	5.32		7.29	5.92	5.19	5.00
FeO					.92				
MgO	.58	.52	.66	.75	.12	1.24	1.24	1.24	1.26
CaO	7.90	6.71	6.38	5.69	1.10	7.77	7.12	6.95	6.84
Na_2O	.04	.05	.06	.07	.01	.05	.06	.06	.06
K_2O	.51	.62	.63	.67	.17	.60	.74	.80	.83
P_2O_5	.90	.97	1.35	1.67	.13	1.08	1.53	1.90	2.28
SO_3	.32	.38	.95	1.58		.50	1.23	1.34	1.21
S					1.18				
H_2O^-	.78	.29	.32	.50		.17	.23	.20	.29
LOI	7.13	6.58	6.12	6.67	73.75	2.03	2.64	3.93	5.17
TOTAL	98.24	100.71	100.58	100.76	99.89	101.87	102.32	101.29	100.93
Rb	28	36	38	41	12	34	43	47	48
Sr	784	1028	1276	1393	281	1301	1790	1967	2042
Y	58	76	89	96	21	96	123	128	129
Zr	400	517	531	521	145	545	588	577	562
Nb	31	42	48	50	11	45	54	54	54
Mo	4	8	16	24	2	7	15	20	26
U	8	8	13	14	4	9	13	14	18
Th	29	38	51	56	12	41	55	60	62
Pb	22	49	94	126	38	49	99	121	141
As	3	13	31	53	4	8	28	36	45
Se	2	2	5	10	.6	<.9	2	3	4
Bi	<3.0	<3.2	5	11	<1.6	3	5	10	11
Ge	1	3	10	17	2	1	9	13	16
W	6	7	12	14	4	6	8	12	16
Ga	21	35	66	96	15	36	71	89	109
Br	<1.1	4	<1.1	2	.6	<1.2	<1.2	<1.2	<1.2
Zn	29	43	82	110	20	47	89	109	135
Cu	41	47	57	61	18	45	61	64	65
Ni	60	64	91	105	22	57	80	84	94
Mn	350	308	314	327	63	361	331	328	332
Cs									
Co	20	27	41	52	9	27	43	51	57
Cr	139	161	199	219	54	206	265	289	296
V	117	134	159	210	59	174	247	306	346
Ba	660	854	1062	1233	349	967	1346	1460	1546
Sc	22	28	36	40	10	30	40	44	46
La	72	92	114	120	32	106	139	148	150
Ce	157	192	236	251	65	229	299	322	326
Nd	74	89	103	112	29	107	139	146	146
Quartz	13.2	11.6	8.0	7.3		16.0	7.3	4.9	3.8
Mullite	19.1	30.8	32.5	34.9		26.3	34.8	35.3	34.6
Glass	52.3	44.6	46.7	47.6		47.6	49.8	50.7	51.0
Hematite	.7	.6	1.0	.7		.8	1.1	1.1	.9
Spinel	5.1	4.3	4.0	2.4		5.1	3.6	3.2	3.4
Calcite	.1	-0.1	-0.1	-0.3		-0.1	-0.1	-0.1	-0.2
Portlandite	1.2	.9	.1	.1		.6	.2		
Lime (meas)	1.2	.7	1.7	.7		1.6	.6	.9	1.3
Lime (corr)	2.2	1.4	1.8	.8		2.1	.8	.9	1.3

Table 5.1 : (Continued)

	D6_PF	D6_PFA1	D6_PFA2	D6_PFA3	D6_PFA4	D3_COAL	D3_COMP	D3_PFA1	D3_PFA2
SiO_2	13.23	51.72	53.03	51.21	53.59	12.01	45.66	50.40	45.16
TiO_2	.41	1.43	1.42	1.39	1.42	.41	1.54	1.42	1.51
Al_2O_3	7.69	27.33	25.37	26.46	26.89	7.57	28.15	27.01	27.96
Fe_2O_3		5.62	7.22	5.76	5.90		5.18	4.99	5.08
FeO	1.35					.98			
MgO	.25	.90	.96	.85	.88	.10	2.77	2.36	2.74
CaO	1.51	5.52	6.92	5.68	5.91	1.81	10.73	9.19	10.58
Na_2O	<.02	.05	.04	.04	.04	.02	.49	.42	.47
K_2O	.16	.51	.49	.50	.50	.16	1.11	1.09	1.10
P_2O_5	.22	.63	.72	.62	.63	.84	1.69	.96	1.50
SO_3		.34	.32	.29	.31		1.68	.84	1.43
S	1.50					.67			
H_2O^-		.08	.87	.09	.03		.14	.08	.10
LOI	75.00	5.70	2.14	7.68	4.87	75.00	1.23	1.06	1.30
TOTAL	102.20	99.85	99.49	100.59	100.97	99.61	100.35	99.82	98.92
Rb	9	32	30	31	30	16	64	62	65
Sr	256	828	851	799	802	571	3315	2648	3223
Y	18	59	58	58	58	18	84	76	86
Zr	127	458	506	468	473	118	490	510	490
Nb	10	36	35	35	35	10	51	46	51
Mo	2	6	5	6	5	1	20	11	20
U	3	7	5	7	6	3	8	6	7
Th	11	37	33	35	35	9	47	39	44
Pb	16	46	34	40	38	9	60	37	56
As	3	6	4	4	5	1	17	9	17
Se	.8	1	1	1	<.9	<.4	9	4	7
Bi	2	<3.0	<3.2	<3.0	<3.1	<1.4	8	<3.4	10
Ge	1	1	<1.0	<1.0	<1.0	1	14	6	13
W	4	9	8	5	8	<2.1	14	6	11
Ga	12	29	24	27	27	12	81	50	77
Br	.9	<1.6	<1.7	<1.6	<1.6	<.5	<1.2	<1.2	<1.2
Zn	14	33	30	30	30	13	52	29	51
Cu	14	37	34	35	34	9	58	51	63
Ni	17	52	48	47	45	12	63	52	66
Mn	96	333	390	338	343	82	409	304	367
Cs									
Co	8	22	19	19	22	6	34	19	29
Cr	52	164	154	154	155	46	199	147	188
V	47	103	101	98	98	39	176	107	156
Ba	364	900	886	853	866	600	2337	1948	2274
Sc	8	24	22	22	23	9	36	31	36
La	34	82	72	78	77	31	107	96	109
Ce	64	168	159	160	158	64	232	201	228
Nd	29	69	66	66	66	29	105	88	102
Quartz		17.6	21.5	17.1	18.6		4.8	9.6	5.2
Mullite		30.7	24.6	26.5	27.0		15.4	20.1	18.2
Glass		40.5	43.6	43.7	43.1		71.8	62.2	67.4
Hematite		.2	1.0	.1	.6		.7	.7	1.0
Spinel		3.9	5.1	3.3	4.4		2.4	2.9	2.5
Calcite		.0	.1	.1	-0.1			-0.1	
Portlandite		.7	1.1	.8	.4		.3	.6	.9
Lime (meas)		.6	.7	.6	1.1		3.4	2.9	3.3
Lime (corr)		1.2	1.6	1.2	1.4		3.6	3.3	4.0

Table 5.1 : (Continued)

	D3_PFA3	D3_PFA4	D2_COAL	D2_PFA1	D2_PFA2	D2_PFA3	D2_PFA4	M2_PF	M2_PFA1
SiO_2	43.84	43.76	12.18	51.45	49.79	48.02	46.95	13.14	49.42
TiO_2	1.57	1.65	.41	1.49	1.63	1.68	1.71	.37	1.22
Al_2O_3	28.41	29.42	7.20	28.76	30.45	31.10	31.14	7.78	26.50
Fe_2O_3	5.37	4.84		4.07	3.88	4.10	4.09		5.45
FeO			.60					1.16	
MgO	3.07	2.89	.54	1.94	2.10	2.13	2.14	.54	1.79
CaO	11.98	10.67	2.39	7.83	7.80	7.23	7.32	2.08	7.49
Na_2O	.49	.50	.11	.36	.46	.49	.48	.10	.31
K_2O	1.09	1.09	.21	.89	.97	1.11	1.12	.24	.88
P_2O_5	1.86	2.29	.13	.87	1.31	1.92	2.30	.24	.59
SO_3	1.68	1.93	1.75	.94	1.34	2.00	1.98		.33
S			.70					1.56	
H_2O^-	.11	.15		.10	.09	.17	.22		.21
LOI	1.40	.97	72.50	1.10	.93	.60	.63	72.59	6.64
TOTAL	100.87	100.15	97.43	99.79	100.76	100.55	100.07	100.97	100.82
Rb	63	66	12	54	60	75	74	14	52
Sr	3573	3711	725	2423	2727	2918	3149	582	1850
Y	89	90	18	82	89	96	98	18	65
Zr	483	476	105	523	523	498	493	114	465
Nb	53	56	10	49	53	54	56	10	40
Mo	24	28	2	10	17	30	30	2	7
U	9	9	3	7	9	14	14	2	6
Th	50	51	11	45	50	59	61	11	36
Pb	67	81	23	41	69	108	118	100	26
As	18	23	1	9	17	30	30	3	6
Se	9	16	.8	2	5	10	15	.8	1
Bi	8	14	<1.5	5	10	14	17	<1.5	<3.2
Ge	15	20	.8	5	10	21	21	2	4
W	12	18	<2.2	7	12	19	22	3	6
Ga	86	106	12	48	77	119	129	12	33
Br	<1.3	<1.3	<.5	<1.2	<1.2	<1.2	<1.2	<.5	<1.1
Zn	60	74	7	29	50	94	117	9	17
Cu	68	68	10	49	60	73	80	13	31
Ni	71	74	13	49	64	81	86	14	41
Mn	416	422	80	256	285	320	356	91	325
Cs				11	11	13	13		
Co	32	39	6	17	25	35	37	6	16
Cr	204	210	43	151	187	220	213	43	115
V	180	225	39	110	149	213	239	38	80
Ba	2449	2708	628	1701	1924	2242	2509	605	1374
Sc	38	41	10	32	37	42	45	10	25
La	111	115	32	102	113	120	126	32	79
Ce	235	245	68	205	227	240	247	66	172
Nd	104	111	32	96	103	111	117	30	79
Quartz	3.9	2.8		12.4	7.7	6.6	4.3		8.9
Mullite	15.2	15.7		28.1	25.8	25.2	20.2		24.7
Glass	70.8	74.3		54.5	60.8	65.0	71.8		53.1
Hematite	.9	1.0		.9	.8	1.2	.7		.8
Spinel	2.8	2.2		2.0	1.6	.8	1.3		2.6
Calcite		-0.1		-0.1	-0.1	-0.2	-0.1		-0.1
Portlandite	.9	.3			.3	<.1	<.1		1.2
Lime (meas)	4.0	2.8		1.1	2.2	.9	1.2		2.1
Lime (corr)	4.6	3.0		1.1	2.4	.8	1.1		3.0

Table 5.1 : (Continued)

	M2_PFA2	M2_PFA3	M2_PFA4	M4_PF	M5_COAL	M5_PFA1	M5_PFA2	M5_PFA3	M5_PFA4
SiO_2	44.96	42.35	44.56	12.97	12.66	52.24	48.41	47.32	48.63
TiO_2	1.59	1.43	1.60	.40	.38	1.50	1.55	1.59	1.65
Al_2O_3	29.26	27.87	30.43	7.78	7.30	29.68	29.68	29.95	31.11
Fe_2O_3	4.93	5.05	5.00			4.15	4.72	4.65	4.25
FeO				.87	.95				
MgO	2.21	2.19	2.35	.54	.56	2.06	2.26	2.41	2.29
CaO	7.97	7.92	8.41	2.20	2.14	7.01	8.02	8.77	7.55
Na_2O	.48	.43	.51	.09	.09	.39	.47	.47	.52
K_2O	.87	.89	.98	.20	.23	.89	.91	.91	.97
P_2O_5	1.27	1.34	1.84	.25	.25	.73	1.11	1.22	1.47
SO_3	1.03	1.10	1.38			.95	1.24	1.43	1.68
S				1.40	1.48				
H_2O^-	.18	.30	.13			.17	.09	.17	.15
LOI	4.87	9.48	2.35	73.66	74.29	1.37	2.21	1.99	.87
TOTAL	99.63	100.34	99.53	101.63	101.62	101.14	100.66	100.89	101.14
Rb	63	59	65	11	14	55	55	54	66
Sr	2801	2706	3131	614	649	2260	2635	2810	2867
Y	88	84	93	18	18	80	84	87	81
Zr	514	474	509	122	113	530	514	515	465
Nb	50	48	55	10	10	48	50	52	49
Mo	20	20	27	2	2	11	16	18	26
U	9	10	10	3	3	7	9	10	10
Th	47	48	55	11	11	43	46	49	46
Pb	85	83	112	53	164	42	63	65	87
As	18	19	25	2	2	9	16	17	25
Se	4	5	10	.8	<.4	1.0	4	5	6
Bi	8	7	11	<1.4	<1.5	4	7	7	9
Ge	16	16	21	1	1	7	10	12	16
W	13	13	15	<2.1	4	10	11	14	16
Ga	78	77	104	12	11	48	69	75	87
Br	<1.2	2	<1.2	<.5	.7	<1.1	<1.2	<1.2	<1.2
Zn	50	57	84	7	8	27	44	46	59
Cu	49	49	62	14	15	47	57	58	62
Ni	60	63	75	13	13	51	63	65	69
Mn	368	373	418	90	91	272	335	352	349
Cs									
Co	33	33	40	5	5	22	31	31	36
Cr	171	173	191	47	42	151	176	181	194
V	139	147	190	40	38	108	142	150	184
Ba	1983	1945	2256	619	651	1731	1983	2058	2208
Sc	34	34	39	10	10	31	35	35	37
La	105	100	110	34	31	99	104	109	108
Ce	220	214	237	70	67	220	221	231	231
Nd	103	101	109	32	32	96	98	106	103
Quartz	7.0	3.3	3.4			10.6	7.4	6.7	6.2
Mullite	22.6	20.1	18.7			26.9	24.5	24.3	24.9
Glass	58.7	63.0	70.5			55.5	60.2	60.2	63.3
Hematite	.8	1.0	.8			.7	.8	.8	.8
Spinel	2.5	1.8	1.9			2.1	2.4	2.3	1.7
Calcite	-0.1	-0.1	-0.1			-0.1	-0.1	-0.1	-0.1
Portlandite	.5					.3	.5	.7	.3
Lime (meas)	3.1	1.4	2.5			2.6	1.9	3.2	2.1
Lime (corr)	3.5	1.4	2.5			2.8	2.3	3.8	2.3

Table 5.1 : (Continued)

	M6_PF	M6_LH1	M6_LH2	M6_LH3	M6_LH4	M6_RH1	M6_RH2	M6_RH3	M6_RH4
SiO_2	9.45	48.44	45.00	41.78	41.68	48.42	44.83	41.89	41.04
TiO_2	.27	1.39	1.52	1.59	1.60	1.36	1.51	1.62	1.65
Al_2O_3	5.38	28.06	28.87	28.67	28.84	26.57	28.31	28.44	28.63
Fe_2O_3		5.20	5.29	5.60	5.85	6.10	5.82	6.13	5.66
FeO	.98								
MgO	.50	2.48	2.72	2.92	3.04	2.62	2.94	3.07	3.01
CaO	1.99	9.51	10.16	10.75	11.15	10.64	10.87	11.12	10.82
Na_2O	.11	.59	.69	.70	.70	.52	.71	.74	.76
K_2O	.17	.88	.91	.87	.88	.93	.91	.90	.89
P_2O_5	.22	1.06	1.59	2.23	2.38	.97	1.48	2.23	2.77
SO_3		1.26	1.90	2.47	2.52	1.18	1.81	2.74	3.30
S	1.57								
H_2O^-			.05	.20	.15	<.06		.08	.10
LOI	80.19	1.79	1.68	2.69	2.26	1.46	1.37	1.18	1.28
TOTAL	102.21	100.65	100.37	100.46	101.04	100.71	100.56	100.12	99.91
Rb	11	52	53	53	53	57	58	61	62
Sr	606	2880	3439	3806	3902	2841	3420	3903	4130
Y	15	76	83	87	87	72	79	85	88
Zr	95	473	479	468	471	469	470	479	474
Nb	8	40	45	49	49	40	46	50	52
Mo	3	16	24	34	36	16	24	36	42
U	2	4	5	8	7	3	5	8	9
Th	9	43	51	52	54	36	41	47	50
Pb	11	58	87	107	111	40	66	98	120
As	1	10	18	29	30	11	21	33	40
Se	.8	3	5	8	10	2	4	9	13
Bi	<1.4	5	7	11	13	<3.4	5	10	14
Ge	2	9	16	26	29	6	15	27	33
W	<2.1	8	10	16	15	8	11	21	20
Ga	9	42	64	87	89	36	61	90	107
Br	1.0	<1.7	<1.8	<1.8	<1.8	<1.3	<1.3	<1.3	<1.3
Zn	7	28	45	66	68	24	40	66	85
Cu	11	45	59	65	67	45	58	71	75
Ni	11	52	67	77	79	83	70	98	93
Mn	100	396	457	519	531	421	463	537	574
Cs									
Co	6	28	41	47	48	25	37	48	58
Cr	32	142	171	193	199	133	168	201	205
V	30	102	144	196	199	91	135	195	240
Ba	629	2071	2467	2755	2784	1912	2410	2757	2978
Sc	6	30	35	39	38	27	34	38	41
La	27	98	113	112	112	97	103	109	117
Ce	53	204	233	235	236	199	216	231	233
Nd	24	89	97	101	99	95	102	109	112
Quartz		9.0	5.8	2.9	2.9	11.2	5.8	2.9	2.5
Mullite		25.4	22.5	16.4	15.6	22.3	20.8	19.3	16.3
Glass		55.5	62.0	70.3	71.3	55.2	62.8	68.7	75.0
Hematite		1.1	1.3	1.2	1.3	1.6	1.5	1.5	1.1
Spinel		2.9	2.8	2.6	3.0	3.3	3.0	2.6	1.3
Calcite			-0.1	-0.1		-0.1	-0.1	-0.1	-0.2
Portlandite		1.2	.2	.1		1.1	.3	1.0	.4
Lime (meas)		3.3	3.8	3.8	3.8	3.8	4.5	3.0	2.3
Lime (corr)		4.2	4.0	3.9	3.8	4.6	4.8	3.7	2.6

5.2.2 **Table 5.2 : Major and minor oxide concentrations in PFA glass by electron microprobe analysis.**

	L1_PFA1	L1_PFA1	L1_PFA1	L1_PFA1	L1_PFA1	L1_PFA1	L1_PFA1	L1_PFA1	L1_PFA1
SiO_2	45.0	57.9	42.8	54.2	51.1	51.0	49.8	52.2	52.5
TiO_2	1.0	.3	.8	4.4	4.1	4.1	2.0	2.9	1.7
Al_2O_3	34.8	37.6	33.5	34.8	37.9	36.8	35.9	37.2	37.7
MnO			.1						
MgO	1.5	.2	1.5	.8	1.2	1.7	2.7	1.1	1.7
CaO	8.2	.5	18.2	1.8	3.7	4.0	6.7	4.6	4.1
Na_2O	.2	.3	.2	.2	.2	1.0	.2	.1	.4
K_2O	.2	.6	.2	.4	.4	.5	.6	.3	.5
Fe_2O_3	11.0	4.4	.9	2.8	2.0	2.2	2.5	2.0	1.9
P_2O_5	.3		.6	.1	.1	.2	.3	.2	.4
SrO			.3						
BaO									.3
TOTAL	102.3	101.7	99.2	99.7	100.7	101.5	100.8	100.6	101.2

	L1_PFA1	L1_PFA1	L1_PFA1	L1_PFA1	L1_PFA1	L1_PFA1	L1_PFA1	L1_PFA1	L1_PFA1
SiO_2	53.1	46.0	46.7	52.0	50.1	50.0	71.2	53.3	44.5
TiO_2	2.9	1.0	2.2	2.0	7.1	1.7	.8	.7	2.3
Al_2O_3	38.0	41.5	38.0	38.3	36.5	35.5	23.1	39.8	36.4
MnO									
MgO	1.1	1.8	2.3	1.2	1.1	.6	1.3	1.0	3.2
CaO	3.8	5.5	7.5	4.0	3.2	11.7	4.1	3.7	11.0
Na_2O	.3	.1	.2	.4	.3	.1	.2	.2	.3
K_2O	.3	.1	.2	.5	.6	.2	.5	.3	.3
Fe_2O_3	1.7	1.7	4.5	1.9	2.0	1.4	1.3	1.1	2.1
P_2O_5	.3	.3	.2	.2	.2	.1		.6	.4
SrO		1.3							
BaO		.5							
TOTAL	101.4	99.8	101.8	100.5	101.1	101.4	102.3	100.7	100.4

	L1_PFA2	L1_PFA2	L1_PFA2	L1_PFA2	L1_PFA2	L1_PFA2	L1_PFA2	L1_PFA2	L1_PFA2
SiO_2	51.5	64.0	43.9	54.7	47.3	48.4	43.6	50.0	50.8
TiO_2	1.6	2.4	7.5	2.0	1.5	2.9	2.5	2.0	2.5
Al_2O_3	40.2	21.5	33.3	35.1	36.7	34.7	35.6	37.8	34.8
MnO					.1				
MgO	.5	1.8	1.1	1.3	2.3	.6	4.1	1.0	2.0
CaO	1.6	7.0	11.1	3.0	9.9	13.5	11.9	6.6	5.3
Na_2O	.2	.2	.2	.3	.2	.1	.1	.2	.2
K_2O	.6	.3	.8	.5	.2	.2	.2	.5	.3
Fe_2O_3	1.2	3.4	2.8	1.9	2.2	1.7	3.1	4.6	2.5
P_2O_5			.1		.5	.1	.3	.1	.2
SrO									
BaO									
TOTAL	97.5	100.6	100.9	98.7	100.9	102.1	101.5	102.6	98.5

	L1_PFA2	L1_PFA2	L1_PFA2	L1_PFA2	L1_PFA2	L1_PFA2	L1_PFA2	L1_PFA2	L1_PFA2
SiO_2	51.4	40.7	52.6	54.0	50.2	45.5	49.8	55.7	48.9
TiO_2	1.8	3.2	1.7	.3	1.4	1.3	1.6	1.7	1.5
Al_2O_3	45.5	38.2	38.8	43.7	41.0	32.3	31.5	34.7	35.6
MnO									.1
MgO	.3	1.5	1.2	.1	1.3	2.0	1.3	1.9	3.3
CaO	1.3	8.7	4.1	.1	4.9	7.2	16.4	5.1	2.9
Na_2O	.2	.2	.2	.1	.3	.2	.1	.2	.1
K_2O	.4	.2	.4	.1	.3	.2	.1	.5	.3
Fe_2O_3	.8	1.6	3.4	.5	1.0	3.5	.9	2.2	8.9
P_2O_5		2.5	.1		.6		.2	.1	.2
SrO		1.8							
BaO		.7				9.9			
TOTAL	101.7	99.3	102.5	98.9	101.1	102.2	101.8	102.1	101.9

Table 5.2 : (Continued)

	L1_PFA3	L1_PFA3	D1_PFA1	D1_PFA1	D1_PFA1	D1_PFA1	D1_PFA1	D1_PFA1	D1_PFA1
SiO_2	50.5	34.5	56.4	47.6	52.3	44.0	46.7	43.5	43.7
TiO_2	2.1	.8	1.1	11.6	2.2	5.3	1.4	1.3	2.0
Al_2O_3	37.9	32.8	25.0	36.8	33.2	29.0	25.8	27.9	35.3
MnO			.2						
MgO	1.3	.9	1.5	.5	2.9	.2	2.1	2.3	.8
CaO	5.2	14.1	.7	.7	.7	3.7	20.3	17.4	7.2
Na_2O	.3	.1	.1	.1	.1		.1		.1
K_2O	.5	.1	1.5	.8	2.6	.2	.2	.3	.3
Fe_2O_3	1.6	1.6	11.4	.8	6.2	16.5	2.8	8.6	7.1
P_2O_5	.5	8.9	.2	.3		2.5	1.6	.3	2.5
SrO		2.2							.5
BaO		1.7							.4
TOTAL	99.9	97.8	98.1	99.1	100.2	101.3	101.1	101.6	99.7

	D1_PFA1	D1_PFA1	D1_PFA1	D1_PFA1	D1_PFA1	D1_PFA1	D1_PFA1	D1_PFA1	D1_PFA1
SiO_2	52.9	46.6	48.6	48.0	98.6	39.7	51.5	40.0	55.4
TiO_2	1.0	1.2	.9	2.7		2.2	1.7	.6	1.5
Al_2O_3	21.7	29.6	36.5	34.4	1.1	25.9	39.2	28.9	27.8
MnO									
MgO	.7	4.4	.2	.5		5.3	1.7	.6	.7
CaO	2.6	12.6	7.2	10.8	.1	22.7	3.2	26.6	7.6
Na_2O	.1	.1	.1	.1			.1	.2	.1
K_2O	4.4	.7	.9	.6	.1	.2	.5	.2	.4
Fe_2O_3	17.7	3.9	1.0	1.6		2.5	2.5	1.1	6.1
P_2O_5	.4	.3	2.1	1.9		1.5	.4	2.8	.6
SrO									
BaO									
TOTAL	101.5	99.3	97.4	100.5	99.9	100.0	100.7	100.9	100.1

	D1_PFA1	D1_PFA1	D1_PFA1	D1_PFA1	D1_PFA1	D1_PFA1	D1_PFA3	D1_PFA3	D1_PFA3
SiO_2	82.6	31.0	47.5	44.8	42.9	36.7	22.1	32.1	42.9
TiO_2	.7	.7	1.8	1.6	1.2	.9	2.4	1.1	1.6
Al_2O_3	9.5	20.4	32.8	34.9	31.5	24.0	22.6	26.0	29.8
MnO			.1						
MgO	.7	2.1	.7	.2	5.1	.8	.3	4.4	1.7
CaO	.3	37.1	15.6	12.2	17.2	13.4	29.2	32.5	11.5
Na_2O	.1							.1	.1
K_2O	1.8	.1	.3	.1	.5	.1			.5
Fe_2O_3	3.9	1.8	.8	.5	1.4	13.7	.9	1.5	2.0
P_2O_5	.2	7.0	.3	7.3	.6	7.3	20.2	2.2	7.2
SrO				.3			2.1		2.5
BaO							1.3		1.7
TOTAL	99.8	100.2	100.1	101.9	100.3	97.0	101.1	99.9	101.5

	D1_PFA3	D1_PFA3	D1_PFA3	D1_PFA3	D1_PFA3	D1_PFA3	D1_PFA3	D1_PFA3	D1_PFA3
SiO_2	57.6	33.7	32.6	32.6	98.6	99.8	42.5	98.6	47.8
TiO_2	2.8	.7	.4	3.3	.2	.1	2.3		10.1
Al_2O_3	29.1	28.1	24.6	31.8	1.6	.6	27.7	.1	31.5
MnO			.2						
MgO	.8	.3	10.3	.7	.1		.4	.2	.8
CaO	4.7	22.9	26.1	13.0	.3		6.5	2.6	3.5
Na_2O	.1			.1			.1		
K_2O	.6		.1	.2	.1		.3		.3
Fe_2O_3	1.5	.7	5.5	1.6	.2		20.4		5.1
P_2O_5	1.5	12.7	1.4	10.6			2.3		.4
SrO	.7	.3		4.2					
BaO	.7			1.4					.4
TOTAL	100.2	99.5	101.1	99.4	101.0	100.5	102.5	101.5	99.9

Table 5.2 : (Continued)

	D1_PFA3	D1_PFA3	D1_PFA3	D1_PFA3	D1_PFA3	D1_PFA3	D1_PFA4	D1_PFA4	D1_PFA4
SiO_2	88.4	34.5	48.7	33.5	98.0	44.4	33.5	29.1	50.2
TiO_2	.3	.9	4.7	.7		1.4	1.9	.2	7.5
Al_2O_3	4.6	28.3	27.8	26.3	1.7	33.0	32.0	24.4	31.4
MnO				.3				.2	
MgO	.1	.5	.5	2.0		1.0	.3	4.2	.9
CaO	1.2	26.6	1.4	35.9	.1	16.9	17.1	38.9	6.8
Na_2O						.1	.1	.1	.1
K_2O	.1		.8		.7	.3	.1		.6
Fe_2O_3	7.4	.7	15.3	2.0	.4	.7	2.1	.7	1.1
P_2O_5		6.8	.2	.3		1.5	10.3	2.3	.2
SrO		.6					1.5	.4	
BaO		.6					.8		
TOTAL	102.0	99.6	99.5	101.1	100.8	99.3	99.8	100.4	98.8

	D1_PFA4	D1_PFA4	D1_PFA4	D1_PFA4	D1_PFA4	D1_PFA4	D1_PFA4	D1_PFA4	D1_PFA4
SiO_2	40.7	43.1	23.6	29.5	56.3	42.7	38.6	48.2	45.7
TiO_2	1.8	1.0	.4	.3	.9	2.0	1.2	.8	1.3
Al_2O_3	28.7	32.6	16.7	23.2	15.9	33.6	22.8	27.7	33.7
MnO	.2		.2				.1		
MgO	3.1	1.3	5.5	12.4	1.6	2.1	4.7	2.4	.4
CaO	21.2	19.0	37.9	29.9	17.2	14.1	21.4	19.0	10.1
Na_2O	.1	.1		.1	.1		.1	.1	.1
K_2O	.5	.2	.1		.1	.1	.3	.4	.6
Fe_2O_3	3.5	1.4	14.8	2.4	1.0	1.5	7.7	.9	1.0
P_2O_5	.2	.6	.7	1.9	6.8	3.0	3.4	.2	5.7
SrO		.3							
BaO		.5							
TOTAL	100.0	100.1	99.9	99.6	99.9	98.9	100.3	99.7	98.6

	D1_PFA4	D1_PFA4	D1_PFA4	D1_PFA4	M2_PFA1	M2_PFA1	M2_PFA1	M2_PFA1	M2_PFA1
SiO_2	42.7	47.9	83.9	38.6	66.7	50.3	51.3	53.7	55.3
TiO_2	1.1	1.3	1.1	1.3		.9	1.7	1.2	.5
Al_2O_3	29.4	36.6	11.0	20.7	19.1	36.9	38.4	40.5	17.6
MnO	.2								
MgO	3.2	.7	.5	.3		2.8	1.1	.5	1.3
CaO	20.1	7.0	2.0	5.0	.2	4.9	2.7	.4	22.9
Na_2O	.1	.1	.1	.1	1.2	.4	.3	.7	.1
K_2O	.4	.6	.4	.1	12.7	.5	.5	1.1	.6
Fe_2O_3	1.1	1.4	1.9	33.7		.9	3.7	1.3	1.2
P_2O_5	.7	3.6		1.5		.6	.2		.4
SrO									
BaO	.3				.3				
TOTAL	99.3	99.1	100.9	101.3	100.2	98.2	99.8	99.4	99.9

	M2_PFA1	M2_PFA_	M2_PFA1	M2_PFA1	M2_PFA1	M2_PFA1	M2_PFA1	M2_PFA1	M2_PFA1
SiO_2	60.1	66.6	48.4	34.6	53.9	58.0	55.4	67.9	47.8
TiO_2	.2		4.6	.4	1.3	2.6	1.7		3.9
Al_2O_3	32.3	18.1	37.6	28.2	36.0	29.3	28.9	19.1	39.9
MnO									
MgO	1.5	.1	2.0	5.7	1.5	2.5	2.6		.6
CaO	.7	.3	3.0	30.4	2.2	4.8	4.9	.1	4.1
Na_2O	.2	1.1	.4		.3	.4	.3	.5	.3
K_2O	3.1	11.7	.9		1.8	1.2	.6	11.3	.3
Fe_2O_3	2.7	.6	1.3	.5	1.2	1.0	4.3		1.0
P_2O_5			.2	.3	.3	.2	.2		.1
SrO									
BaO			.3		.5	.5		.3	
TOTAL	100.7	98.5	98.4	100.0	98.9	100.4	98.8	99.3	98.1

Table 5.2 : (Continued)

	M2_PFA1	M2_PFA1	M2_PFA1	M2_PFA1	M2_PFA1	M2_PFA1	M2_PFA1	M2_PFA1	M2_PFA1
SiO_2	54.5	48.8	34.5	71.9	46.6	51.6	54.0	48.7	51.4
TiO_2	3.2	1.2	1.1	1.0	1.0	2.8	2.4	7.2	1.3
Al_2O_3	35.0	30.4	23.1	21.2	38.0	17.5	31.3	36.7	40.9
MnO									
MgO	.7	4.3	.6	.6	.4	5.4	2.3	.6	.4
CaO	2.7	11.3	19.9	1.4	.9	20.9	4.8	1.9	.3
Na_2O	.4	.2	.2	.3	.6	.2	.4	.6	.5
K_2O	1.1	.9	.1	1.1	.8	.3	1.3	.8	1.0
Fe_2O_3	.9	1.8	19.4	.7	12.2	1.1	1.4	1.2	1.1
P_2O_5	.1	.2	1.9			.2	.5		
SrO								.3	
BaO					.5		.3	.5	
TOTAL	98.6	99.0	100.8	98.2	101.0	100.0	98.8	98.5	96.9

	M2_PFA1	M2_PFA2	M2_PFA2	M2_PFA2	M2_PFA2	M2_PFA2	M2_PFA2	M2_PFA2	M2_PFA2
SiO_2	52.9	47.6	48.4	41.2	52.2	49.1	52.4	56.7	51.2
TiO_2	.7	.8	.6	1.0	.9	1.0	2.2	.9	2.3
Al_2O_3	36.3	38.2	31.7	35.5	37.7	38.8	34.5	35.5	40.7
MnO									
MgO	1.1	3.4	4.4	.7	2.2	2.7	2.1	1.5	.5
CaO	5.1	7.6	12.8	11.3	4.5	7.4	3.7	.7	3.4
Na_2O	.3	.2	.2	.2	.5	.4	.6	.3	.3
K_2O	.4	.2	.5	.2	.4	.6	.8	2.5	.3
Fe_2O_3	1.2	2.0	1.1	10.5	.6	.4	2.6	3.3	.9
P_2O_5	.1	.2	.6	.3	.2	.2	.1		.2
SrO									
BaO									
TOTAL	98.2	100.0	100.4	100.9	99.2	100.7	99.1	101.3	99.7

	M2_PFA2	M2_PFA2	M2_PFA2	M2_PFA2	M2_PFA2	M2_PFA2	M2_PFA2	M2_PFA2	M2_PFA2
SiO_2	45.3	33.3	45.9	41.4	40.2	59.5	75.5	34.3	63.1
TiO_2	.9	.6	1.1	.6	.4	1.0	2.8	10.3	1.8
Al_2O_3	36.8	22.3	22.9	41.3	24.3	35.6	17.3	37.4	29.7
MnO		.2							
MgO	2.0	11.6	3.6	1.0	7.2	.5	.7	1.3	1.5
CaO	11.6	29.8	19.8	5.0	23.4	.3	.5	10.7	1.7
Na_2O	.2	.1		.2	.1	.5	.3	.1	.2
K_2O	.1	.0		.3	.0	.9	1.6	.1	2.4
Fe_2O_3	1.1	1.6	1.0	1.6	1.0	1.1	1.0	1.1	1.2
P_2O_5	.5	.3	3.4		3.4			.3	.1
SrO		.3	2.2	5.0	1.0			1.0	
BaO			1.1	3.4	.5			1.4	.3
TOTAL	98.6	100.3	100.9	99.8	101.6	99.4	99.6	97.9	101.9

	M2_PFA2	M2_PFA2	M2_PFA2	M2_PFA2	M2_PFA3	M2_PFA3	M2_PFA3	M2_PFA3	M2_PFA3
SiO_2	34.1	51.2	68.3	60.6	54.8	57.1	29.8	30.2	51.7
TiO_2	2.8	.9	.1	.7	.5	.2	.4	.4	3.4
Al_2O_3	24.4	39.2	19.1	26.4	36.8	37.6	13.1	13.1	38.5
MnO							.2	.2	
MgO	9.2	.6	.3	2.7	1.6	.3	12.0	12.1	1.1
CaO	24.4	1.6	.8	.8	1.3	2.4	41.4	43.6	.4
Na_2O		.5	.8	.4	.5	.7	.1		.6
K_2O		1.7	10.0	3.1	2.3	1.0			1.3
Fe_2O_3	1.3	1.8	.4	5.1	2.0	1.2	.6	.7	3.1
P_2O_5	1.5			.1	.3		1.2	1.1	.1
SrO	.9								
BaO	1.1		.3						
TOTAL	99.8	97.4	100.1	100.0	100.1	100.5	98.8	101.5	100.3

Table 5.2 : (Continued)

	M2_PFA3	M2_PFA3	M2_PFA3	M2_PFA3	M2_PFA3	M2_PFA3	M2_PFA3	M2_PFA3	M2_PFA3
SiO_2	30.9	35.8	50.1	56.6	24.0	51.7	48.2	53.5	59.1
TiO_2	1.4	.5	.8	.6	.2	2.0	.8	.6	.6
Al_2O_3	21.2	30.2	5.8	27.6	17.9	36.9	41.7	40.0	30.7
MnO	.2		.2		.3				
MgO	1.0	.5	11.0	2.2	8.5	1.2	.3	.5	2.0
CaO	42.8	33.3	31.2	.4	45.9	4.8	.6	1.9	.9
Na_2O		.1		.3		.5	.3	.6	.4
K_2O				4.8		.4	1.2	.9	2.7
Fe_2O_3	1.4	.4	1.0	5.7	1.3	1.9	2.0	1.0	4.0
P_2O_5	1.7	.7	.4	.1	.9		.6	.1	
SrO					.4		1.5		
BaO							.8		
TOTAL	100.6	101.5	100.5	98.4	99.5	99.4	98.0	99.2	100.3

	M2_PFA3	M2_PFA3	M2_PFA3	M2_PFA3	M2_PFA3	M2_PFA3	M2_PFA3	M2_PFA3	M2_PFA3
SiO_2	94.9	52.1	62.1	56.5	69.8	52.9	41.4	49.3	61.6
TiO_2	.2	4.3	.2	2.0		.7	3.2	2.1	1.1
Al_2O_3	2.4	39.4	17.5	34.2	19.8	40.3	37.1	48.7	21.5
MnO									
MgO	1.1	.7	1.1	1.0	.1	.3	4.6	.2	1.1
CaO	2.6	.4	16.2	1.5	.4	.5	10.6	.2	4.3
Na_2O	.1	.3	.2	.4	.6	.4	.2	.1	.3
K_2O	.2	1.3	.9	1.3	8.9	1.4	.2	.7	1.2
Fe_2O_3	.2	.7	2.6	1.0	.5	1.6	1.5	.6	.3
P_2O_5		.1		.1			.2		4.4
SrO							1.0		2.5
BaO				.3			.6		.8
TOTAL	101.6	99.4	100.8	98.5	100.1	98.2	100.6	101.8	99.1

	M2_PFA3	M2_PFA3	M2_PFA3	M2_PFA3	M2_PFA3	M2_PFA4	M2_PFA4	M2_PFA4	M2_PFA4
SiO_2	21.0	55.9	48.9	71.4	47.4	45.2	57.9	40.5	97.5
TiO_2	.1	3.5	.7	3.1	3.5	1.0	1.8	3.6	.5
Al_2O_3	21.3	32.0	24.3	22.4	42.1	17.4	35.9	37.8	.2
MnO								.2	
MgO	.2	1.0	1.7	.5	.4	11.9	.8	4.8	.3
CaO	32.3	3.7	18.9	.4	1.6	21.7	1.2	9.2	.1
Na_2O		.4	.1	.4	.3	.1	.5	.6	.1
K_2O		.7	.4	.9	.3		1.2	.2	.1
Fe_2O_3	.3	1.7	3.4	.7	2.2	3.2	.7	.8	.2
P_2O_5	22.4	.5		.2		.6	.1	.7	
SrO	.8	.4			1.0			1.6	
BaO	1.6	.5			.7			.8	
TOTAL	99.8	100.3	98.5	99.9	99.5	101.1	100.1	100.8	98.9

	M2_PFA4	M2_PFA4	M2_PFA4	M2_PFA4	M2_PFA4	M2_PFA4	M2_PFA4	M2_PFA4	M2_PFA4
SiO_2	48.5	49.0	46.8	53.9	66.6	41.4	58.6	46.7	55.5
TiO_2	1.1	2.7	1.2	2.1		1.2	.1	1.4	2.6
Al_2O_3	23.6	22.4	38.3	40.2	24.0	8.8	34.3	31.8	33.1
MnO						.2		.1	
MgO	6.9	9.3	1.9	.8	.5	12.3	1.4	6.7	1.8
CaO	18.7	16.3	4.7	1.2	3.3	34.4	.7	12.7	2.8
Na_2O	.1	.1	.5	.4	2.2	.2	.5	.4	.6
K_2O	.2	.1	.6	.8	1.0	.1	2.5	.2	1.5
Fe_2O_3	1.1	.7	6.7	.9	2.0	1.9	3.4	.6	2.4
P_2O_5	.5	.4	.1	.2		.6		.2	.2
SrO									
BaO									
TOTAL	100.7	100.9	100.7	100.5	99.6	101.0	101.6	100.8	100.4

Table 5.2 : (Continued)

	M2_PFA4	M2_PFA4	M2_PFA4	M2_PFA4	M2_PFA4	M2_PFA4	M2_PFA4	M2_PFA4
SiO_2	64.3	49.1	48.1	47.1	44.8	70.2	70.7	39.5
TiO_2		.3	2.0	.8	1.4			4.7
Al_2O_3	19.0	37.0	33.1	31.1	21.3	20.7	19.7	29.0
MnO				.2				
MgO		.7	4.1	5.8	.7	.1	.7	.7
CaO	.1	4.7	9.7	10.4	31.0	.2	2.3	17.9
Na_2O	.6	.6	.2	.3	.1	.4	.6	.1
K_2O	11.9	5.3	.2	.5	.1	8.7	5.3	
Fe_2O_3		2.8	.6	1.8	1.1	.4	.7	.6
P_2O_5			.7	1.1	1.5			2.0
SrO			1.3					3.8
BaO	2.5	.5	.7					1.8
TOTAL	98.4	101.0	100.7	99.1	101.9	100.6	100.0	100.0

5.2.3 **Table 5.3 : Major and minor oxide concentrations in PFA Fe oxides by electron microprobe analysis.**

	D5_PFA1	D5_PFA1	D5_PFA1	D5_PFA1	D5_PFA1	D5_PFA1	D5_PFA1	D5_PFA1	D5_PFA1
SiO_2	1.2	.1	.2	.1	.1	.1	.2		.1
TiO_2	.3	.2					.1		.1
Al_2O_3	10.1	4.3	3.7	4.4	1.1	7.8	7.9	1.9	8.4
Cr_2O_3									
FeO	9.1	27.6	31.5	19.0	30.8	19.2	71.5	18.3	.3
Fe_2O_3	66.3	65.8	65.3	70.3	67.8	65.5		71.3	70.6
MnO	.6			.7		.5	.4	.8	.5
MgO	15.1	2.9	.1	8.1		8.2	14.5	5.7	19.6
CaO	1.5	.2	.1	.2	.1	.2	2.3	2.5	1.5
TOTAL	101.1	101.2	100.8	102.8	99.9	101.5	97.0	100.5	101.1

	D5_PFA1	D5_PFA1*	D5_PFA1	D5_PFA1	D5_PFA1	D5_PFA1	D5_PFA1	D5_PFA1	D5_PFA1
SiO_2	.1	6.3	.1	.7			.3	.1	.1
TiO_2	.2	.3	.3	.5			.1	.2	.1
Al_2O_3	3.7	3.6	8.1	16.9	4.0	2.5	1.1	7.2	1.8
Cr_2O_3				.1					
FeO	16.3		23.0	15.4		2.4	31.7	32.0	31.6
Fe_2O_3	70.3	45.8	63.1	53.7	76.8	76.8	68.4	61.3	67.3
MnO	.4			.4	.6	.6			
MgO	9.7	3.1	5.8	12.2	18.8	17.1		.4	.1
CaO	.6	37.8	.3	1.0	2.5	1.7	.1	.1	.1
TOTAL	101.4	97.0	100.7	101.0	102.7	101.1	101.7	101.2	101.0

	D5_PFA1	D5_PFA1	D5_PFA1	D5_PFA1	D5_PFA1	D5_PFA1	D5_PFA1	D5_PFA1	D5_PFA1
SiO_2			1.6	.6	1.9	.6	.2	.3	
TiO_2				.2	.2		.2	.4	.3
Al_2O_3	3.9	2.3	1.7	19.9	9.0	.6	4.9	7.8	10.9
Cr_2O_3									
FeO	20.2	30.4	31.6	10.7	31.8	29.9	32.0	.1	.9
Fe_2O_3	69.6	67.6	64.3	53.6	55.2	68.1	63.1	70.3	68.7
MnO	.7			.6				.6	.4
MgO	6.7	.2	.4	14.6	1.6	.1	.2	20.2	20.1
CaO	.2	.5	.6	1.6	.3	1.5	.1	1.4	1.0
TOTAL	101.3	101.0	100.2	101.8	99.9	100.8	100.7	101.1	102.3

	D5_PFA1	L1_PFA1	L1_PFA1	L1_PFA1	L1_PFA1	L1_PFA1	L1_PFA1	L1_PFA1	L1_PFA1
SiO_2	.7	.6	1.8	3.6	.1	.1		1.7	.2
TiO_2	.5	.4	.4	.4		.3	.1	.6	.2
Al_2O_3	16.2	11.0	8.8	9.8	4.9	10.4	5.9	15.0	3.7
Cr_2O_3		.1			.1				
FeO	26.3	33.2	34.6	36.6	19.7		89.1	32.5	
Fe_2O_3	50.5	53.4	54.7	51.1	66.8	89.8		47.5	97.1
MnO	.2								
MgO	5.0	.3	.4	.9	5.8	.3	4.4	2.0	.1
CaO	.5	.1	.2	.4	1.8	.1	.5	.3	.1
TOTAL	99.9	99.1	100.0	102.9	99.3	101.0	100.1	99.6	101.4

	M5_PFA1	M5_PFA1	M5_PFA1	M5_PFA1	M5_PFA1	M5_PFA1	M5_PFA1	M5_PFA1	M5_PFA1
SiO_2		.1	.1	3.4		.2		.6	.1
TiO_2		.2	.1	.5	.1		.2	.1	
Al_2O_3	1.4	8.9	2.2	7.7	3.1	.2	4.2	1.3	.7
Cr_2O_3									
FeO	30.5	32.6	30.7	35.5			31.1	31.2	30.1
Fe_2O_3	68.5	58.1	66.6	50.7	97.9	102.3	63.9	64.9	67.3
MnO									
MgO		.2	.4	.7			.1	.1	.1
CaO			.2	.1		.1		.1	.1
TOTAL	100.3	100.0	100.3	98.5	101.1	102.8	99.4	98.4	98.5

* = excluded from discussion

Table 5.3 : (Continued)

	M5_PFA1	M5_PFA1	M5_PFA1	M5_PFA1	M5_PFA1	M5_PFA1	M5_PFA1	M5_PFA1	M5_PFA1
SiO_2		.3		.4	1.8	.6	3.7	.3	.2
TiO_2					.1	.2	.4		.4
Al_2O_3	2.4	8.6	.5	.3	3.3	8.1	9.8	.7	8.4
Cr_2O_3						.1			
FeO	30.3	32.1		30.6	32.5	.3	35.3	30.8	29.1
Fe_2O_3	66.9	57.7	93.8	67.4	59.5	91.5	49.3	68.3	60.0
MnO									
MgO		.1	1.6		.3	.3	1.6	.1	2.0
CaO	.1	.2	3.8	.1	.2	.1	.2		.2
TOTAL	99.7	99.1	99.6	98.7	97.7	101.2	100.3	100.1	100.3

	M5_PFA1	M5_PFA1	M5_PFA1	M5_PFA1	M5_PFA1	M5_PFA1
SiO_2	.1	.3	.2	.1	10.9	.2
TiO_2	.3	.1	.2	.1	.1	.2
Al_2O_3	6.4	2.1	4.5	4.5	6.8	7.7
Cr_2O_3						
FeO	31.3	31.6	30.5	26.5	41.5	20.0
Fe_2O_3	61.7	65.4	63.7	65.7	34.5	63.9
MnO					1.3	
MgO	.5	.1	.8	3.1	1.8	7.9
CaO	.2			.5	.2	.3
TOTAL	100.4	99.6	99.8	100.5	97.0	100.2

5.2.4 **Table 5.4 : Particle size distributions expressed as cumulative weight percent.**

Duvha (1):

diameter μm	cumulative weight %	diameter μm	cumulative weight %		
	field 1		field 2	field 3	field 4
564.0	0.0	564	0.0		
261.6	4.4	261.6	0.3	0.0	
160.4	22.5	160.4	1.9	0.2	
112.8	40.6	112.8	4.9	2.0	0.0
84.3	53.0	84.3	9.7	6.6	0.1
64.6	62.1	64.6	16.0	9.5	0.6
50.2	70.6	50.2	23.8	13.7	2.2
39.0	77.7	39.0	33.7	21.4	5.3
30.3	83.2	30.3	45.1	30.0	9.5
23.7	87.8	23.7	56.0	38.3	16.8
18.5	91.4	17.7	69.6	50.7	26.2
14.5	93.8	13.6	77.5	61.5	37.1
11.4	95.9	10.5	84.2	71.8	49.7
9.1	97.6	8.2	90.1	80.1	61.7
7.2	98.5	6.4	93.8	87.9	74.6
5.8	99.2	5.0	96.5	93.7	86.1
		3.9	98.3	96.3	92.5
		3.0	99.2	97.8	95.7
		2.4	99.9	99.5	98.5
		1.9	100.0	99.8	99.5
		1.5		100.0	99.7
		1.2			

Duvha (6):

diameter μm	cumulative weight %			
	field 1	field 2	field 3	field 4
564.0	0.0	0.0	0.0	0.0
261.6	3.0	4.9	2.9	5.5
160.4	10.7	22.9	15.2	19.7
112.8	21.3	44.6	34.3	35.7
84.3	33.7	62.0	50.4	49.7
64.6	46.4	74.3	61.7	60.4
50.2	57.8	83.7	71.9	69.5
39.0	67.3	89.7	80.0	77.7
30.3	75.6	93.6	85.5	83.8
23.7	82.3	95.9	89.6	88.3
18.5	87.0	97.2	92.7	91.7
14.5	90.3	97.9	94.4	93.9
11.4	93.0	98.5	95.9	95.7
9.1	95.2	99.0	97.2	97.1
7.2	96.8	99.3	98.1	98.1
5.8	98.2	99.6	98.9	99.0

Table 5.4 : (Continued)

Matla (2):

diameter μm	cumulative weight %		diameter μm	cumulative weight %	
	field 1	field 2		field 3	field 4
564.0			118.4	0.0	
261.6	0.0		54.9	0.3	
160.4	2.1	0.0	33.7	1.8	0.0
112.8	8.7	0.2	23.7	4.5	0.2
84.3	16.8	1.2	17.7	9.1	1.3
64.6	24.4	3.1	13.6	15.8	4.3
50.2	33.2	6.6	10.5	24.3	10.3
39.0	43.2	10.7	8.2	34.1	18.8
30.3	52.1	15.6	6.4	44.9	29.8
23.7	59.2	22.0	5.0	56.6	43.7
17.7	67.1	30.5	3.9	67.0	56.3
13.6	74.0	40.1	3.0	75.2	65.3
10.5	80.1	50.4	2.4	82.1	73.9
8.2	85.2	59.6	1.9	87.7	81.5
6.4	89.6	69.1	1.5	90.8	86.7
5.0	93.4	79.2	1.2	92.8	92.1
3.9	95.8	86.5			
3.0	97.2	91.2			
2.4	98.2	95.7			
1.9	98.9	98.4			
1.5	99.2	99.0			
1.2	99.4	99.3			

Matla (RH6):

diameter μm	cumulative weight %	diameter μm	cumulative weight %	diameter μm	cumulative weight %	
	field 1		field 2		field 3	field 4
564.0	0.0	188.0	0.0	118.4	0.0	
261.6	1.0	87.2	2.8	54.9	0.1	
160.4	3.8	53.5	11.8	33.7	1.3	0.0
112.8	8.5	37.6	23.0	23.7	5.4	0.2
84.3	15.2	28.1	33.0	17.7	12.9	2.1
64.6	24.5	21.5	42.4	13.6	21.4	7.2
50.2	36.9	16.7	51.6	10.5	32.3	15.9
39.0	49.2	13.0	60.0	8.2	43.0	25.8
30.3	59.3	10.1	67.8	6.4	54.7	37.0
23.7	67.5	7.9	75.3	5.0	67.0	49.6
21.5	69.9	6.2	81.6	3.9	76.3	60.6
16.7	76.6	4.8	86.4	3.0	82.8	69.6
13.0	81.9	3.8	90.4	2.4	89.1	78.5
10.1	86.2	3.0	93.6	1.9	94.0	86.8
7.9	90.0	2.4	95.8	1.5	95.9	89.6
6.2	92.9	1.9	97.3	1.2	97.0	90.5
4.8	95.0					
3.8	96.6					
3.0	97.9					
2.4	98.7					
1.9	99.2					

Table 5.4 : (Continued)

Lethabo (1) Malvern Data:

diameter μm	cumulative weight %		diameter μm	cumulative weight %				
	field 1	field 2		field 3	field 4	field 5	field 6	field 7
564.0	0.0		118.4	0.0		0.0		
261.6	3.4	0.0	54.9	2.1	0.0	.1		
160.4	17.8	.6	33.7	5.4	.2	.2	0.0	0.0
112.8	27.9	3.7	23.7	8.4	1.4	.5	.1	.1
84.3	37.7	6.5	17.7	13.0	4.2	1.9	.5	.8
64.6	45.2	9.3	13.6	21.0	10.0	5.3	2.8	3.5
50.2	52.7	11.4	10.5	35.1	20.8	12.9	10.1	10.4
39.0	58.5	16.4	8.2	51.7	35.8	25.5	22.5	22.4
30.3	64.2	21.9	6.4	69.9	53.7	43.1	40.1	40.0
23.7	69.2	26.8	5.0	84.8	71.7	63.0	60.3	60.2
17.7	76.3	34.6	3.9	91.8	83.7	78.2	75.3	75.2
13.6	81.0	43.1	3.0	95.0	90.4	87.5	84.7	84.7
10.5	85.4	55.2	2.4	98.1	95.3	93.3	91.9	92.0
8.2	90.3	68.5	1.9	99.3	97.7	96.4	95.8	95.9
6.4	94.2	82.8	1.5	99.5	98.5	97.6	97.1	97.1
5.0	97.0	93.2	1.2	99.6	98.9	98.2	97.9	97.8
3.9	98.6	96.5						
3.0	99.3	97.8						
2.4	99.8	99.7						
1.9	99.9	100.0						
1.5	100.0							

Lethabo (5):

diameter μm	cumulative weight %		diameter μm	cumulative weight %	
	field 1	field 2		field 3	field 4
564.0	0.0		118.4		
261.6	5.2		54.9	0.0	
160.4	22.1	0.0	33.7	0.5	0.0
112.8	35.8	0.2	23.7	2.3	0.1
84.3	47.7	1.2	17.7	5.8	1.2
64.6	56.2	3.1	13.6	12.4	4.8
50.2	62.7	6.6	10.5	20.8	12.1
39.0	69.1	10.7	8.2	31.2	21.4
30.3	74.0	15.6	6.4	43.1	33.3
23.7	77.8	22.0	5.0	56.8	48.6
17.7	83.0	30.5	3.9	69.2	63.2
13.6	86.4	40.1	3.0	78.7	74.6
10.5	89.1	50.4	2.4	86.8	84.5
8.2	92.0	59.6	1.9	92.3	91.1
6.4	94.5	69.1	1.5	94.5	93.7
5.0	96.5	79.2	1.2	95.9	95.3
3.9	97.9	86.5			
3.0	98.7	91.2			
2.4	99.4	95.7			
1.9	99.7	98.4			
1.5		99.0			
1.2		99.3			

Table 5.4 : (Continued)

Lethabo (1) Sedigraph Data:

diameter μm	Cumulative weight %						
	field 1	field 2	field 3	field 4	field 5	field 6	field 7
500.0							
353.0							
250.0	0.2	0.2					
177.0	3.0	0.8	0.1				
125.0	13.1	2.4	1.0				
88.0	22.7	4.5	2.3				
62.0	31.9	8.2	3.0	1.2	0.3	0.4	0.5
44.0	40.2	12.9	3.8	1.2	0.5	0.7	0.5
31.0	52.6	19.4	6.5	1.9	1.1	1.1	0.9
22.0	63.7	27.1	10.8	4.2	3.6	2.5	1.7
16.0	73.0	36.6	16.7	7.3	6.8	4.7	3.1
11.0	80.5	47.1	24.8	13.5	11.7	8.2	5.5
7.8	86.5	57.6	35.3	22.9	18.9	13.6	9.8
5.5	90.8	67.1	48.0	35.1	29.4	22.6	16.7
3.9	94.2	75.6	64.0	50.7	44.7	37.3	29.7
2.7	96.5	82.1	78.7	67.4	62.6	56.6	49.8
1.9	98.2	86.8	89.2	81.1	78.6	75.4	71.2
1.3	99.3	89.5	94.8	90.3	89.9	88.6	87.4
0.9	99.8	91.1	97.5	94.9	95.4	95.2	94.9
0.6	100.0	91.6	98.3	96.7	97.7	97.6	97.5
0.4					98.1	98.2	98.0
0.3							98.2
0.2							98.9

CHAPTER 6

RESULTS AND DISCUSSION

6.1 INCORRECTLY LABELLED SAMPLES

Three sets of samples received for analysis in this study appeared to be anomalous. D2 and D3 (supposedly Duvha) almost certainly belonged to Matla. Both data sets have glass and mullite concentrations which follow trends seen in the Matla ash (see later in chapter). The D3 lime and spinel concentrations plot within the Matla field, while D2 lime and spinel concentrations lie just on the edge of the range defined by the Matla samples. The possibility that these two sample sets are in actual fact Matla samples is supported by the results of a Discriminant Function Analysis performed on the data set which classified the samples into the Matla field, using MgO, K_2O, LOI, Pb, Cu, Co, Cr, Ba, Nd, quartz and spinel as the discriminant variables. The similarity between the first two canonical variables for Matla and for D2 and D3 are shown in Fig. 6.1. D2 and D3 sample sets have thus been excluded from the following discussion. D2 and D3 may represent coal mined from a different seam to that normally mined, as it is known that Duvha did reclaim from a different seam at about that time.

Four D6 samples (supposedly Duvha fields 1 to 4) all appear to belong to Duvha field 1 on the basis of similar particle size distributions and a very narrow chemical and mineral compositional range. This is supported by the results of a Discriminant Function Analysis which selected As as the discriminant variable. The similarity between the canonical variable for known Duvha field 1 samples and between the D6 samples is shown in Fig. 6.2. These four samples have thus been used as an indication of the total error (analytical + sampling) due to the heterogeneity of the source material.

The apparent mislabelling of the D2, D3 and D6 data sets is certainly a lesson in the necessity for collecting one's own samples, regardless of cost.

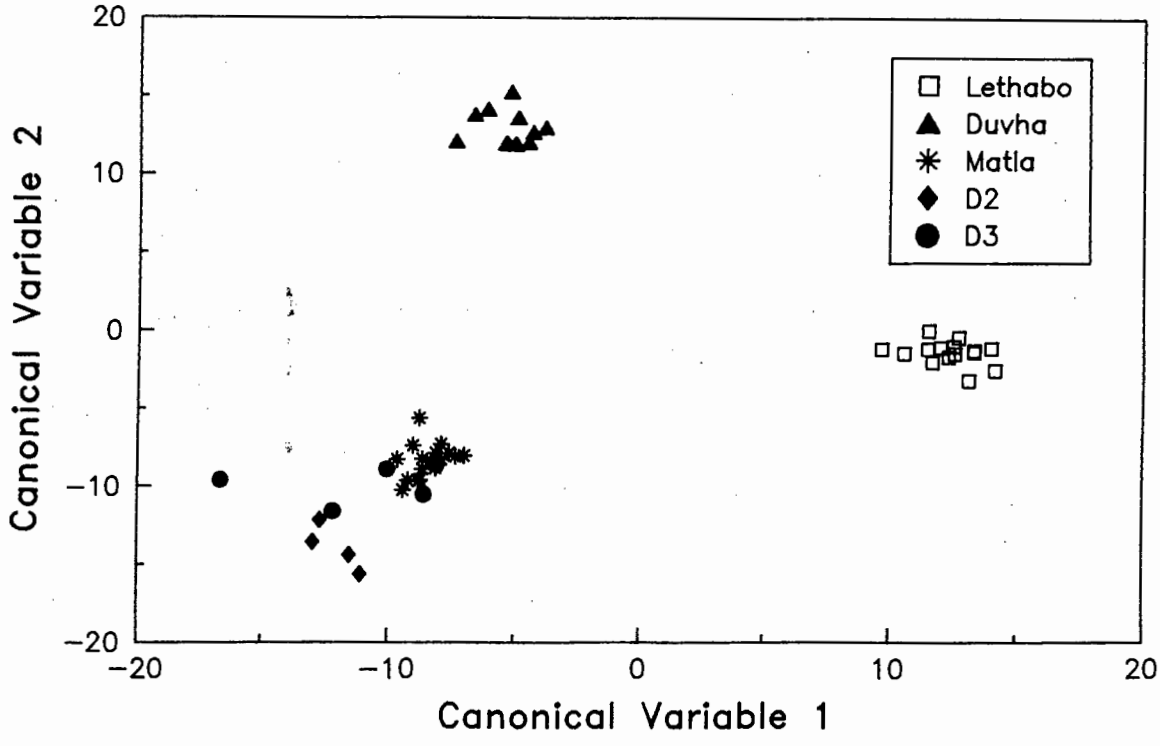

Fig. 6.1 : Comparison of the first two canonical variables for D2 and D3 (fields 1 to 4) with known Lethabo, Duvha and Matla samples (fields 1 to 4), determined with the BMDP program 7M.

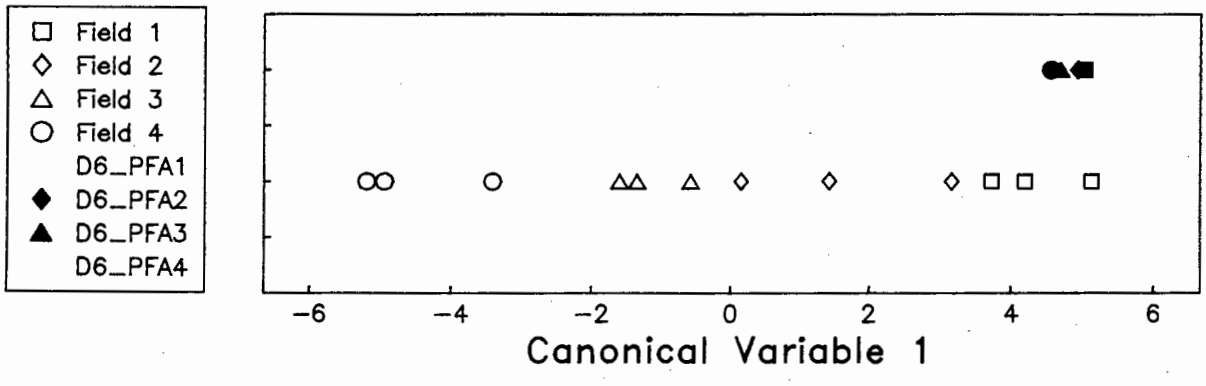

Fig. 6.2 : Comparison of the first canonical variable for D6_PFA1, 2, 3 and 4 with known Duvha PFA samples from fields 1 to 4, determined using the BMDP program 7M.

6.2 SIZE ANALYSIS

6.2.1 Comparison of Sedigraph and Malvern Particle Sizer Data

The particle size distribution of the L1 sample suite was determined with both a Malvern Particle Sizer (sample in slurry) and the Sedigraph-Settling Column combination. The former method underestimates the amount of material finer than approximately 20μm by as much as 20% when compared with the Sedigraph data (Fig. 6.3(a)). This results in a shift of the Malvern particle size distribution curve towards the coarser particle sizes (Fig. 6.3(b)). There is a relatively good agreement between the two methods for FA from fields 1 and 2.

Disagreement between the two methods is to be expected considering the different methods of measurement (settling and light-scattering) and the non-ideal nature of the particles (translucent, hollow cores in the case of the cenospheres and plerospheres, and deviation from sphericity).

An important difference between the two results is that whereas for the Malvern data the size distributions for FA from fields 5, 6 and 7 are almost identical, the Sedigraph data indicate that for each of these fields the FA is finer than in the previous field. This is shown in Fig. 6.4 where the value of the 50^{th} percentile (in microns) is compared for the two methods. These values are usually higher for the Malvern data compared with the Sedigraph data. The Sedigraph is thus considered to be more suitable for detecting differences in particle size of the finer particles, although the length of time taken to measure the fine fraction made it unsuitable for routine use in this work.

6.2.2 Malvern Particle Sizer (Dry Sample)

Initially particle size measurements were determined on dry FA and coal samples. Fig. 6.5 shows a typical particle size distribution. The presence of free lime makes the particles very susceptible to agglomeration caused by surface moisture holding the particles together, and possibly by chemical reactions involving the free lime. Dry particle sizing was discontinued following these results.

6.2.3 Coal

Coal is ground to standard size limits in each of the power stations. The theoretical particle size distribution of the pulverised coal which is accepted into the combustion chamber is listed for each station in Table 6.1. Duvha coal is ground to a much coarser particle size than

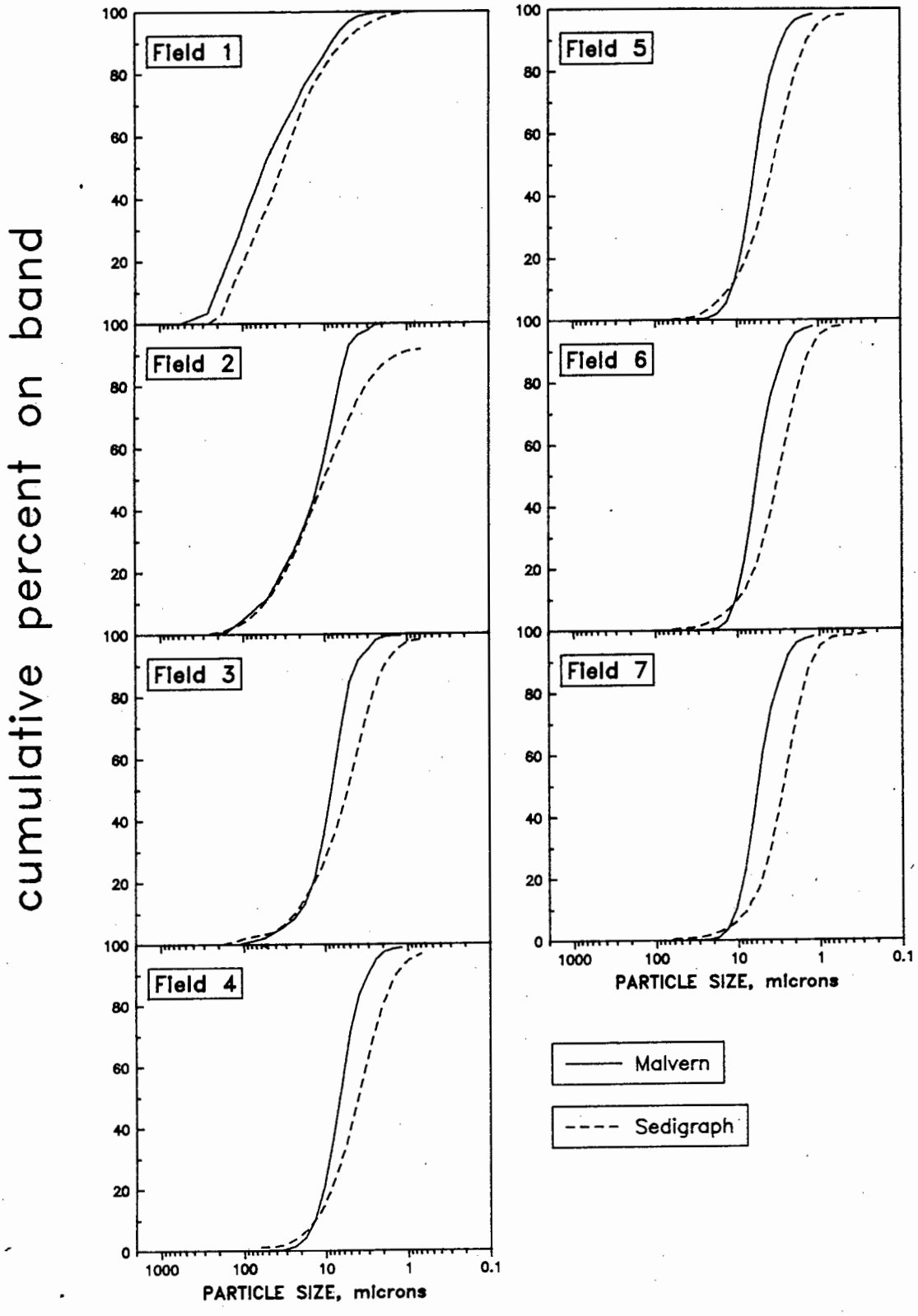

Fig. 6.3(a) : Comparison of the cumulative frequency plots for the Lethabo L1 data set determined with the Sedigraph and Malvern Sizer (sample in slurry).

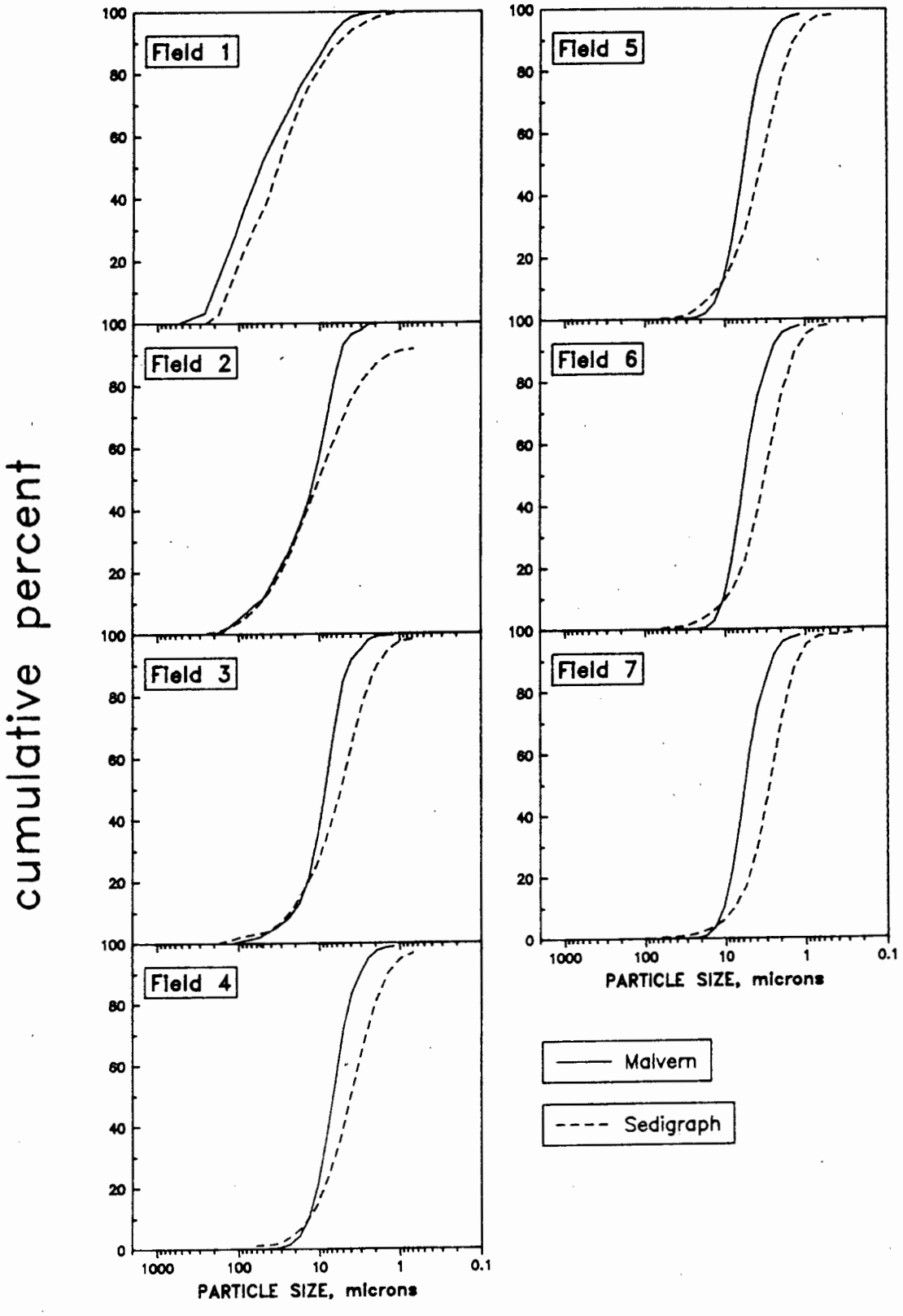

Fig. 6.3(a) : Comparison of the cumulative frequency plots for the Lethabo L1 data set determined with the Sedigraph and Malvern Sizer (sample in slurry).

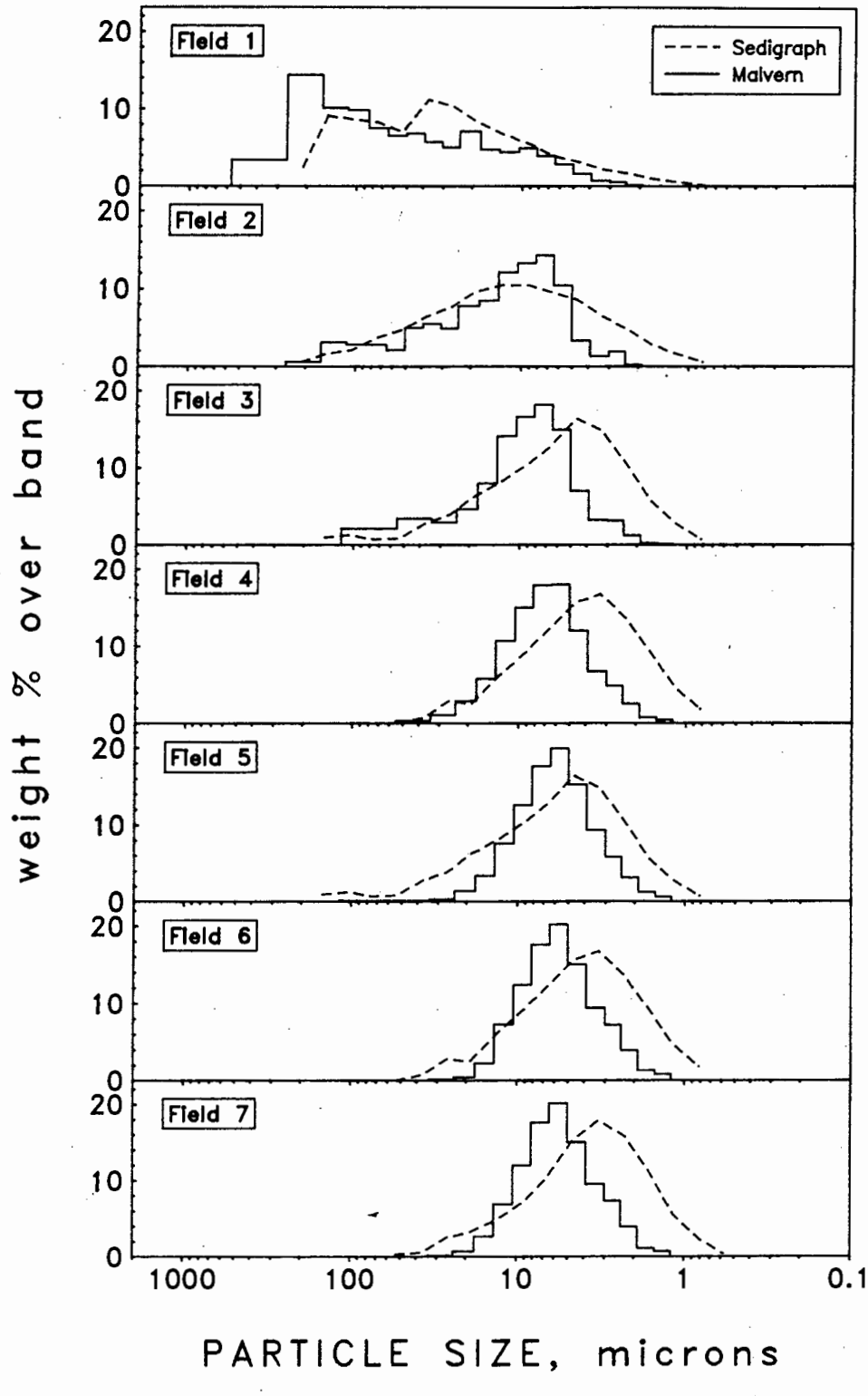

Fig. 6.3(b) : Comparison of the frequency distribution plots for the Lethabo L1 data set determined with the Sedigraph and Malvern Sizer (sample in slurry).

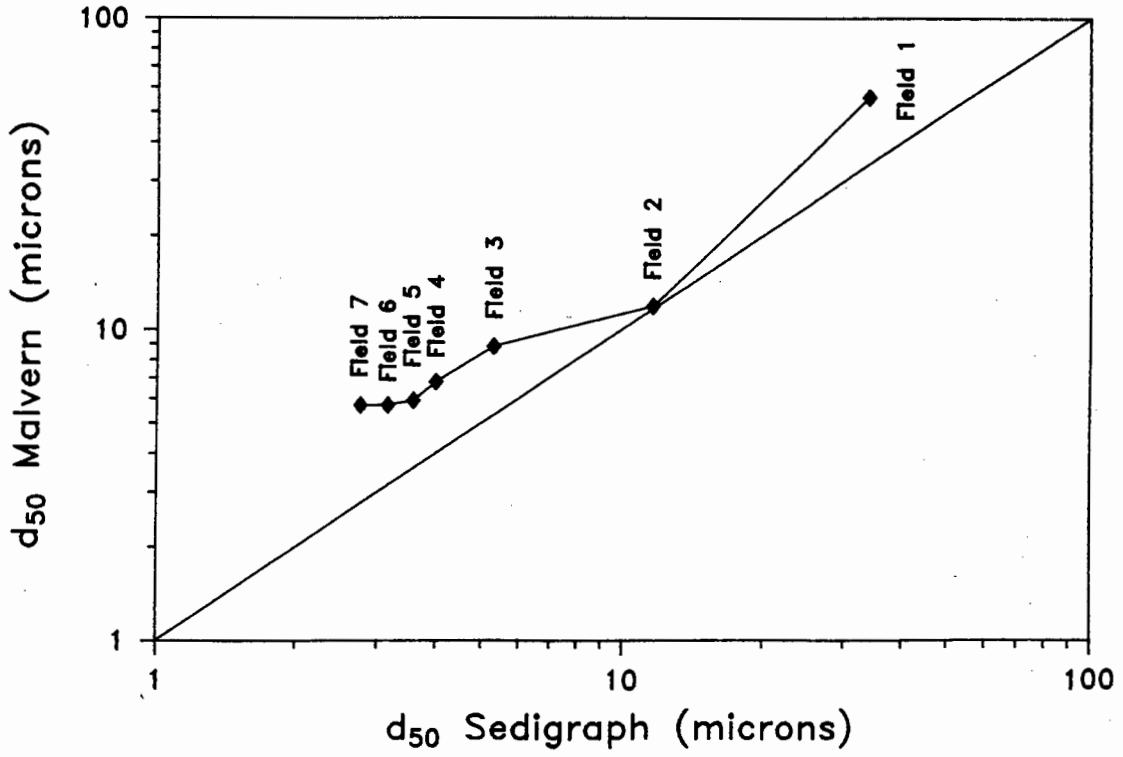

Fig. 6.4 : Comparison of the 50th percentile (in microns) for data from the Sedigraph and Malvern Counter for Lethabo L1.

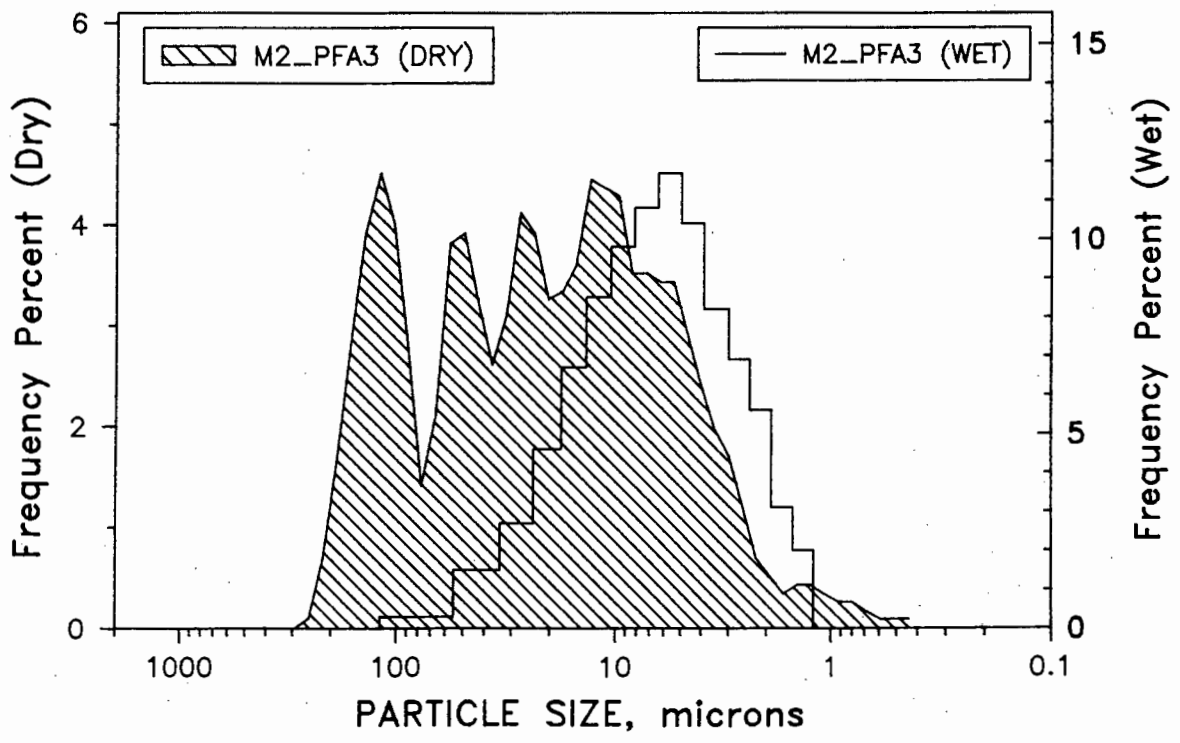

Fig. 6.5 : Particle size frequency distribution of M2 PFA3 (dry) determined with a Malvern Particle Sizer.

either Lethabo or Matla coal.

Lethabo		Matla		Duvha	
Mesh (μm)	Weight % on sieve	Mesh (μm)	Weight % on sieve	Mesh (μm)	Weight % on sieve
+300	2.25	+300	<0.2	+300	0.2
+150	7.30	+150	4-7	+150	7.7-13.7
+105	13.71			+106	21.0-33.9
+75	24.33	+75	25-28	+75	31.7-47.8

Table 6.1 : Particle size distributions of input coal expressed as percent retained on sieve. Data kindly supplied by ESKOM staff.

6.2.4 FA

Particle size frequency distributions determined with the Malvern Particle Sizer (wet sample) are shown in Fig. 6.6. The particle size distribution of all three power stations decreases significantly in FA from fields 1 to 4, although the difference between FA from the first two fields is much greater than the difference between the later fields. There is very little difference in the particle size of FA from fields 4-7 of Lethabo 1, which is in agreement with data from Heinichen and Willis (1987). The two data sets for Lethabo and Matla taken 18 months apart have similar particle size distributions, indicating very little variation in the size distribution of the ash with time. The particle size distributions of Duvha field 1 FA and Lethabo field 1 FA are similar, while that of Duvha field 4 FA is slightly coarser than FA from field 4 of either Lethabo or Matla. This may be due to the much coarser particle size to which the Duvha coal is ground.

The frequency distribution of field 1 ash is skewed to the smaller particle sizes for all three stations when plotted on a log scale. The size distributions of FA from the remaining precipitator fields have approximately log normal distributions, i.e. FA from fields 3 to 7 of Lethabo, and 2 to 4 of Matla and Duvha.

6.2.5 Reproducibility and Sampling Error

The particle size distributions of the four D6 field 1 samples are compared in Fig. 6.7. Samples II, III and IV have nearly identical particle size distributions and are similar to the

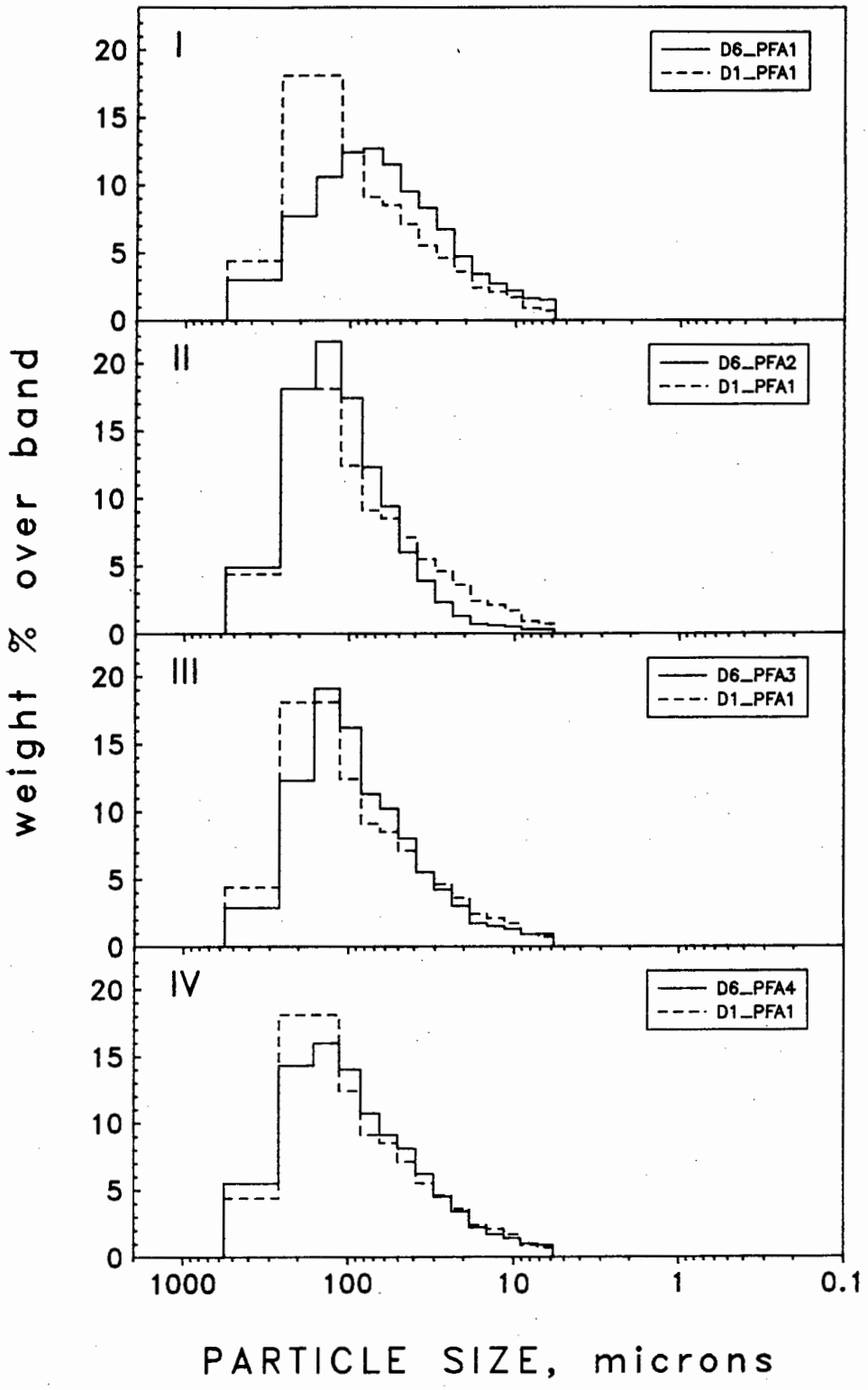

Fig. 6.7 : Particle size frequency distribution for replicate samples of Duvha 6 (D6) PFA.

particle size distribution of D1_PFA1. Sample I has a mean shifted towards the finer particle size, and has a more log-normal distribution, compared with the skewed distributions of the other three samples. If the assumption is true that that these four samples are all from Duvha field 1, then these variations are representative of the small degree of heterogeneity of the source material. Alternatively, if the samples can be assumed to be identical, then the results represent the reproducibility of the measurement technique.

6.3 MINERAL COMPOSITION

6.3.1 Coal

The mineralogy of samples of input coal from each of the power stations was determined by the National Institute for Coal Research (CSIR). These results are listed in Table 6.2. The kaolinite concentration is highest in Lethabo coal and lowest in Matla coal. The pyrite concentration is highest in Duvha coal and lowest in Lethabo coal.

	Lethabo					Duvha		Matla		
Mineral	TH8_16*	TH8_17*	L1_PF	L3_PF	L4_PF	D4_PF	D5_COAL	M2_PFA	M4_PF	M5_COAL
Quartz	3.3	3.3	4.5	5.0	4.8	4.6	8.3	2.2	3.8	4.1
Kaolinite	33.4	29.6	34.7	30.5	34.1	24.0	20.7	18.5	21.7	22.6
Feldspar							1.7			
Calcite	1.3	1.6	1.9	1.5	1.5	2.7	1.3	2.0	1.6	1.5
Dolomite		0.9		0.8	0.8		0.7	1.8	1.3	1.5
Siderite		0.3		0.5	0.4	0.5	0.4	0.1		0.1
Pyrite	0.4	0.5	0.5	0.5	0.5	1.8	1.9	1.4	1.6	0.5

Table 6.2 : Mineral compositions of selected coal samples. Analyses provided by the National Institute of Coal Research of the CSIR.

* = Samples collected at the same time

6.3.2 PFA

The general mineralogy of South African PFA is well known. The major phases are glass, mullite and quartz (Willis 1987; Lesch and Cornell 1987). Other phases which have been identified are lime, portlandite, hematite, and an Fe-oxide phase identified as maghemite (γ-Fe_2O_3) (Lesch and Cornell 1987). An X-ray diffractogram from a magnetic concentrate of Duvha PFA is compared in Fig. 6.8 with the peak positions for magnetite, magnesioferrite (low) and maghemite. Peak positions are close to those of magnesioferrite. On the basis of the chemical composition of spinels from Lethabo and Matla, however (see later), they are reported in this work as a ferrite spinel. With the exception of lime and portlandite, the phases identified are typical of low-calcium/Class F ashes (ASTM classification) derived from bituminous coal (McCarthy 1988). Variations in fly ash mineralogy can be attributed to differences in the inorganic components of the source coal, in the coal preparation and combustion conditions, and in ash collection and handling methods (McCarthy 1988).

In the discussion which follows, two data points are considered to have significantly different values if their difference is greater than 4 standard deviations (95% confidence). Mineral concentrations in PFA samples collected during 1980 from Duvha and Matla power stations have been reported by both Willis (1987) and by Lesch and Cornell (1987), and are compared here with the concentrations reported in this work.

6.3.2.1 Glass:

The glass concentration in the PFA samples has been determined using two methods: method (i) measures the glass and mineral concentrations directly and normalises the data to 100%, and method (ii) calculates glass by difference from 100% of the total mineral concentration.

The correlation between measured and calculated glass concentrations is shown in Fig. 6.9. Glass concentrations from Duvha and Lethabo PFA determined by both methods are equally distributed about the 1:1 correspondence line, whereas Matla glass concentrations calculated by difference tend to be higher than measured values, particularly for concentrations greater than 65%.

Because glass is the largest mineral component any errors in the glass values will introduce significant errors in the other mineral components if the mineral and glass values are normalised to 100%. Therefore, since the total error in mineral components is relatively small (see later), the glass concentrations presented in this work have been calculated by difference.

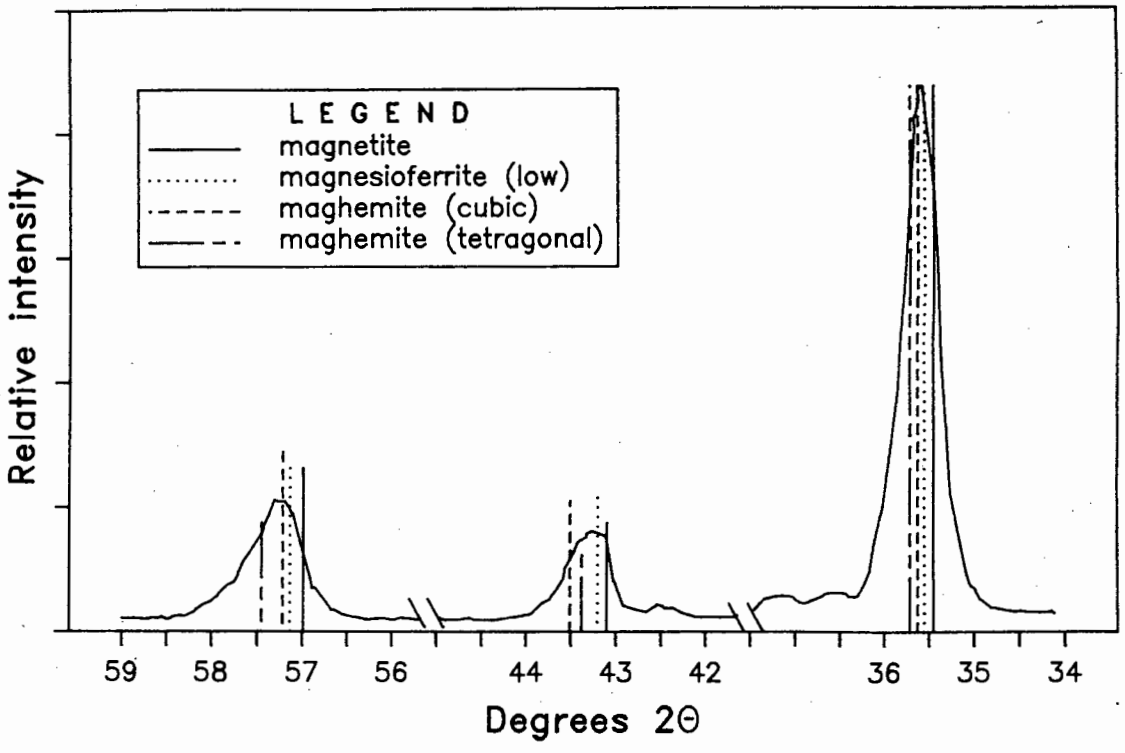

Fig. 6.8 : X-ray diffractogram of the magnetic concentrate from Duvha PFA.

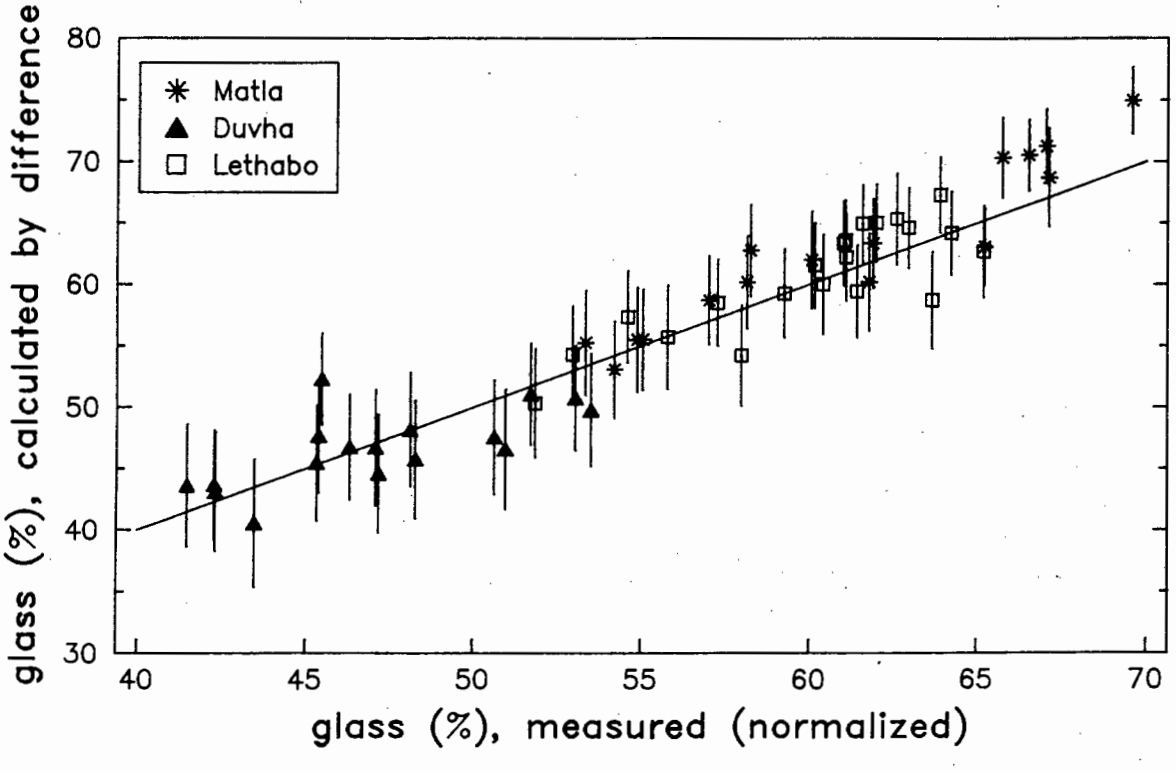

Fig. 6.9 : Comparison of glass values in all PFA samples determined (i) by measurement and then normalised, and (ii) by calculating glass as the difference between the sum of the mineral components and 100%. Error bars are ± 2 standard deviations.

Glass concentration data are shown in Fig. 6.10. Three sets of Lethabo samples, L1, L3 and L4, show no significant difference from each other, with the exception of L1_PFA4 and L3_PFA4. L5 glass concentrations remain constant in PFA from fields 1 to 4, but are significantly higher in PFA from fields 1 and 2 than in corresponding fields from the other Lethabo PFA samples. In contrast, L3 and L4 glass concentrations increase significantly in PFA from fields 1 to 4, and L4 glass remains constant in PFA from fields 4 to 6. Glass concentration increases significantly in L1 PFA from fields 1 to 6. There is no significant difference between L1 bottom ash, mixed ash and PFA from field 1. The glass concentrations in L5_PFA1 and L5_PFA2 are significantly higher than in the other Lethabo samples, and thus there is a real variation in glass content in PFA from these fields with time. The range is within analytical error for PFA from fields 3, 4, 5 and 6.

The glass concentration range for PFA from each field of Duvha samples D1, D4 and D5 is within analytical error, and there is thus no significant difference in the glass concentrations of PFA from fields 1 to 4. There is no significant difference between D1 composite ash and PFA from D1 fields 1 to 4.

The glass concentration range in the Duvha PFA samples is 44.6-52.3%. This is in contrast with data reported by Willis (1987) for the 1980 samples, in which there is a sharp increase in the Duvha PFA glass concentrations from fields 1 to 4 of 23-46%. Only concentrations in PFA from fields 3 and 4 reported by Willis plot within the range determined in this study. There has thus been a significant change in the glass concentration of PFA from Duvha fields 1 and 2 between 1980 and 1987/88.

The Matla glass concentrations increase significantly in all PFA samples from fields 1 to 4. For each particular field the concentration range is within analytical error, and thus there is no significant variation in glass content over time. There is no significant difference between PFA from the left and right hand fields of M6.

Lesch and Cornell (1987) also noted the increase in the glass concentrations in PFA from fields 1 to 4 of Matla. The concentration range reported by these authors is the same as that determined in this work. The glass concentrations determined by Willis (1987) in PFA from fields 3 and 4 (1980 samples) are within the range reported in this work. The compositions reported by Willis for PFA from fields 1 and 2 are higher by 10-20% than the concentrations reported in this work.

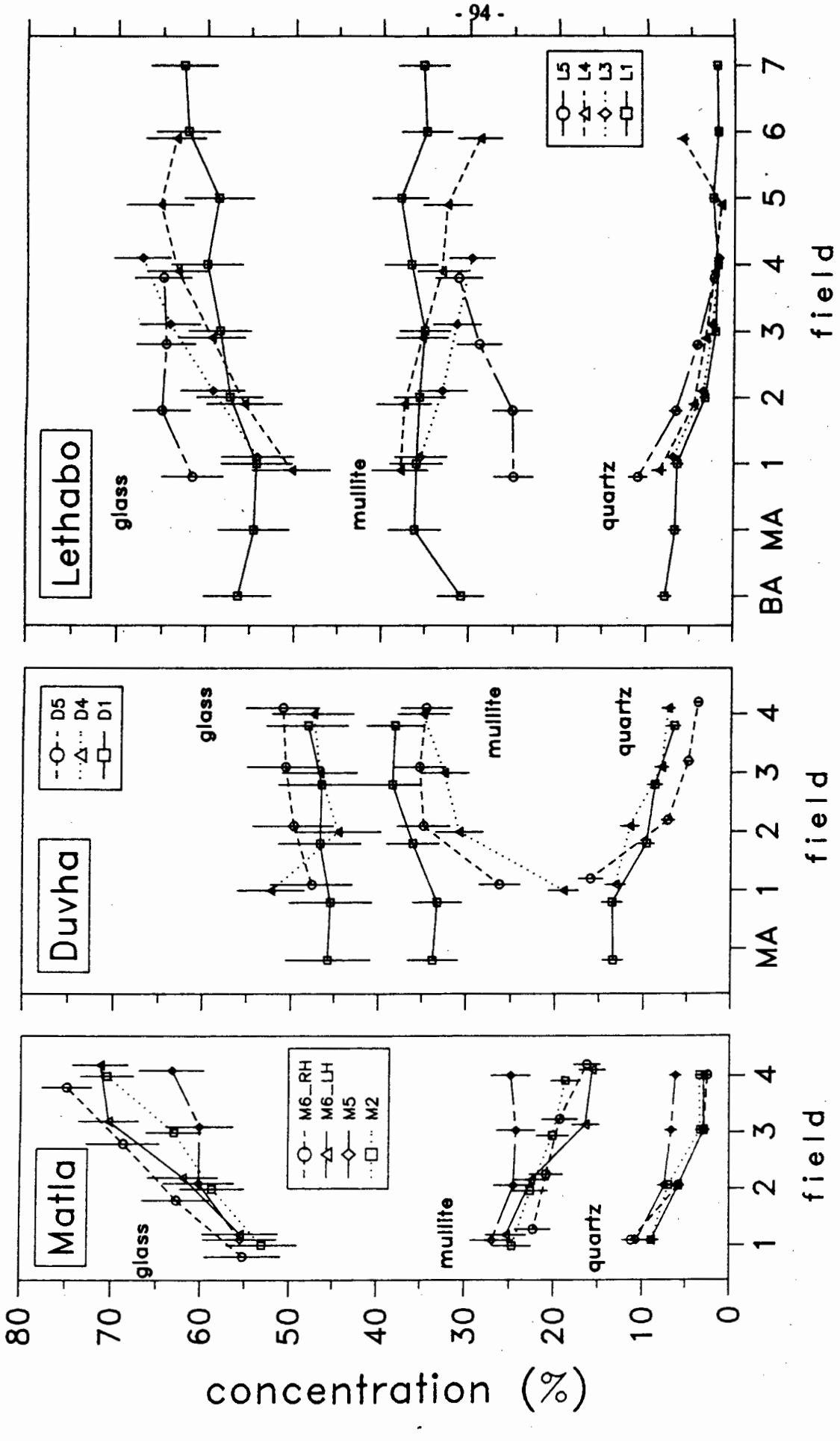

Fig. 6.10 : Variations in the glass, mullite and quartz concentrations in PFA from different sites in the power stations. BA = bottom ash, MA = mixed ash. Error bars are ± 2 standard deviations.

6.3.2.2 Mullite:

Mullite is a common mineral in Class F fly ash. The mullite concentrations are shown in Fig. 6.10. For the Lethabo L1 PFA samples, there is no significant difference in the mullite concentration of the bottom ash, the mixed ash, and in PFA from fields 1 to 7. In contrast, mullite in L3 PFA decreases significantly from fields 1 to 4, and the mullite in L4 PFA decreases significantly from fields 1 to 6. In L5 ash however, mullite increases significantly from fields 1 to 4. There is thus no single trend discernable for mullite in Lethabo ash, but varies considerably. The mullite concentration ranges of L1, L3 and L4 PFA from fields 1 and 2 are within analytical error, whereas L5 PFA has significantly less mullite in PFA from the first two fields compared with equivalent fields from the other samples. The mullite concentration range in PFA from fields 1 and 2 is thus greater than the analytical error, and represents a real variation in the mullite concentration of PFA from these fields with time.

For D1 PFA there is no significant difference in the mullite concentration of the composite ash and of PFA from fields 1 to 4. D4 and D5 however both have significantly less mullite in PFA from field 1 compared with field 2, and mullite in PFA from fields 2, 3 and 4 remains constant within the 95% confidence limits. The mullite concentration range in field 1 PFA is greater than the analytical error, and thus there is a real variation with time of the mullite concentration in PFA from this field.

Willis (1987) reported only the nett mullite peak to nett internal standard peak intensity ratios for Duvha PFA. Changes in these ratios indicated a sharp increase in the mullite concentration in PFA from field 1 to 2, and that PFA from fields 2, 3 and 4 had similar mullite concentrations. This agrees with the trends noted in this work for PFA from D4 and D5.

In Matla PFA, the mullite concentration decreases significantly from fields 1 to 4 for all samples except M5. The concentration range in PFA from each field is greater than the analytical error and thus indicates a minor variation in the mullite concentration in PFA from each field with time. There is no significant difference between PFA from the left and right hand fields of M6.

Lesch and Cornell (1987) also noted the decrease in mullite concentration in Matla PFA from fields 1 to 4. The concentration range reported by these authors is the same as that determined in this work. There was no obvious trend in the mullite ratios reported by Willis

(1987).

6.3.2.3 Quartz:

Quartz is observed in all fly ashes and is believed to be quartz from the original coal which survived combustion (McCarthy 1988). This is confirmed by the angular to sub-angular morphology of most quartz grains observed under the microscope, which is typical of sedimentary quartz.

The quartz concentrations are shown in Fig. 6.10. Quartz decreases significantly in all Lethabo samples from fields 1 to 4, and is constant, within analytical error, in PFA from fields 4 to 7 for L1. L1 mixed ash and bottom ash have essentially the same quartz concentration as field 1 PFA. L4_PFA6 has an unexpectedly high quartz content. The decrease of quartz in PFA with each subsequent precipitator has been related to the preferential extraction of the large quartz grains by the first few precipitators (Willis 1987). The quartz concentration range in PFA from fields 1, 2 and 3 is larger than that due to analytical error, and thus represents a real variation in the quartz content from each of these fields with time.

At Duvha, the quartz concentration decreases considerably in PFA from fields 1 to 4, with D1 composite ash having the same concentration as PFA from field 1. The range of quartz concentrations for PFA from each specific field is greater than that due to analytical error, and thus indicates a real variation in the quartz content in PFA from each field with time.

The quartz concentrations reported by Willis (1987) are higher by as much as 12% in Duvha PFA from fields 1 and 2, compared with the maximum concentrations reported in this work, and are within the range for PFA from fields 3 and 4. Willis also noted the decrease in quartz content in PFA from fields 1 to 4.

The quartz concentration of Matla ash decreases significantly from fields 1 to 4 in all samples. The range of quartz concentrations in PFA from each specific field is greater than that due to analytical error, and thus indicates a real variation in the quartz content of PFA from each field with time. The quartz concentration range of M6_LH1 and M6_RH1 is larger than the analytical error, but is within the analytical error for 100% confidence levels. Fields 2 to 4 are within the analytical error for 95% confidence levels.

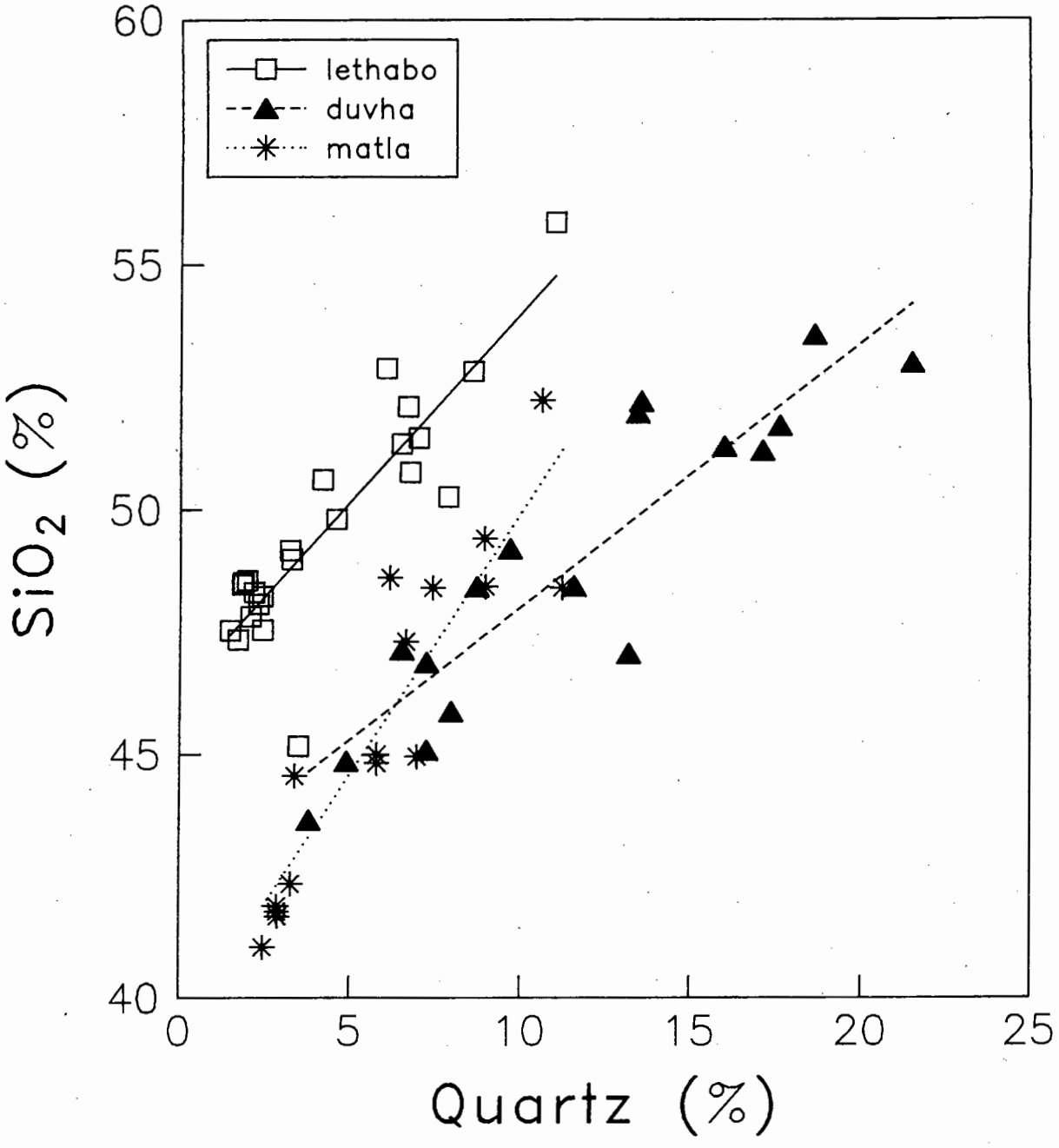

Fig. 6.11 : Correlation between the quartz and SiO_2 concentrations in PFA.

Quartz concentrations in Matla PFA reported by Willis (1987), and by Lesch and Cornell (1987), also decrease in concentration in PFA from fields 1 to 4, and are within the concentration range reported in this work.

The quartz-SiO_2 relationships are shown in Fig. 6.11. Each of the stations defines a positive but separate trend. Duvha and Matla overlap each other and Lethabo ash has the least quartz for any particular SiO_2 concentration. Willis (1987) noted that there is in general a good correlation between the quartz and SiO_2 concentrations in South African PFA.

6.3.2.4 Spinel:

The spinel concentrations are shown in Fig. 6.12. Four sets of Lethabo samples, L1, L3, L4 and L5, have significantly less spinel in field 4 PFA than in field 1 PFA. There is no significant difference in the spinel concentration of PFA from fields 4 to 7 of L1, and of PFA from fields 4 and 6 of L4. L1 bottom ash and mixed ash both have significantly less spinel than PFA from field 1. The concentration range in PFA from each field is greater than that due to analytical error, and thus represents a real variation in spinel concentration in PFA from each field with time. Hematite in Lethabo PFA was detected only in bottom ash (0.6%) and in L4_PFA5 (0.3%). The latter is associated with a significantly low spinel value, i.e. spinel probably inverted to hematite for reasons unknown.

At Duvha the spinel concentration decreases considerably in PFA from fields 1 to 4. The concentration range in PFA from each field is greater than the analytical error, and thus indicates a real variation with time of the spinel content in PFA from each field.

Matla spinel concentrations (except M6_LH4) decrease significantly in PFA from fields 1 to 4. There is no significant difference in PFA from the left and right hand fields of M6 for fields 1 to 3. The concentration range in PFA from fields 1, 3 and 4 is greater than the analytical error, and thus indicates a real variation in spinel content of PFA from these fields with time.

The straight line relationship between the Fe_2O_3 and spinel concentrations is shown in Fig. 6.13. A regression line passed independently through each of the stations is parallel with a regression line passed through all the data points collectively, and thus the intra-station trend is the same as the inter-station trend. All samples had spinel concentrations greater than the lower limit of detection (LLD) of 0.15%. A minimum concentration of approximately 2-3% Fe_2O_3 in the ash is thus required before spinel formation will commence.

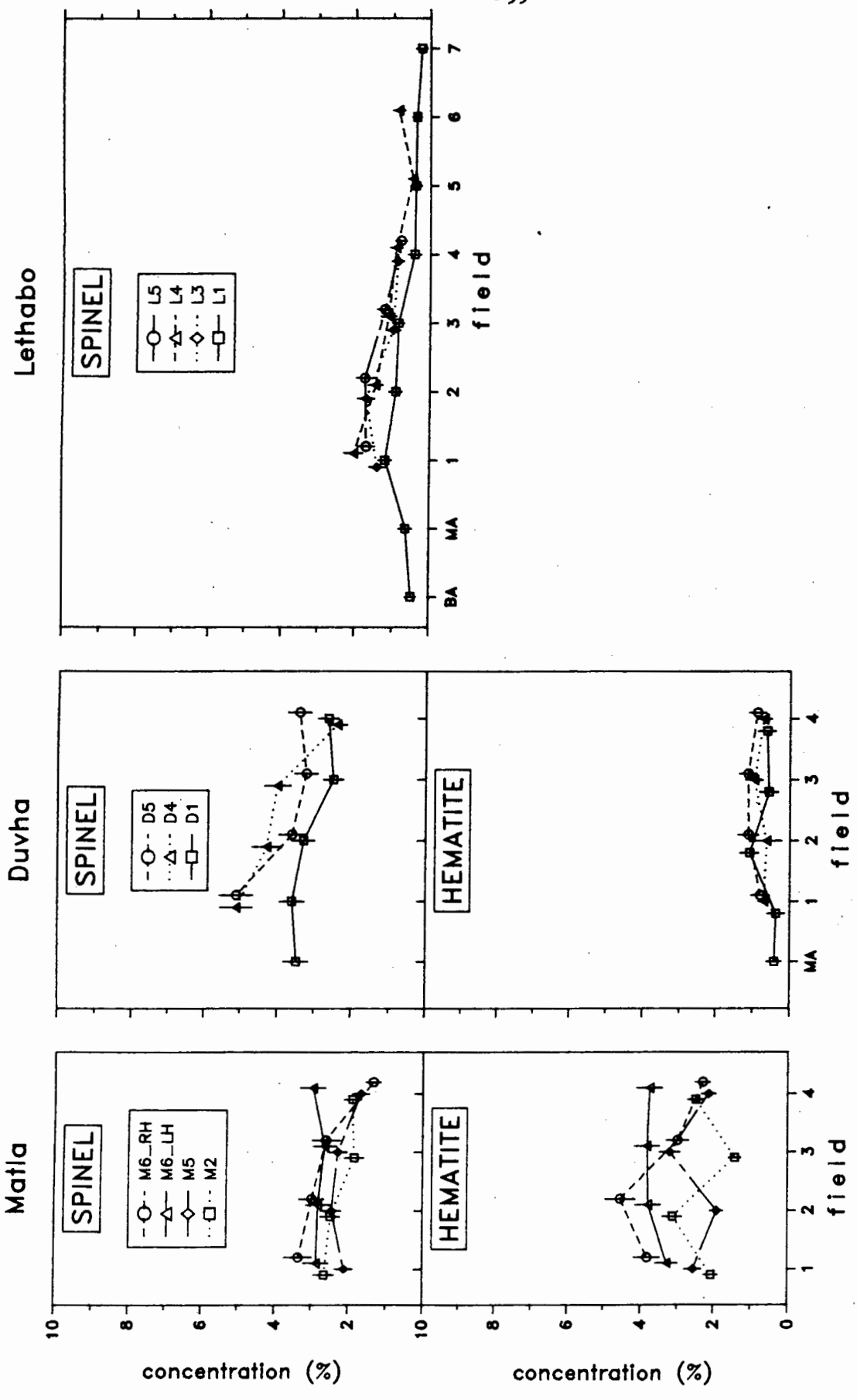

Fig. 6.12 : Variations in the spinel and hematite concentrations in PFA from different sites in the power stations. BA = bottom ash, MA = mixed ash. Error bars are ± 2 standard deviations.

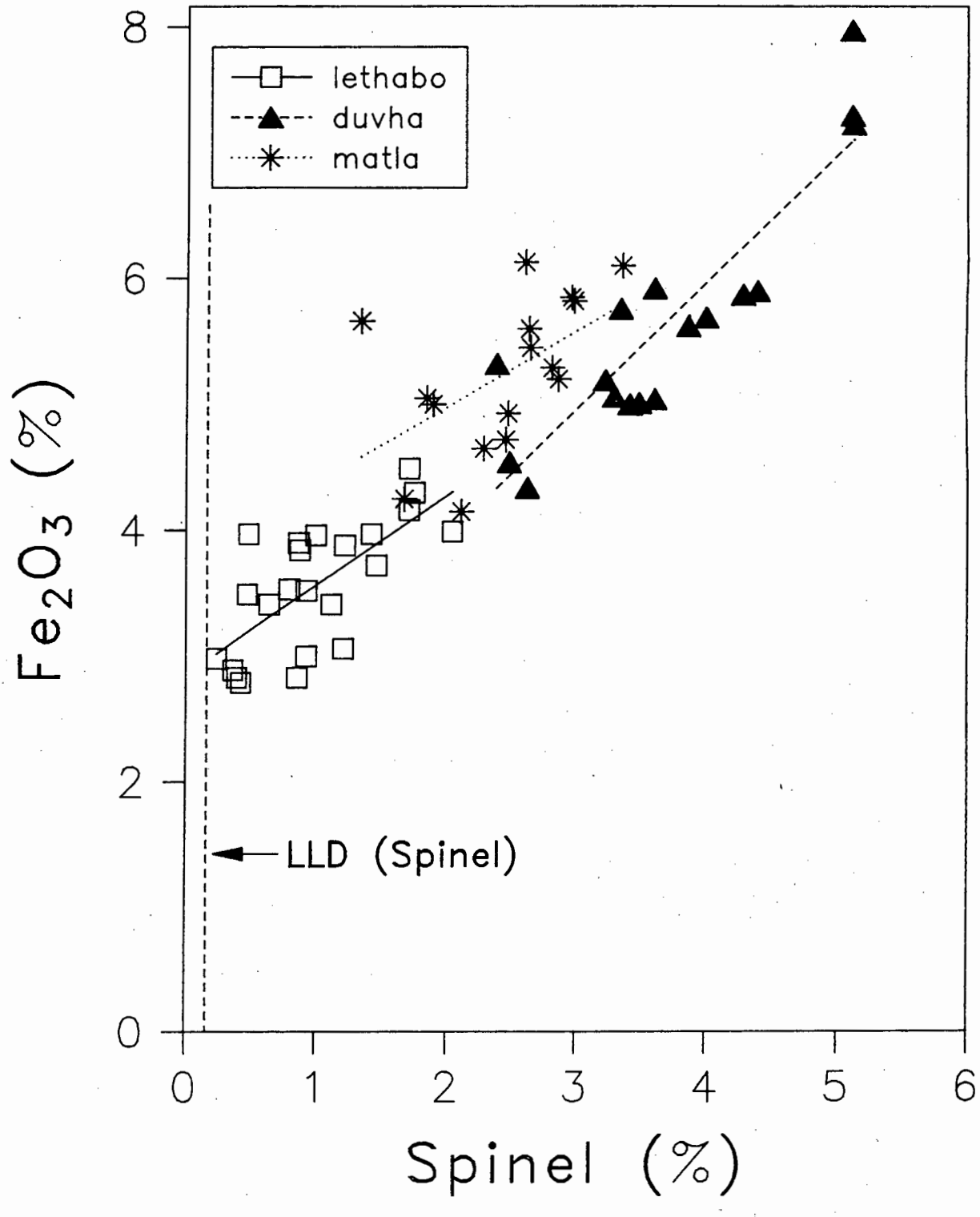

Fig. 6.13 : Correlation between the spinel and Fe_2O_3 concentrations in PFA.

6.3.2.5 Hematite:

The Hematite concentrations are shown in Fig. 6.12 for PFA from Duvha and Matla. Except for two samples (see above), hematite is below the detection limit in Lethabo PFA. The concentration range in PFA for each field of Duvha is within the analytical error, and thus there is no significant variation in the hematite concentration.

There is no significant difference in the Matla PFA hematite concentrations from fields 1 to 4, and there is no significant difference between PFA from the left and right hand fields of M6. The concentration range in the PFA for fields 1 and 2 is greater than the analytical error, but is within analytical error for PFA from fields 3 and 4. There is thus a real variation with time in the hematite concentration of PFA from the first two fields.

6.3.2.6 Lime:

Lime is affected by the alteration to portlandite. The lime values reported here are true only for the time of analysis, and not for the time of sample collection. The same comment applies to the portlandite concentration data. The measured lime concentrations are shown in Fig. 6.14.

Lethabo PFA lime concentrations are as low as -0.7% for some samples (LLD = 0.08%), which is clearly impossible. Lime is corrected for overlap from mullite, hematite, spinel, portlandite and calcite (not detected), as well as for the influence of the glass bulge, and has obviously been overcorrected. Therefore, unless fairly large concentrations of lime are present, comparisons are difficult. L3 and L5 have significantly greater lime in field 2 PFA compared with field 1 PFA, whereas PFA from fields 1 and 2 of L1 and L4 cannot be distinguished at the 95% confidence level.

Lime was detected in all samples of Duvha PFA. The concentration range of Duvha lime within PFA from each field is greater than the analytical error, and thus there is a significant variation of lime in PFA from each field with time, although there are no consistent trends between PFA from the different precipitators.

The lime concentration of M6_LH remains constant in PFA from fields 1 to 4, but decreases in PFA from M6_RH. This disagrees with Lesch and Cornell (1987) who noted an increase in lime for some samples of Matla PFA. The concentration difference between PFA from the left and right hand fields 2 to 4 of M6 is greater than the analytical error. The concentration

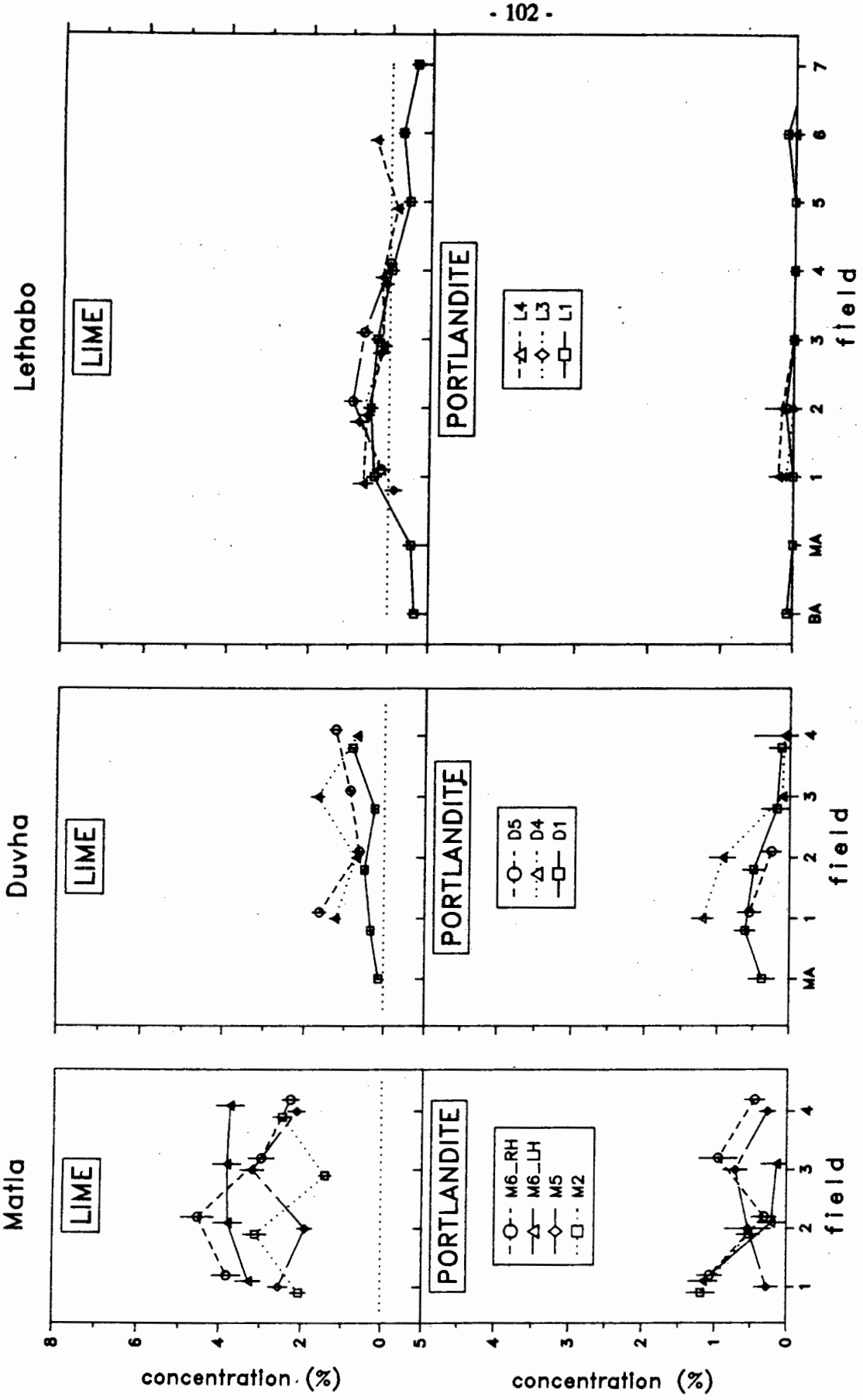

Fig. 6.14 : Variations in the lime and portlandite concentrations in PFA from different sites in the power stations. BA = bottom ash, MA = mixed ash. Error bars are ± 2 standard deviations.

range in PFA from each field is greater than the analytical error, and thus indicates a real variation with time of the lime content in PFA from each field.

6.3.2.7 Portlandite:

Portlandite concentration data are shown in Fig. 6.14. Portlandite is never greater than 0.3% in any of the Lethabo samples. The portlandite concentration decreases significantly in PFA from fields 1 to 4 for all Duvha samples. The concentration range for PFA from fields 1 and 2 is greater than the analytical error, and thus represents a real variation with time of the portlandite concentration in PFA from each field.

6.3.2.8 Total Crystalline Lime:

All of the portlandite measured in the PFA is probably due to the alteration of lime. The total crystalline lime concentration was calculated from the sum of lime plus portlandite recalculated as lime, and is probably more representative of the total free lime concentration at the time of PFA formation. A plot of total crystalline lime is shown in Fig. 6.15. The concentration in each sample is slightly higher than for the Lime data, but in general the trends remain the same.

The correlation between total crystalline lime and CaO is shown in Fig. 6.16. All three stations plot on a regression line with a slope equal to 1.42. When the CaO concentration is between 4-6%, the total measurable crystalline lime is zero. CaO in PFA is present both in free lime (or portlandite) and in the glass, and thus 4-6% must occur as dissolved CaO in the glass. McCarthy et al (1984) estimates that no more than 1/3 of the total CaO occurs as free lime in lignite and sub-bituminous coal ashes. This is true for Lethabo and Duvha PFA (CaO < 8%), but not for Matla PFA which has a higher CaO concentration range.

6.3.2.9 Sampling Error:

Mineral concentrations in the four supposedly replicate D6 field 1 samples are compared in Fig. 6.17. The glass and lime concentration range are within analytical error. The ranges of mullite, quartz, spinel and hematite are somewhat greater than the analytical error, and thus represent heterogeneity of the source material.

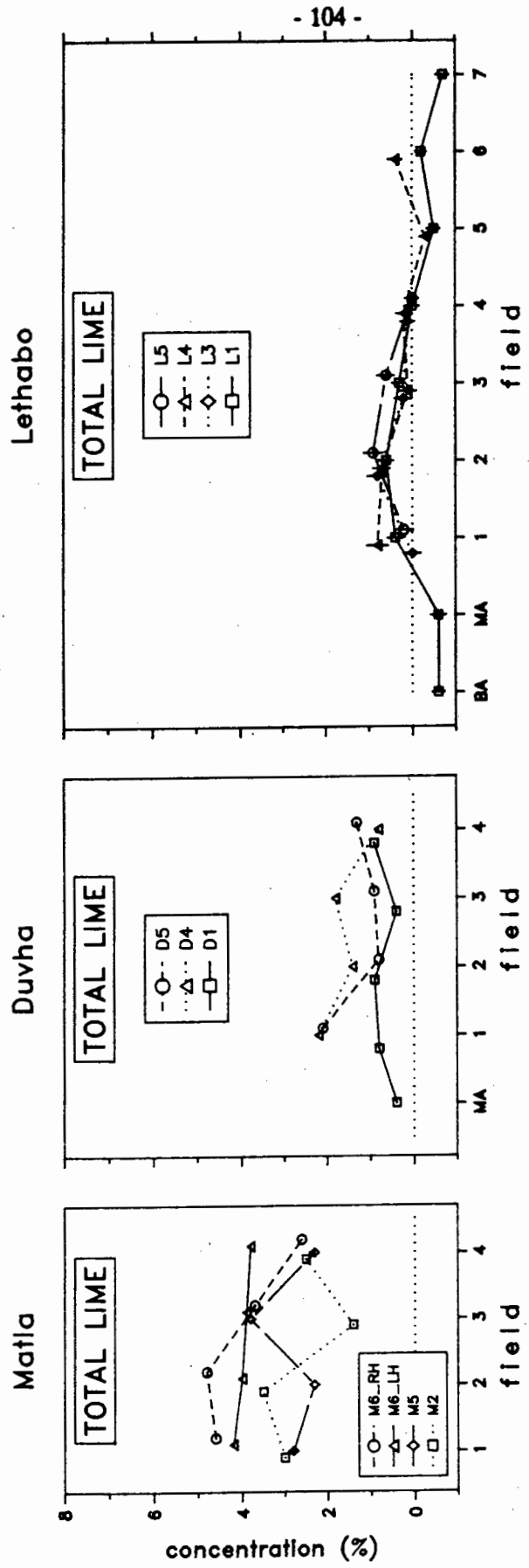

Fig. 6.15 : Variations in the total crystalline lime concentrations in PFA from different sites in the power stations. BA = bottom ash, MA = mixed ash.

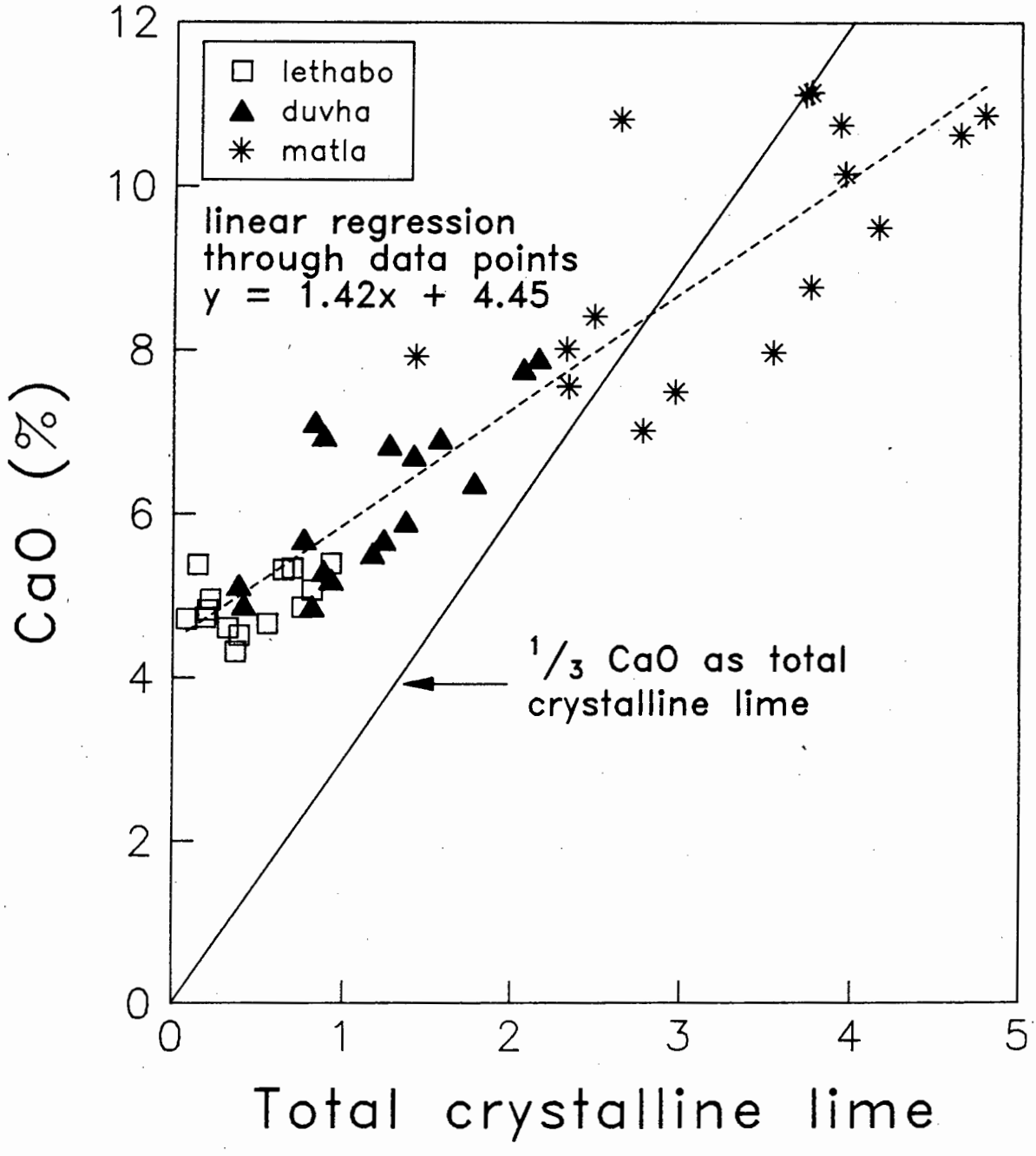

Fig. 6.16 : Correlation between the total crystalline lime and CaO concentrations in PFA samples from all three stations.

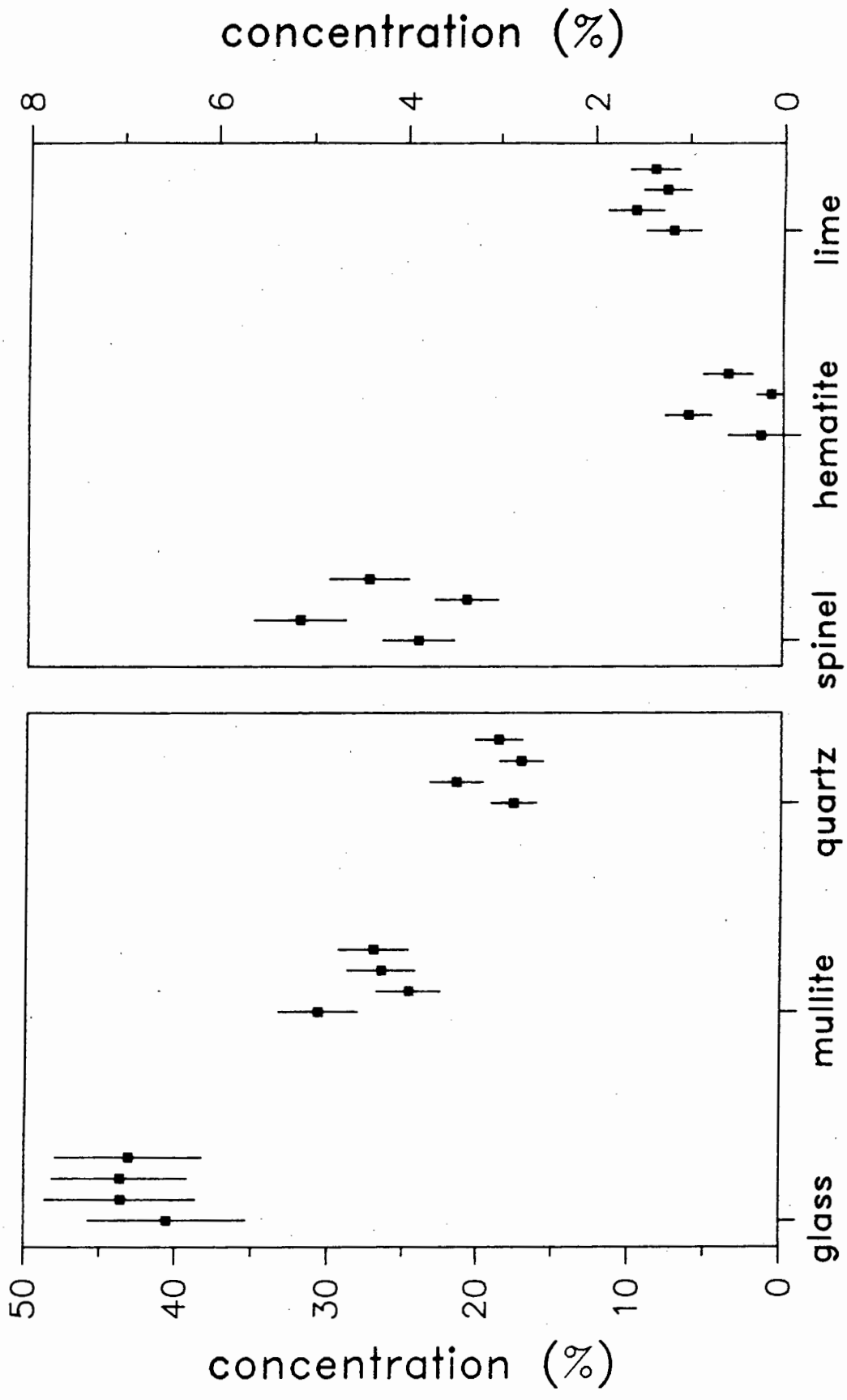

Fig. 6.17 : Variation in mineral concentrations of the four replicate D6 samples.

6.4 CHEMICAL COMPOSITION

6.4.1 Coal

Ranges of the major element oxides and the trace elements of the coal bulk chemical composition are listed in Table 6.3, and are shown graphically in Fig. 6.18. The following oxides have narrow concentration ranges in the input coal from a particular station: SiO_2, Al_2O_3, TiO_2, CaO, K_2O and P_2O_5 in all stations, FeO, MgO and Na_2O in Lethabo and Matla PFA, and S in Duvha and Matla PFA. The remaining oxides have wider concentration ranges. LOI is lower in Lethabo PFA than in PFA from either Duvha and Matla, resulting in higher concentrations of the major mineral forming oxides such as SiO_2 and Al_2O_3. The concentrations of FeO, MgO, CaO and Na_2O are lowest in Duvha PFA and equal in PFA from Lethabo and Matla.

Many trace elements occur at high concentrations in the Lethabo coal and low concentrations in the Matla coal, due to the higher ash content of the former, e.g. Zr, Nb, U, Th, As, Ga, Zn, Cu, Ni, Co, Cr, V, La, Ce and Nd. Ba and Sr are highest in Matla coal.

6.4.2 PFA

6.4.2.1 Bulk Chemical Composition:

Concentration ranges of the major element oxides and the trace elements of the PFA bulk chemical compositions are listed in Tables 6.4 (a-c). Enrichment ratios of the oxides and trace elements are listed in Table 6.5. The relationship between the precipitator field number and concentrations of the major oxides is shown in Fig. 6.19(a), and a comparison of the enrichment ratios (field 4 concentration / field 1 concentration) are shown for each oxide in Fig. 6.19 (b).

SiO_2 and Al_2O_3 have the highest concentrations in the ash (>20%), with CaO and Fe_2O_3 in the concentration range 3-10%. The remaining oxides TiO_2, MgO, K_2O, Na_2O, P_2O_5 and SO_3 have concentrations of less than 3% and often less than 1%.

SiO_2 has similar concentrations in PFA from all three stations. Al_2O_3 and TiO_2 are highest in Lethabo PFA and lowest in Matla PFA, and CaO, K_2O, P_2O_5 and SO_3 are highest in Matla PFA and lowest in Lethabo PFA. Duvha PFA has the highest Fe_2O_3 concentration and the lowest MgO and Na_2O concentrations.

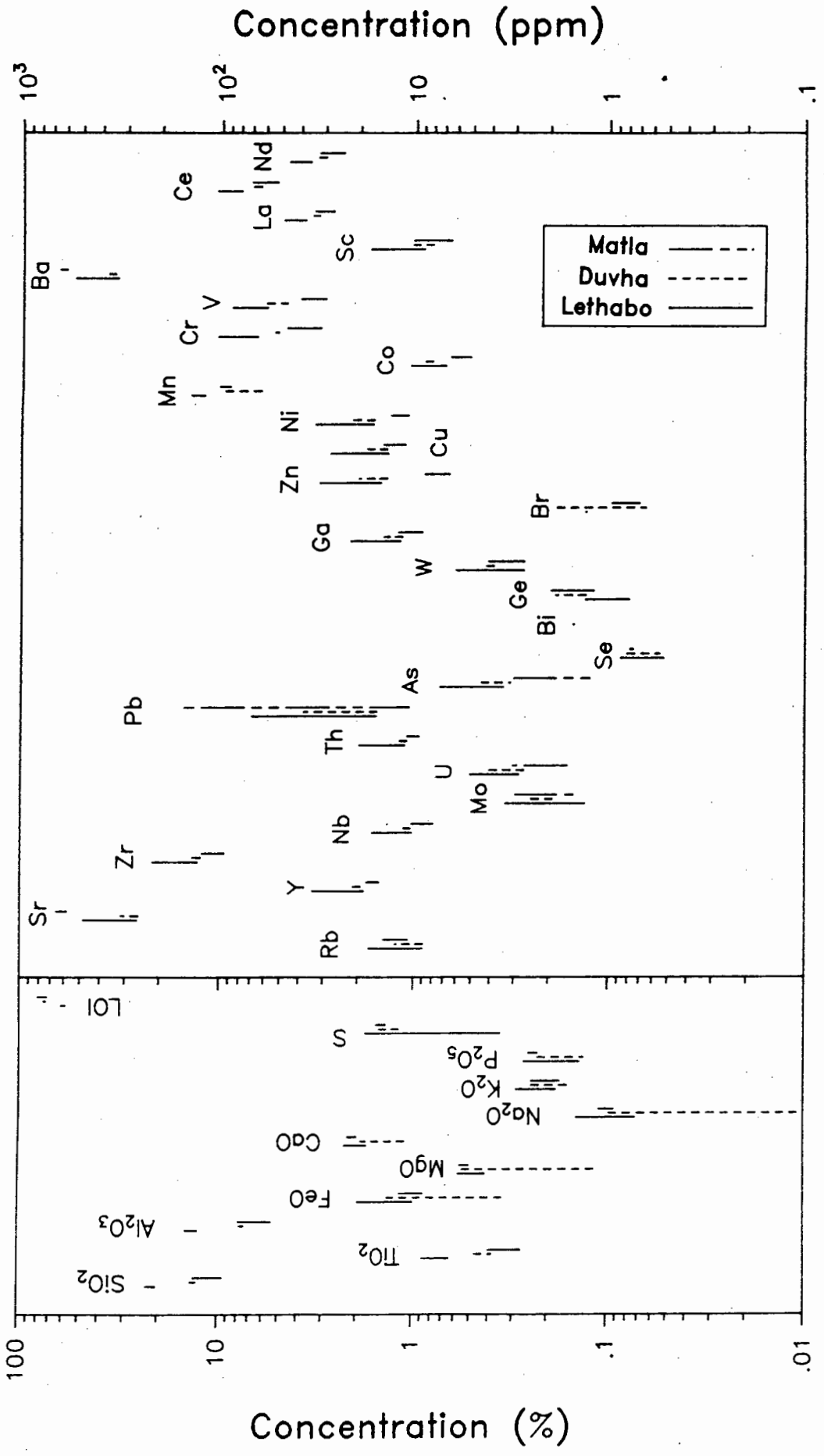

Fig. 6.18 : Major oxide and trace element composition ranges of coal samples received from the input coal of Lethabo, Duvha and Matla.

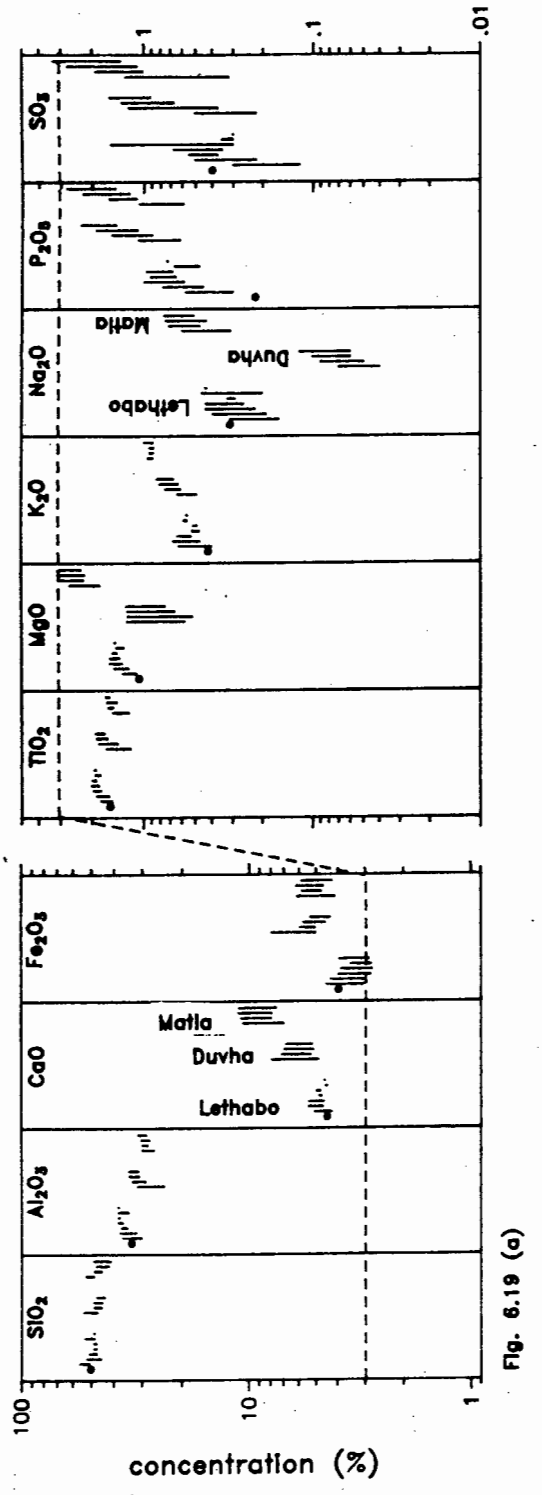

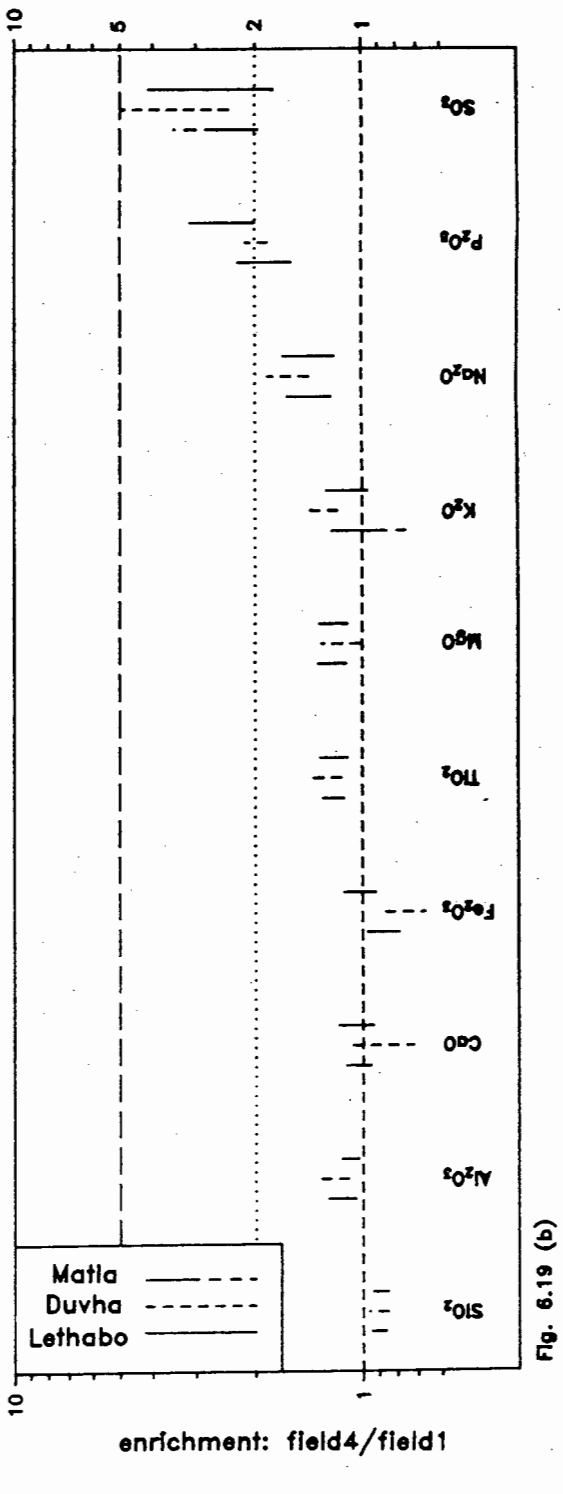

Fig. 6.19(a) : Major oxide composition ranges in the PFA samples. From left to right for each oxide: Lethabo bottom ash ( ), fields 1, 2, 3, 4, 5, 6, 7; Duvha fields 1, 2, 3, 4; and Matla fields 1, 2, 3, 4.

Fig. 6.19(b) : Enrichment ranges of the major oxides in the PFA samples.

	Lethabo n = 6			Duvha n = 3			Matla n = 4		
	Min		Max	Min		Max	Min		Max
SiO_2	20.26	-	22.59	12.79	-	13.50	9.45	-	13.14
TiO_2	.63	-	.88	.38	-	.47	.27	-	.40
Al_2O_3	12.63	-	14.38	7.36	-	7.69	5.38	-	7.78
FeO	.99	-	1.95	.34	-	1.35	.87	-	1.16
MgO	.41	-	.57	.12	-	.54	.50	-	.56
CaO	1.77	-	2.28	1.10	-	1.88	1.99	-	2.20
Na_2O	.07	-	.14	<.01	-	.10	.09	-	.11
K_2O	.18	-	.28	.16	-	.24	.17	-	.24
P_2O_5	.14	-	.26	.13	-	.22	.22	-	.25
S	.35	-	1.80	1.18	-	1.50	1.40	-	1.57
LOI	58.76	-	61.38	73.75	-	75.00	72.59	-	80.19
Rb	9	-	17	9	-	12	11	-	14
Sr	259	-	479	256	-	312	582	-	649
Y	19	-	34	18	-	21	15	-	18
Zr	129	-	216	125	-	145	95	-	122
Nb	10	-	17	10	-	11	8	-	10
Mo	1	-	3	2	-	2	2	-	3
U	3	-	5	3	-	4	2	-	3
Th	11	-	20	11	-	12	9	-	11
Pb	16	-	69	16	-	38	11	-	164
As	3	-	7	3	-	4	1	-	3
Se	.5	-	.9	.6	-	.8	.8	-	.8
Bi	<1.7			<1.5	-	2	<1.4		
Ge	.8	-	1	1	-	2	1	-	2
W	3	-	6	4	-	4	3	-	4
Ga	12	-	22	12	-	15	9	-	12
Br	<.6			.6	-	2	.7	-	1.0
Zn	15	-	32	14	-	20	7	-	9
Cu	14	-	28	14	-	18	11	-	15
Ni	17	-	33	17	-	22	11	-	14
Mn	121	-	140	63	-	96	90	-	100
Co	7	-	11	8	-	9	5	-	6
Cr	66	-	103	52	-	54	32	-	47
V	59	-	88	47	-	59	30	-	40
Ba	336	-	544	349	-	371	605	-	651
Sc	9	-	18	8	-	10	6	-	10
La	38	-	49	32	-	35	27	-	34
Ce	80	-	105	64	-	72	53	-	70
Nd	36	-	46	29	-	33	24	-	32

Table 6.3 : Concentration ranges of oxides and trace elements in the coal samples. < x indicates a value below the detection limit of x.

	Bottom Ash n = 1	Mixed Ash n = 1	Field 1 n = 4			Field 2 n = 4			Field 3 n = 4		
SiO_2	50.27	50.77	51.35	-	55.87	45.17	-	52.11	47.55	-	50.61
TiO_2	1.57	1.67	1.54	-	1.76	1.59	-	1.87	1.77	-	1.94
Al_2O_3	33.35	35.23	30.06	-	36.33	31.76	-	37.40	34.69	-	36.87
Fe_2O_3	3.97	3.41	3.06	-	4.49	3.00	-	4.30	2.83	-	3.96
MgO	1.06	1.20	1.11	-	1.31	1.23	-	1.47	1.34	-	1.58
CaO	4.46	4.36	4.24	-	5.07	4.66	-	5.39	4.61	-	5.38
Na_2O	.31	.28	.16	-	.31	.19	-	.39	.22	-	.43
K_2O	.42	.46	.40	-	.62	.47	-	.67	.53	-	.63
P_2O_5	.22	.36	.30	-	.57	.45	-	.77	.58	-	.99
SO_3	.40	.42	.12	-	.30	.22	-	.50	.37	-	.55
H_2O^-	.29	.39	.04	-	.16	.08	-	5.74	.10	-	.19
LOI	4.35	2.25	.37	-	1.96	.15	-	2.26	.53	-	3.21
Rb	27	31	27	-	39	30	-	44	37	-	42
Sr	759	837	767	-	1306	870	-	1573	945	-	1745
Y	88	94	69	-	94	76	-	105	82	-	112
Zr	567	571	452	-	586	458	-	600	470	-	655
Nb	46	47	41	-	48	46	-	52	49	-	65
Mo	3	6	5	-	6	7	-	9	9	-	10
U	11	12	9	-	12	12	-	14	12	-	15
Th	45	49	45	-	50	50	-	57	54	-	68
Pb	31	79	65	-	77	104	-	117	134	-	166
As	3	14	9	-	15	23	-	28	29	-	37
Se	<.9	2	1	-	2	2	-	3	3	-	5
Bi	<3	3	<3			6	-	7	11	-	11
Ge	<1	2	1	-	2	4	-	5	6	-	7
W	7	7	7	-	10	10	-	13	12	-	16
Ga	33	56	36	-	55	58	-	79	78	-	108
Br	<1	<1	<1			<1			<1		
Zn	35	81	35	-	79	62	-	137	90	-	183
Cu	50	59	39	-	61	48	-	75	55	-	78
Ni	88	92	45	-	96	53	-	112	67	-	126
Mn	413	371	248	-	358	278	-	388	315	-	413
Cs	11	13		-	13		-	15		-	14
Co	23	24	16	-	24	19	-	28	24	-	29
Cr	231	257	177	-	257	211	-	285	241	-	287
V	164	191	119	-	192	153	-	233	180	-	260
Ba	743	868	800	-	1124	937	-	1393	1123	-	1480
Sc	39	43	32	-	44	37	-	50	42	-	52
La	102	113	97	-	110	103	-	119	110	-	124
Ce	217	234	202	-	232	215	-	247	230	-	260
Nd	99	104	83	-	106	86	-	113	95	-	118

Table 6.4(a) : Concentration ranges of oxides and trace elements in the Lethabo PFA samples.

	Field 4 n = 4			Field 5 n = 3			Field 6 n = 2			Field 7 n = 1
SiO_2	47.35	-	48.48	47.54	-	48.41	48.52	-	52.89	48.56
TiO_2	1.82	-	1.99	1.90	-	1.96	1.78	-	1.90	1.91
Al_2O_3	36.50	-	38.07	37.59	-	38.21	34.31	-	38.24	38.13
Fe_2O_3	2.79	-	3.84	2.83	-	3.49	2.89	-	3.90	2.98
MgO	1.39	-	1.55	1.44	-	1.51	1.31	-	1.44	1.47
CaO	4.71	-	4.82	4.79	-	4.95	4.46	-	4.52	4.56
Na_2O	.26	-	.43	.29	-	.32	.20	-	.45	.43
K_2O	.47	-	.52	.49	-	.51	.56	-	.58	.56
P_2O_5	.65	-	.90	.68	-	.96	.47	-	.66	.73
SO_3	.35	-	.67	.30	-	1.55	.30	-	.35	.30
H_2O^-	.11	-	.43	.08	-	.42	.07	-	.16	.10
LOI	.28	-	1.20	.34	-	1.08	.33	-	.87	.67
Rb	31	-	35	32	-	35	37	-	39	38
Sr	993	-	1653	1045	-	1699	1029	-	1089	1185
Y	84	-	110	89	-	113	76	-	109	112
Zr	504	-	586	496	-	582	454	-	573	566
Nb	54	-	57	54	-	55	47	-	55	57
Mo	8	-	10	10	-	10	7	-	8	7
U	11	-	14	12	-	15	11	-	13	14
Th	60	-	62	59	-	62	52	-	61	63
Pb	158	-	166	176	-	180	134	-	179	185
As	26	-	33	28	-	31	17	-	25	26
Se	4	-	6	5	-	6	4	-	6	7
Bi	12	-	16	14	-	17	9	-	16	18
Ge	4	-	7	5	-	7	4	-	5	6
W	13	-	15	14	-	17	12	-	15	15
Ga	94	-	105	103	-	108	66	-	107	110
Br	<1			<1			<1			<1
Zn	101	-	204	122	-	217	75	-	226	235
Cu	61	-	83	70	-	84	54	-	88	96
Ni	79	-	129	90	-	132	61	-	127	128
Mn	373	-	483	406	-	487	318	-	495	518
Cs		-	14		-	14		-	15	14
Co	23	-	32	26	-	34	19	-	34	34
Cr	250	-	293	275	-	290	231	-	277	269
V	187	-	273	213	-	271	153	-	239	241
Ba	1148	-	1623	1206	-	1643	1119	-	1358	1437
Sc	45	-	56	47	-	56	40	-	54	54
La	119	-	128	123	-	132	103	-	133	139
Ce	246	-	268	258	-	272	222	-	270	275
Nd	99	-	120	114	-	122	94	-	122	124

Table 6.4(a) : Continued

	Composite Ash n = 1	Field 1 n = 4			Field 2 n = 4			field 3 n = 4			Field 4 n = 4		
SiO_2	51.98	47.08	-	53.59	4.92	-	48.45	44.86	-	48.44	43.66	-	47.15
TiO_2	1.65	1.19	-	1.63	1.42	-	1.81	1.63	-	1.85	1.69	-	1.90
Al_2O_3	31.34	23.83	-	31.15	28.84	-	32.92	30.90	-	33.91	31.09	-	34.22
Fe_2O_3	5.01	5.04	-	7.97	5.06	-	5.92	4.54	-	5.69	4.34	-	5.32
MgO	.82	.58	-	1.24	.52	-	1.24	.66	-	1.24	.75	-	1.26
CaO	4.89	4.87	-	7.90	5.30	-	7.12	5.13	-	6.95	5.20	-	6.84
Na_2O	.07	.04	-	.07	.05	-	.09	.06	-	.10	.06	-	.12
K_2O	.62	.49	-	.63	.61	-	.74	.63	-	.80	.67	-	.83
P_2O_5	.75	.62	-	1.08	.90	-	1.53	1.09	-	1.90	1.46	-	2.28
SO_3	.27	.22	-	.50	.37	-	1.22	.67	-	1.35	.92	-	1.57
H_2O^-	.12	.03	-	.87	.23	-	.57	.11	-	.32	.10	-	.50
LOI	2.74	2.03	-	7.68	2.22	-	6.58	2.84	-	6.12	3.03	-	6.67
Rb	38	28	-	39	36	-	43	38	-	47	41	-	48
Sr	1034	784	-	1301	1028	-	1790	1276	-	1967	1393	-	2042
Y	90	58	-	96	76	-	123	89	-	128	96	-	129
Zr	546	400	-	545	517	-	603	531	-	594	521	-	593
Nb	46	31	-	45	42	-	54	48	-	55	50	-	57
Mo	7	4	-	7	8	-	15	16	-	20	24	-	28
U	9	5	-	9	8	-	13	13	-	15	14	-	18
Th	43	29	-	41	38	-	55	51	-	60	56	-	64
Pb	52	22	-	49	49	-	99	94	-	121	126	-	141
As	11	3	-	10	13	-	28	31	-	36	45	-	53
Se	<.9	1	-	2	1	-	2	3	-	5	4	-	10
Bi	<3	3	-	3	5	-	7	5	-	10	8	-	11
Ge	3	1	-	3	3	-	9	10	-	13	16	-	20
W	7	5	-	9	7	-	10	12	-	14	14	-	18
Ga	38	21	-	37	35	-	71	66	-	89	96	-	109
Br	<1	<1			<1	-	4	<1			<1	-	2
Zn	82	29	-	73	43	-	125	82	-	157	110	-	209
Cu	49	34	-	45	47	-	61	57	-	64	61	-	74
Ni	93	45	-	90	64	-	113	84	-	121	94	-	145
Mn	233	233	-	390	241	-	331	244	-	328	258	-	332
Co	33	19	-	33	27	-	43	41	-	51	52	-	57
Cr	163	139	-	206	161	-	265	199	-	289	219	-	296
V	129	98	-	174	134	-	247	159	-	306	210	-	346
Ba	974	660	-	967	854	-	1346	1062	-	1460	1233	-	1617
Sc	30	22	-	30	28	-	40	36	-	44	40	-	46
La	105	72	-	109	92	-	139	114	-	148	120	-	150
Ce	196	157	-	229	192	-	299	236	-	322	251	-	326
Nd	99	66	-	107	89	-	139	103	-	146	112	-	146

Table 6.4(b) : Concentration ranges of oxides and trace elements in the Duvha PFA samples.

	Field 1 n = 4			Field 2 n = 4			field 3 n = 4			Field 4 n = 4		
SiO_2	48.42	-	52.24	44.83	-	48.41	41.78	-	47.32	41.04	-	48.63
TiO_2	1.22	-	1.50	1.51	-	1.59	1.43	-	1.62	1.60	-	1.65
Al_2O_3	26.50	-	29.68	28.31	-	29.68	27.87	-	29.95	28.63	-	31.11
Fe_2O_3	4.15	-	6.10	4.72	-	5.82	4.65	-	6.13	4.25	-	5.85
MgO	1.79	-	2.62	2.21	-	2.94	2.19	-	3.07	2.29	-	3.04
CaO	7.01	-	10.64	7.97	-	10.87	7.92	-	11.12	7.55	-	11.15
Na_2O	.31	-	.59	.47	-	.71	.43	-	.74	.51	-	.76
K_2O	.88	-	.93	.87	-	.91	.87	-	.91	.88	-	.98
P_2O_5	.59	-	1.06	1.11	-	1.59	1.22	-	2.23	1.47	-	2.77
SO_3	.32	-	1.27	1.02	-	1.90	1.10	-	2.74	1.37	-	3.29
H_2O^-	.14		-	.21		-	.18	.08	-	.30	.10	-
LOI	1.37	-	6.64	1.37	-	4.87	1.18	-	9.48	.87	-	2.35
Rb	52	-	57	53	-	63	53	-	61	53	-	66
Sr	1850	-	2880	2635	-	3439	2706	-	3903	2867	-	4130
Y	65	-	80	79	-	88	84	-	87	81	-	93
Zr	465	-	530	470	-	514	468	-	515	465	-	509
Nb	40	-	48	45	-	50	48	-	52	49	-	55
Mo	7	-	16	16	-	24	18	-	36	26	-	42
U	3	-	7	5	-	9	8	-	10	7	-	10
Th	36	-	43	41	-	51	47	-	52	46	-	55
Pb	26	-	58	63	-	87	65	-	107	87	-	120
As	6	-	11	16	-	21	17	-	33	25	-	40
Se	1	-	3	4	-	5	5	-	9	6	-	13
Bi	4	-	5	5	-	8	7	-	11	9	-	14
Ge	4	-	9	10	-	16	12	-	27	16	-	33
W	6	-	10	10	-	13	13	-	21	15	-	20
Ga	33	-	48	61	-	78	75	-	90	87	-	107
Br	<1			<1			<1	-	2	<1		
Zn	17	-	28	40	-	50	46	-	66	59	-	85
Cu	31	-	47	49	-	59	49	-	71	62	-	75
Ni	41	-	83	60	-	70	63	-	98	69	-	93
Mn	272	-	421	335	-	463	352	-	537	349	-	574
Co	16	-	28	31	-	41	31	-	48	36	-	58
Cr	115	-	151	168	-	176	173	-	201	191	-	205
V	80	-	108	135	-	144	147	-	196	184	-	240
Ba	1374	-	2071	1983	-	2467	1945	-	2757	2208	-	2978
Sc	25	-	31	34	-	35	34	-	39	37	-	41
La	79	-	99	103	-	113	100	-	112	108	-	117
Ce	172	-	220	216	-	233	214	-	235	231	-	237
Nd	79	-	96	97	-	103	101	-	109	99	-	112

Table 6.4(c) : Concentration ranges of oxides and trace elements in the Matla PFA samples.

	Lethabo n = 4			Duvha n = 4			Matla n = 4		
	Min		Max	Min		Max	Min		Max
SiO_2	.861	-	.944	.851	-	.958	.848	-	.931
TiO_2	1.128	-	1.288	1.148	-	1.415	1.101	-	1.310
Al_2O_3	1.048	-	1.248	1.098	-	1.304	1.028	-	1.148
Fe_2O_3	.787	-	.968	.667	-	.860	.918	-	1.126
MgO	1.109	-	1.327	1.013	-	1.296	1.111	-	1.315
CaO	.951	-	1.114	.720	-	1.067	1.017	-	1.172
Na_2O	1.223	-	1.616	1.413	-	1.836	1.201	-	1.662
K_2O	.756	-	1.217	1.105	-	1.395	.967	-	1.122
P_2O_5	1.575	-	2.351	1.842	-	2.122	2.001	-	3.093
SO_3	1.958	-	3.456	2.403	-	4.984	1.767	-	4.119
Rb	.816	-	1.171	1.140	-	1.492	1.025	-	1.232
Sr	1.265	-	1.619	1.569	-	1.776	1.269	-	1.693
Y	1.170	-	1.263	1.310	-	1.652	1.024	-	1.431
Zr	1.000	-	1.116	1.032	-	1.302	.877	-	1.094
Nb	1.150	-	1.313	1.207	-	1.619	1.016	-	1.364
Mo	1.457	-	1.901	3.967	-	5.612	2.192	-	3.651
U	.932	-	1.310	1.745	-	1.992	1.462	-	3.267
Th	1.190	-	1.329	1.524	-	1.953	1.075	-	1.539
Pb	2.059	-	2.559	2.857	-	5.718	1.901	-	4.236
As	1.888	-	2.791	5.256	-	17.677	2.688	-	4.445
Se	2.000	-	3.971	2.861	-	5.813	3.574	-	9.019
Bi		-		3.240	-	3.240	2.233	-	2.449
Ge	2.318	-	3.622	7.735	-	16.098	2.386	-	5.690
W	1.283	-	2.065	2.357	-	2.500	1.658	-	2.491
Ga	1.917	-	2.596	2.866	-	4.633	1.812	-	3.157
Br	.992	-	1.034	.958	-	1.000	1.040	-	1.058
Zn	1.687	-	3.138	2.858	-	3.778	2.174	-	4.865
Cu	1.296	-	1.570	1.435	-	1.637	1.305	-	1.968
Ni	1.346	-	1.734	1.617	-	1.767	1.115	-	1.842
Mn	1.279	-	1.527	.919	-	1.108	1.282	-	1.363
Co	1.258	-	1.486	1.705	-	2.539	1.621	-	2.434
Cr	1.101	-	1.482	1.434	-	1.569	1.284	-	1.662
V	1.355	-	1.646	1.743	-	1.992	1.705	-	2.632
Ba	1.405	-	1.723	1.599	-	1.866	1.275	-	1.643
Sc	1.264	-	1.386	1.527	-	1.773	1.217	-	1.538
La	1.148	-	1.243	1.221	-	1.664	1.094	-	1.387
Ce	1.154	-	1.237	1.328	-	1.592	1.049	-	1.378
Nd	1.137	-	1.231	1.257	-	1.508	1.069	-	1.366

Table 6.5 : Range of enrichment factors for oxides and trace elements in PFA from Lethabo, Duvha and Matla.

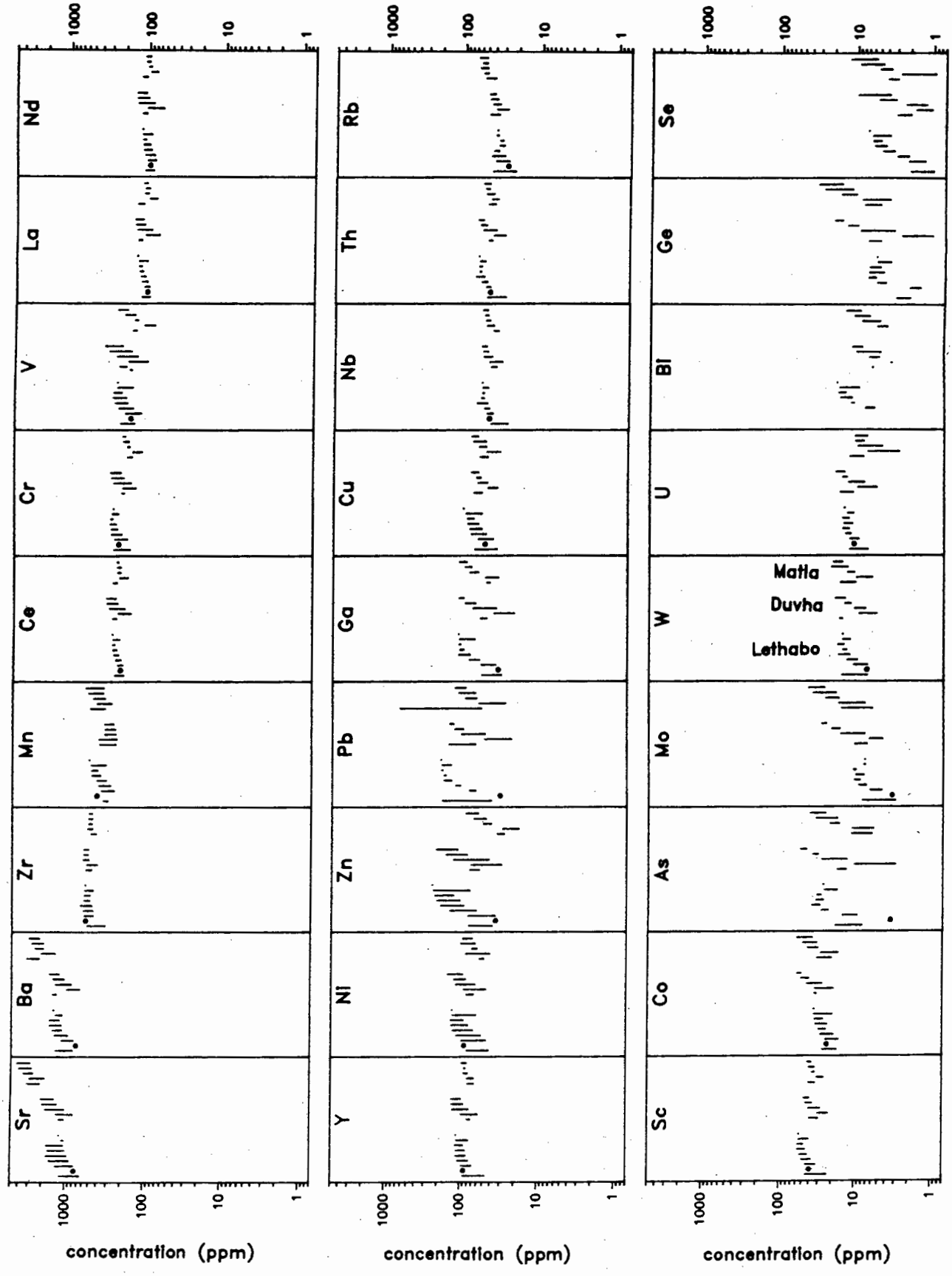

Fig. 6.20(a) : Trace element composition ranges in the PFA samples. From left to right for each oxide: Lethabo coal ash, bottom ash ( ), fields 1, 2, 3, 4, 5, 6, 7; Duvha coal ash, fields 1, 2, 3, 4; and Matla coal ash, fields 1, 2, 3, 4. Values for coal ash were calculated from the coal compositions.

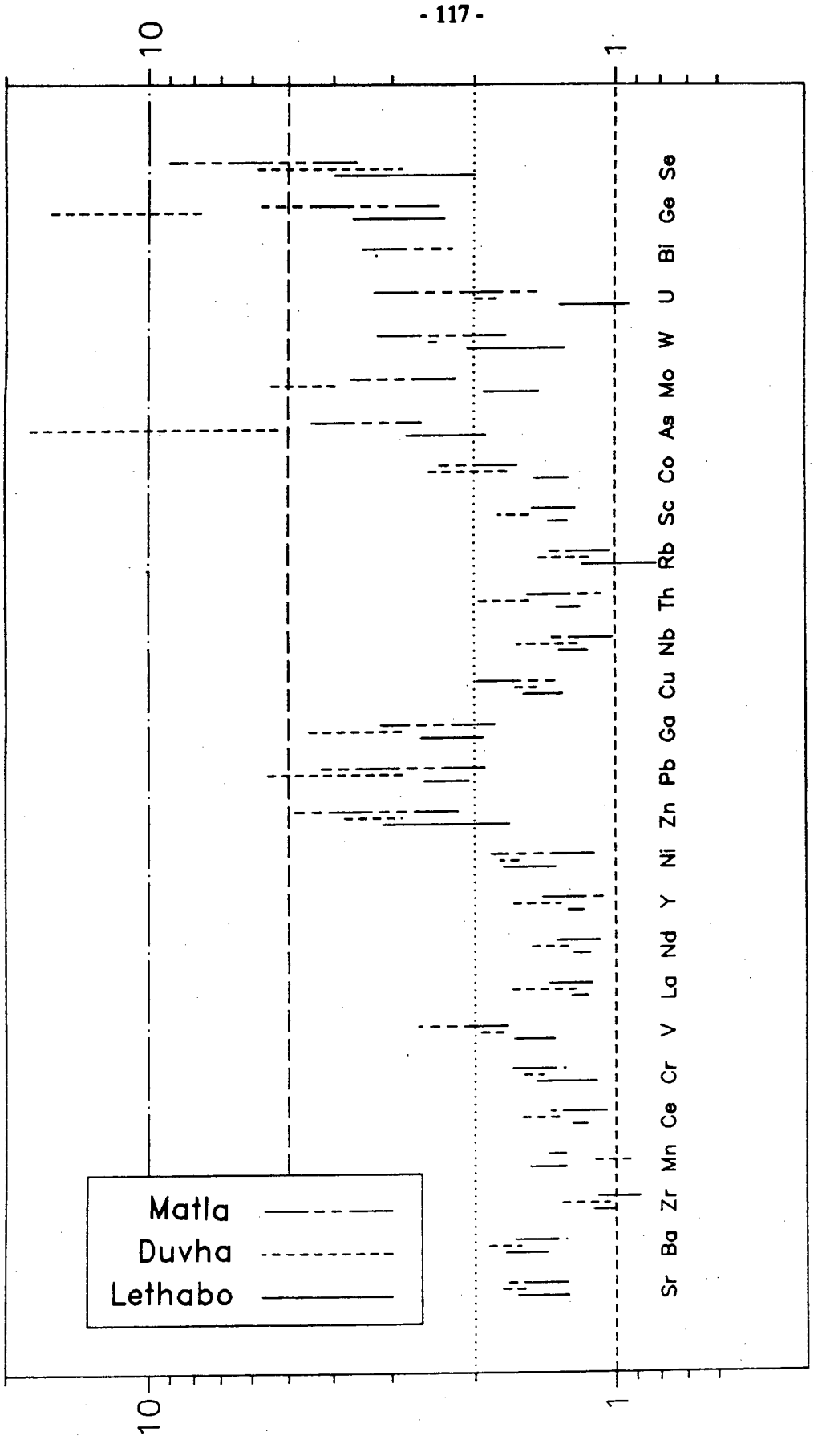

Fig. 6.20(b) : Ranges of trace element enrichment in PFA. Elements are arranged from left to right in approximate order of decreasing concentration.

The enrichment factors for SiO_2 (<1) are similar for PFA from Lethabo, Duvha and Matla PFA. The concentration thus decreases in PFA from fields 1 to 4 in all cases, but remains approximately constant in PFA from the last precipitator fields of Lethabo. CaO remains constant in PFA from fields 1 to 4 of all stations. Fe_2O_3 remains constant in Matla PFA, but decreases in concentration in PFA from fields 1 to 4 of Duvha and Lethabo, and K_2O remains constant in PFA from Matla and Lethabo but increases slightly in Duvha PFA. In all cases Na_2O, P_2O_5 and SO_3 increase considerably in concentration in PFA from fields 1 to 4, and the concentrations remain constant in PFA from the last four precipitator fields of Lethabo. SO_3 has the highest enrichment factors (2-5X) of all the oxides.

Lethabo Bottom Ash is enriched in Na_2O and SO_3 relative to PFA from field 1, and depleted in MgO and P_2O_5 (Fig. 6.19(a)). The oxides SiO_2, Al_2O_3, CaO, Fe_2O_3 (the refractory oxides) and K_2O have similar concentrations in Bottom Ash and in PFA from field 1.

Trace element concentration ranges for PFA from each field of Matla, Duvha and Lethabo, as well as for the coal ash (calculated from the LOI values), are shown graphically in Fig. 6.20(a). Most trace elements have similar concentration ranges in PFA from all three stations, except for Sr and Ba which are highest in Matla PFA. Trace element concentrations are similar in both the Lethabo coal ash and in PFA from field 1. Trace element concentrations are depleted in field 1 PFA relative to the coal ash for Ba, Ce, Cr, V, La, Nd, Pb, Cu, Sc, W, U and Se in both Duvha and Matla PFA, for Ga, Th, Rb, As, Mo and Ge in Duvha PFA, and for Zn in Matla PFA. The concentrations in field 1 PFA relative to concentrations in the coal ash are probably a function of power station design.

A comparison of the range of enrichment factors for each element is shown in Fig. 6.20(b). High enrichment factors (> 5) are found for As and Ge in Duvha PFA, and for Se in Matla PFA. Factors in the range 2-5X are found for Pb, Ga and Zn in PFA from all three stations, for Mo, Bi and W in PFA from Matla and Duvha, for Ge and As in Matla and Lethabo PFA, for Se in Duvha and Lethabo PFA, and for U in some samples of Matla PFA. Some samples have enrichment factors >2 for Co in Matla and Duvha PFA and for V in Matla PFA. Certain trace elements such as Ga, Th, As, Mo and Ge have higher enrichment factors in Duvha PFA than in PFA from the other stations. This feature was noted by Willis (1987) Trace elements which remain constant in concentration in PFA from fields 1 to 4 are Zr in all three stations, Rb in Lethabo PFA, and Mn in Duvha PFA. The remaining trace elements have enrichment factors in the range 1-2X. The high enrichment factors for Duvha PFA are due to the low initial trace element concentrations in field 1 PFA (compared with concentrations in the coal ash). Lethabo PFA, which generally has the lowest enrichment

factors, does not show this depletion in field 1 concentrations compared with the coal ash.

Many of the trace elements showing large enrichment factors have low concentrations in PFA from field 1. These are As, Mo, Ge and Se, and to a lesser extent W, U (in Duvha and Matla) and Bi. The only elements with both high enrichment factors and high concentrations are Pb, Zn and Ga.

Many elements which increase in concentration in PFA from fields 1 to 4 of Lethabo remain constant in PFA from the last four precipitator fields. These are Sr, Ba, Mn, Ce, Cr, V, Zn, Pb, Ga, Ni, La, Nd, Cu, Th, Co, Sc, Nb, W, U, Bi and Se. As and Ge have concentration maxima in the vicinity of fields 3 to 5 of Lethabo PFA followed by a decrease in concentration in fields 6 and 7.

Lethabo Bottom Ash is depleted relative to PFA from field 1 in Pb, As, Mo, Ge, Bi and Se, but is relatively enriched in Mn. The remaining trace elements have similar concentrations in both the bottom ash and in field 1 PFA.

The trace element enrichment in PFA from fields 1 to 4 is associated with a decrease in particle size. The inverse relationship between particle size and the trace element concentration has been noted by many researchers. Natusch et al (1974) noted that As, Cr, Pb, Ni, Se, Zn as well as other trace elements concentrated in samples with the smallest particle size. Campbell et al (1978) noted that the concentrations of As, Cr, Ga and Pb increased with decreasing particle size, and that for Si and possibly Zr the concentrations increase with increasing particle size. Kaakinen et al (1975) noted that Al, Fe, Rb, Sr, Y and Nb remain approximately constant in samples taken downstream in a power station, and that Cu, Zn, As, Mo, Pb and Se are lowest in the bottom ash and increase downstream. The same authors noted a decrease in the Zr concentration in the downstream samples. Willis (1983) reported that for Grootvlei power station Mo, Ge, As and Bi showed the greatest enrichment, V, W, Pb, Se and U the least enrichment, and Ga, Zn, P and S intermediate degrees of enrichment.

Coles et al (1979) recognised three classes of element based on the enrichment as a function of particle size. These are: elements which have little or no enrichment in the smaller particle size (Al, Ca, Fe, K, Mg, Mn, Na, Rb, Ti, Ce, La and Nd); elements which are enriched in the smaller particles (As, Ga, Mo, Pb, Se, W and Zn); and elements whose behaviour is

intermediate between the two groups (Ba, Sr, Cr, Cu, Ni, U and V). These categories are in agreement with the trace element behaviour recognised in this work.

Attempts have been made to explain the inverse relationship between concentration and particle size by a model involving vaporisation in the combustion chamber followed by condensation onto particle surfaces as the temperature of the flue gas cools, with smaller particles having larger surface area / volume ratios and subsequently higher trace element concentrations. Smith et al (1980) have been able to show that some of the elements which have the largest enrichment factors reported in this work (Se and As) and Br are completely volatilised by 1400°C in reheating experiments on fly ash. The concentration maxima in PFA from fields 4, 5 and 6 of certain trace elements from Lethabo PFA (Ge and As) cannot be explained by the surface area - volume model noted above as there is no significant difference in the particle size distributions of PFA from Lethabo fields 4, 5, 6 and 7. If condensation of a particular phase was complete by field 4, then that element would remain constant in PFA from fields 4, 5, 6 and 7, due to PFA from those fields having similar particle size distributions. The observed decrease in concentration can be explained if Ge and As are still undergoing condensation from fields 4 and 7. This is supported by the low temperatures of sublimation of the oxides of these phases (GeO sublimes at 710°C and As_2O_3 sublimes at 193°C). Other phases which sublime at relatively low temperatures are SeO_2 (350°C) and Ga_2O (>500°C), both of which show strong enrichments in PFA from fields 1 to 4 and remain constant in PFA from fields 4, 5, 6 and 7. An alternative explanation could be the preferential extraction of As and Ge bearing particles by the electrostatic precipitators.

6.4.2.2 Chemical Composition of Glass:

Histograms of the SiO_2 and Al_2O_3 compositions of the glass phase determined with the electron microprobe are presented in Figs 6.21 and 6.22 respectively for L1 (fields 1 to 2), D1 (fields 1 to 3) and M2 (fields 1 to 4). It was decided to limit the fields studied in the case of D1 and L1 as it was felt that selection of suitably sized particles (>15μm) from samples with a small particle size distribution caused bias in the results.

SiO_2 has a bimodal distribution in Duvha and Matla glass, and a unimodal distribution in Lethabo glass. The average SiO_2 concentration is similar in all three stations. High SiO_2 concentrations in Matla and Duvha glasses are associated with low Al_2O_3 concentrations (<10%) in some samples. Hulett et al (1980) noted that quartz was associated with an Al_2O_3

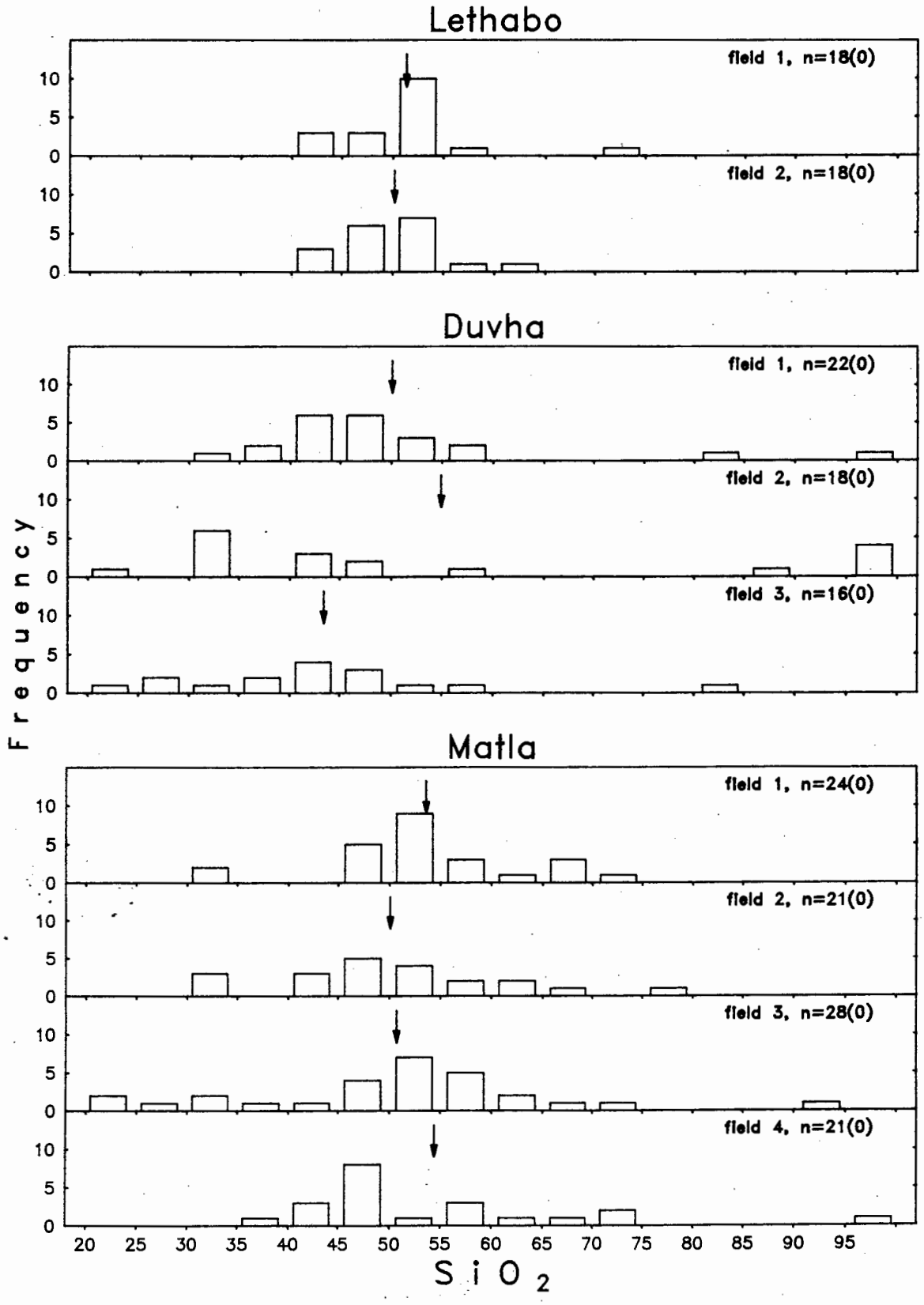

Fig. 6.21 : Histograms of the SiO_2 distribution in PFA glass analyses. Mean values are indicated by an arrow. The number in bracketts is the number of analyses below the detection limit.

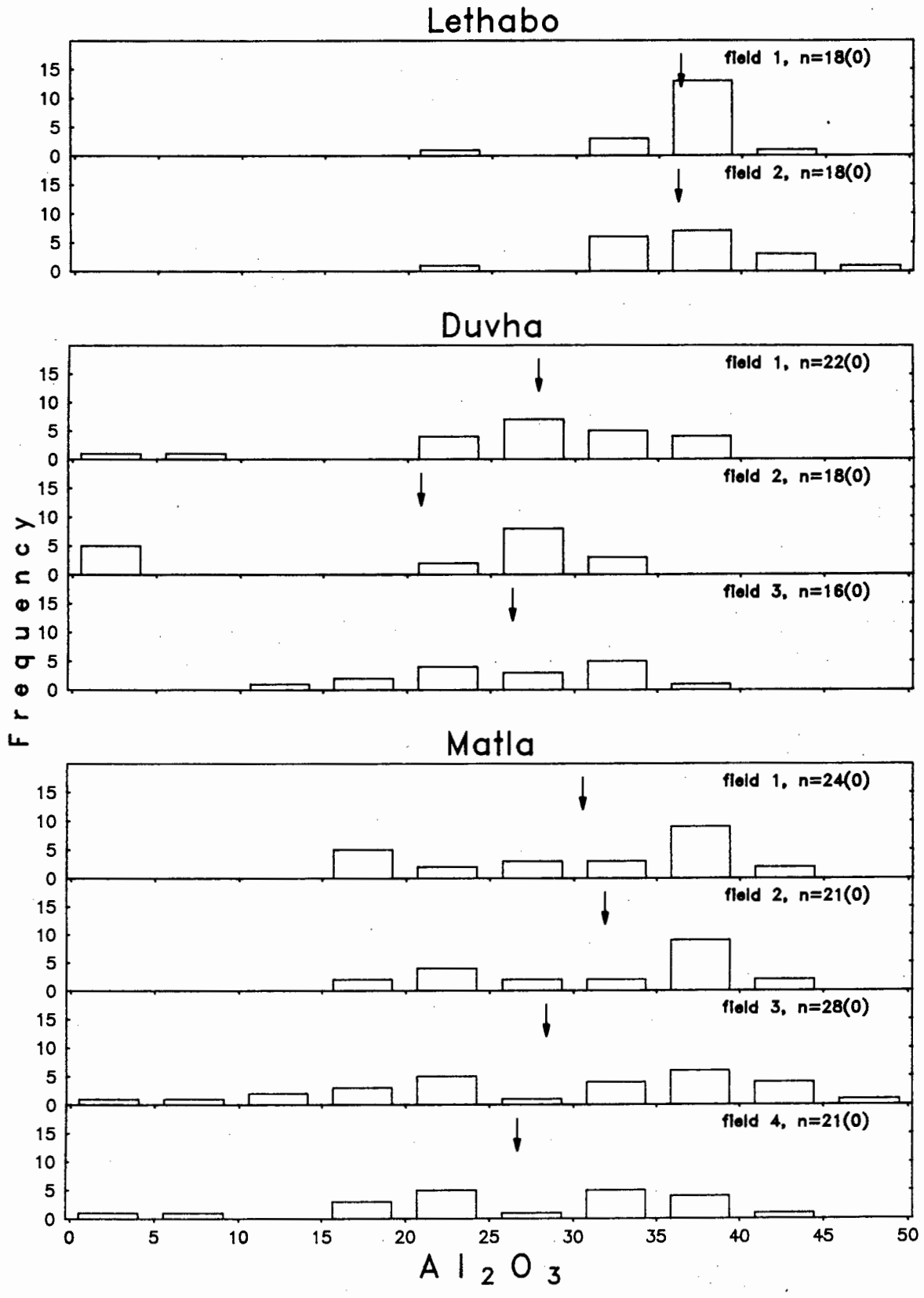

Fig. 6.22 : Histograms of the Al_2O_3 distribution in PFA glass analyses. Mean values are indicated by an arrow. The number in bracketts is the number of analyses below the detection limit.

concentration of < 10%.

Lethabo and Matla PFA glass both have a mode between 35-40%, and Matla glass has a second mode between 15-25%. Duvha glass has a mode between 25-35%.

A plot of Al_2O_3 versus SiO_2 in glass is shown in Fig. 6.23. Also shown on the same diagram are points representing quartz (SiO_2) and kaolinite ($Al_2Si_2O_5(OH)_4$) (expressed as OH free), which are the two major Al_2O_3 and SiO_2 bearing mineral phases of the input coal. Most analyses plot within the area bounded by the kaolinite-quartz tie line (mixing line) and the kaolinite dilution line (dilution by other than aluminosilicate bearing phases), although several analyses plot on the high Al_2O_3 side of the latter line. No analyses plot outside the kaolinite-quartz tie-line. The control of glass analyses by this tie line is particularly obvious for Matla PFA. The difference in composition between kaolinite and the glass can be explained by mixing between kaolinite, quartz and a third class of components which contain no silica or aluminium and thus do not plot on this diagram, e. g. lime and spinel.

The extent of kaolinite mixing with quartz and with phases which contain no SiO_2 and Al_2O_3 is further demonstrated in Fig. 6.24. Duvha and especially Lethabo glass compositions are largely controlled by mixing between kaolinite and phases other than quartz, whereas Matla glass has large contributions from both quartz and non-quartz phases.

Lauf (1985) noted that glass droplets of considerably different compositions can coexist in the combustor, and suggested that little mixing of droplets occurs during combustion. However, a considerable amount of initial mixing must occur while the droplets are liquid in order to explain the compositional variations of the glass. Similar trends on the SiO_2-Al_2O_3-"other oxide" ternary diagram were reported by Ramsden and Shibaoka (1982) and were attributed to variable proportions of quartz, clay and other minerals in the original coals.

Histograms showing the extent of assimilation of CaO, TiO_2, Fe_2O_3, MgO, P_2O_5, K_2O, Na_2O, BaO and SrO into the glass phase are shown in Figs 6.25-6.33.

The CaO frequency distributions (Fig. 6.25) of Matla and Duvha glass have a mode at less than 2% in PFA from all the fields (except Duvha field 3), although concentrations as high as 40% are found in Duvha glass and 46% in Matla glass. The CaO concentration of Lethabo glass has a mode at 4-6%, with no values greater than 20%.

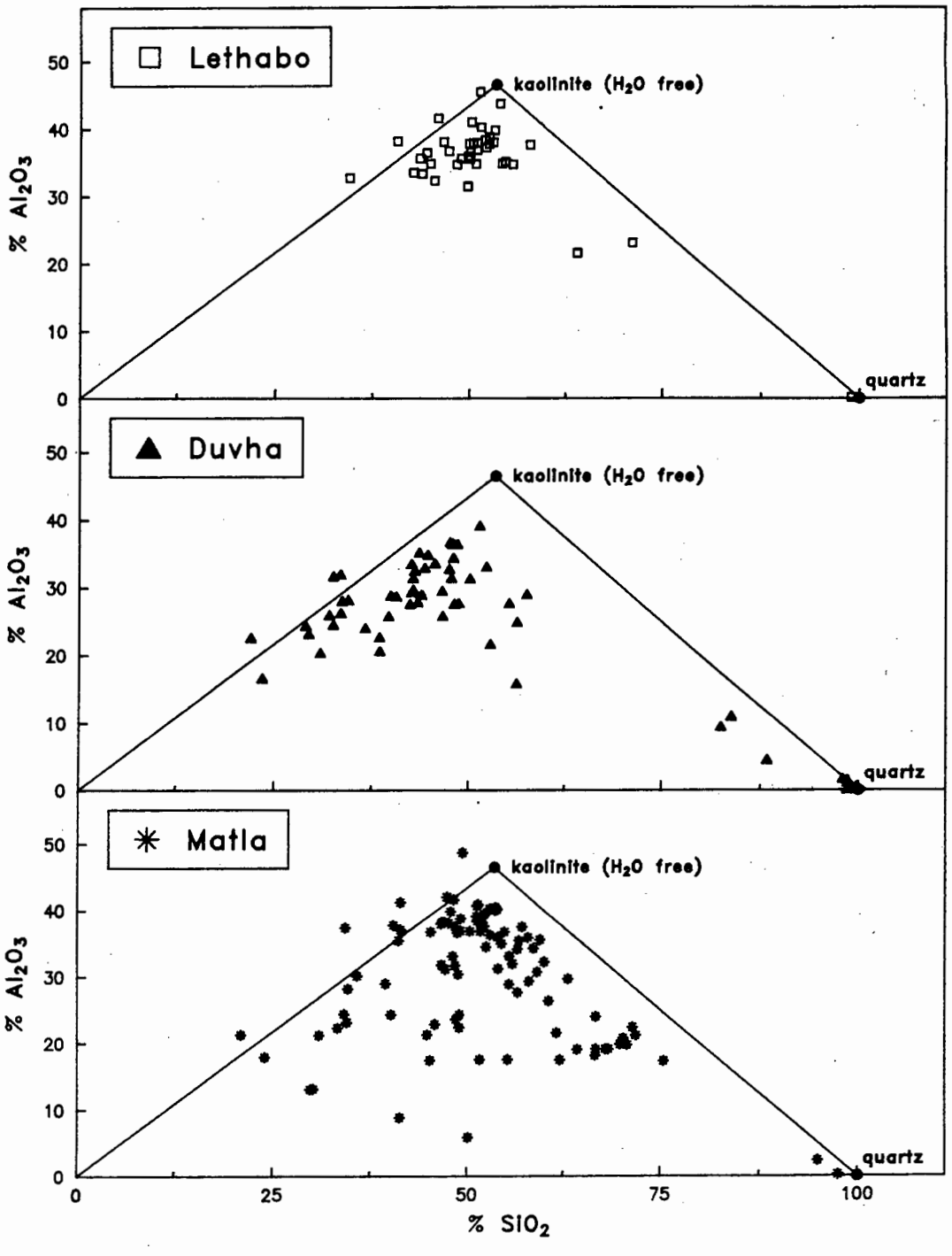

Fig. 6.23 : Al_2O_3 vs SiO_2 in glass analyses from Lethabo, Duvha and Matla.

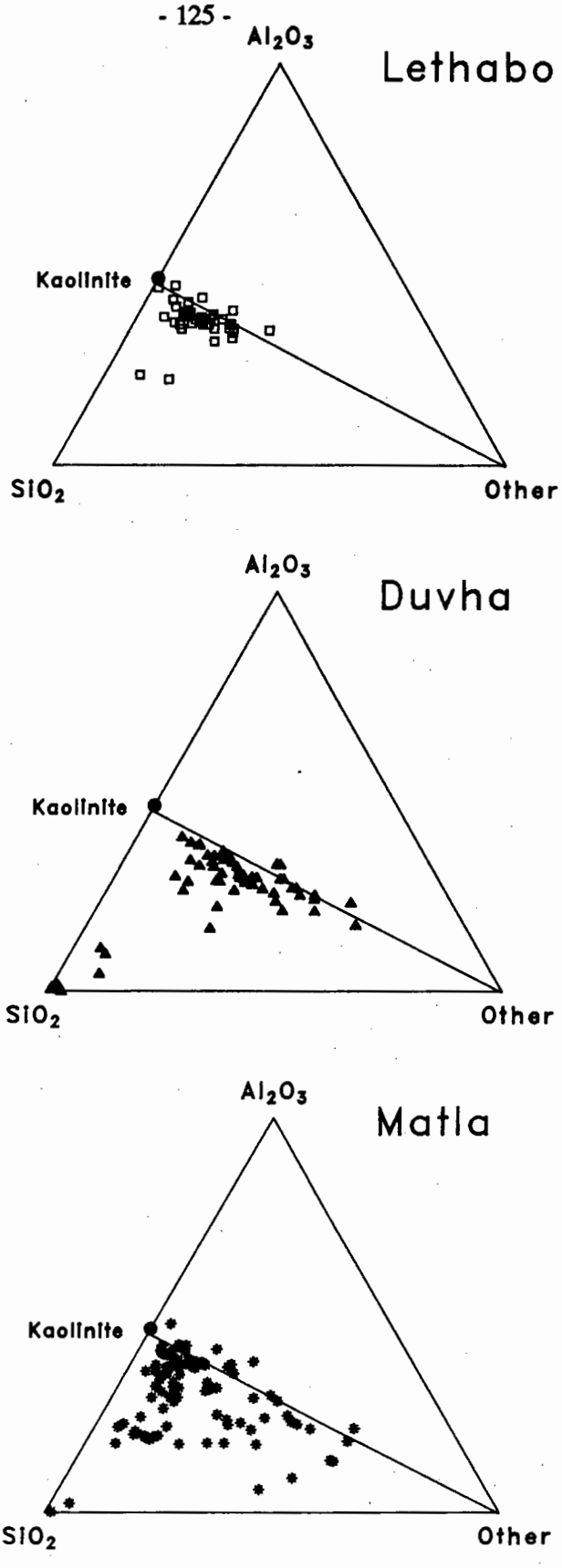

Fig. 6.24 : Trigonal diagrams of Al_2O_3, SiO_2, and Fe_2O_3 + MgO + CaO + P_2O_5 + SrO + Na_2O + K_2O + BaO in PFA glass analyses.

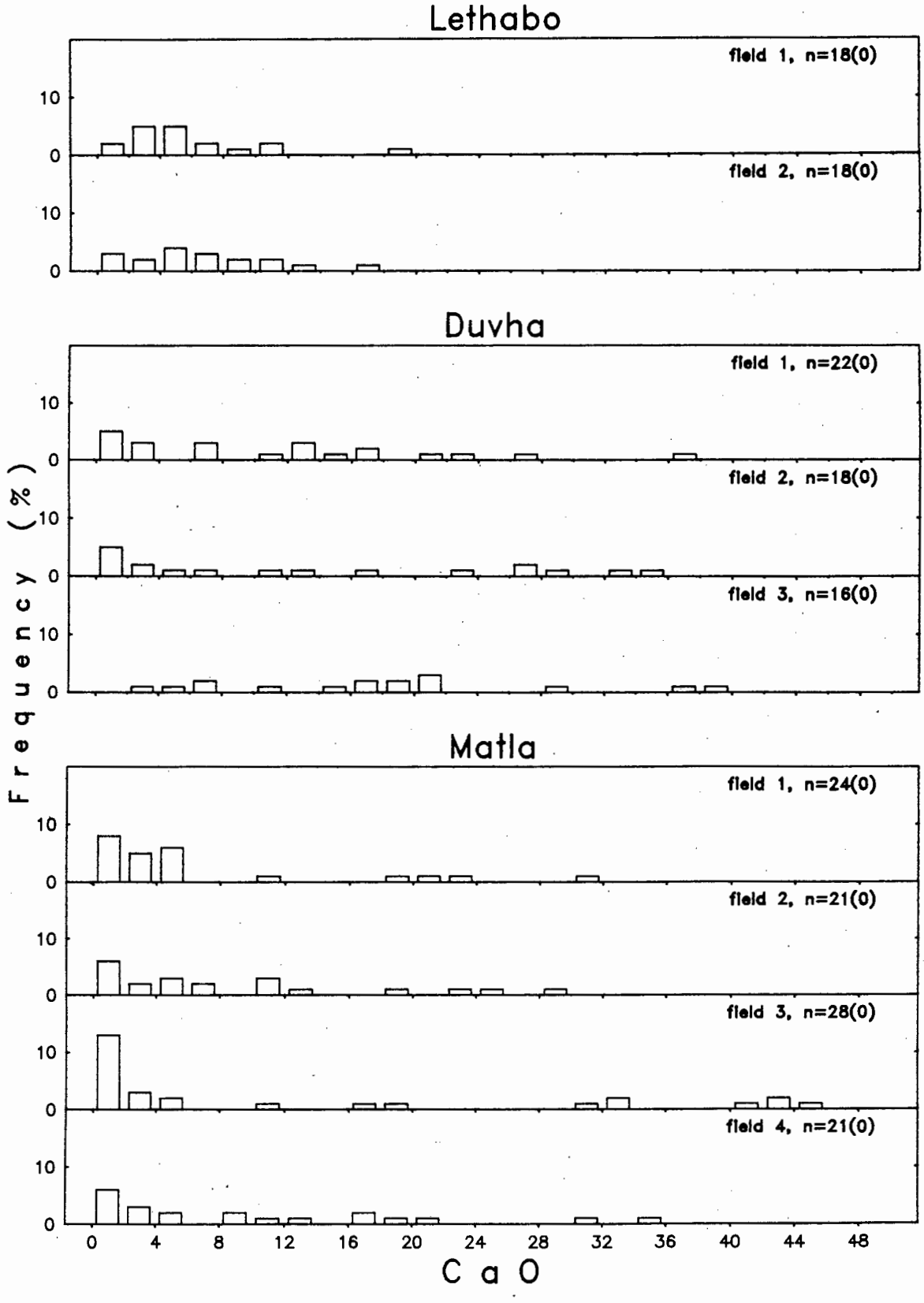

Fig. 6.25 : Histograms of the CaO distribution in PFA glass analyses.

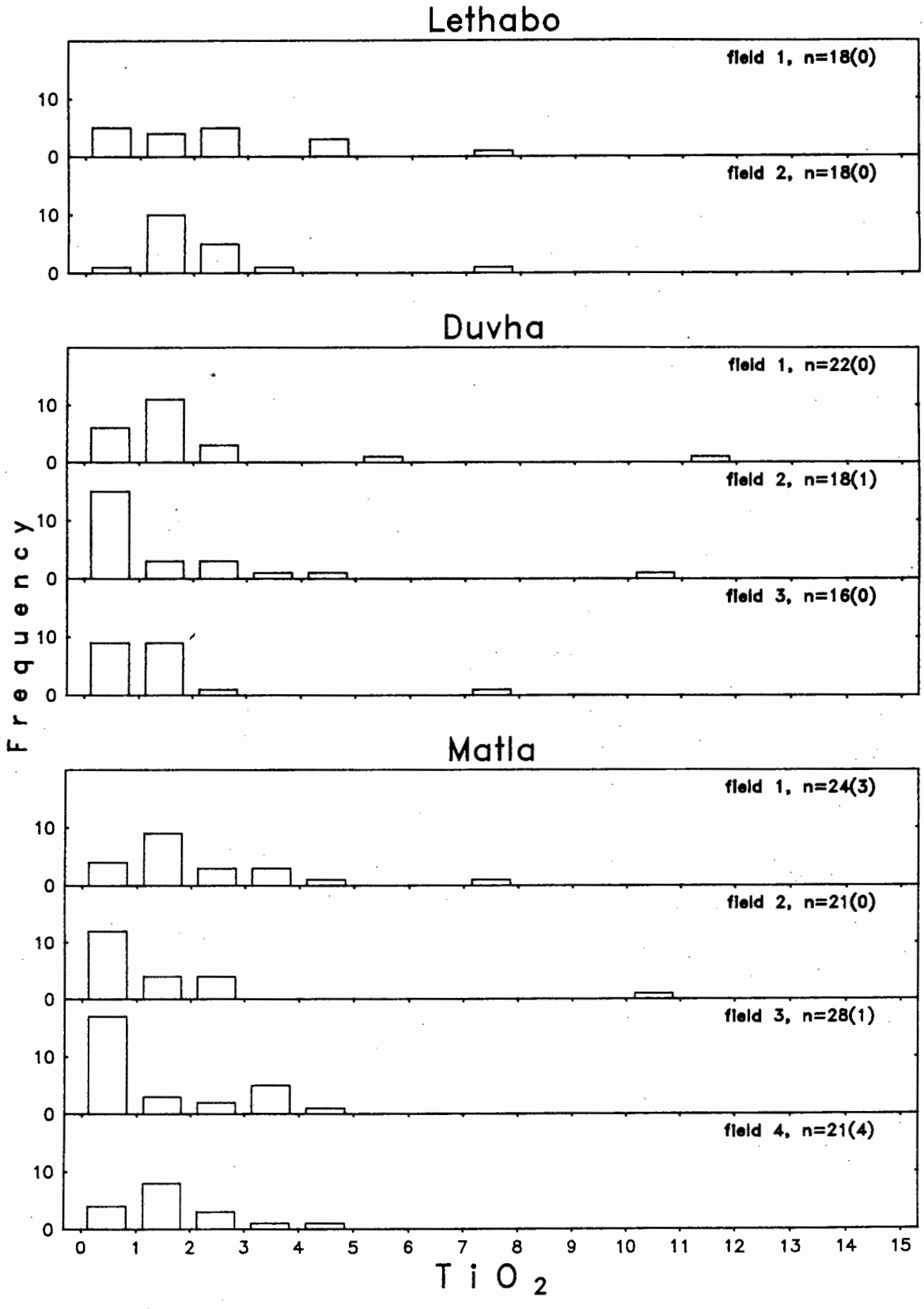

Fig. 6.26 : Histograms of the TiO_2 distribution in PFA glass analyses.

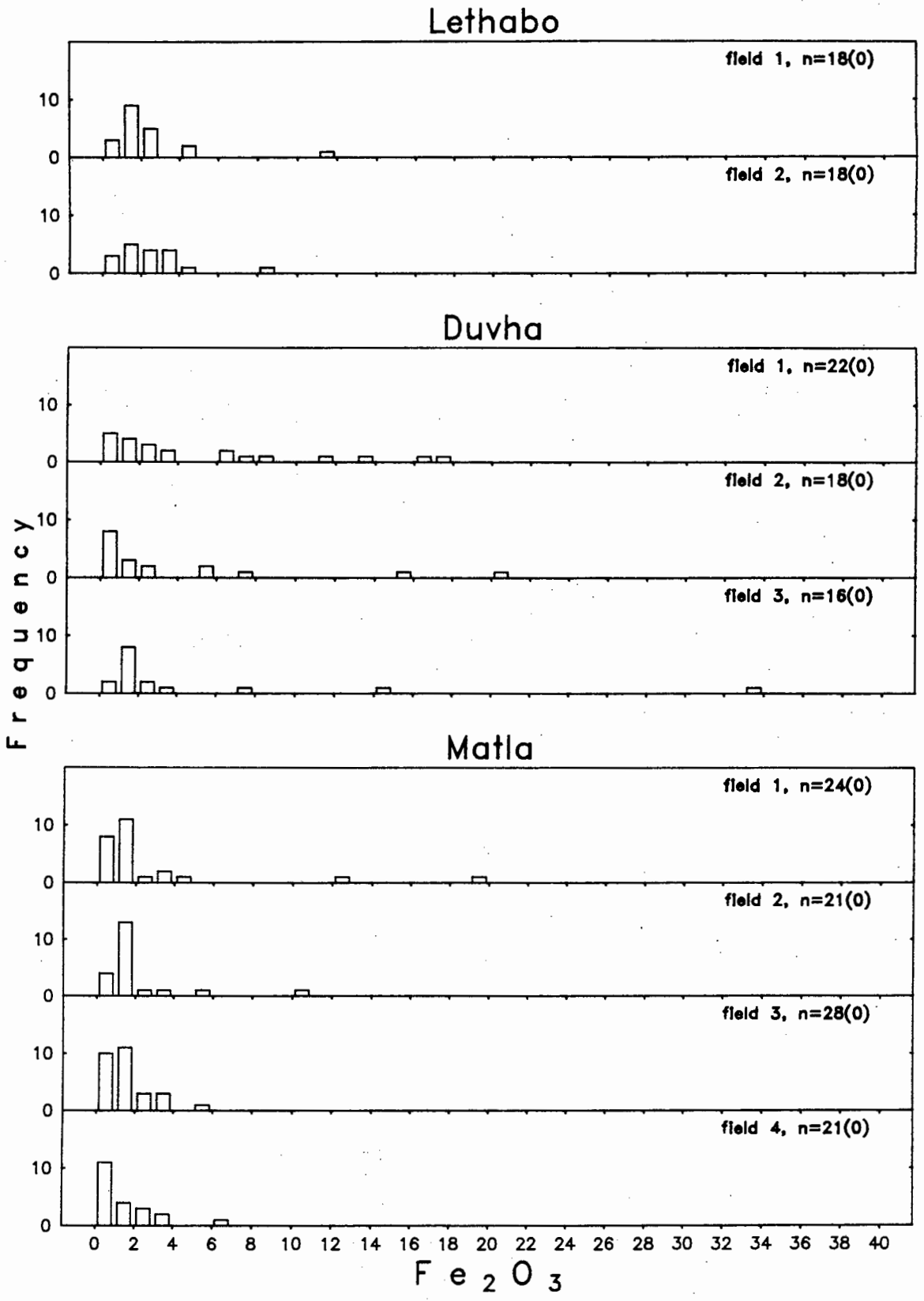

Fig. 6.27 : Histograms of the Fe_2O_3 distribution in PFA glass analyses.

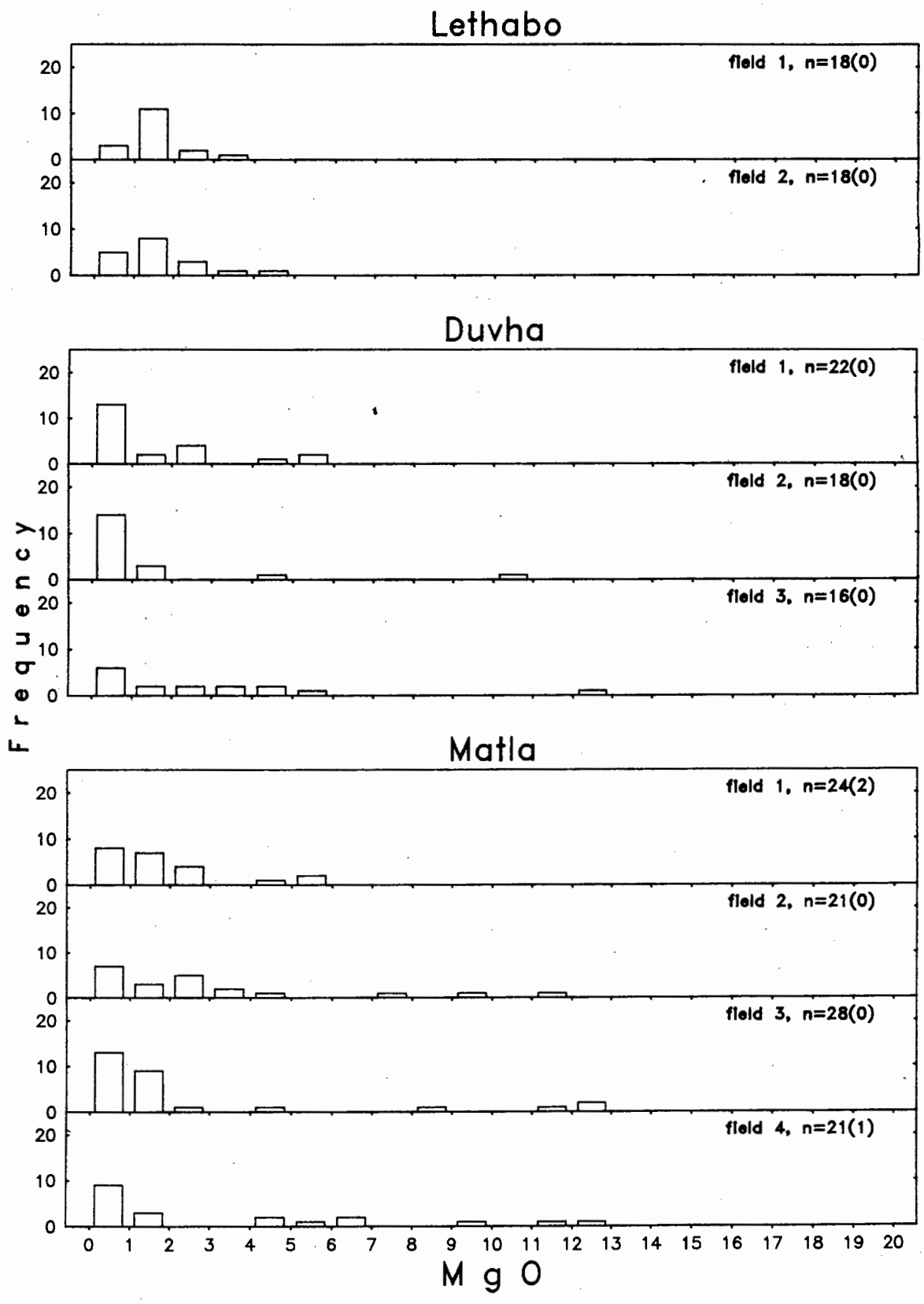

Fig. 6.28 : Histograms of the MgO distribution in PFA glass analyses.

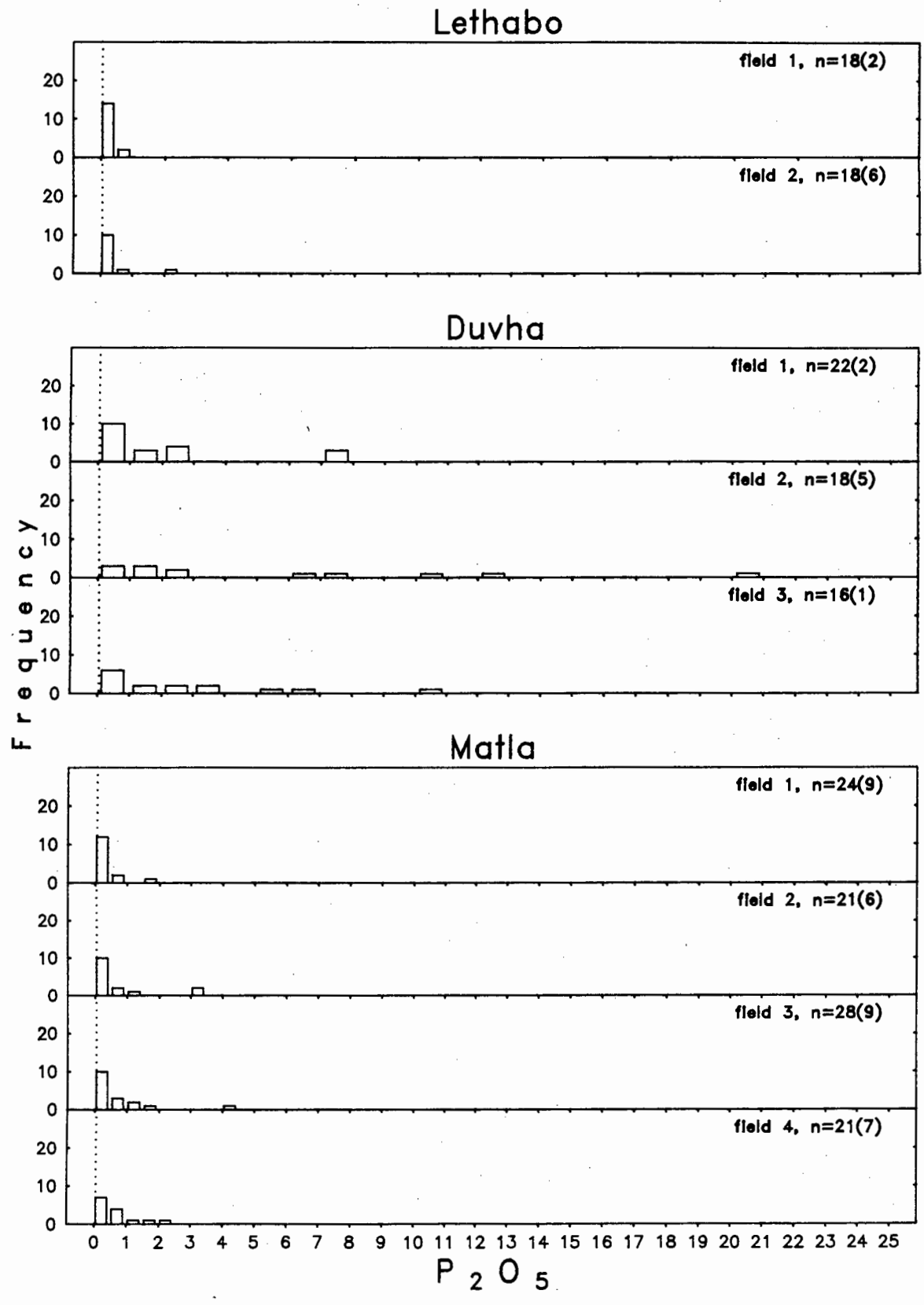

Fig. 6.29 : Histograms of the P_2O_5 distribution in PFA glass analyses. The lower limit of detection is marked by the dotted vertical line.

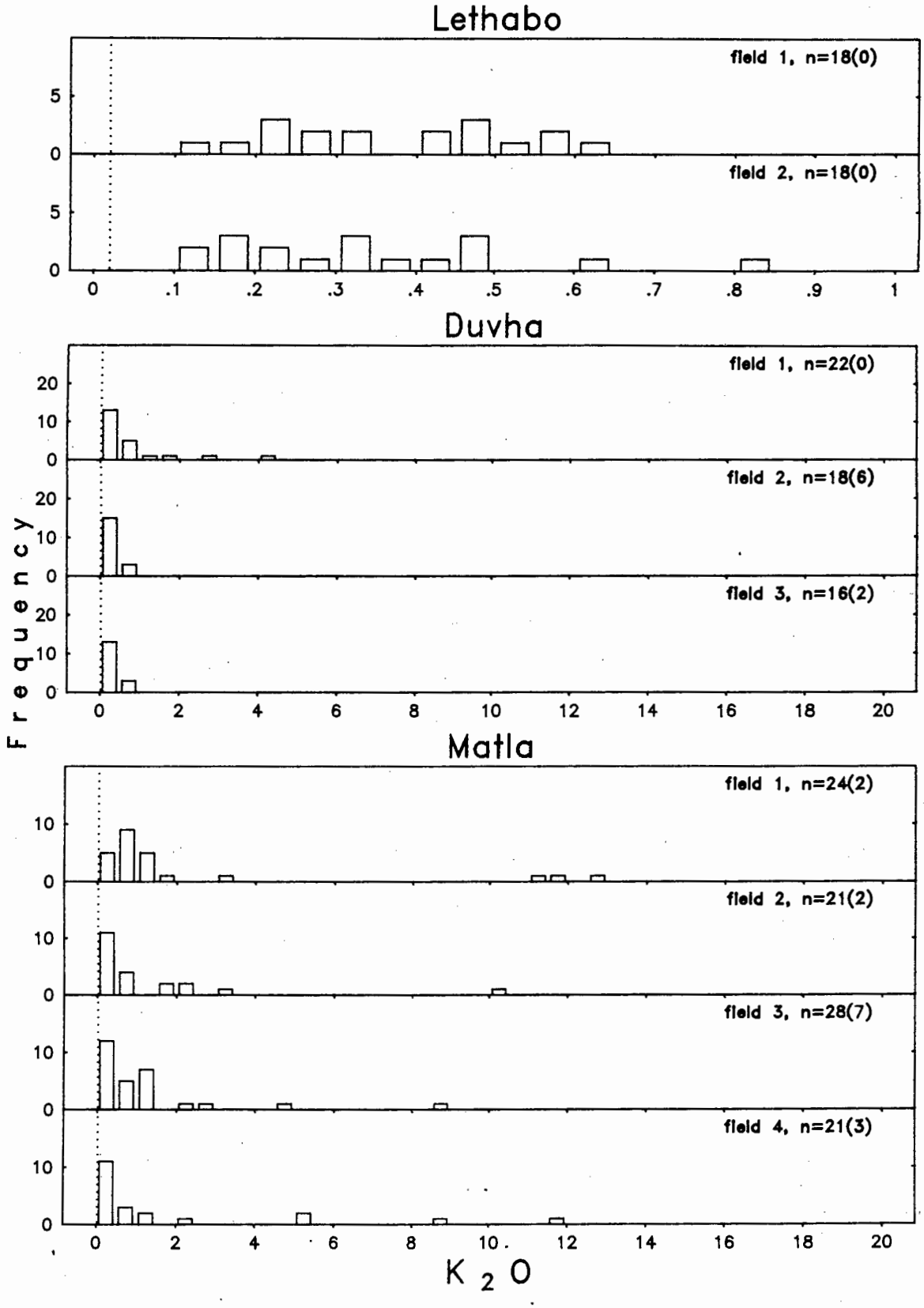

Fig. 6.30 : Histograms of the K_2O distribution in PFA glass analyses. The lower limit of detection is marked by the dotted vertical line.

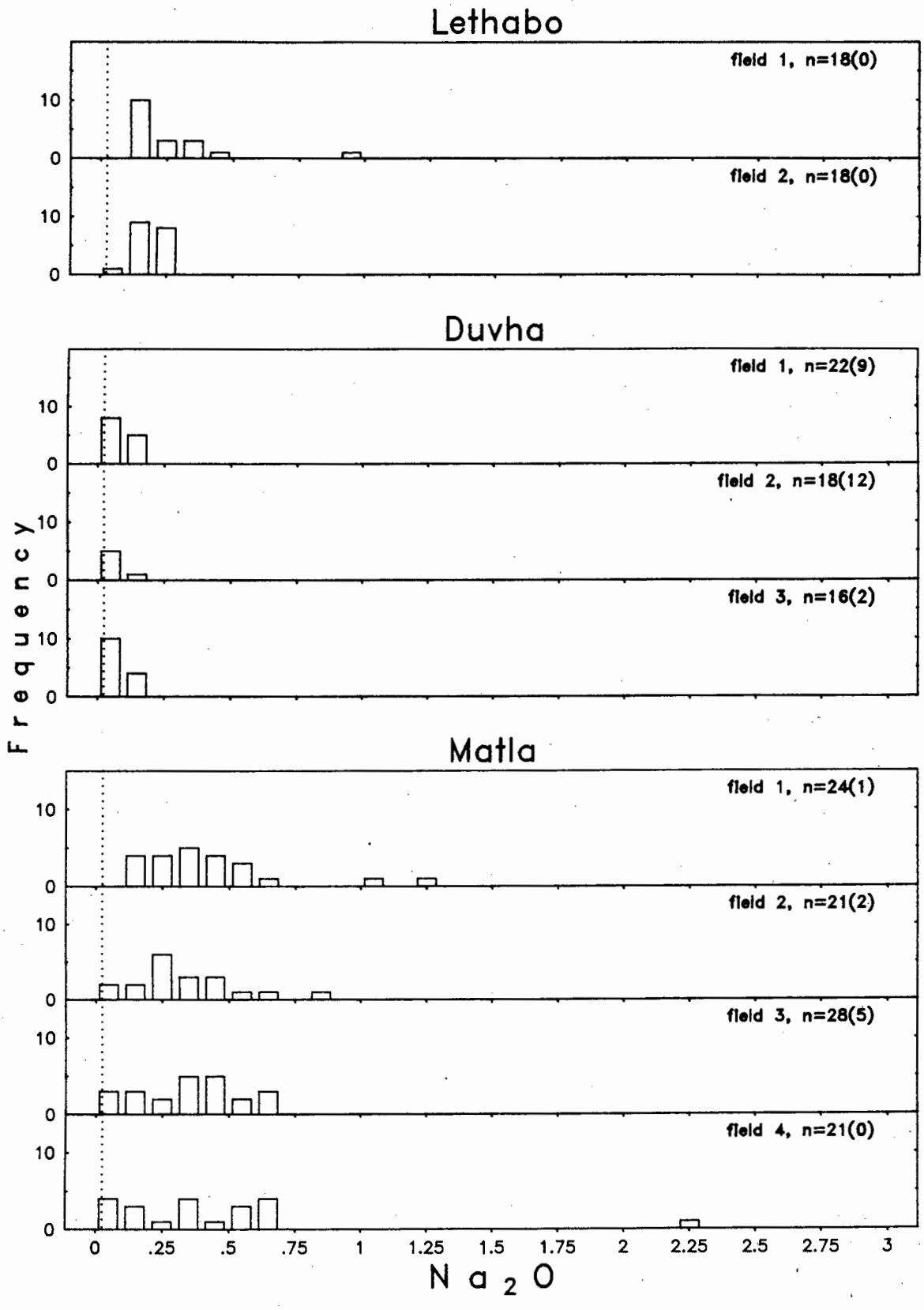

Fig. 6.31 : Histograms of the Na_2O distribution in PFA glass analyses. The lower limit of detection is marked by the dotted vertical line.

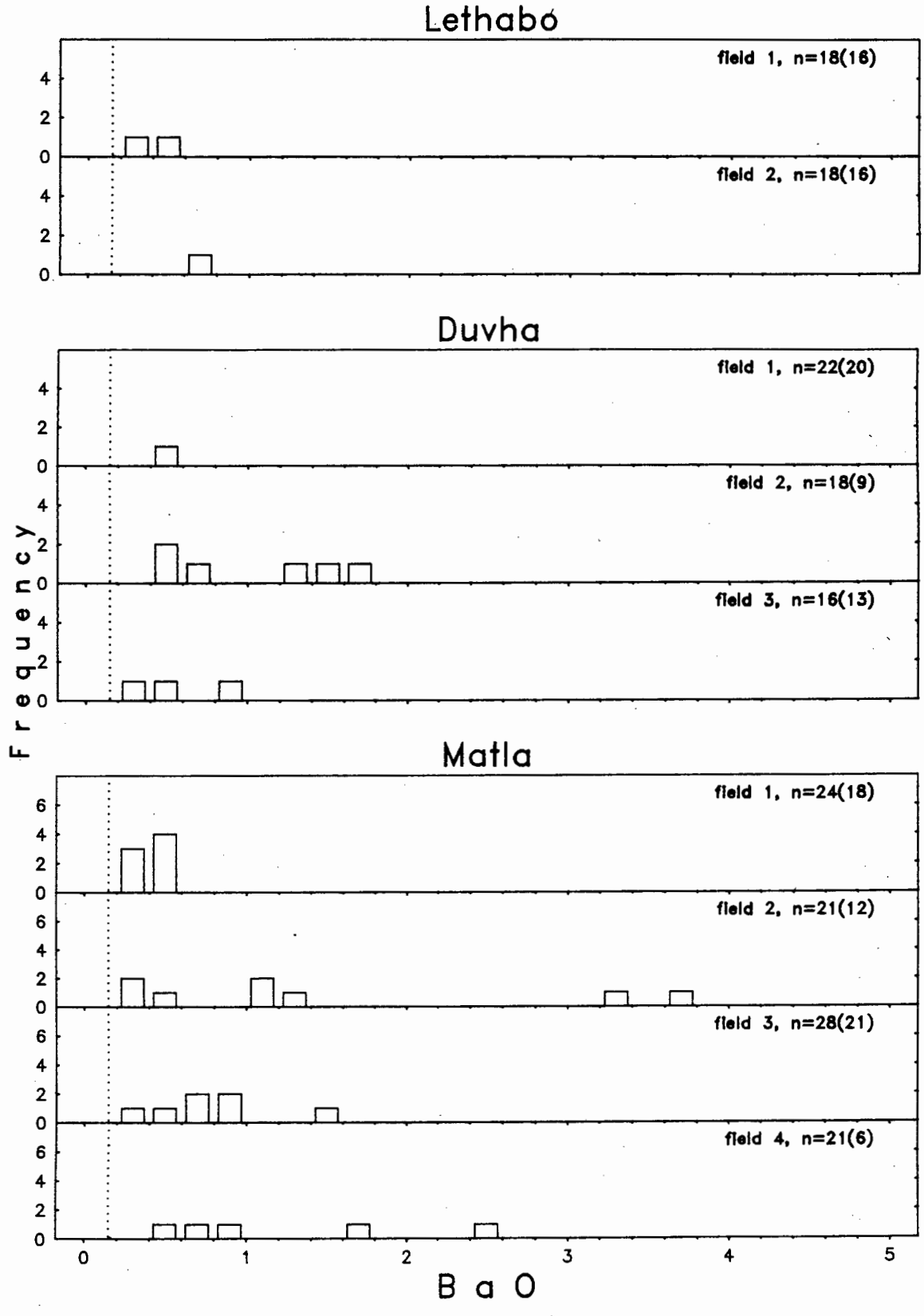

Fig. 6.32 : Histograms of the BaO distribution in PFA glass analyses. The lower limit of detection is marked by the dotted vertical line.

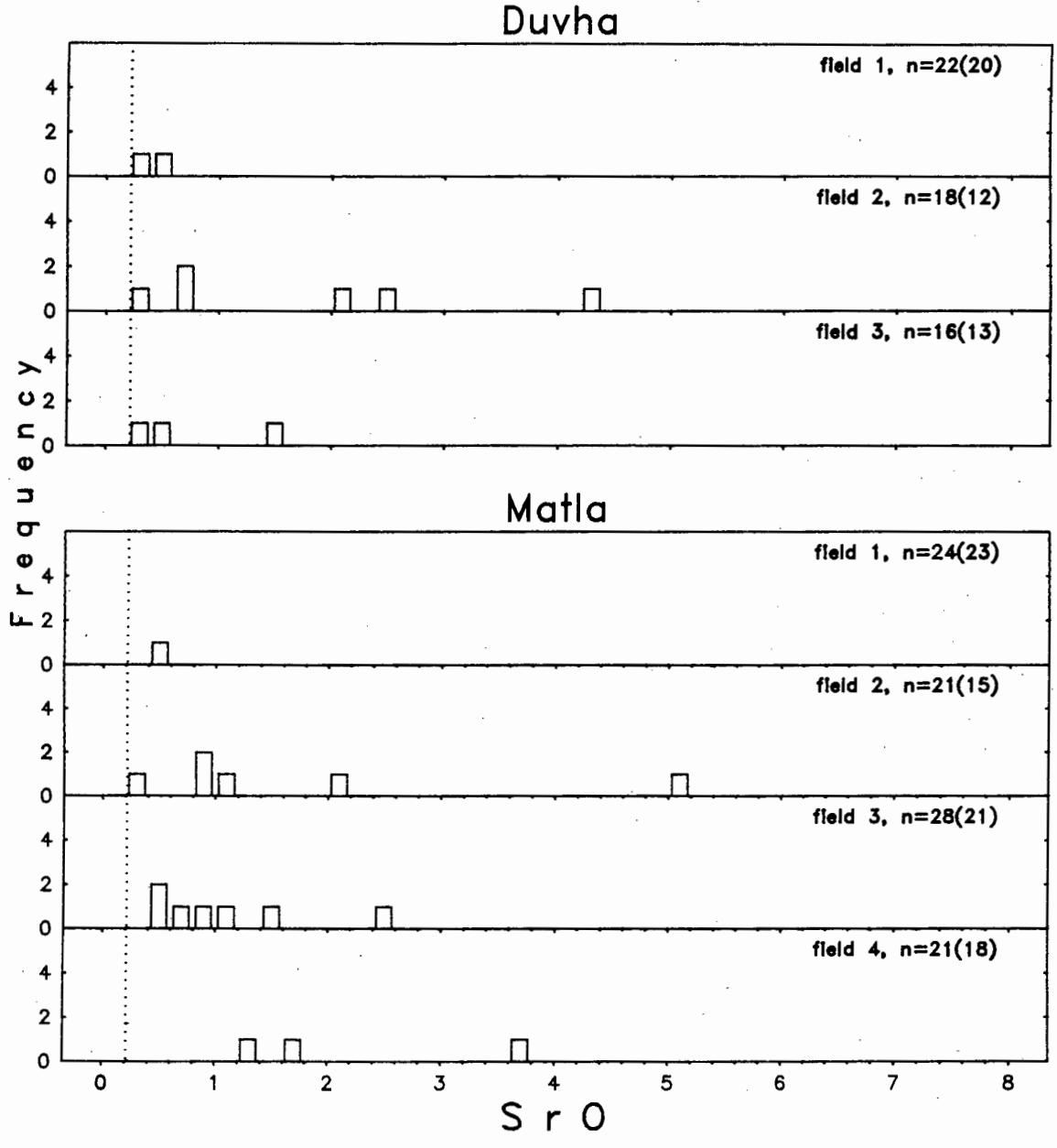

Fig. 6.33 : Histograms of the SrO distribution in PFA glass analyses. The lower limit of detection is marked by the dotted vertical line. SrO was below the detection limit in Lethabo glass analyses.

The TiO_2 frequency distribution has a mode at less than 2% in glass from both Duvha and Matla, with very few analyses in the range 4-12%.

Fe_2O_3 in Lethabo glass has a skewed distribution in PFA from fields 1 and 2, with a mode between 1-2%. Duvha and Matla PFA both have a mode at less than 2%. The Fe_2O_3 concentration decreases exponentially in glass from Duvha fields 1 and 2 and in glass from Matla field 4, and is a skewed distribution in glass from Duvha field 3 and Matla fields 1-3.

The MgO frequency distribution in Lethabo glass has an approximately normal distribution with a mode between 1-2% in PFA from fields 1 and 2. Duvha and Matla glasses have a mode of less than 1% and the MgO distribution decreases exponentially.

The P_2O_5 frequency distribution decreases exponentially in glass from all three stations. Duvha glass has a larger concentration range than either Lethabo or Matla glass, with values as high as 21%. The K_2O frequency distribution decreases exponentially in glass from Duvha and Matla. The K_2O concentration in Lethabo PFA is much lower than in either Duvha or Matla. Na_2O in Matla glass has a maximum concentration of less than 0.7%, although occasional samples were analysed with concentrations as high as 2.3%. The Na_2O mode is lowest in Duvha glass and highest in Matla glass.

BaO and SrO were below the detection limits in most of the glass analyses, and SrO was below the detection limit in all the Lethabo glasses.

There is a strong negative correlation between CaO and SiO_2 when the SiO_2 concentration is less than ±65% (Fig. 6.34). When SiO_2 is greater than ±65% the CaO concentration is always less than 5%.

Assuming that all Al in glass was derived from kaolinite, the "kaolinite" content of the glass can be calculated as:

$$\text{Kaolinite} = Al_2O_3 \times K \qquad (6.1)$$

K = the $SiO_2 + Al_2O_3$ / Al_2O_3 ratio in kaolinite

The frequency distribution derived from the above calculation is shown in Fig. 6.34. Lethabo glass generally contains more than 70% kaolinite, with a mode between 70-80%. This high value is probably due to the high kaolinite content of Lethabo coal. Duvha PFA has a bimodal

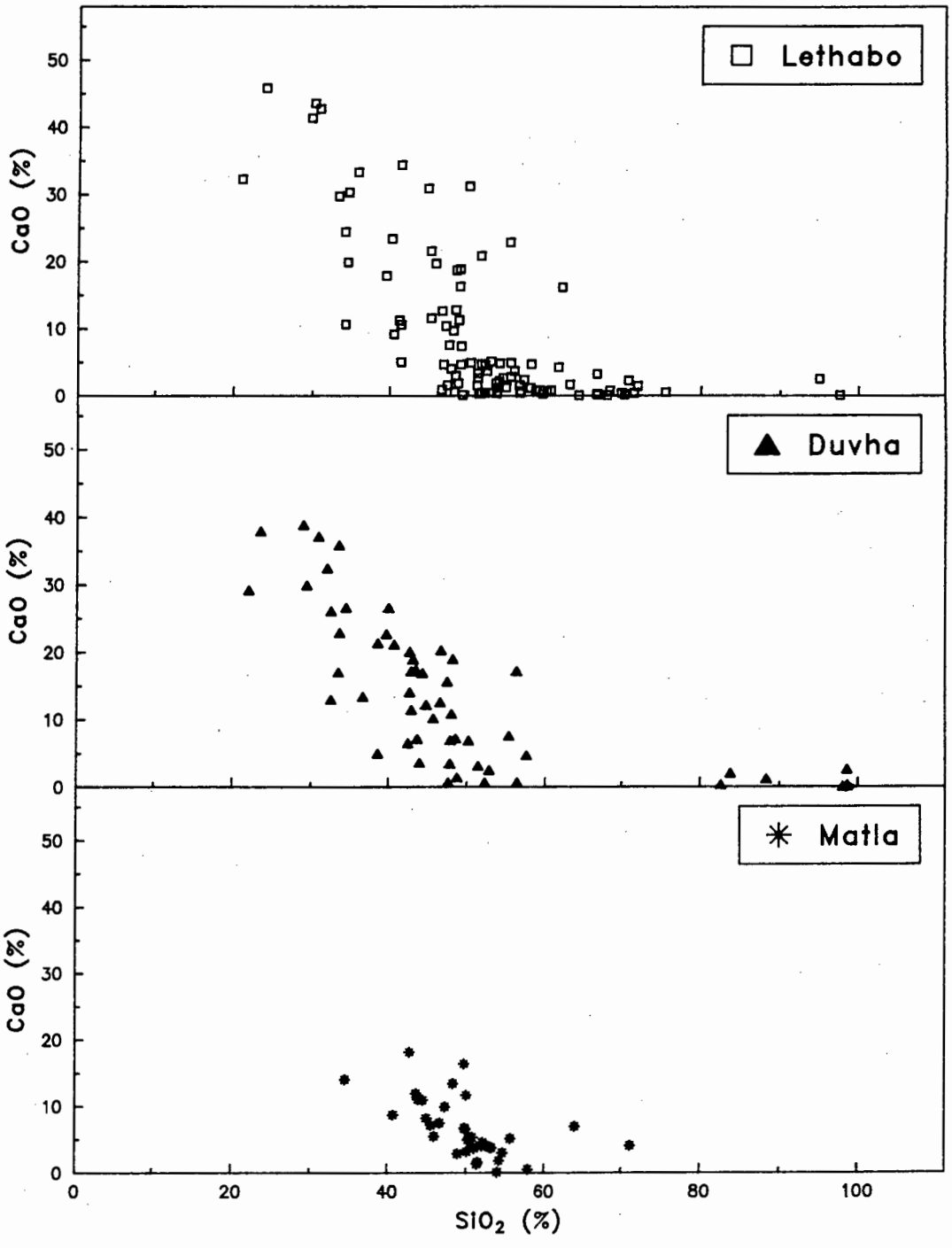

Fig. 6.34 : CaO vs SiO_2 in PFA glass analyses.

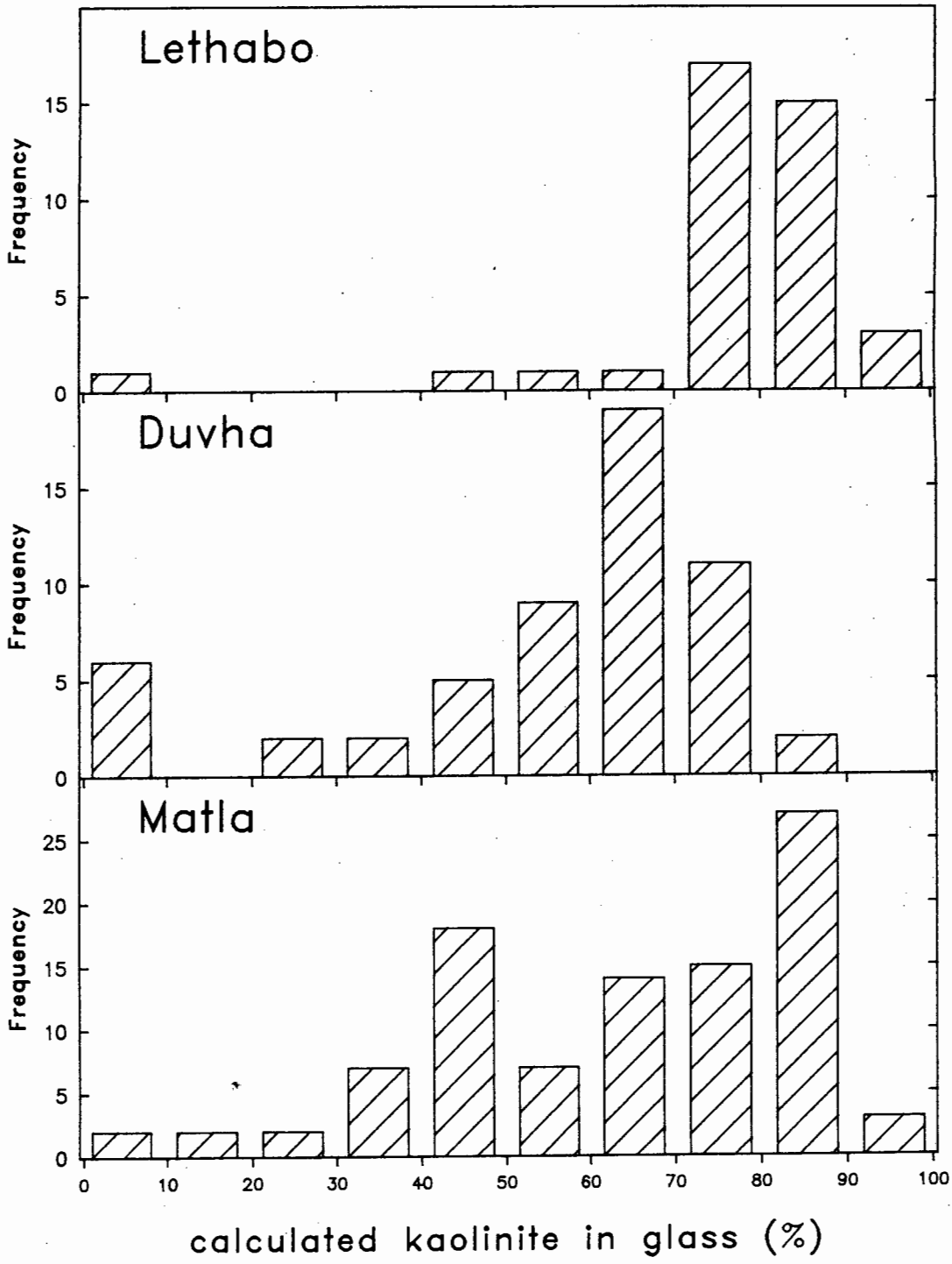

Fig. 6.35 : Histograms of the calculated kaolinite concentrations in glass grains.

frequency distribution of kaolinite in glass, with modes between 0-10% and 60-70% kaolinite. Matla PFA has a broad range of values of kaolinite in glass (0-100%), with a bimodal frequency distribution having modes between 40-50% and 80-90%.

6.4.2.3 Chemical Composition of Spinel:

Spinels are commonly found as blocky and/or columnar dendritic Fe-oxide crystals in the glass phase, and more rarely as solid Fe-rich spheres. The latter spheres occasionally formed cenospheres. Similar occurrences of spinel in fly ash from Australian power plants have been described by Ramsden and Shibaoka (1982), and in South African ash by Lesch and Cornell (1987). Transitional varieties between solid glass and dendritic and solid Fe-rich spheres were noted in PFA from all three power stations. Ramsden and Shibaoka (1982) consider that such an assemblage reflects variations in the initial composition of individual particles and in their thermal and impact histories. Lauf (1985) described the presence in fly ash of "ferrospheres" consisting of spinel (an impure aluminium ferrite) and small amounts of aluminosilicates, which he considered to be the oxidised remains of framboidal pyrite from the coal.

Spinels from Duvha PFA accept up to 25% MgO and Al_2O_3 in their structure (Fig. 6.36), whereas spinel compositions from Lethabo and Matla PFA tend to lie along an Fe_2O_3-Al_2O_3 tie-line with a maximum MgO content of 5%. McCarthy et al (1988) noted that the ferrite spinel composition of low-calcium/Class F ashes is close to the magnetite end member, based on unit cell parameter measurements. Substitution of MgO and Al_2O_3 for Fe_2O_3 has been noted in ferrite spinels formed from lignite gasification ash (McCarthy et al 1984, Stevenson 1984).

There is a positive correlation between TiO_2 and Al_2O_3 in spinels from each station (Fig. 6.37(a)), and a negative correlation between FeO and Al_2O_3 (Fig. 6.37(b)). There is a negative correlation between FeO and MgO in Duvha spinels, but not in Matla or Lethabo spinels (Fig. 6.37(c)). The negative correlations indicate that Al_2O_3, MgO and TiO_2 substitute for FeO in the spinel structure, with MgO substitution dominant in Duvha spinels. The major MgO bearing mineral in the coal is dolomite ($FeMg(CO_3)_2$), but the dolomite content of Duvha coals is low (< 0.7%) compared with Matla coals (1.3-1.8%), and is similar to Lethabo coals (< 0.9%). It is thus unlikely that the presence of dolomite could explain the preferential substitution of MgO for FeO in spinel in Duvha PFA. The low glass content of

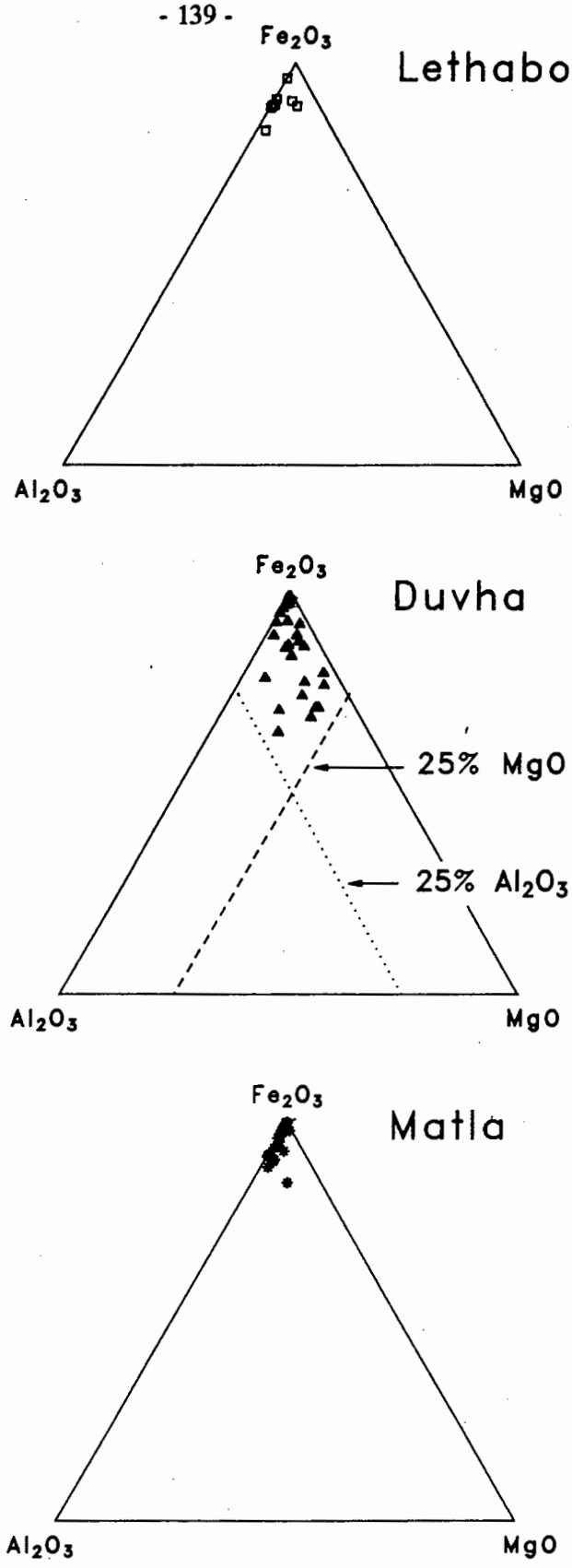

Fig. 6.36 : Trigonal diagrams of Fe_2O_3 - Al_2O_3 - MgO in spinel analyses.

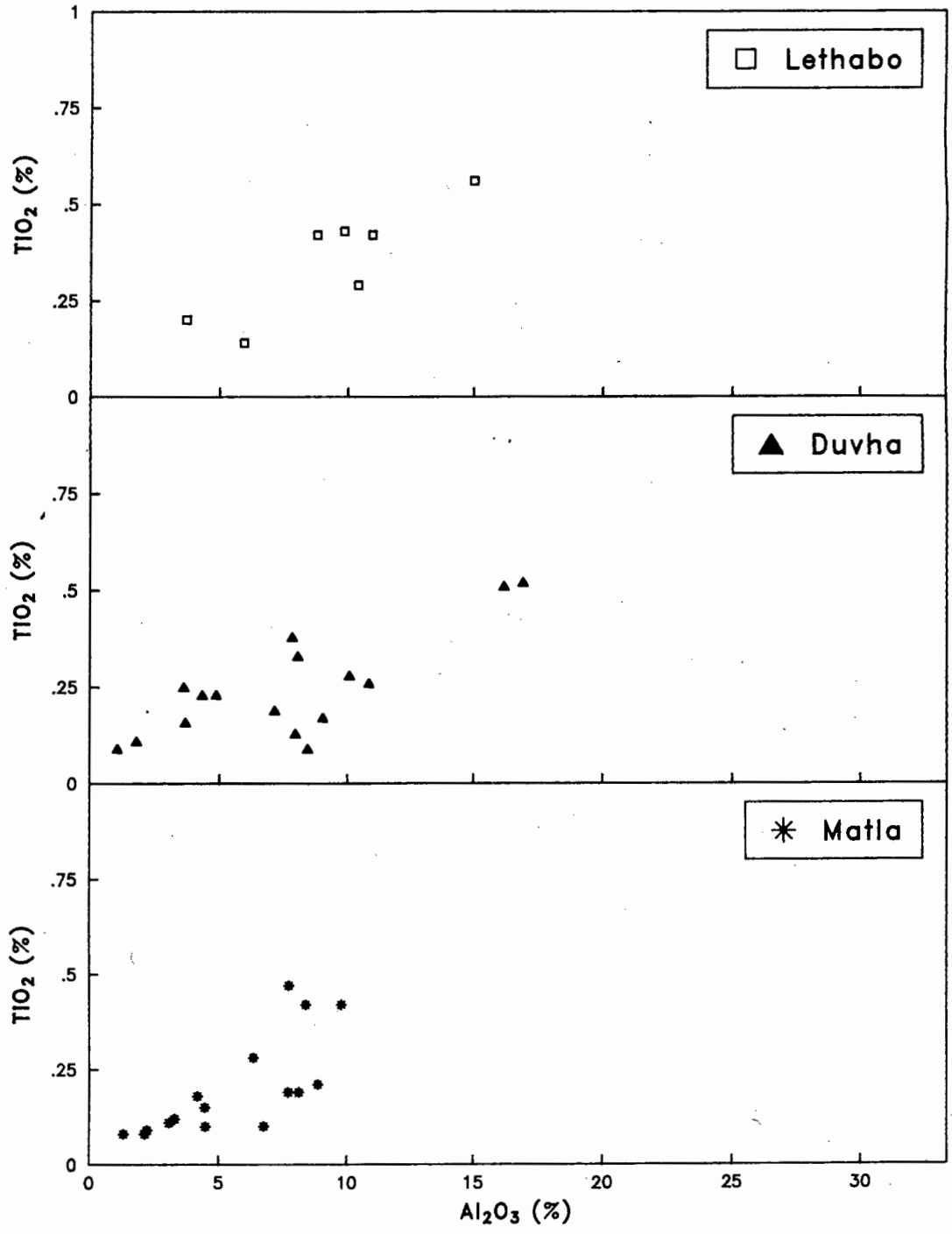

Fig. 6.37(a) : TiO_2 vs Al_2O_3 for spinel analyses.

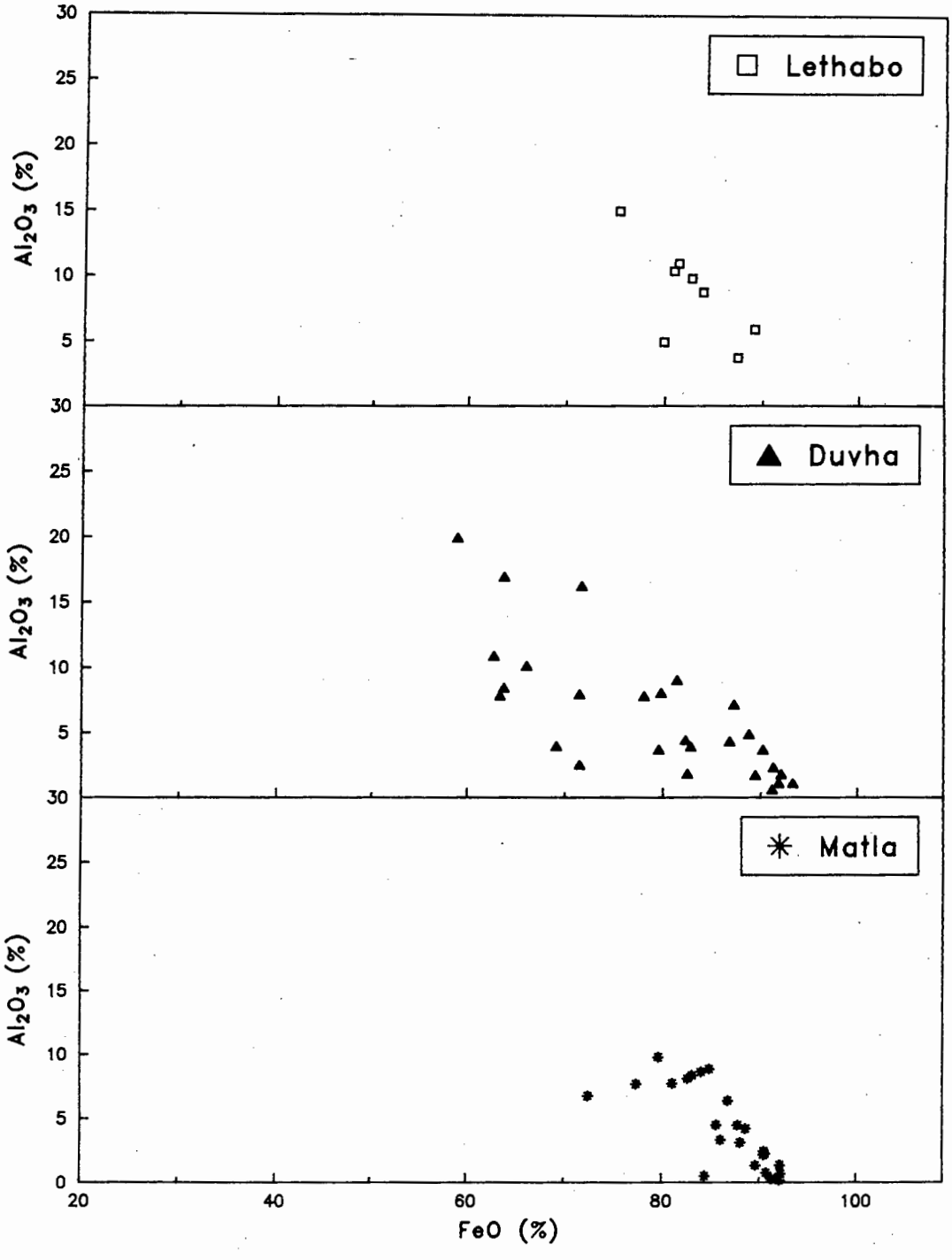

Fig. 6.37(b) : Al_2O_3 vs FeO for spinel analyses. Total Fe expressed as FeO.

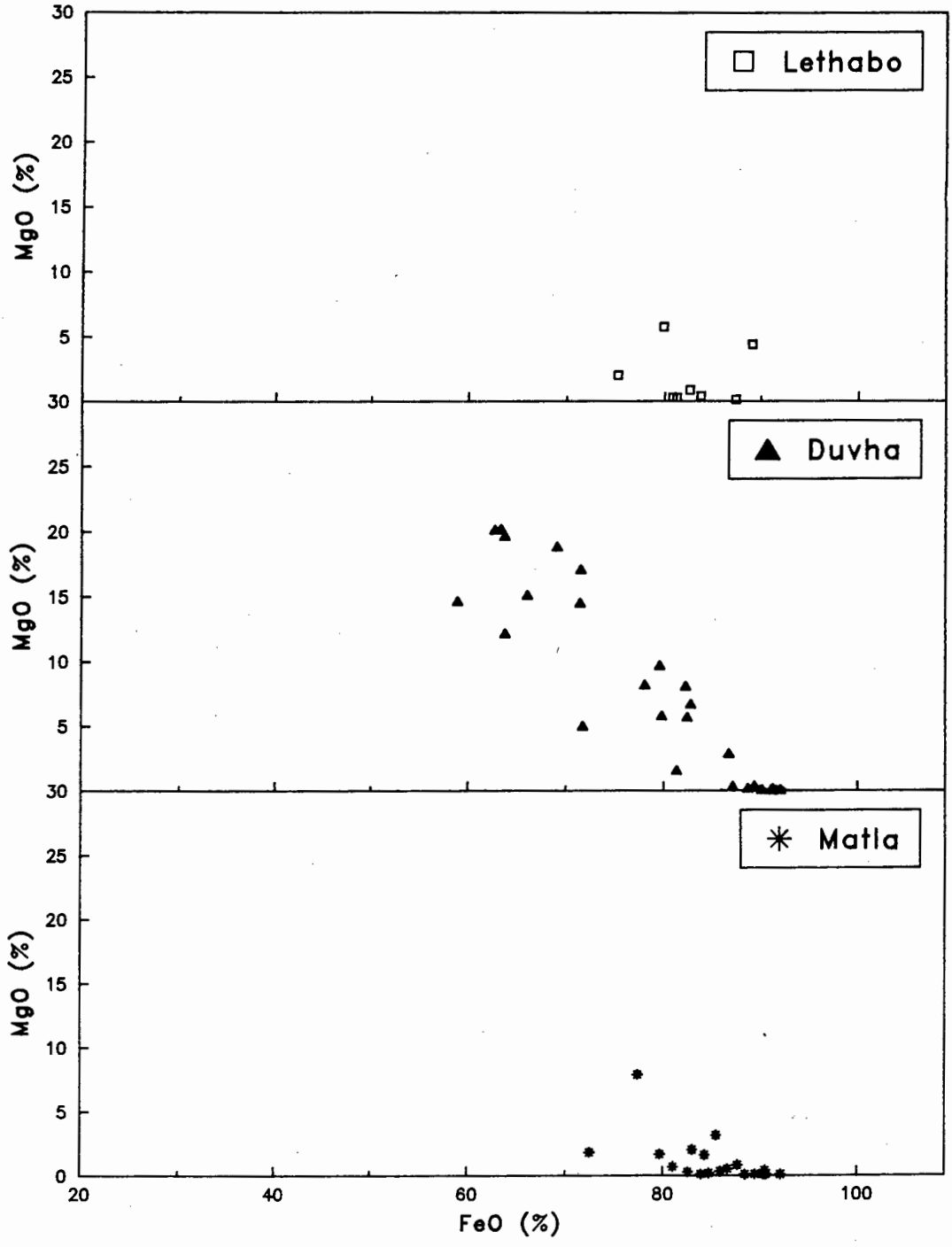

Fig. 6.37(c) : MgO vs FeO for spinel analyses.

Duvha PFA may result in MgO entering the spinel phase (in which it is compatible), rather than remaining at a high concentration in the glass.

6.5 MULLITE-GLASS CONCENTRATION RATIO

Various researchers have reported that there is a correlation between the CaO concentration of the PFA and the glass content (Lesch and Cornell 1987). The relationship between total CaO and glass is shown in Fig. 6.38. Matla and Duvha both plot close to the regression line noted by Lesch. Lethabo plots off the regression line and has a much higher glass content than anticipated from the CaO concentration. The high glass content of Lethabo PFA may be related to the high kaolinite content of the coal.

The CaO_{glass}/Al_2O_3 ratio versus the mullite concentration in the glass-mullite mixture is compared in Fig. 6.39(a). The x-axis term represents the relative concentration of CaO in the glass. Duvha and Matla plot adjacent to each other and have negative slopes which are subparallel with each other. Lethabo plots as a field on the regression line passed through Matla. The complete data set also defines a negative trend. Thus for Duvha and Matla, and for all three stations together, it is noted that an increase in the CaO_{glass}/Al_2O_3 ratio is associated with a decrease in the percentage of mullite in the glass-mullite mixture. The presence of CaO in the glass thus limits the crystallisation of mullite.

The mullite concentration versus the Na_2O/Al_2O_3 ratio is compared in Fig. 6.39(b). The three stations together define a strong negative trend. Duvha PFA has very little variation in the Na_2O/Al_2O_3 ratio, but has a large variation in the mullite/mullite+glass ratio. Lethabo PFA plots as a field and Matla PFA has a negative trend parallel with the inter-station trend. Thus, in general an increase in the Na_2O/Al_2O_3 ratio is associated with a decrease in the percentage of mullite in the glass-mullite mixture. The effect of MgO and K_2O on mullite formation is shown in Figs. 6.39(c) and (d). The presence of Na_2O, CaO, MgO and possibly K_2O in the glass have a very marked effect on the mullite concentration, higher concentrations of these oxides leading to lower concentrations of mullite.

In power stations, glass and mullite are believed to form as alteration products of kaolinite during the combustion process. When slowly heated, kaolinite normally dehydrates at about

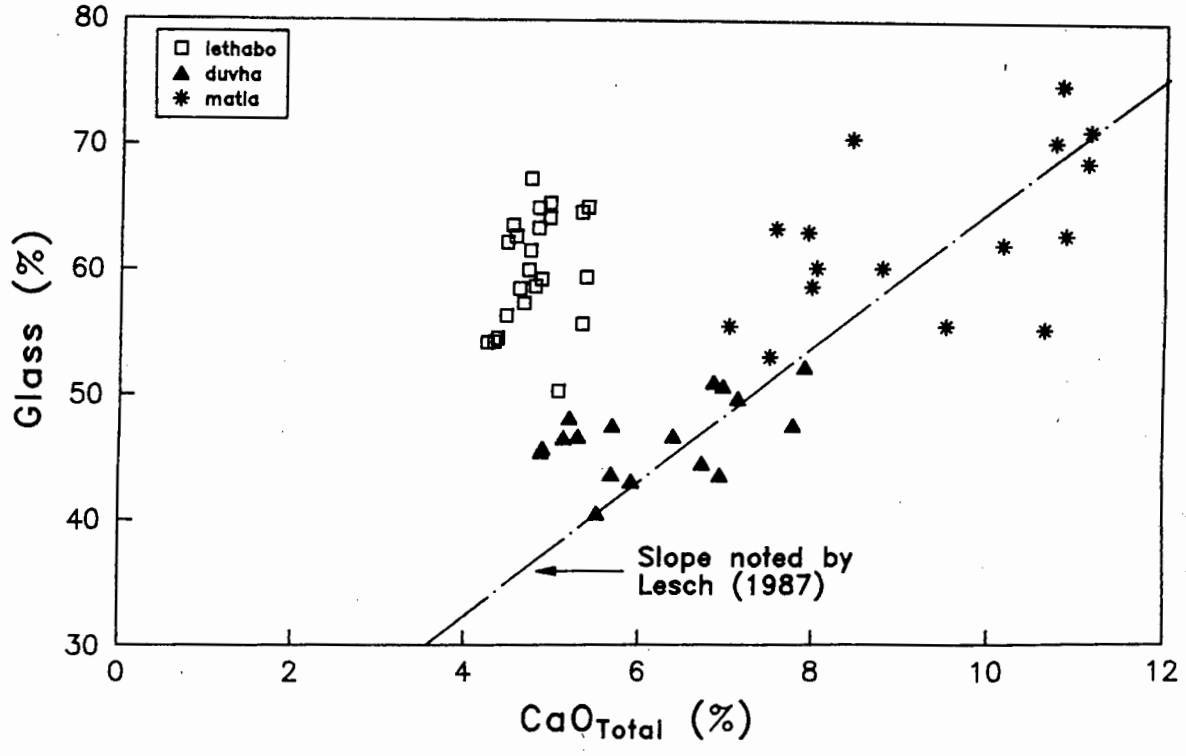

Fig. 6.38 : CaO vs glass concentrations in the PFA samples. CaO_{Total} = total CaO determined in the PFA by XRF analyses.

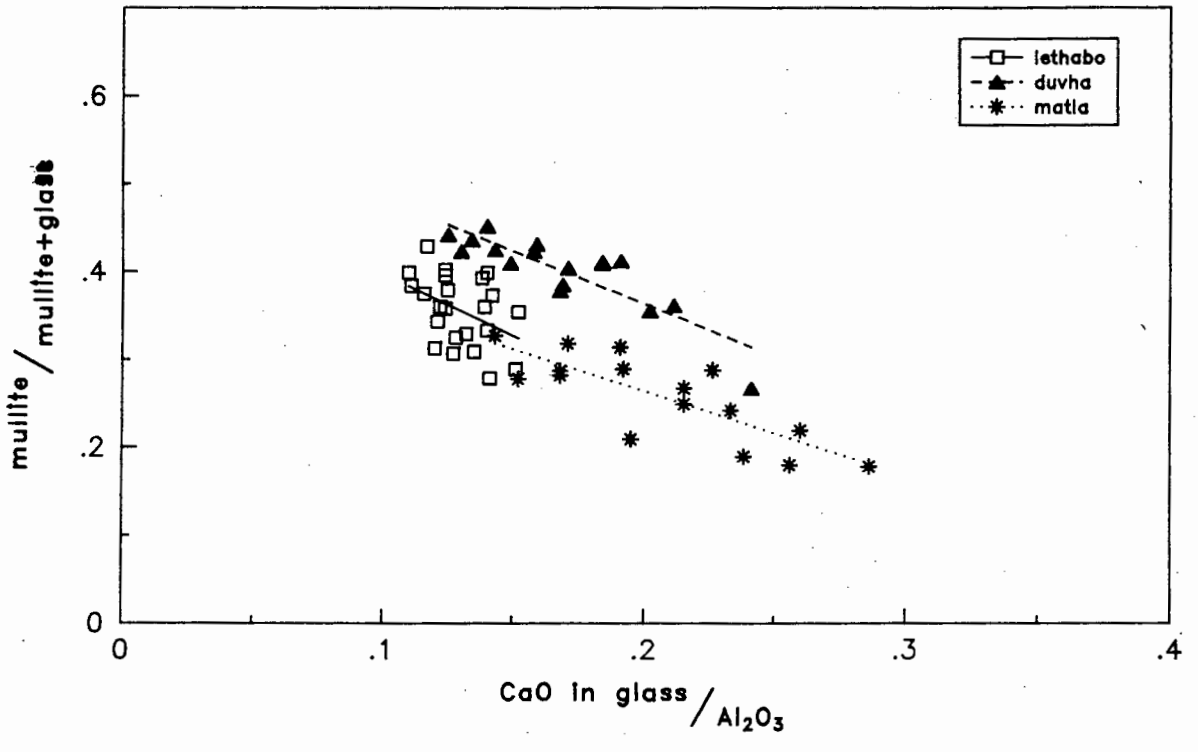

Fig. 6.39(a) : Scatter diagram showing the negative correlation between CaO (in glass) / Al_2O_3 vs the mullite / mullite + glass ratio.

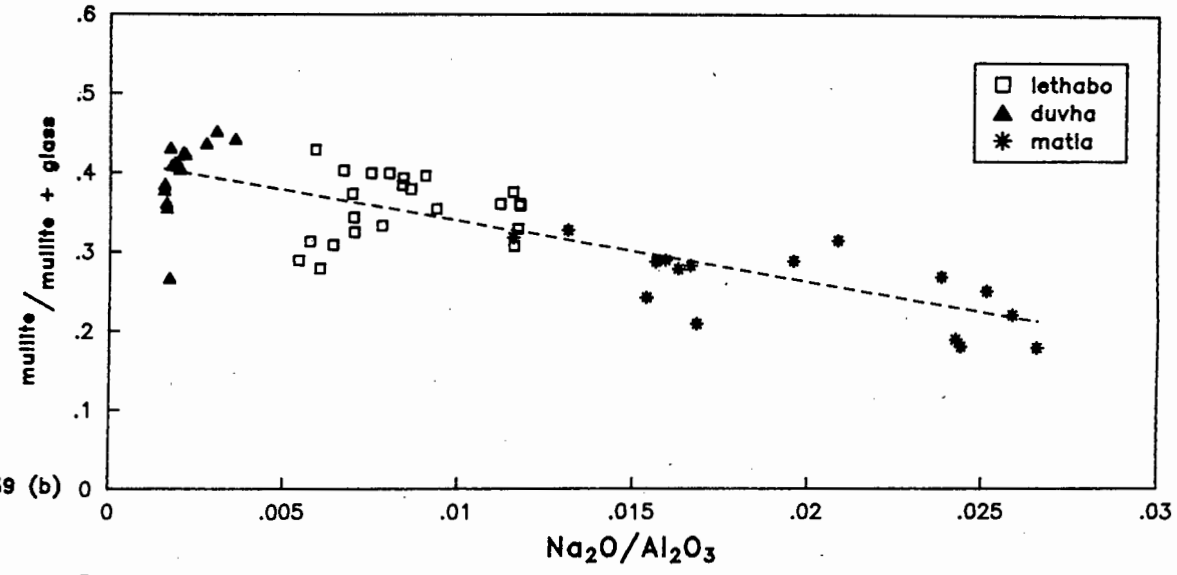

Fig. 6.39 (b)

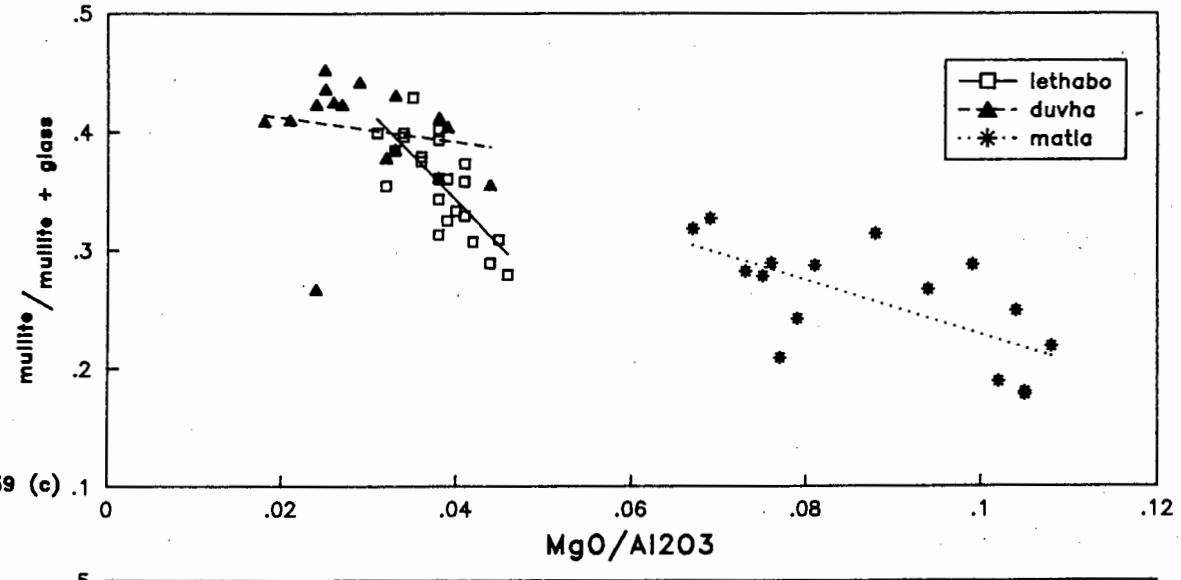

Fig. 6.39 (c)

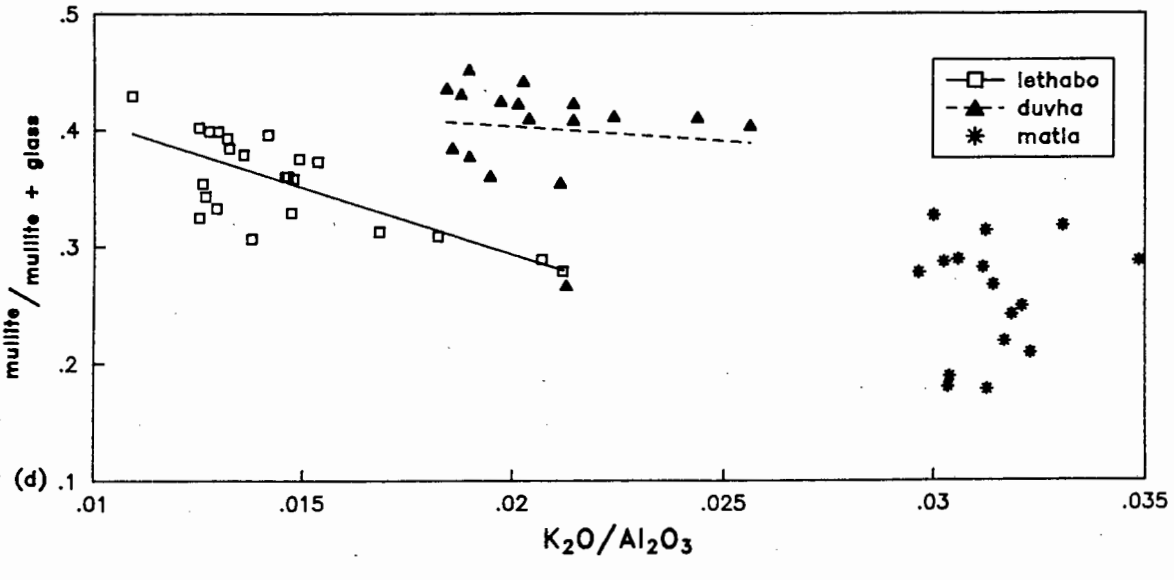

Fig. 6.39 (d)

Fig. 6.39(b-d) : Scatter diagrams showing the negative correlations between Na_2O, MgO and K_2O / Al_2O_3 ratios vs the mullite / mullite + glass ratio.

500°C to form metakaolinite, which subsequently alters to a mixture of mullite and cristobalite at 1200°C-1400°C (Brindley and Nakahira 1959). Cristobalite was not observed in the fly ash samples. Ramsden (1969) suggests that kaolinite initially retains its water within the structural lattice when flash-heated, and that on the microscopic scale the presence of this structural water results in melting rather than decomposition of the mineral. Hubbard and McGill (1984) however, consider that flash-heating of kaolinite results in destruction of the lattice and formation of a mullite-bearing, amorphous aggregate, without melting of the grain. These aggregates were observed in PFA from Duvha field 1 (D1_PFA1). Hubbard and McGill (1984) state that illite melts on flash-heating due to the presence of fluxing agents such as H_2O and potasium in the structure. In such a case the glass formation is restricted to milliseconds, and mullite would form from devitrification of the glass. Kaolinite was the major component of the coals in this study however, with illite never present in more than trace proportions.

The presence of K_2O, CaO and other oxides in the glass must be due to assimilation of adjacent particles, which acted as fluxes to melt the kaolinite grains. Mullite in the PFA studied thus either formed as an alteration product directly from kaolinite, prior to the formation of the glass, or crystallised from a previously formed glass phase. In the former case, the alkali and alkaline earth elements would act as fluxes for the formation of glass.

Hulett et al (1980) conducted a series of etching experiments on PFA and noted that alkali, rare-earth and many transition elements were concentrated in the glass phase compared with the mullite-quartz phase. These observations were supported by Grossman (1983) who conducted a similar set of etching experiments and who noted that the concentrations of most minor elements in the mullite-quartz mixture were lower than in the other components of the PFA.

If the hypothesis that mullite crystallised from the glass is correct, then the observed relationship between Na_2O, CaO, MgO and K_2O can be explained by a process in which the rejected solute builds up in the glass ahead of the crystallising mullite. This solute needs to be removed for further crystal growth to take place, and can thus can act as a rate control to retard crystal growth. An alternative explanation could be that the glass would remain stable if the concentration of fluxing elements was high enough. If not, then mullite would crystallise out, due to supersaturation of Al in the glass.

Both amorphous aggregates and glass spheres have been observed in the PFA, and thus both mechanisms discussed above for the formation of mullite are likely to take place.

6.6 MIXING

It was demonstrated in section 6.2.2.2 that assimilation of particulate mineral matter into the glass took place. Therefore, final mineral concentrations of the PFA must be lower than that derived from the coal ash prior to formation of glass and assimilation. The concentration of SiO_2 and CaO in the glass derived from the assimilation of quartz and lime respectively can be calculated as shown below:

$$CaO_{glass} = CaO_{total} - CaO_{lime} \quad (6.2)$$

CaO_{glass} = CaO concentration in the glass (due to assimilation of lime).
CaO_{total} = total measured CaO concentration.
CaO_{lime} = CaO concentration calculated from the measured free lime.

$$SiO_{2\ glass} = SiO_{2\ total} - SiO_{2\ kaolinite} - SiO_{2\ quartz} \quad (6.3)$$

$SiO_{2\ glass}$ = SiO_2 concentration in the glass (due to assimilation of quartz).
$SiO_{2\ total}$ = total measured SiO_2 concentration.
$SiO_{2\ kaolinite}$ = SiO_2 concentration in glass (derived from kaolinite).
$SiO_{2\ quartz}$ = SiO_2 concentration found as free quartz.

These calculations assume that all the crystalline SiO_2 is found as free quartz, and that all the crystalline CaO is found as free lime. $SiO_{2\ kaolinite}$ is calculated from the assumption that the only source of Al_2O_3 in the PFA is from kaolinite in the coal. Feldspar (also a source of Al_2O_3) was detected in Duvha coal (< 1.7%), but this can be ignored for the purpose of this calculation. $SiO_{2\ Kaolinite}$ is thus determined from:

$$SiO_{2\ kaolinite} = Al_2O_3 \times K \quad (6.4)$$

K = the SiO_2/Al_2O_3 ratio of kaolinite.

Fe_2O_3 in glass could not be calculated using this method as it was not possible to differentiate between ferrite spinel occurring in the glass and as free grains not associated with the glass.

The total concentration of quartz prior to assimilation is thus:

$$quartz_{total} = quartz_{measured} + SiO_{2\ glass} = SiO_{2\ total} - SiO_{2\ kaolinite} \quad (6.5)$$

$quartz_{measured}$ = measured quartz concentration.

Similarly, the total concentration of lime prior to assimilation is:

$$lime_{total} = lime_{measured} + CaO_{glass} = CaO_{total} \quad (6.6)$$

$lime_{measured}$ = total crystalline lime.

It is thus possible to calculate the percentage of quartz and lime that has been assimilated into the glass.

The negative correlations between total lime and quartz (calculated) versus the percentages of each assimilated into the glass is shown in Fig. 6.40. There is an inverse relationship between the total CaO concentration of the bulk ash and the proportion of the total original lime which is assimilated into the glass. Total lime concentrations of less than approximately 5% are completely assimilated into the glass phase, as noted previously, whereas only 40-60% is assimilated for total lime concentrations of 10%. Quartz, which has a concentration range from 9.8-23.5% shows well defined trends for Duvha and Matla, but not for Lethabo. There is no obvious trend for the three stations taken collectively.

The effect of the (total lime or quartz)/glass+mullite ratio on the percent assimilated is shown in Fig 6.41. Lime has a negative correlation, and for a lime/glass+mullite ratio of .05 as much as 85-100% of the total lime will be assimilated, whereas for a ratio of 0.10 only 55-

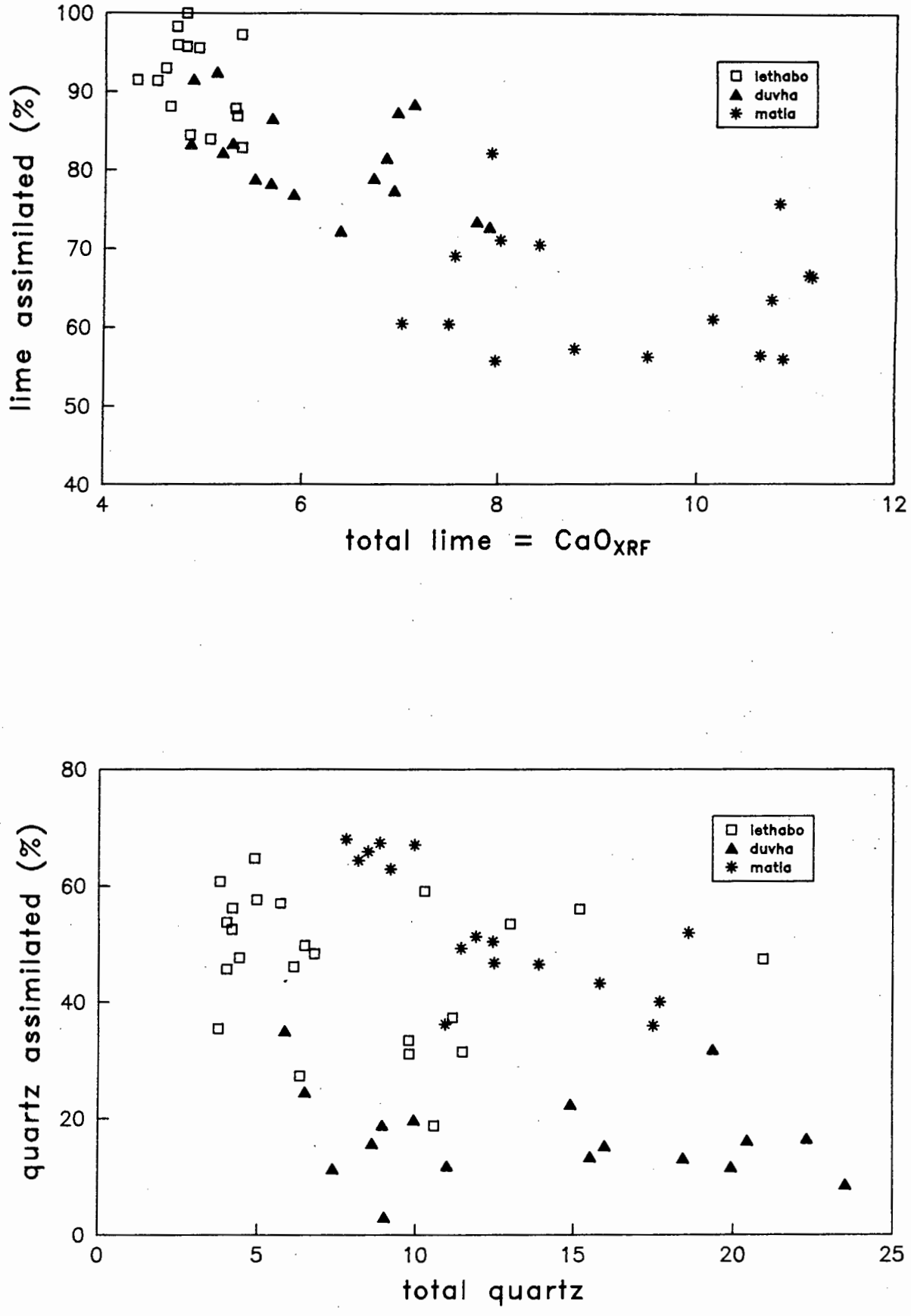

Fig. 6.40 : Total lime and total quartz vs the percentage of each assimilated into the glass.

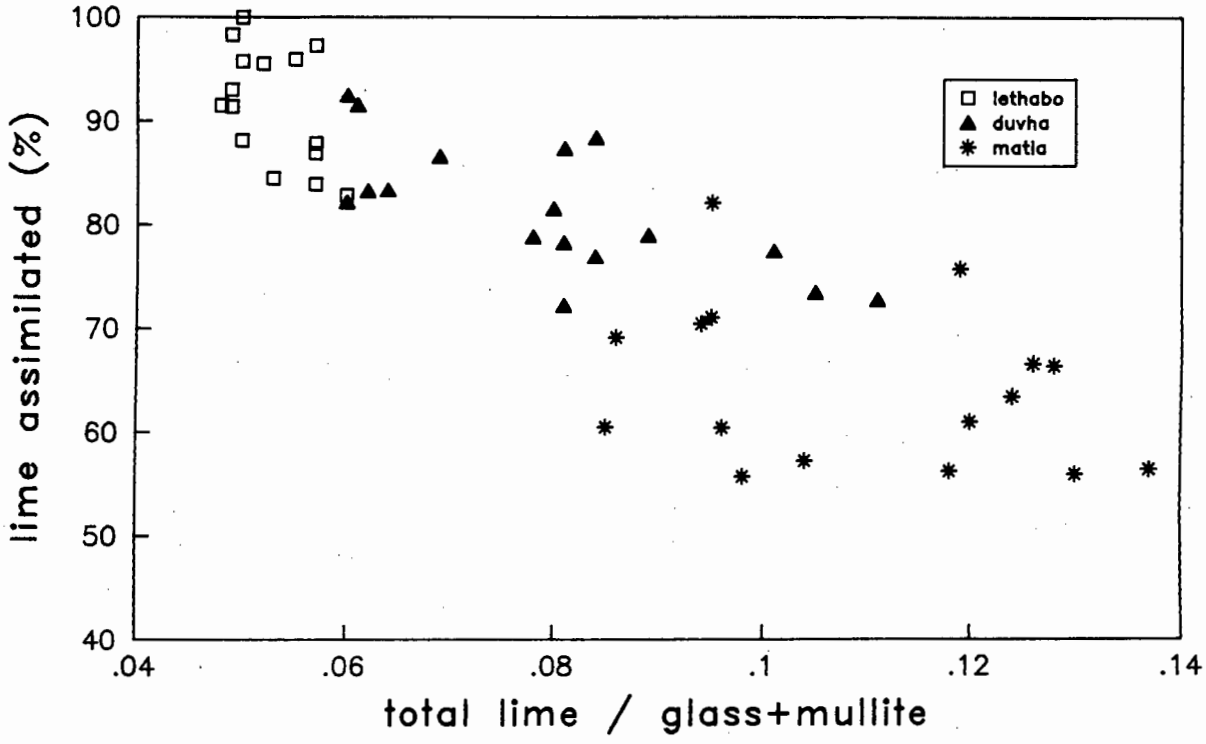

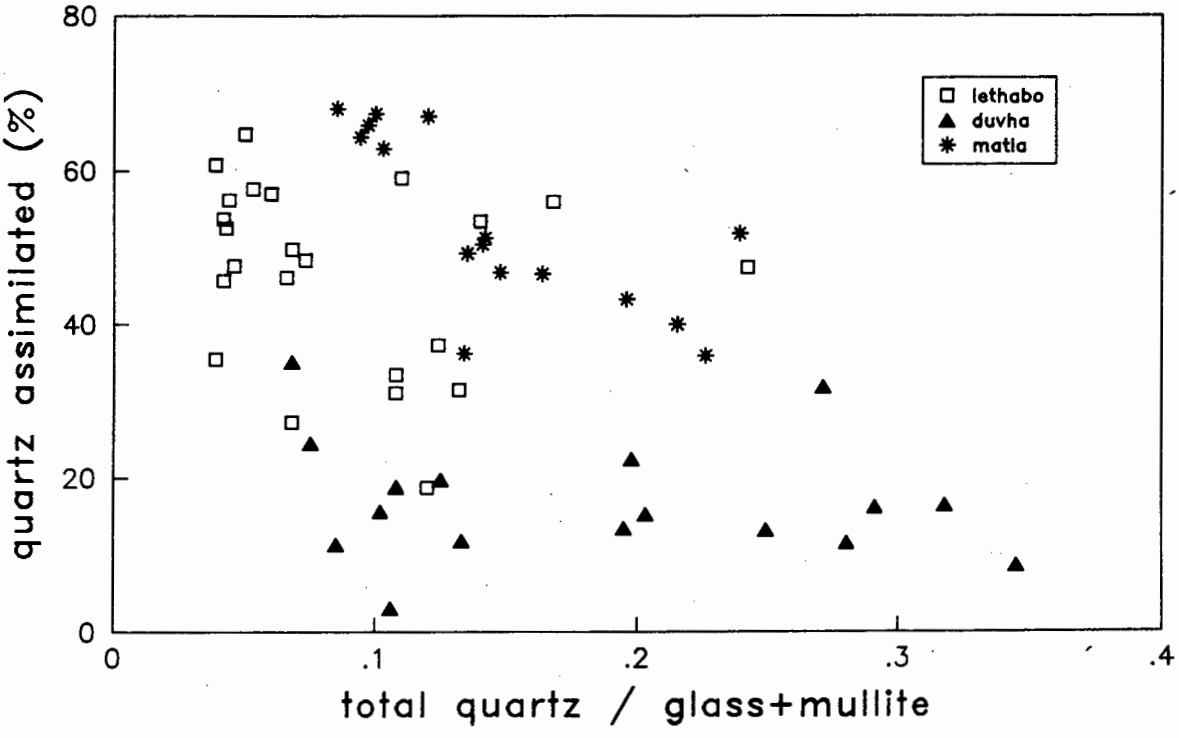

Fig. 6.41 : Total lime / (glass + mullite) and total quartz / (glass + mullite) vs the percentages of each phase assimilated into the glass.

75% will be assimilated.

Quartz plots over a broad range. Matla quartz plots on a similar trend to that defined for the lime. Duvha quartz has a low percentage assimilation.

It is evident from Figs 6.40 and 6.41 that quartz and lime behave differently in the combustion chamber. A significant difference between quartz and lime in coal is that quartz (and kaolinite) occur as finely dispersed grains throughout the coal, whereas lime is derived from carbonate minerals which are generally autochthonous and often form large particles and veins. The carbonate minerals thus may not be in contact with the silica minerals until they are exposed to the turbulent high temperature conditions of the combustion chamber. Raask (1984) considers that melting and assimilation of micro-crystalline clay minerals in the pulverised coal particles occurs on exposure to the high temperatures in the combustion chamber, and that once these particles are liberated from their coal hosts they are prevented from colliding by the electrostatic forces on each particle. Mixing between kaolinite and quartz would thus occur mainly in-situ in unburnt coal, whereas carbonate minerals derived from vein material would not be exposed to the in-situ mixing hypothesis discussed above. Quartz is also less likely to melt as easily in the glass as lime.

The concentration - assimilation relationship noted above for lime suggests that if the concentration of a phase in the input coal is known, then it is possible to estimate the proportion of the phase which will be assimilated into the glass.

6.7 MASS BALANCE CALCULATIONS

6.7.1 Mineral

A mass balance calculation has been performed on the L1 data set. L1 PFA was used as this is the only data set for which bottom ash was available. The percentage ash collected in each of the precipitators and the bottom ash is shown in Table 6.6 (Heinichen and Willis (1987); and specifications kindly supplied by the staff of Lethabo power station). The mineralogy of the bulk ash was calculated from the known proportions of PFA collected by each precipitator, and is compared in Table 6.7 with the mineralogy of the input coal (expressed as LOI free). Total quartz is calculated from measured quartz plus quartz assimilated in glass

(calculated), and is similar to the quartz concentration of the coal ash. Kaolinite in coal ash is similar to the sum of mullite and glass in the PFA corrected for the assimilation of quartz and lime. No correction is made for the assimilation of Fe_2O_3 bearing phases into the glass as this could not be calculated. The sum of calcite and dolomite in the coal agrees closely with calculated total lime in the bulk ash (measured lime + lime calculated from portlandite + lime assimilated into the glass). The agreement between coal mineralogy and the bulk ash mineralogy corrected for the effects of assimilation is generally very close, and within the limits of analytical error.

Collection site	% Collected
Bottom Ash	10.0
Field 1	55.9
Field 2	21.2
Field 3	8.0
Field 4	3.0
Field 5	1.2
Field 6	0.4
Field 7	0.2

Table 6.6 : Distribution of the PFA between bottom ash and the precipitator fields for Lethabo power station. The bottom ash data were kindly supplied by power station staff. Data for fields 1 to 7 were taken from Heinichen and Willis (1987).

L1 Coal Ash		Bulk L1 PFA	
Quartz	9.6	8.4	$Quartz_{total} = quartz_{lost\ into\ glass} + quartz_{measured}$
Kaolinite	84.0	80.8	$Mullite + glass - quartz_{lost\ in\ glass} - lime_{lost\ in\ glass}$
Dolomite + calcite	4.9	4.4	$Lime_{total} = lime_{lost\ in\ glass} + lime_{measured} = CaO_{measured\ by\ XRF}$

Table 6.7 : Comparison of the mineralogy of the bulk L1 PFA and the mineral concentrations in the L1 coal ash (calculated from the mineralogy of the input coal and corrected for LOI).

6.7.2 Chemical

A chemical mass balance calculation has been performed on the L1 data set. Table 6.8 compares the composition of the coal ash for L1_PF (calculated) with the bulk PFA (calculated). S is lower in the bulk PFA by 92%. The concentrations of Al_2O_3, Y, Zr, Nb, Mo, As, Ga, Zn, Ni, Mn and Sc were higher in the bulk ash. Of these elements the most

significant increases were for Zn which increased from 78ppm in the coal ash to 101ppm in the bulk ash, and for Ni which increased from 80 to 102ppm. Toxic elements such as Se, B and V have similar concentrations in the coal ash and the bulk ash. Of the elements determined the only one released in significant proportions to the environment is S.

	L1_PF Ash (calculated)	L1 Bulk PFA (calculated)
SiO_2	51.61	50.22
TiO_2	1.68	1.70
Al_2O_3	33.24	35.88
FeO	2.41	2.79[1]
MgO	1.00	1.17
CaO	4.51	4.45
Na_2O	0.27	0.29
K_2O	0.44	0.47
P_2O_5	0.34	0.36
S	0.95	0.08[2]
Rb	32	31
Sr	761	813
Y	83	97
Zr	527	586
Nb	41	48
Mo	5	6
U	12	12
Th	49	51
Pb	68	87
As	12	17
Se	2	2
Bi	<4	3
Ge	2	3
W	10	9
Ga	51	63
Br	<1.5	<1.1
Zn	78	101
Cu	68	65
Ni	80	102
Mn	341	380
Cs	12	13
Co	22	26
Cr	251	263
V	215	207
Ba	820	866
Sc	41	46
La	112	113
Ce	237	238
Nd	105	108
B	209	218

Table 6.8 : Chemical mass balance of the L1_PF coal ash (calculated from the coal composition) and the calculated L1 bulk ash composition. B data kindly supplied by B. Pougnet of the Department of Analytical Science at UCT. 1 = all Iron expressed as FeO, 2 = all Sulphur expressed as S

CHAPTER 7

SUMMARY AND RECOMMENDATIONS

7.1 SUMMARY

This work has aimed to provide the basic chemical and mineralogical data necessary to assist in the development and promotion of PFA utilisation in South Africa. Ash from three of South Africa's largest power stations, Duvha, Lethabo and Matla was collected over the period 1987-1988 to determine the long term variations in the chemical and mineralogical composition and particle size distribution of the ash.

These three stations were selected for study for the following reasons: The glass and calcium content is lower in Duvha PFA and higher in Matla PFA than in most other South African fly ashes (Lesch and Cornell 1987; Willis 1987); and Lethabo coal is ground to a finer size than normal, has the highest ash content of all South African power stations, and seven sequential electrostatic precipitator fields are used where Duvha and Matla have four.

The mineralogy of the PFA was determined using a semi-quantitative X-ray diffraction method developed by the author. The method was based on integrated counts over peak areas using silicon as an internal standard. Correction factors for peak overlap and interference were determined using interference standards. Concentration standards were prepared for each phase determined in the samples. A computer program in FORTRAN 77 was written to process the intensity data.

Bulk chemical concentrations of major, minor and trace elements were determined using X-ray fluorescence spectrometry.

Compositions of the glass and ferrite spinel phases were determined by electron microprobe analysis.

Particle size distributions were determined with a Malvern Instruments Particle Sizer on PFA in both dry and slurry form, with comparative results obtained for some samples with a Micromeritics Sedigraph.

The particle size distribution decreases in PFA from fields 1 to 4, although the size difference in PFA from the first two fields is greater than the difference between the later fields.

There is no significant difference in the particle size of PFA from fields 4 to 7 of Lethabo.

The particle size distribution of PFA from each field of Matla and Lethabo has remained constant over a period of 18 months.

The particle size distribution of PFA from Duvha field 4 is slightly coarser than PFA from field 4 of either Lethabo or Matla, which may be due to the much coarser particle size to which the Duvha coal is ground.

The glass concentration generally increases in Lethabo PFA from fields 1 to 4, and remains constant from fields 4 to 7. No particular trend was noticed in the mullite concentration. The quartz concentration decreases in PFA from fields 1 to 4 and remains constant from fields 4 to 7.

The glass concentration remains constant in Duvha PFA from fields 1 to 4, whereas samples taken in 1980 showed a sharp increase in concentration from fields 1 to 4 (Willis 1987). The mullite concentration increases sharply from field 1 to 2 in both samples studied in this work and in the 1980 samples. Quartz decreases from fields 1 to 4 in both PFA in the present study and in the 1980 samples, although the quartz concentration in the 1980 samples was higher than in the samples in the present study.

The glass concentration in the Matla PFA samples increases from fields 1 to 4, and the mullite and quartz concentrations decrease from fields 1 to 4. The trends and concentration ranges reported in this work for mullite, quartz and glass in Matla PFA agree with data reported by Lesch and Cornell (1987) for samples collected in 1980.

There is a positive correlation between the SiO_2 and quartz concentrations for all the samples studied.

The spinel concentration decreases in PFA from fields 1 to 4 in all the Duvha and Lethabo samples, and in most of the Matla samples. Hematite shows no trend, and was below the detection limit in most of the Lethabo PFA samples. There is a positive correlation between the Fe_2O_3 and spinel concentrations for all the samples. A minimum concentration of of 2-3% Fe_2O_3 is required in the ash before spinel formation commences.

Lime in the PFA samples gradually alters to portlandite. Lethabo lime generally decreases in concentration in PFA from fields 1 to 4. There is a positive correlation between CaO and the

lime concentration for all the samples. Below a total CaO concentration of 5%, all the CaO is dissolved in the glass phase.

The glass concentration is highest in Matla PFA and lowest in Duvha PFA. Mullite is low in Matla PFA and high in Lethabo and Duvha PFA. Quartz is highest in Duvha PFA. Spinel is highest in Duvha PFA and lowest in Lethabo PFA. Lime is highest in Matla PFA and lowest in Lethabo PFA.

The mineral phases in PFA from Duvha and Matla tend to show a small variation in concentration with time, but generally remain within well defined concentration limits. An exception is the glass concentration in the Duvha PFA.

SiO_2 decreases in concentration in PFA from fields 1 to 4 in all three stations. CaO, Fe_2O_3 and K_2O generally remain constant in concentration. Considerable enrichments are shown by Na_2O, P_2O_5 and SO_3 in PFA from fields 1 to 4 in all three stations. Zr, Rb and Mn generally have no or very low enrichments in PFA from fields 1 to 4. High enrichment factors (> 5) were found for As, Ge and Se.

Trace elements generally have the highest enrichments in Duvha PFA and the lowest in Lethabo PFA. This is due to depletion of trace elements in PFA from field 1 of Duvha compared with the coal ash. Trace elements have similar concentrations in Lethabo field 1 PFA and in the coal ash.

Glass in PFA is derived from kaolinite in the coal which has melted and undergone mixing with the other coal minerals.

Ferrite spinel in PFA can incorporate Al_2O_3, MgO and TiO_2 as substitutions for FeO, with the MgO substitution dominant in Duvha spinels. This may be due to the lower glass concentration in Duvha PFA being unable to accommodate the MgO.

There is a negative correlation for all the stations between the mullite concentration and the ratios of CaO, Na_2O, MgO and K_2O concentrations with Al_2O_3. These elements are incompatable in the mullite structure, and the negative correlation can be explained if the rate of mullite formation in the glass is retarded by the buildup of a rejected solute containing these elements. This solute would need to be removed before further crystallisation could occur. An alternative explanation could be that the glass would remain stable if the

concentration of fluxing elements was high enough. If not, then mullite would crystallise out, due to supersaturation of Al in the glass.

There is a negative correlation between the CaO concentration of the PFA and the proportion of the total CaO (= total original lime) which has been assimilated into the glass phase. This relationship is not seen for quartz. A possible explanation could be that quartz in PFA is derived from finely dispersed quartz grains throughout the coal, whereas lime is derived from carbonate minerals which are generally autochthonous and often form veins. The carbonates would thus only be exposed to molten kaolinite following liberation of the latter from their coal hosts, whereas quartz grains would be in contact with molten kaolinite in the unburnt coal particles. Quartz however is less likely to be absorbed into glass as easily as CaO.

A mass balance calculation for the Lethabo L1 data set shows a good correlation between coal mineralogy and the mineralogy of the bulk ash (corrected for the effects of assimilation).

A chemical mass balance calculation performed on the L1 data set indicates that of the elements determined, the only one released in significant proportions to the environment is S (92%).

7.2 RECOMMENDATIONS

Three sets of incorrectly labelled samples were received in this study. It is extremely important that sample collection should be undertaken by researchers themselves, regardless of cost.

The mineralogy and chemistry of South African PFA collected by the precipitators is now well established. The mineralogy, chemistry and particle size distribution of PFA which is released to the atmosphere has to date only been estimated from the results of PFA taken from the precipitators. An essential future study should analyse material captured after the final precipitator field. This would be of particular importance from an environmental point of view as the smaller size fraction of PFA, which is the fraction released to the atmosphere, is enriched in many trace elements compared with the bulk ash. The chemical composition of the flue gas should also receive further investigation, particularly with regard to environmentally sensitive elements such as N and S, which are responsible for acid rain, and for toxic volatile elements such as Hg, Be and Tl.

Future studies of PFA should include bottom ash samples. Without data from these samples it is impossible to accurately calculate the bulk ash composition, or carry out mass balance calculations.

The control by the alkali and alkaline earth elements over the formation of mullite in the glass is important and should receive further investigation. Interest has been expressed in the extraction of Al from PFA. Al which occurs in glass is much easier (and less costly) to extract than Al which is bound in the mullite phase. Future studies should thus consider the economic viability of adding CaO, Na_2O or MgO to the input coal in order to increase glass formation and reduce the crystallisation of mullite, which would assist in Al extraction from the PFA at a later date. However, this could result in 'sticky' ash which would clog burners or precipitators.

Future studies should also investigate the leaching of elements from the different phases present in the PFA. Different phases will leach at different rates, and it is thus important to know in which phases the toxic elements are likely to be found, as well as their rate of release.

ACKNOWLEDGMENTS

A note of thanks must go towards the following persons, without whom this project would have remained in the ether.

Dr Richard Kruger of Ash Resources, previously of the CSIR, whose constant dedication to PFA utilisation recognised the need for a project of this nature, and for supplying the samples for analysis.

Prof. James Willis of the Department of Geochemistry, UCT, for his supervision over the period and for invaluable assistance in the field of analysis.

The staff of ESKOM, for their assistance throughout the project, and for making samples available for analysis.

Chris Jones of PPC at De Hoek, for making available the Malvern Instruments Particle Sizer, and for his kind assistance.

Dr Don Ball and Jonathan Knight of the Department of Physics, UCT, for assisting in the particle size analysis.

Dr John Rogers and Mathew Smith of the Marine Geoscience Unit, UCT, for making available the Sedigraph, and in assisting where help was needed.

Prof. Andy Duncan and Dave Hill of the Department of Geochemistry, UCT, for giving me so much assistance with the computer systems, and Dr Dick Rickard for assistance with the electron microprobe.

Bruno Pougnet of Analytical Science, UCT, for his assistance with regards to size analysis.

And my wife Delene, whose kind patience and understanding supported me when all else failed.

REFERENCES

1. Alexander, L. E. (1977), Forty years of quantitative diffraction analysis, Advances in X-Ray Analysis, Vol. 20, 1-13.

2. Alexander, L. and Klug, H. P. (1948), Basic aspects of x-ray absorption, Analytical Chemistry, Vol. 20, 886-889.

3. Bayliss, P. (1986), Quantitative analysis of sedimentary minerals by powder x-ray diffraction, Powder Diffraction, Vol. 1, 37-39.

4. Bertin, E. P. (1975), Principles and practise of x-ray spectrometric analysis, Plenum Press, 1079pp, 2nd Edition.

5. Block, C. and Dams, R. (1976), Study of fly ash emission during combustion of coal, Environmental Science and Technology, Vol. 10, 1011-1017.

6. Brindley, G. W. (1945), The effect of grain or particle size on x-ray reflections from mixed powders and alloys considered in relation to the quantitative determination of crystalline substances, Phil. Mag., Vol. 36, 347-369.

7. Brindley, G. W. and Nakahira, M. (1959), The kaolinite-mullite reaction series: I, A survey of outstanding problems, Journal of the American Ceramic Society, Vol. 42, 311-314.

8. Burnet, G., Murtha, M. J. and Dunker, J. W. (1984), Recovery of metals from coal ash. An annotated bibliography (Revised), U. S. Department of Energy, IS-4833 (rev), UC-90.

9. Campbell, J. A., Laul, J. C., Nielson, K. K. and Smith, R. D., (1978), Separation and chemical characterization of finely-sized fly-ash particles, Anal. Chem., Vol. 50, 1032-1040.

10. Chung, F. H. (1974), Quantitative interpretation of x-ray diffraction patterns of mixtures. I. Matrix-flushing method for quantitative multicomponent analysis, Journal of

Applied Crystallography, Vol. 7, 519-525.

11. Clark, G. L. and Reynolds, D. H. (1936), Quantitative analysis of mine dusts, Ind. Eng. Chem., Anal. Ed., Vol. 8, 36-40.

12. Clark, N. H. and Preston, R. J. (1974), Dilution methods in quantitative x-ray diffraction analysis, X-Ray Spectrometry, Vol. 3, 21-25.

13. Coles, D. G., Ragaini, R. C., Ondov, J. M., Fisher, G. L., Silberman, D. and Prentice, B. A. (1979), Chemical studies of stack fly ash from a coal-fired power plant, Environmental Science and Technology, Vol. 13, 455-459.

14. Copeland, L. E. and Bragg, R. H. (1958), Quantitative x-ray diffraction analysis, Analytical Chemistry, Vol. 30, 196-208.

15. Davidson, R. L., Natusch, D. F. S., Wallace, J. R. and Evans, C. A., Jr, (1974), Trace elements in fly ash. Dependence of concentration on particle size, Environmental Science and Technology, Vol. 8, 1107-1113.

16. Diamond, S. (1983), On the glass present in low-calcium and in high-calcium fly ashes, Cement and Concrete Research, Vol. 13, 459-464.

17. Eskom Annual Report (1988), Eskom Communication Department, 44pp.

18. Feather, C. E. and Willis, J. P. (1976), A simple method for background and matrix correction of spectral peaks in trace element determination by x-ray fluorescence spectrometry, X-Ray Spectrometry, Vol. 5, 41-48.

19. Fisher, G. L., Chang, D. P. Y. and Brummer, M. (1976), Fly ash collected from electrostatic precipitators: Microcrystalline structures and the mystery of the spheres, Science, Vol. 192, 555-556.

20. Furuya, K., Miyajima, Y., Chiba, T. and Kikuchi, T. (1987), Elemental characterization of particle size-density separated coal fly ash by spectrophotometry, inductively coupled plasma emission spectrometry, and scanning electron microscopy-energy dispersive x-ray analysis, Environmental Science and Technology, Vol. 21, 898-903.

21. Grossman, S. L. (1983), The chemistry and mineralogy of the fly ash generated by the Hadera M. D. Power Station, Unpublished M.Sc thesis, Hebrew University of Jerusalem, 39pp.

22. Heinichen, D. and Willis, J. P. (1987), Size classification and metal enrichment of pulverized fuel ash by electrostatic precipitation, Proc. Third International Conf. Electrostatic Precipitation, 1075-1084.

23. Hubbard, F. H. and McGill, R. J. (1984), Clay and pyrite transformations during ignition of pulverised coal, Min. Mag., Vol. 48, 251-256.

24. Hulett, L. D., Jr, Weinberger, A. J., Northcutt, K. J. and Ferguson, M. (1980), Chemical species in fly ash from coal-burning power plants, Science, Vol. 210, 1356-1358.

25. Hull, A. W. (1919), A new method of chemical analysis, Journal of the American Chemical Society, Vol. 41, 1168-1175.

26. Hussein, A. T. and Gad, G. M. (1966), On the chemical determination of glassy phases in alumino-silicate refractories, Journ. of Chem. UAR, Vol. 9, 365-374.

27. Jenkins, R., Fawcett, T. G., Smith, D. K., Visser, J. W., Morris, M. C. and Frevel, L. K. (1988), JCPDS - International centre for diffraction data: Sample preparation methods in x-ray powder diffraction, Powder Diffraction, Vol. 1, 51-63.

28. Kaakinen, J. W., Jorden, R. M., Lawasani, M. H. and West, R. E. (1975), Trace element behaviour in coal-fired power plant, Environmental Science and Technology, Vol. 9, 862-869.

29. Klein, D. H., Andren, A. W., Carter, J. A., Emery, J. F., Feldman, C., Fulkerson, W., Lyon, W. S., Ogle, J. C., Talmi, Y., Van Hook, R. I. and Bolton, N. (1975), Pathways of thirty-seven trace elements through coal-fired power plant, Environmental Science and Technology, Vol. 9, 973-979.

30. Klug, H. P. and Alexander, L. E. (1974), X-ray diffraction procedures, 1974, 2nd Edition, John Wiley and Sons, 966pp.

31. Kruger, R. A., Willis, J. P. and Bosch, G. L. (1989), What minerals can be economically recovered from fly ash?, Total Utilization of Coal Resources, S. A. Institute of Mining and Metallurgy Journal, In press.

32. Lauf, R. J. (1982), Microstructures of coal fly ash particles, Ceramic Bulletin, Vol. 61, 487-490.

33. Lauf, R. J. (1985), Characterization of the mineralogy and microchemistry of fly ash, Nuclear and Chemical Waste Management, Vol. 5, 231-236.

34. Lennox, D. H. (1957), Monochromatic diffraction-absorption technique for direct quantitative x-ray analysis, Analytical Chemistry, Vol. 29, 766-770.

35. Leroux, J., Lennox, D. H. and Kay, K. (1953), Direct quantitative x-ray analysis by diffraction-absorption technique, Analytical Chemistry, Vol. 25, 740-743.

36. Lesch, W. (1987), The mineral and glass content of South African fly ash, Unpublished M.Sc Thesis, University of Stellenbosch, 188pp.

37. Lesch, W. and Cornell, D. H. (1987), The mineralogy and morphology of fly ash from South African power stations, Ash - A valuable resource, CSIR, Vol. 3, 13pp.

38. Linton, R. W., Loh, A. and Natusch, D. F. S. (1976), Surface predominance of trace elements in airborne, Science, Vol. 191, 852-854.

39. McCarthy, G. J. (1988), X-ray powder diffraction for studying the mineralogy of fly ash, Fly Ash and Coal Conversion By-Products; Characterization, Utilization and Disposal IV, Mat. Res. Soc. Proc., Vol. 113, Materials Research Society, Pittsburgh, 75-86.

40. McCarthy, G. J., Gehringer, R. C. Smith, D. K., Injaian, V. M., Pfoertsch, D. E. and Kabel, R. L. (1981), Internal standards for quantitative x-ray phase analysis: crystallinity and solid solution, Advances in X-Ray Analysis, Vol. 24, 253-264.

41. McCarthy, G. J., Johansen, D. M., Steinwand, S. J. and Thedchanamoorthy, A. (1988), X-ray diffraction analysis of fly ash, Advances in X-Ray Analysis, Vol. 31, 331-342.

42. McCarthy, G. J., Swanson, K. D., Keller, L. P. and Blatter, W. C. (1984), Mineralogy of western fly ash, Cement and Concrete Research, Vol. 14, 471-478.

43. McCarthy, G. J. and Thedchanamoorthy, A. (1989), Semi-quantitative x-ray diffraction analysis of fly ash by the reference intensity ratio method, Fly Ash and Coal Conversion By-Products; Characterisation, Utilization and Disposal V, Res. Soc. Symp. Proc. Vol. 136 (Materials Research Society, Pittsburgh, 1989), 67-76.

44. Natusch, D. F. S., Wallace, J. R., Evans, C. A., Jr, (1974), Toxic trace elements: Preferential concentration in respirable particles, Science, Vol. 183, 202-204.

45. Norrish, K. and Hutton, J. T. (1969), An accurate x-ray spectrographic method for the analysis of a wide range of geological samples, Geochim. Cosmochim. Acta, Vol. 33, 431-453.

46. Parrish, W. and Huang, T. C. (1983), Accuracy and precision of intensities in x-ray polycrystalline diffraction, Advances in X-Ray Analysis, Vol. 26, 35-44.

47. Raask, E. (1984), Creation, capture and coalescence of mineral species in coal flames, Journal of the Institute of Energy, Vol. 57, 231-239.

48. Ramsden, A. R. (1969), A microscopic investigation into the formation of fly-ash during the combustion of a pulverized bituminous coal, Fuel, Vol. 48, 121-137.

49. Ramsden, A. R. and Shibaoka, M. (1982), Characterization and analysis of individual fly-ash particles from coal-fired power stations by a combination of optical microscopy, electron microscopy and quantitative electron microprobe analysis, Atmospheric Environment, Vol. 16, 2191-2206.

50. Smith, R. D., Campbell, J. A. and Nielson, K. K. (1980), Volatility of fly ash and coal, Fuel, Vol. 59, 661-665.

51. Stevenson, R. J. (1984), Mineralogical characterization of a lignite gasification ash from a low-BTU fixed-bed gassifier II. Scanning electron microscope phase analysis, Cement and Concrete Research, Vol. 14, 485-490.

52. Tao, G. Y., Pella, P. A. and Rousseau, R. M. (1985), NBSGSC - A fortran program for quantitative x-ray fluoresence analysis, NBS Technical Note 1213, U. S. Department of Commerce, National Bureau of Standards, 118pp.

53. Tatlock, D. B. (1966), Rapid modal analysis of some felsic rocks from calibrated x-ray diffraction patterns, Bull. U. S. Geol. Survey, Vol. 1209, 1-41.

54. Valkovic, V., Makjanic, J., Jaksic, M., Popovic, S., Bos, A. J. J., Vis, R. D., Wiederspahn, K. and Verheul, H. (1984), Analysis of fly ash by x-ray emission spectroscopy and proton microbeam analysis, Fuel, Vol. 63, 1357-1362.

55. Verbaan, B. (1987), The utilization of South African power station fly ash for the recovery of aluminium products, Ash - A Valuable Resource, CSIR, Vol. 3, 15pp.

56. Willis, J. P. (1983), Trace-element studies on South African coals and fly ash, Special Publication of the Geological Society of South Africa, Vol. 7, 129-135.

57. Willis, J. P. (1987), Variations in the composition of South African fly ash, Ash - A valuable resource, 2-6 February 1987, CSIR, Vol. 3, 12pp.

58. Willis, J. P. (1989), Compton scatter and matrix correction for trace element analysis of geological materials, X-Ray Fluorescence Analysis in the Geological Sciences. Advances in Methodology, Short Course Vol. 7, GAC-MAC Annual Meeting, Montreal, quebec, 1989, 91-140.

59. Willis, J. P., Bosch, G. L. and Kruger, R. A. (1989), The chemical and mineralogical composition of South African fly ash, Proc. Fifteenth Biennial Low-Rank Fuels Symposium, May 1989, In press.

60. Zevin, L. S. (1977), A method of quantitative phase analysis without standards, Journal of Applied Crystalography, Vol. 10, 147-150.

Analytical parameters used for QXRD.

Analyte Peak/ Background	2θ range	Overlapping/Interfering Peak								MFAC	GFAC	Calibration Curve Slope	LLD (%)
		Silicon	Quartz	Mullite	Hematite	Spinel	Calcite	Portlandite	Lime				
Mullite (110)	15.50 - 17.00					0.006						0.0114	0.60
Portlandite (001)	17.19 - 19.00			0.003		0.109						0.0444	0.15
Quartz (100)	19.70 - 21.70										0.018	0.0200	0.35
Hematite (012)	23.70 - 24.65		0.020									0.0313	0.22
Silicon (111)	27.85 - 29.00		0.011			0.016	0.014[c] 0.106[p] 0.017[l]	0.406[p] 0.506[l]			-0.025		
Calcite (104)	29.00 - 29.70	0.007	0.005			0.032		0.052[p] 0.048[l]			0.041	0.2228	0.03
Spinel (220)	29.75 - 30.60		0.003	0.029			0.127[l]	0.024[c]			0.004	0.0415	0.15
Lime (111)	31.70 - 32.65			0.026	0.075	0.040	0.001[c] 0.154[p] 0.041[l]	0.055[p] 0.073[l]			0.027	0.0680	0.08
Glass	11.50 - 38.20											0.0118	
background	11.50									0.108			
background	15.13									0.231			
background	17.19			0.020				0.070[p] 0.289[l]		0.251			
background	19.45									0.218			
background	22.20									0.219			
background	24.75		0.012		0.026					0.255			
background	29.70	0.001	0.005			0.142	0.338[c] 0.626[p] 0.211[l]	0.027[p] 0.041[l]		0.209			
background	34.75			0.128	0.052	0.155		0.288[p] 0.796[l]		0.171			
background	38.20									0.140			

c = factor determined with calcite interference standard
p = factor determined with portlandite interference standard
l = factor determined with lime interference standard
MFAC = mullite correction factor for background
GFAC = glass correction factor

Appendix 1

Appendix 2(a)

Background positions used to calculate the area of the background below each analyte peak.

Peak	Background Positions (°2θ)
Mullite(110)	11.50 15.13 17.19
Portlandite(001)	15.13 17.19 19.45
Quartz(100)	17.19 19.45 22.20
Hematite(104)	19.45 22.20 24.75
Silicon(111)	24.75 29.70 34.75
Calcite(104)	24.75 29.70 34.75
Spinel(220)	24.75 29.70 34.75
Lime(111)	24.75 29.70 34.75

Appendix 2(b)

Domain limits and background positions used to calculate the area of the glass bulge.

Domain	2θ Range	Background Positions (°2θ)
I	11.50 - 17.19	11.50 15.13 17.19
II	17.19 - 19.45	15.13 17.19 19.45
III	19.45 - 22.20	17.19 19.45 22.20
IV	22.20 - 24.75	19.45 22.20 24.75
V	24.75 - 34.75	24.75 29.70 34.75
VI	34.75 - 38.20	29.70 34.75 38.20

Appendix 3(a)

An example of an input parameter file for program XRDGLASS is shown. Lines 1 and 2 are ignored by the program. Peaks and backgrounds are listed in order of increasing degrees 2θ.

Column 1 (Descrp): Name of peak or background position.

Column 2 (Rw): Position number in detection order.

Columns 3 and 4 (Ba): Background calculation instructions. Two negative numbers having the same value alongside a peak in columns 3 and 4 (e.g. -1 -1) instruct the program to calculate the background at that position using the quadratic equation determined from backgrounds which are designated by the same negative number. The background with the lowest 2θ value used to calculate the equation has the same number (e.g. -1) in column 3 only, and the background with the highest 2θ value has the same number (e.g. -1) in column 4 only. Backgrounds with 2θ values intermediate to these two background positions are included in the calculation. For each set of background positions defined in this manner, a quadratic equation is calculated through the glass bulge and through the background below the bulge (using calculated intensities).

Columns 5 (Bf1), 6 (Mul) and 7 (Mp): Factors used to calculate the background below the glass bulge. Bf1 = Factor BFAC used to calculate background due to quartz alone, using background intensities at 11.5 and 38.2°2θ determined with the quartz interference standard. Mul = MFAC (see text), and Mp indicates the row number (Rw) of mullite.

Columns 8 (Pf1) and 9 (P1): Pf1 = overlap and interference correction factor, i.e. PFAC and BFAC. P1 = Row number (Rw) of overlapping/interfering peak which must be multiplied by Pf1. Similar pairs are listed in columns 10-11, 12-13, 14-15 and 16-17.

Column 18 (Pf6): Pf6 = GFAC and is multiplied by the total glass bulge area to correct the nett peaks for error contributed from the glass.

Column 19 (Ps): Position in output data file. The internal standard must correspond to Ps = 1.

Column 20 (Lim): Domain limits for the glass area calculation. Values in rows 1 and 2 are used as the integral limits for domain I. Area in domain I between the glass bulge and the the background below the bulge are calculated using quadratic equation -1 (columns 3 and 4). Similarly, domain II uses the integral limits from rows 2 and 3, and uses the quadratic equation -2, etc.

```
XRD PARAMETER FILE
Descrp Rw Ba Ba Bf1 MulMp Pf1 P1 Pf2 P2 Pf3 P3 Pf4 P4 Pf5 P5 Pf6 Ps Lim
BACK13  1 -1  0 000 108 3 000  0 000  0 000  0 000  0 000  0 000 0 11.50
BACK1   2 -2  0 627 231 3 000  0 000  0 000  0 000  0 000  0 000 0 17.19
MUL110  3 -1 -1 000 000 0 006 14 000  0 000  0 000  0 000  0 000 2 19.45
BACK2   4 -3 -1 485 251 3 020  3 289  5 000  0 000  0 000  0 000 0 22.20
PTL001  5 -2 -2 000 000 0 003  3 109 14 000  0 000  0 000  0 000 3 24.75
BACK3   6 -4 -2 373 218 3 000  0 000  0 000  0 000  0 000  0 000 0 34.75
QTZ100  7 -3 -3 000 000 0 000  0 000  0 000  0 000  0 000  0 018 4 38.20
BACK4   8  0 -3 266 219 3 000  0 000  0 000  0 000  0 000  0 000 0
HMT012  9 -4 -4 000 000 0 020  7 000  0 000  0 000  0 000  0 000 5
BACK5  10 -5 -4 185 255 3 012  7 026  9 000  0 000  0 000  0 000 0
SIL111 11 -5 -5 000 000 0 011  7 016 14 017 12 506  5 000  0-025 1
CAL104 12 -5 -5 000 000 0 007 11 005  7 032 14 048  5 000  0 041 6
```

BACK6	13	-6	0	081	209	3	001	11	005	7	142	14	211	12	041	5	000	0
MGF220	14	-5	-5	000	000	0	003	7	029	3	127	12	000	0	000	0	004	7
LIM111	15	-5	-5	000	000	0	026	3	075	9	040	14	041	12	073	5	027	8
BACK7	16	0	-5	021	171	3	128	3	052	9	155	14	796	5	000	0	000	0
BACK8	17	0	-6	000	140	3	000	0	000	0	000	0	000	0	000	0	000	0

Appendix 3(b)

An example of an input data file for program XRDGLASS. Lines 1 and 2 are ignored by the program. The sample name is taken from the third line. Data columns from left to right are: Name of peak or background, angle in degrees 2θ at beginning of scan window, angle in degrees 2θ at end of scan window, position of peak maximum in degrees 2θ (the last three columns have the same entries in the case of backgrounds), total counts measured in window, counting time in thousandths of a second, and intensity of background 13 and 8 (11.5 and 38.2°2θ respectively) measured with the quartz interference standard. The colon after the first sample indicates that another sample follows.

```
sample data  Feb 1989
DESCRIP THETA1  THETA2   THETA  COUNTS    TIME    QUARTZ
D3_COMPA
BACK13   11.50   11.50   11.50  279130   200000   254537
BACK1    15.13   15.13   15.13  226295   200000    47090
MUL110   15.50   17.00   16.45  457509   360017
BACK2    17.19   17.19   17.19  226150   200000
PTL001   17.19   19.00   18.10  508330   434501
BACK3    19.45   19.45   19.45  240794   200000
QTZ100   19.70   21.70   20.85  653777   480022
BACK4    22.20   22.20   22.20  269891   200000
HMT012   23.70   24.65   24.10  619964   455893
BACK5    24.75   24.75   24.75  124150    94114
SIL111   27.85   29.00   28.44 1115083   552010
CAL104   29.00   29.70   29.48  355014   335927
BACK6    29.70   29.70   29.70  205467   200000
MGF220   29.75   30.60   30.19  439356   407960
LIM111   31.70   32.65   32.22  495430   455961
BACK7    34.75   34.75   34.75  149697   200000
BACK8    38.20   38.20   38.20  106973   200000
:
D3_COMPB
BACK13   11.50   11.50   11.50  288344   200000   254537
BACK1    15.13   15.13   15.13  233196   200000    47090
MUL110   15.50   17.00   16.45  470244   359895
BACK2    17.19   17.19   17.19  231166   200000
PTL001   17.19   19.00   18.10  520531   434450
BACK3    19.45   19.45   19.45  247115   200000
QTZ100   19.70   21.70   20.85  670059   480073
BACK4    22.20   22.20   22.20  253442   182009
HMT012   23.70   24.65   24.10  639467   455909
BACK5    24.75   24.75   24.75  271983   200000
SIL111   27.85   29.00   28.44 1095360   551846
CAL104   29.00   29.70   29.48  367835   336025
BACK6    29.70   29.70   29.70  212294   200000
MGF220   29.75   30.60   30.19  454213   407835
LIM111   31.70   32.65   32.22  512492   455970
BACK7    34.75   34.75   34.75  155386   200000
BACK8    38.20   38.20   38.20  110447   200000
```

Appendix 3(c)

```
      program  xrdglass
      implicit     none
      character*63 fname,fname1,fname2,fname3
      character*28 name
      character*5  dummy
      character*8  sname,intact
      character*6  des(0:50),backa(50),backb(50),nam(50)
      character*4  gdat,end
      character*1  ans,ans1,ans2,ans3
      real         a,c,gtheta(50),gcps(50),thtmin(50),thtmax(50),
     +             theta(50),bpeak(50),npeak(0:50),ratio1(50),
     +             cps(50),time(50),rat1(50),npeaq(0:50),
     +             denom1,brate(50),tback(50),lld(50),sd(50),
     +             nett(50),tback1,tback2,ratio,div,q(20),xp(20),
     +             x1(50),x2(50),x3(50),
     +             xxp,yyp,sy,sy2,syc,syc2,sst,ssr,r2(100),
     +             bfac1(0:100),pfac1(0:100),cpsaaa(100),b(20,20),
     +             qstart(-100:0),qstop(-100:0),area1,bulge,
     +             pfac2(0:100),rr2(100),xx1(100),xx2(100),xx3(100),
     +             s(100),botcps(0:100),pfac3(0:100),d(100,4),area2,
     +             cpsold(100),cps1(50),
     +            npeak1(50),npeak2(50),botcp1(50),botcp2(50),pfac4(100)
     +            ,b_area(100),cps3(100),npeak3(100)
     +            ,pfac5(100),cps2(50),mfac(100),pfac6(0:100)
      logical      eflag
      integer*4    counts(100)
      integer      bk1(0:100),bk2(0:100),itrm,i,values,afile,ios,ilp,
     +             k,tick,ofile,ios1,kb,tickb,pos(100),quad,numqod,l,
     +             count,countb,stepq,backin,bakout,j,ios2,ios4,
     +             baca(100),bacb(100),peak1(0:100),pnum,row(100),
     +             f,p,m,bfile,start(-100:0),stopp(-100:0),n,iti,repeat,
     +             peak2(0:100),peak3(0:100),times,peak5(100)
     +             ,error,ios3,gfile,peak4(0:100),qtz13,
     +             qtz8,mpeak(0:100)
c
c
      itrm = 6
      ilp  = 6
      write(itrm,1000)
c
c     ***************** send output file to printer ********************
c
      call spprt (ilp,itrm,name,eflag)
          if (eflag) then
              write (itrm,3001)
              stop 'program aborted'
          end if
c
c
c     **************** format statements *********************
c
998   format  (/)
999   format  (a8)
1000  format  (/,'program xrd_glass  -  rev. %i%')
1002  format  (a6,2x,f6.2,2x,f6.2,2x,f6.2,1x,i7,2x,f7.3,2x,i7)
1012  format  (a6,1x,3(i2,1x),2(f3.3,1x),i1,5(1x,f3.3,1x,i2),f4.3,
     +         i2,1x,f5.2)
1020  format  (a)
1010  format  (/,'enter filedescriptor of xrd (glass) data file:  _)
1060  format  (/,'enter filedescriptor of output data:    _)
```

```
1062  format  (/,'enter filedescriptor of parameter file:    _)
1063  format  (/,'enter filedescriptor of grafit data file:    _)
3000  format  (/,'error opening file,iostat=',i5,/,'file=',a63,/,
     +         'abort? (y/n) [n]:  _)
1014  format  (1x,'glass',60x,f11.3,17x,f7.3)
1013  format  (29x,'integral limits : ',(:,10f6.2))
1015  format  (/,/,10x,'sample name:',3x,8a)
1016  format  (/,10x,a6,1x,'to',1x,a6,1x,'  upper curve:  cps=',f8.3
     +        ,1x,'2theta**2+  ',f8.3,'  2theta+ ',f9.3,4x,'r2=',f5.2)
1017  format  (29x,'lower curve:  cps=',f8.3,1x,'2theta**2+  ',f8.3
     +          ,'  2theta+ ',f9.3,4x,'r2=',f5.2)
1032  format  (/,10x,'background corrections and interferences',/,19x,
     +        'glass bulge',54x,'baseline')
1033  format  (10x,'descrip',1x,'peak1',2x,'pfac1',2x,'peak2',2x,'pfac2'
     +         ,2x,'peak3',2x,'pfac3',2x,'peak4',2x,'pfac4',2x,'peak5',
     +         2x,'pfac5',6x,'bfac',2x,'backa',1x,'backb',2x,'mull',1x,
     +         'glass')
1019  format  (10x,a6,2x,5(a6,1x,f5.3,2x),4x,f5.3,1x,a6,1x,a6,2x,f5.3
     +         ,2x,f5.3)
2000  format  (//,1x,'mineral bk1 bk2  2-theta  2-theta  total  time  '
     +   ,'    orignl    glass     peak      base      nett     std dev'
     +         ,'lld     ratio1          '
     +        ,/,1x,'peak              begin    end      counts (secs)  '
     +    ,'  cps       bulge     base      line      peak     ( % ) '
     +    ,'  (cps)    (s111)          ',/)
2001  format  (/,10x,'number of iterations = ',i2)
1008  format  ('1')
2010  format  (1x,a6,2x,2(i2,2x),f7.3,2x,f7.3,1x,i7,2x,f7.3,1x,
     +        6(f8.3,2x),2(f6.3,2x))
3001  format  (/,'error in opening spool file')
3020  format  (a8,8x,'0',1x,'0',5x,'                        ',10x
     +        ,10(:,/,9f8.3))
3021  format  ('data')
3022  format  (f6.2,2x,f8.3,2x,f8.3,5x,'?')
3023  format  (' -        -        -        -')
3024  format  ('end')
3025  format  (f6.2,5x,'?',8x,'?',5x,f8.3)
c
c
      afile  = 80
      ofile  = 70
      bfile  = 75
      gfile  = 72
      gdat   = 'data'
      end    = 'end'
      intact = 'interact'
c
c
c     ****************  enter names of input and output ****************
c     ****************  data files, parameter file, and ****************
c     ****************  grafit readable file            ****************
c
1     write   (*,1010)
      read    (*,1020) fname
3     write   (*,1060)
      read    (*,1020) fname1
4     write   (*,1062)
      read    (*,1020) fname2
6     write   (*,1063)
      read    (*,1020) fname3
c
c     ******************open input data file ****************************
```

```
c
      open    (afile,file=fname,status='old',iostat=ios)
          if (ios .ne. 0) then
              write (*,3000) ios,fname
              read (*,1020) ans
                  if (ans .eq. 'y') stop 'program aborted'
                  go to 1
          end if
c
c     ******************open parameter file ****************************
c
      open    (bfile,file=fname2,status='old',iostat=ios2)
          if (ios2 .ne. 0) then
              write (*,3000) ios2,fname2
              read (*,1020) ans2
                  if (ans2 .eq. 'y') stop 'program aborted'
                  go to 4
          end if
c
c     *****************open output data file ***************************
c
      open (ofile,file=fname1,status='old',access='sequential',
     +     iostat=ios1)
          if (ios1 .ne. 0) then
              write (*,3000) ios1,fname1
              read (*,1020) ans1
                  if (ans1 .eq. 'y') stop 'program aborted'
                  go to 3
          end if
c
c     **************** open output data file to grafit *****************
c     ****************           readable file        *****************
c
      open (gfile,file=fname3,status='new',iostat=ios3)
          if (ios3 .ne. 0) then
              write (*,3000) ios3,fname3
              read (*,1020) ans3
                  if (ans3 .eq. 'y') stop 'program aborted'
                  go to 6
          end if
          do 16 i=1,1000
16            read (ofile,1020,end=110) dummy
c
c     ***************** read data from the parameter file *************
c
110   repeat=0
      read (bfile,998)
          do 7 i=1,1000
           read (bfile,1012,end=993,iostat=ios4) nam(i),row(i),bk1(i),
     +          bk2(i),bfac1(i),mfac(i),mpeak(i),pfac1(i),peak1(i),
     +          pfac2(i),peak2(i),pfac3(i),peak3(i),pfac4(i),peak4(i),
     +          pfac5(i),peak5(i),pfac6(i),pos(i),s(i)
7         continue
c
c     ***************** read data from the input file ******************
c
993    read (afile,998)
995    read (afile,999) sname
           read (afile,1002,iostat=ios) des(1),thtmin(1),
     +           thtmax(1),theta(1),counts(1),time(1),qtz13
           read (afile,1002,iostat=ios) des(2),thtmin(2),
     +           thtmax(2),theta(2),counts(2),time(2),qtz8
```

```
          do 5 i=3,1000
           read (afile,1002,end=13,iostat=ios) des(i),thtmin(i),
     +          thtmax(i),theta(i),counts(i),time(i)
           if (des(i).eq.':') then
               iti=0
               go to 12
           end if
5     continue
13    iti=1
c
c     ***************** set variables to zero **************************
c
12    bk1(0)=0
      bk2(0)=0
      peak1(0)=0
      peak2(0)=0
      peak3(0)=0
      peak4(0)=0
      bfac1(0)=0
      mfac(0)=0.0
      des(0)=' '
      area2=0.0
      botcps(0)=0.0
      npeaq(0)=0.0
      npeak(0)=0.0
      mpeak(0)=0.0
      pfac1(0)=0.0
      pfac2(0)=0.0
      pfac3(0)=0.0
      pfac4(0)=0.0
      pfac5(0)=0.0
      pfac6(0)=0.0
c
c     ************ calculate the count rate per second  *****************
c     ************ and 2-theta in centre of window, and *****************
c     ************ set variables to zero                *****************
c
      values=i-1
       qtz13=qtz13/time(1)
       qtz8=qtz8/time(values)
       do 15 i=1,values
           cps(i)=counts(i)/time(i)
           cpsold(i)=cps(i)
           bpeak(i)=cps(i)
           botcps(i)=cps(i)
           cps1(i)=0.0
           cps2(i)=0.0
           botcp1(i)=0.0
           botcp2(i)=0.0
           b_area(i)=0.0
           npeaq(i)=0.0
           npeak(i)=0.0
           npeak1(i)=0.0
           npeak2(i)=0.0
           npeak3(i)=0.0
15     continue
c
c     ************ count number of quadratic equations  *****************
c
      repeat=repeat+1
      if (repeat.ne.1) then
          go to 991
```

```
      end if
      numqod = 0
      do 1021 f=1,values
         if (bk1(f).lt.0.and.bk2(f).ne.bk1(f).and.bk1(f).lt.(-1*numqod))
     +   then
              numqod=-1*bk1(f)
         end if
1021  continue
c
c     *********** determine upper and lower limit of   ****************
c     *********** each quadratic equation              ****************
c
      do 1030 quad=-1,-1*numqod,-1
          do 1025 i=1,values
              if (bk1(i).eq.quad.and.bk2(i).ne.bk1(i)) then
                  qstart(quad)=theta(i)
                  start(quad)=i
              else
                  if (bk2(i).eq.quad.and.bk1(i).ne.bk2(i)) then
                      qstop(quad)=theta(i)
                      stopp(quad)=i
                  end if
              end if
1025  continue
1030  continue
c
c     *********** record measured intensity of each    *****************
c     ***********          peak and background         *****************
c
991   do 19 i=1,values
              cpsaaa(i)=cps(i)
19    continue
c
      times=-1
992   do 99 p=1,50
          do 910 i=1,values
              cps1(i)=cps2(i)
              botcp1(i)=botcp2(i)
              npeak1(i)=npeak2(i)
910       continue
          times=times+1
c
c     *********** calculate intensity of background under *************
c     ********* the glass bulge at each background position ***********
c
          botcps(row(1))=qtz13+(mfac(1)*npeak(mpeak(1)))
          do 1043 i=2,values
              if (mfac(i).ne.0) then
                  botcps(i)=((bfac1(i)*(qtz13-qtz8))+qtz8)+
     +                              (mfac(i)*npeak(mpeak(i)))
              else
                  botcps(i)=0.0
              end if
1043      continue
c
c
c     ************** quadratic fit to background under glass *************
c
c     ********* select 2-theta and count rate for background ***********
c
       stepq=0
26     tickb=0
```

```
      do 380 quad=-1,-1*numqod,-1
        stepq=stepq+1
        backin=0
        bakout=0
        countb=0
290       do 300 i=start(quad),stopp(quad)
            if (bk1(i).ne.bk2(i).and.bk1(i).le.0.or.bk2(i).eq.0) then
              tickb=tickb+1
              gcps(tickb)=botcps(i)
              gtheta(tickb)=theta(i)
              countb=countb+1
              if (backin .eq. 0) then
                  backin=i
              end if
              bakout=i
            end if
300         continue
c             if (numqod .eq. 0) then
c                 go to 351
c             end if
c
c     ********** calculate quadratic equations for background ********
c     **********              below the glass bulge           ********
c
      do 700 i=1,3
          q(i)=0.0
          xp(i)=0.0
              do 701 j=1,3
                  b(i,j)=0.0
701           continue
700   continue
      do 702 i=tickb-countb+1,tickb
          xp(1)=1.0
          do 703 j=2,3
              xp(j)=xp(j-1)*gtheta(i)
703       continue
          do 704 j=1,3
              do 705 k=1,3
                  b(j,k)=b(j,k)+xp(j)*xp(k)
705           continue
              q(j)=q(j)+xp(j)*gcps(i)
704       continue
702   continue
      do 750 i=1,3
          div=b(i,i)
755       do 810 j=1,3
              b(i,j)=b(i,j)/div
810       continue
          q(i)=q(i)/div
          do 770 j=1,3
              if (i-j) 760,770,760
760           ratio=b(j,i)
              do 780 k=1,3
                  b(j,k)=b(j,k)-ratio*b(i,k)
780           continue
              q(j)=q(j)-ratio*q(i)
770       continue
750   continue
      n=1
      do 790 i=tickb-countb+1,tickb
          d(n,1)=gtheta(i)
          d(n,2)=gcps(i)
```

```
          xxp=1
          yyp=0
          do 795 j=1,3
              yyp=yyp+xxp*q(j)
              xxp=xxp*d(n,1)
795       continue
          d(n,3)=yyp
          d(n,4)=d(n,2)-yyp
      n=n+1
790   continue
      sy=0.0
      sy2=0.0
      syc=0.0
      syc2=0.0
      sst=0.0
      ssr=0.0
      r2(stepq)=0.0
      do 820 i=1,3
          sy=sy+d(i,2)
          sy2=sy2+d(i,2)*d(i,2)
          syc=syc+d(i,3)
          syc2=syc2+d(i,3)*d(i,3)
820   continue
      sst=sy2-sy*sy/float(countb)
      ssr=syc2-syc*syc/float(countb)
      r2(stepq)=ssr/sst
      backa(stepq)=des(backin)
      backb(stepq)=des(bakout)
      x1(stepq)=q(3)
      x2(stepq)=q(2)
      x3(stepq)=q(1)
380       continue
351       continue
c
c     ******** quadratic for background fit through glass bulge *******
c
c     *********** select 2-theta and count rate for backgrounds *******
c
       stepq=0
27     tickb=0
       do 982 quad=-1,-1*numqod,-1
         stepq=stepq+1
         backin=0
         bakout=0
         countb=0
291        do 901 i=start(quad),stopp(quad)
             if (bk1(i).ne.bk2(i).and.bk2(i).le.0.or.bk2(i).eq.0)
     +       then
                tickb=tickb+1
                gcps(tickb)=cps(i)
c                   if (bfac1(i).ne.0.and.peak1(i).ne.0.or.bfac1(i).ne.
c     +                 0.and.baca(i).ne.0) then
c                       gcps(tickb)=cpsaaa(i)
c                   end if
                gtheta(tickb)=theta(i)
                countb=countb+1
                if (backin .eq. 0) then
                   backin=i
                end if
                bakout=i
             end if
901        continue
```

```
c
c     ********** calculate quadratic equation for glass bulge  *******
c
      do 900 i=1,3
          q(i)=0.0
          xp(i)=0.0
              do 902 j=1,3
                  b(i,j)=0.0
902           continue
900   continue
      do 903 i=tickb-countb+1,tickb
          xp(1)=1.0
          do 904 j=2,3
              xp(j)=xp(j-1)*gtheta(i)
904       continue
          do 905 j=1,3
              do 906 k=1,3
                  b(j,k)=b(j,k)+xp(j)*xp(k)
906           continue
              q(j)=q(j)+xp(j)*gcps(i)
905       continue
903   continue
      do 951 i=1,3
          div=b(i,i)
956       do 811 j=1,3
              b(i,j)=b(i,j)/div
811       continue
          q(i)=q(i)/div
          do 971 j=1,3
              if (i-j) 961,971,961
961           ratio=b(j,i)
              do 981 k=1,3
                  b(j,k)=b(j,k)-ratio*b(i,k)
981           continue
              q(j)=q(j)-ratio*q(i)
971       continue
951   continue
      n=1
      do 791 i=tickb-countb+1,tickb
          d(n,1)=gtheta(i)
          d(n,2)=gcps(i)
          xxp=1
          yyp=0
          do 996 j=1,3
              yyp=yyp+xxp*q(j)
              xxp=xxp*d(n,1)
996       continue
          d(n,3)=yyp
          d(n,4)=d(n,2)-yyp
      n=n+1
791   continue
      sy=0.0
      sy2=0.0
      syc=0.0
      syc2=0.0
      sst=0.0
      ssr=0.0
      rr2(stepq)=0.0
      do 921 i=1,3
          sy=sy+d(i,2)
          sy2=sy2+d(i,2)*d(i,2)
          syc=syc+d(i,3)
```

```
          syc2=syc2+d(i,3)*d(i,3)
921    continue
       sst=sy2-sy*sy/float(countb)
       ssr=syc2-syc*syc/float(countb)
       rr2(stepq)=ssr/sst
       backa(stepq)=des(backin)
       backb(stepq)=des(bakout)
       xx1(stepq)=q(3)
       xx2(stepq)=q(2)
       xx3(stepq)=q(1)
c
c
c      ***************  calculate background below peak  ****************
c
           do 950 i=1,values
                if (bk1(i).eq.quad.and.bk2(i).eq.quad.and.thtmin(i).ne.
     +              thtmax(i).or.i.ge.start(quad).and.i.le.stopp(quad)
     +              .and.bk2(i).le.0.and.thtmin(i).ne.thtmax(i).and.
     +              bk1(i).ne.bk2(i)) then
                    b_area(i)=(((xx1(stepq)*(thtmax(i)**3))/3+(xx2(stepq)
     +                    *thtmax(i)**2)/2+(xx3(stepq)*thtmax(i)))-
     +                    (((xx1(stepq)*(thtmin(i)**3))/3+(xx2(stepq)*
     +                    thtmin(i)**2)/2+(xx3(stepq)*thtmin(i))))))/
     +                    (thtmax(i)-thtmin(i))
                   bpeak(i)=xx1(stepq)*(theta(i)**2)+xx2(stepq)*
     +                      theta(i)+xx3(stepq)
                end if
                if (bk1(i).eq.quad.and.bk2(i).eq.quad.and.thtmin(i).eq.
     +              thtmax(i).or.i.ge.start(quad).and.i.le.stopp(quad)
     +              .and.bk2(i).le.0.and.thtmin(i).eq.thtmax(i)) then
                    bpeak(i)=xx1(stepq)*(theta(i)**2)+xx2(stepq)*theta(i)
     +                     +xx3(stepq)
                    b_area(i)=0.0

                end if
950        continue
982        continue
c
c      ***************** peak on peak overlap corrections **************
c
       pnum=0
       do 830 i=1,values
           if (bk1(i).eq.bk2(i).and.bk2(i).lt.0.and.thtmin(i).ne.
     +     thtmax(i)) then
               npeak(i)=cpsaaa(i)-b_area(i)-pfac1(i)*npeak(peak1(i))-
     +                  pfac2(i)*npeak(peak2(i))-pfac3(i)*npeak(peak3(i))
     +                 -pfac4(i)*npeak(peak4(i))-pfac5(i)*npeak(peak5(i))
     +                 -pfac6(i)*(area1/(s(stepq+1)-s(1)))
           end if
           if (bk1(i).eq.bk2(i).and.bk2(i).lt.0.and.thtmin(i).eq.
     +     thtmax(i)) then
               npeak(i)=cpsaaa(i)-bpeak(i)-pfac1(i)*npeak(peak1(i))-
     +                  pfac2(i)*npeak(peak2(i))-pfac3(i)*npeak(peak3(i))
     +                 -pfac4(i)*npeak(peak4(i))-pfac5(i)*npeak(peak5(i))
     +                 -pfac6(i)*(area1/(s(stepq+1)-s(1)))
           end if
830    continue
c
c      ******** peak on background interference corrections ***********
c
           do 353 i=1,values
                if (npeak(i).lt.0) then
```

```
                npeaq(i)=0.0
            else
                npeaq(i)=npeak(i)
            end if
353       continue
          do 352 i=1,values
            if (bk1(i).ne.bk2(i).and.bk2(i).le.0.and.pfac1(i).ne.0.
     +          or.bk2(i).eq.0.and.pfac1(i).ne.0) then
                cps(i)=cpsaaa(i)-pfac1(i)*npeaq(peak1(i))-pfac2(i)*
     +                npeaq(peak2(i))-pfac3(i)*npeaq(peak3(i))-
     +              pfac4(i)*npeaq(peak4(i))-pfac5(i)*npeaq(peak5(i))
                bpeak(i)=cps(i)
            end if
352       continue
c
c     ******************** glass bulge area calculation ****************
c
      area1=0
      do 831 l=1,stepq
          area1=((xx1(l)*s(l+1)**3)/3-(xx1(l)*s(l)**3)/3
     +        +(xx2(l)*s(l+1)**2)/2-(xx2(l)*s(l)**2)/2
     +        +(xx3(l)*s(l+1))-(xx3(l)*s(l))
     +        -(x1(l)*s(l+1)**3)/3+(x1(l)*s(l)**3)/3
     +        -(x2(l)*s(l+1)**2)/2+(x2(l)*s(l)**2)/2
     +        -(x3(l)*s(l+1))+(x3(l)*s(l)))+area1
831   continue
c
c     ************** Compare background and nett peak intensities *******
c     ************** with results from the previous iteration,    *******
c     ************** and repeat calculations if there are any     *******
c     ************** significant differences                      *******
c
      m=0
      do 1001 l=1,values
         cps2(l)=cps(l)
         cps3(l)=(cps2(l)-cps1(l))/cps2(l)
          if (bk1(l).ne.bk2(l).and.bk2(l).le.0.or.bk2(l).eq.0) then
              if (cps3(l).gt.-0.0001.and.cps3(l).lt.0.0001) then
                  continue
              else
                  m=1
              end if
          end if
          if (bk1(l).eq.bk2(l).and.bk2(l).lt.0.or.bk2(l).gt.0) then
              npeak2(l)=npeak(l)
              npeak3(l)=(npeak2(l)-npeak1(l))/npeak2(l)
              if (cps3(l).gt.-0.0001.and.cps3(l).lt.0.0001.or.
     +            npeak3(l).gt.-0.0001.and.npeak3(l).lt.0.0001) then
                  continue
              else
                  m=1
              end if
          end if
1001  continue
      if (m.eq.0) then
          continue
      else
          go to 992
      end if
      go to 994
99    continue
994   continue
```

```
c
c     *** calculate ratio of the nett peak to the internal standard ****
c                      and determine counting error
c
          do 355 i=1,values
               if (pos(i) .eq. 1) then
                    denom1=npeak(i)
               end if
355       continue
          area2=area1/(s(stepq+1)-s(1))
          bulge=area2/denom1
          do 356 i=1,values
               if (bk1(i).eq.bk2(i).and.bk1(i).ne.0.or.bk1(i).gt.0) then
                    ratio1(i)=npeak(i)/denom1
                    brate(i)=cps(i)-npeak(i)
                      do 410 k=i,values
                          if(bk1(k)*bk2(k).le.0.or.bk1(k)*bk2(k).gt.0
     +                    .and.bk1(k).ne.bk2(k)) then
                              tback1=time(k)
                              go to 420
                          end if
410                     continue
420                     do 430 k=i,1,-1
                          if (bk1(k)*bk2(k).le.0.or.bk1(k)*bk2(k).gt.0
     +                    .and.bk1(k).ne.bk2(k)) then
                              tback2=time(k)
                              go to 440
                          end if
430                     continue
440                     if (tback1+tback2 .gt. time(i)) then
                          tback(i)=time(i)
                        else
                          tback(i)=tback1+tback2
                        end if
                    sd(i)=(((cps(i)/time(i)+brate(i)/tback(i))**0.5)
     +                                        *100)/(cps(i)-brate(i))
                    lld(i)=3*((brate(i)/tback(i))**0.5)
               else
                    ratio1(i)=0.0
                    sd(i)=100/((cps(i)*time(i))**0.5)
                    lld(i)=0.0
               end if
               if (npeak(i).lt.lld(i).and.npeak(i).gt.(-1*lld(i))) then
                    npeak(i)=0.0
                    ratio1(i)=0.0
               end if
356       continue
c
c     ************************ print the data ***************************
c
          write (ilp,1015) sname
          do 460 l=1,stepq
              write (ilp,1016) backa(l),backb(l),xx1(l),xx2(l),xx3(l),rr2(l)
              write (ilp,1017) x1(l),x2(l),x3(l),r2(l)
              write (ilp,1013) (s(i),i=l,l+1)
460       continue
          write (ilp,1032)
          write (ilp,1033)
          do 480 i=1,values
            if (mfac(i).gt.0.or.pfac1(i).gt.0.or.pfac6(i).ne.0) then
            write (ilp,1019) des(i),des(peak1(i)),pfac1(i),des(peak2(i)),
     +                      pfac2(i),des(peak3(i)),pfac3(i),des(peak4(i)),
```

```
     +                  pfac4(i),des(peak5(i)),pfac5(i),bfac1(i),
     +                  des(baca(i)),des(bacb(i)),mfac(i),pfac6(i)
        end if
480   continue
      write (ilp,2001) times
      write (ilp,2000)
      do 30 i=1,values
30    write (ilp,2010) des(i),bk1(i),bk2(i),thtmin(i),thtmax(i),
     +                 counts(i),time(i),
     +                 cpsold(i),bpeak(i),b_area(i),botcps(i),npeak(i),
     +                 sd(i),lld(i),ratio1(i)
      write (ilp,1014) area2,bulge
      write (ilp,1008)
c
c     ************* remove the zero values in the ratio list **********
c
      tick=0
      k=1
      count=0
60          do 35 i=k,values
                if (pos(i) .ne. 0) then
                      rat1(pos(i))=ratio1(i)
                      nett(pos(i))=npeak(i)
                      count=count+1
                else
                      k=i+1
                      tick=tick+1
                           if (k .gt. values) then
                                go to 35
                           else
                                go to 60
                           end if
                end if
35          continue
c
c     ******************** write data to file *************************
c
      write (ofile,3020) sname,bulge,(rat1(i),i=1,count),area2,
     +                  (nett(i),i=1,count),(bpeak(i),i=1,values),
     +                  (botcps(i),i=1,values)
c
c     ********** write background data to grafit readable file ********
c
      if (repeat.eq.1) then
          write (gfile,3021)
      end if
      do 708 i=1,values
          if (bk1(i).ne.bk2(i).and.bk1(i).le.0.or.bk2(i).eq.0) then
              write (gfile,3022) theta(i),bpeak(i),botcps(i)
          else
              write (gfile,3025) theta(i),bpeak(i)
          end if
708   continue
      if (iti.eq.0) then
          write (gfile,3023)
      else
          write (gfile,3024)
      end if
      if (iti.eq.0) then
         go to 995
      end if
      close (afile)
```

```
      close (ofile)
      close (bfile)
      close (gfile)
      call spcls (ilp,name)
c
      end
```

Appendix 3(d)

An example of an output data file from program XRDGLASS in the format of files used in the Department of Geochemistry. Line 1 is the title. Line 2 is the number of samples and the number of variables respectively. The variable names occupy lines 3 - 7. A format statement is on line 8. Lines 1 to 8 are entered by the user. Line 9 is the sample name, followed by the data. These data are output by the program. The variables have the following order: Glass area/silicon ratio; Analyte peak/silicon ratio in the order defined by the parameter file (Ps); Nett glass area; Nett analyte peaks in the order defined by the parameter file; Corrected backgrounds through glass bulge for all background and peak positions in order of increasing degrees 2θ. Corrected backgrounds through background below glass glass for all background and peak positions in order of increasing degrees 2θ.

```
XRD SAMPLES: Feb 1989
  2 52
GlassrS111r M110r P001r Q100r H012r C104r M220r L111r GlassnS111n M110n
P001n Q100n H012n C104n M220n L111n B13t  B1t   M110t B2t   P001t B3t
Q100t B4t   H012t B5t   S111t C104t B6t   M220t L111t B7t   B8t   B13b
B1b   M110b B2b   P001b B3b   Q100b B4b   H012b B5b   S111b C104b B6b
M220b L111b B7b   B8b
(8A2,I1,I2,5X,16A2,10(:,/,9F8.3))
D3_COMPA         0 0
    .555   1.000    .164    .013    .094    .022   -.010    .094    .216
 517.755 933.168 153.355  12.405  87.904  20.342  -9.324  87.395 201.511
1395.6731131.4481114.8571124.0981145.2221204.3051271.4641348.7891340.833
1317.5611090.4081026.5761013.043 983.044 858.786 704.377 534.7161288.564
 920.627    .000 776.440    .000 655.235    .000 544.429    .000 465.954
    .000    .000 351.051    .000    .000 283.003 256.471
D3_COMPB         0 0
    .638   1.000    .186    .017    .098    .024   -.008    .105    .241
 549.641 861.871 159.946  14.914  84.596  20.844  -6.711  90.591 207.795
1441.7321165.9641143.0891148.3211170.0541235.9561308.5301391.7151383.351
1358.3581126.0131060.5891046.7101015.938 888.333 729.460 552.0911289.277
 922.153    .000 778.099    .000 656.675    .000 545.876    .000 467.638
    .000    .000 352.432    .000    .000 284.133 257.396
```

Appendix 3(e)

An example of an output data file from program XRDGLASS in the format of a file readable by the graph program GRAFIT. Samples are separated by the tilde symbol in each data column. From left to right the columns are: Position of analyte peak and background in degrees 2θ; Background intensities through the glass bulge; Background intensities (calculated) for the background below the glass; Background intensities below peaks.

```
DATA
 11.50  1436.754  1237.000      ?
 15.13  1277.222   860.643      ?
 16.45     ?         ?       1329.328
 17.19  1384.230   717.365      ?
 18.10     ?         ?       1470.056
 19.45  1641.423   604.357      ?
 20.85     ?         ?       1810.614
 22.20  1981.056   496.394      ?
 24.10     ?         ?       2029.348
 24.75  2010.297   414.665      ?
 28.44     ?         ?       1812.185
 29.48     ?         ?       1728.284
 29.70  1708.709   309.729      ?
 30.19     ?         ?       1642.307
 32.22     ?         ?       1387.133
 34.75  1114.030   249.189      ?
 38.20   821.947   228.000      ?
 ~         ~         ~          ~
 11.50  1453.219  1236.000      ?
 15.13  1296.903   861.135      ?
 16.45     ?         ?       1343.185
 17.19  1393.185   718.425      ?
 18.10     ?         ?       1477.165
 19.45  1649.092   605.865      ?
 20.85     ?         ?       1819.104
 22.20  1991.461   498.330      ?
 24.10     ?         ?       2034.009
 24.75  2011.606   416.925      ?
 28.44     ?         ?       1814.538
 29.48     ?         ?       1730.019
 29.70  1710.328   312.405      ?
 30.19     ?         ?       1642.862
 32.22     ?         ?       1383.668
 34.75  1106.446   252.105      ?
 38.20   810.334   231.000      ?
END
```

Appendix 3(f)

An example of the printout from program XRDGLASS is shown on the following page. Numbers in italics have been added for the purpose of this explanation.

Section (1): Quadratic equations of the upper and lower background curves in each domain, and the backgrounds used in the calculation.

Section (2): Background interference and overlap correction factors used to correct the nett counts for each analyte peak. BFAC are the factors used to calculate directly the background due to quartz. MFAC and GFAC are discussed in the text.

Section (3): From left to right: Peak or background name, Ba as in the parameter file (columns 2 and 3), scan range (columns 4 and 5), total counts, time counted at each position, measured intensities, corrected intensity of background through the glass bulge, background area under each peak, calculated intensity through the background below the glass bulge, nett peak, standard deviation of nett peaks and backgrounds, lower limit of detection, and the ratio of the nett peak to the nett peak of Silicon (111).

Appendix 3(f) (Continued)

SAMPLE NAME: D3_COMPA

(1)

```
BACK13 TO BACK2    UPPER CURVE:  CPS=  12.173 2THETA**2+  -396.977  2THETA+  4350.976    R2= 1.00
                   LOWER CURVE:  CPS=   5.513 2THETA**2+  -248.177  2THETA+  3413.481    R2= 1.00
                   INTEGRAL LIMITS :  11.50 17.19

BACK1  TO BACK3    UPPER CURVE:  CPS=   8.997 2THETA**2+  -294.332  2THETA+  3525.134    R2= 1.00
                   LOWER CURVE:  CPS=   3.781 2THETA**2+  -192.176  2THETA+  2962.724    R2= 1.00
                   INTEGRAL LIMITS :  17.19 19.45

BACK2  TO BACK4    UPPER CURVE:  CPS=   3.487 2THETA**2+   -92.386  2THETA+  1681.636    R2= 1.00
                   LOWER CURVE:  CPS=   2.643 2THETA**2+  -150.399  2THETA+  2580.869    R2= 1.00
                   INTEGRAL LIMITS :  19.45 22.20

BACK3  TO BACK5    UPPER CURVE:  CPS= -12.199 2THETA**2+   560.633  2THETA+ -5085.050    R2=  .99
                   LOWER CURVE:  CPS=   1.771 2THETA**2+  -114.002  2THETA+  2202.451    R2= 1.00
                   INTEGRAL LIMITS :  22.20 24.75

BACK5  TO BACK7    UPPER CURVE:  CPS=    .037 2THETA**2+   -63.526  2THETA+  2867.078    R2= 1.00
                   LOWER CURVE:  CPS=    .972 2THETA**2+   -76.127  2THETA+  1754.684    R2= 1.00
                   INTEGRAL LIMITS :  24.75 34.75

BACK6  TO BACK8    UPPER CURVE:  CPS=   1.388 2THETA**2+  -150.484  2THETA+  4258.228    R2= 1.00
                   LOWER CURVE:  CPS=    .672 2THETA**2+   -56.751  2THETA+  1443.819    R2= 1.00
                   INTEGRAL LIMITS :  34.75 38.20
```

(2)

BACKGROUND CORRECTIONS AND INTERFERENCES

GLASS BULGE										BASELINE				
DESCRIP	PEAK1	FAC1	PEAK2	FAC2	PEAK3	FAC3	PEAK4	FAC4	PEAK5	FAC5	BFAC	BACKA	BACKB	MFAC	GFAC
BACK13		.000		.000		.000		.000		.000	.000			.108	.000
BACK1		.000		.000		.000		.000		.000	.627			.231	.000
MUL110	MGF220	.006		.000		.000		.000		.000	.000			.000	.000
BACK2	MUL110	.020	PTL001	.289		.000		.000		.000	.485			.251	.000
PTL001	MUL110	.003	MGF220	.109		.000		.000		.000	.000			.000	.000
BACK3		.000		.000		.000		.000		.000	.373			.218	.000
QTZ100		.000		.000		.000		.000		.000	.000			.000	.018
BACK4		.000		.000		.000		.000		.000	.266			.219	.000
HMT012	QTZ100	.020		.000		.000		.000		.000	.000			.000	.000
BACK5	QTZ100	.012	HMT012	.026		.000		.000		.000	.185			.255	.000
SIL111	QTZ100	.011	MGF220	.016	CAL104	.017	PTL001	.506		.000	.000			.000	-.025
CAL104	SIL111	.007	QTZ100	.005	MGF220	.032	PTL001	.048		.000	.000			.000	.041
BACK6	SIL111	.001	QTZ100	.005	MGF220	.142	CAL104	.211	PTL001	.041	.081			.209	.000
MGF220	QTZ100	.003	MUL110	.029	CAL104	.127		.000		.000	.000			.000	.004
LIM111	MUL110	.026	HMT012	.075	MGF220	.040	CAL104	.041	PTL001	.073	.000			.000	.027
BACK7	MUL110	.128	HMT012	.052	MGF220	.155	PTL001	.796		.000	.021			.171	.000
BACK8		.000		.000		.000		.000		.000	.000			.140	.000

NUMBER OF ITERATIONS = 5

(3)

MINERAL PEAK	BK1	BK2	THETA BEGIN	THETA END	TOTAL COUNTS	TIME (SECS)	ORIGNL CPS	GLASS BULGE	PEAK BASE	BASE LINE	NETT PEAK	STD DEV (%)	LLD (CPS)	RATIO (S111)
BACK13	-1	0	11.500	11.500	279130	200.000	1395.650	1395.673	.000	1288.564	.000	.189	.000	.000
BACK1	-2	0	15.130	15.130	226295	200.000	1131.475	1131.448	.000	920.627	.000	.210	.000	.000
MUL110	-1	-1	15.500	17.000	457509	360.017	1270.798	1114.857	1116.919	.000	153.355	1.680	5.285	.164
BACK2	-3	-1	17.190	17.190	226150	200.000	1130.750	1124.098	.000	776.440	.000	.211	.000	.000
PTL001	-2	-2	17.190	19.000	508330	434.501	1169.917	1145.222	1147.525	.000	12.405	19.053	5.103	.013
BACK3	-4	-2	19.450	19.450	240794	200.000	1203.970	1204.305	.000	655.235	.000	.204	.000	.000
QTZ100	-3	-3	19.700	21.700	653777	480.022	1361.973	1271.464	1264.750	.000	87.904	2.792	5.354	.094
BACK4	0	-3	22.200	22.200	269891	200.000	1349.455	1348.789	.000	544.429	.000	.192	.000	.000
HMT012	-4	-4	23.700	24.650	619964	455.893	1359.889	1340.833	1337.789	.000	20.342	13.497	6.402	.022
BACK5	-5	-4	24.750	24.750	124150	94.114	1319.145	1317.561	.000	465.954	.000	.284	.000	.000
SIL111	-5	-5	27.850	29.000	1115083	552.010	2020.041	1090.408	1091.332	.000	933.168	.291	5.767	1.000
CAL104	-5	-5	29.000	29.700	355014	335.927	1056.819	1026.576	1034.552	.000	-9.324	-27.908	5.712	-.010
BACK6	-6	0	29.700	29.700	205467	200.000	1027.335	1013.043	.000	351.051	.000	.222	.000	.000
MGF220	-5	-5	29.750	30.600	439356	407.960	1076.958	983.044	983.966	.000	87.395	2.588	4.719	.094
LIM111	-5	-5	31.700	32.650	495430	455.961	1086.562	858.786	861.541	.000	201.511	1.064	4.462	.216
BACK7	0	-5	34.750	34.750	149697	200.000	748.485	704.377	.000	283.003	.000	.266	.000	.000
BACK8	0	-6	38.200	38.200	106973	200.000	534.865	534.716	.000	256.471	.000	.306	.000	.000
GLASS											517.755			.555

Appendix 4

Composition of the standards used to construct the calibration curves used in QXRD.

Glass standards				
	Weight percent components			Glass
	Glass	Duvha PFA	Quartz	Total
1	0	33.4	66.6	14.5
2	0	100	0	43.4
3	50	50	0	71.7

Mullite/quartz standards				
	Weight Percent Components			
	Quartz	Mullite/quartz Concentrate	Quartz Total	Mullite Total
1	0	100	22.2	86.1
2	40	60	47.3	51.7
3	60	40	64.9	34.4
4	80	20	82.4	17.2

Quartz standards (II)		
	Glass	Quartz
1	95	5
2	85	15
3	75	25

Spinel/hematite standards					
	Weight Percent Components				
	Duvha PFA magnetic concentrate	Quartz	Hematite	Spinel Total	Hematite Total
1	30	70	0	25.7	4.3
2	20	46.8	33.2	17.1	36.1
3	10	23.4	66.6	8.6	68.1

Calcite standards		
	Quartz	Calcite
1	95	5
2	90	10
3	85	15

Portlandite standards		
	Quartz	Portlandite
1	95	5
2	90	10
3	85	15

Lime standards		
	Quartz	Lime
1	95	5
2	85	10
3	75	15